

https://dspace.org/

A CO2 capture technology using carbon nanotubes with polyaspartamide surfactant

Ngoy, Jacob Masiala

2016-07-13
http://hdl.handle.net/10539/20570

Downloaded from a DSpace repository. https://dspace.org/

A CO_2 CAPTURE TECHNOLOGY USING CARBON NANOTUBES WITH POLYASPARTAMIDE SURFACTANT



Jacob Masiala Ngoy

A thesis submitted to the Faculty of Engineering and the Built Environment, University of the Witwatersrand, Johannesburg, in fulfilment of the requirements for the degree of Doctor of Philosophy

Johannesburg, 2016

DECLARATION

I declare that this thesis is the fruit of my own work. It is being submitted for the degree of Doctor of Philosophy of Engineering in the University of the Witwatersrand, Johannesburg, South Africa. It has not been submitted before for any degree or examination in any other University.

Signed……...

……day of……2016

ABSTRACT

Technologies for the separation of CO_2 from flue gas require a feat of engineering for efficient achievement. Various CO_2 capture technologies, including absorption, adsorption, cryogenics and membranes, have been investigated globally. The absorption technology uses mainly alkanolamine aqueous solutions, the most common being monoethanolamine (MEA); however, further investigation is required to circumvent its weakness due to degradation through oxidation, material corrosion and high energy costs required for regeneration. Attractive advantages in adsorption technology, including the ability to separate the more diluted component in the mixture with a low energy penalty, have been a motivation for many researchers to contribute to the advancement of adsorption technology in CO_2 capture. The challenge in CO_2 adsorption technology is to design a hydrophobic and biodegradable adsorbent with large CO_2 uptake, high selectivity for CO_2, adequate adsorption kinetics, water tolerance, and to require low levels of energy for regeneration processes. The existing adsorbent such as activated carbon, silica gel, zeolites, metal organic frameworks and others, have been ineffective where moisture occurs in flue gas. This work provides an advanced adsorption technology through a novel adsorbent, MWNT-PAA, designed from the non-covalent functionalization of multi-walled carbon nanotubes (MWNTs) by polyaspartamide (PAA) as product of amine grafted to polysuccinimide (PSI). Three types of PAA were prepared using ethylenediamine (EDA), 1, 3 propanediamine (PDA) and monoethanolamine (MEA) drafted to PSI to give PSI-EDA, PSI-PDA and PSI-MEA respectively. The CO_2 adsorption capacity was 13.5 mg-CO_2/g for PSI-PDA and 9.0 mg-CO_2/g for PSI-MEA, which decreased significantly from PSI where the CO_2 adsorption capacity was 25 mg-CO_2/g. PSI-EDA was selected as PAA, because the CO_2 adsorption capacity was 52 mg-CO_2/g which doubled from PSI. The polymer polyethylenimine (PEI), the most commonly polymer used in CO_2 capture, was found to be non-biodegradable, while the polymer PAA showed the presence of CONH as a biodegradable bond functionality, occurring in the MWNT-PAA, as confirmed through Fourier Transform Infrared (FTIR) analysis. The adsorbent MWNT-PAA was demonstrated to have a water tolerance in the temperature range 25-55 ℃, where CO_2 adsorption capacity increased with the increase of water in the adsorbent. The highest CO_2 adsorption capacity recorded was 71 mg-CO_2/g for the moist MWNT-PAA using 100% CO_2 and 65 mg-CO_2/g for the mixture of 14% CO_2 with air. Under the same conditions, the dry MWNT-PAA adsorbed 70 and 46 mg-CO_2/g respectively (100%, 14% CO_2). The

regenerability efficiency of the MWNT-PAA absorbent was demonstrated at 100 ^{o}C; after 10 cycles of adsorption-desorption 99% of adsorbed gas was recovered in the desorption process. The heat flow for the thermal swing adsorption system resulted in the net release of heat over the complete cycle; a cycle includes adsorption (heat release) and desorption (heat absorbance). Thus, this MWNT-PAA adsorbent demonstrates an advantage in terms of overall energy efficiency, and could be a competitive adsorbent in CO_2 capture technology.

DEDICATION

To the Holy Ghost: The Spirit of God the Creator

The Spirit of wisdom, understanding and science

The Spirit of dominion and reign

The Spirit of counsel and might

The Spirit of knowledge and of the fear of the Lord

I dedicate this work.

ACKNOWLEDGEMENT

Particular thanks are due to Professor Nicola Wagner, Professor Olav Bolland and Professor J. Herman Potgieter, my supervisors, for the many hours spent offering advice, encouragement, suggestions and guidance to make the completion of this project possible.

Thanks to the EnPe grant under the Norad funding mechanism.

To Esther Masiala my wife, I say thanks for the attention that you have given to this research by providing every day a refreshing framework.

To my daughters, Souviel Masiala and Gael Masiala, I say thanks, in your presence I could relax with a discharged mind.

I finally say thanks to everyone who has contributed directly or indirectly for the achievement of this project.

TABLE OF CONTENTS

DECLARATION ii

ABSTRACT iii

DEDICATION v

ACKNOLEDGEMENT vi

TABLE OF CONTENTS vii

LIST OF FIGURES xiv

LIST OF TABLES xix

LIST OF ABREVIATION xxi

NOMENCLATURE xxiv

LIST OF GREEK SYMBOLS xxvi

CHAPTER ONE: INTRODUCTION 1

1.0. INTRODUCTION 1

1.1. BACKGROUND OF STUDY 2

1.2. PROBLEM STATEMENT 4

1.3. RESEARCH AIMS AND OBJECTIVES 6

1.4. RESEARCH HYPOTHESIS AND QUESTIONS 6

1.5. RESEARCH TECHNIQUES 7

1.6. EXPECTED CONTRIBUTION TO KNOWLEDGE 7

1.7. ORGANIZATION OF THESIS 8

CHAPTER TWO: LITERATURE REVIEW 9

2.0. INTRODUCTION 9

2.1. CO_2 EMISSIONS SOURCES 10

2.1.1. Fuel and fuel production 9

2.1.1.1. Solid fuel 12

2.1.1.2. Liquid fuel 14
2.1.1.3. Gaseous fuel 15
2.1.2. Other industrial sources of CO_2 16
2.1.2.1. Cement production 16
2.1.2.2. Refineries 17
2.1.2.3. Iron and steel 17
2.1.2.4. Petrochemical industry 17
2.2. CO_2 CAPTURE, TRANSPORT AND STORAGE 18
2.2.1. CO_2 capture 18
2.2.2. CO_2 compression and transport 21
2.2.3. Storage 22
2.2.3.1. Underground storage 23
2.2.3.2. Ocean storage 25
2.2.3.3. Mineral carbonation 25
2.2.3.4. Industrial use – products 26
2.2.4. CO_2 capture economy cost evaluation 26
2.3. CO_2 CAPTURE TECHNOLOGY 30
2.3.1. Absorption 30
2.3.2. Adsorption 31
2.3.3. Membranes 32
2.3.4. Cryogenics separation 32
2.4. ADSORPTION TECHNOLOGY 33
2.4.1. Introduction 33
2.4.2. Fundamentals factors for designing adsorbents 34
2.4.2.1. Fluid flow through packed bed 36
2.4.2.2. Mass transfer and adsorption kinetics 37
2.4.2.3. Potential energies for adsorption 40
2.4.2.4. Heat of adsorption 41
2.4.3. Adsorption separation process 42
2.4.3.1. Regeneration of spent adsorbent 42
2.4.3.2. Regeneration methods 42
2.4.4. Adsorption technology for CO_2 capture 45
2.4.4.1. Adsorption technology for CO_2 capture using fixed bed 45
2.4.4.2. CO_2 adsorption technology using moving bed 47

2.4.4.3. CO_2 adsorption using fluidized bed reactors (FBRs) 48
2.4.5. Adsorbent materials for CO_2 capture 50
2.4.5.1. Activated carbon 50
2.4.5.2. Silica gel 51
2.4.5.3. Zeolite 51
2.4.5.4. Metal organic frameworks 52
2.4.6. Modification of surface characteristic of adsorbents 52
2.4.7. Moisture effects on adsorbents for CO_2 capture 57
2.4.8. Specific characterization for adsorbents evaluation 59
2.4.8.1. Nuclear magnetic resonance spectroscopy 59
2.4.8.2. Fourier transform infrared and Raman spectra 59
2.4.8.3. High resolution transmission electron microscope 59
2.4.8.4. Brunauer, Emmett, and Teller 60
2.4.8.5. Thermogravimetric analyser 61
2.5. SUMMARY 62

CHAPTER THREE: METHODOLOGY 64

3.0. INTRODUCTION 64
3.1. EQUIPMENT AND CHEMICALS 65
3.1.1. Equipment 65
3.1.2. Chemicals 65
3.2. CHARACTERIZATION 66
3.3. EXPERIMENTAL PROCEDURE 68
3.3.1. Detailed description of adsorbents synthesis 69
3.3.1.1. Design of polyaspartamides (PAAs) 69
3.3.1.2. Preparation of poly-αβ-DL-succinimide (PSI) 71
3.3.1.3. PAA synthesis from EDA to produce PSI-EDA 72
3.3.1.4. PAA synthesis from PDA to produce PSI-PDA 73
3.3.1.5. PAA synthesis from MEA to produce PSI-MEA 73
3.3.1.6. . Coating of multi-walled carbon nanotube (MWNT) by PSI to give MWNT-PSI 74
3.3.1.7. Coating of multi-walled carbon nanotube (MWNT) by PAA to give MWNT-PAA 74
3.3.2. Adsorption and desorption experiments 75
3.3.2.1. CO_2 adsorption using thermogravimetry analyzer (TGA) 75
3.3.3. Desorption experiments 76

3.4. SUMMARY 78

CHAPTER FOUR: RESULTS AND DISCUSSION 79

4.0. INTRODUCTION 79
4.1. POLYASPARTAMIDES (PAAs) 82
4.1.2. Characterization of PAAs 82
4.1.2.1. Polysuccinimide (PSI) 82
4.1.2.2. PAA using EDA to produce PSI-EDA 85
4.1.2.3. PAA using PDA to produce PSI-PDA 87
4.1.2.4. PAA using MEA to produce PSI-MEA 90
4.1.2.5. Comparison of PAAs 92
4.1.3. Adsorption at 25 ◦C for PAA selection 93
4.1.3.1. PSI 93
4.1.3.2. PAA of type PSI-EDA 93
4.1.3.3. PAA of type PSI-PDA 94
4.1.3.4. PAA of type PSI-MEA 95
4.1.3.5. Comparison and PAA selection 95
4.2. NON-COVALENT FUNCTIONALISATION OF MULTI-WALLED CARBON NANOTUBES WITH POLYASPARTAMIDE (MWNT-PAA) 97
4.2.1. Characterization of MWNT with PAAs 97
4.2.1.1. Multi-walled carbon nanotubes (MWNTs) 97
4.2.1.2. Multi-walled carbon nanotube with polysuccinimide (MWNT-PSI) 100
4.2.1.3. Multi-walled carbon nanotube with polyaspartamide (MWNT-PAA) 102
4.2.2. Comparison study of growth of adsorbent characterization 105
4.3. TEMPERATURE EFFECTS ON CO_2 ADSORPTION USING 100% CO_2 107
4.3.1. CO_2 adsorption at 25 ◦C 107
4.3.2. CO_2 adsorption at 35 ◦C 110
4.3.3. CO_2 adsorption at 45 ◦C 112
4.3.4. CO_2 adsorption at 55 ◦C 113
4.3.5. CO_2 adsorption at 65 ◦C 115
4.3.6. CO_2 adsorption at 75 ◦C 116
4.3.7. CO_2 adsorption at 85 ◦C 117
4.3.8. Conclusion of effect of increasing temperature on adsorbents 100% CO_2 119

4.4. TEMPERATURE EFFECTS ON CO_2, N_2 AND O_2 ADSORPTION 121
4.4.1. N_2 and O_2 adsorption at 25 ◦C compared to CO_2 adsorption 121
4.4.2. N_2 and O_2 adsorption at 35 ◦C compared to CO_2 adsorption 123
4.4.3. N_2 and O_2 adsorption at 45 ◦C compared to CO_2 adsorption 124
4.4.4. N_2 and O_2 adsorption at 55 ◦C compared to CO_2 adsorption 126
4.4.5. Section Summary 127
4.5. CO_2 ADSORPTION FROM FLUE GAS WITH VARIABLE CO_2 CONCENTRATION 128
4.5.1. CO_2 adsorption at 25 ◦C 128
4.5.1.1. PAA 128
4.5.1.2. MWNT-PAA 130
4.5.2. CO_2 adsorption at 35 ◦C 132
4.5.2.1. PAA 132
4.5.2.2. MWNT-PAA 133
4.5.3. CO_2 adsorption at 45 ◦C 135
4.5.3.1. PAA 135
4.5.3.2. MWNT-PAA 136
4.5.4. CO_2 adsorption at 55 ◦C 137
4.5.4.1. PAA 137
4.5.4.2. MWNT-PAA) 138
4.5.5. Discussion of variable CO_2 concentration on adsorption 140
4.6. THE BEHAVIOR OF MOIST ADSORBENTS ON ADSORPTION 143
4.6.1. The effects of moist adsorbents on O_2 adsorption with change of temperature 144
4.6.2. The effects of moist adsorbents using variable CO_2 concentration in gas stream at variable temperatures 145
4.6.2.1. Gas stream with 100% CO_2 Content 145
4.6.2.2. Effluent stream gas with 14% CO_2 content 153
4.6.2.3. Discussion of CO_2 adsorption using moist adsorbents at varying CO_2 Concentration 161
4.7. ADSORPTION-DESORPTION CYCLES 163
4.7.1. Adsorption at 25 ◦C with desorption at 90 ◦C for 10 cycles 164

4.7.2. Adsorption at 25 ◦C with desorption at 100 ◦C for 10 cycles 167

4.8. THERMODYNAMICS EVALUATION OF THERMAL SWING ADSORPTION 171
4.8.1. Evaluation of heat flow in the sweeping process 171
4.8.2. Evaluation of heat flow in the adsorption process 175
4.8.3. Evaluation of heat flow in the desorption process 176
4.8.4. Heat flow depending on adsorption time 177
4.9. EVALUATION OF NUMBERS OF BEDS FOR TSA SYSTEMS 179
4.10. COMPARISON OF DESIGNED ADSORBENTS TO THE EXISTING ADSORBENTS FOR CO_2 CAPTURE 186

CHAPTER FIVE: SUMMARY, CONCLUSIONS AND RECOMMENDATION 188

5.1. SUMMARY 188
5.2. CONCLUSIONS 193
5.3. RECOMMENDATION 195

CHAPTER SIX: CONTRIBUTION OF THE WORK TO SCIENTIFIC ADVANCEMENT AND ACHIEMENTS 197

6.1. ACHIEVEMENT OF ADSORBENTS DESIGN 198
6.2. ACHIEVEMENT OF ADSORPTION AND DESORPTION PROCESS 200
6.3. ACHIEVEMENT OF THERMODYNAMICS STUDIES 203
6.4. PAPERS + CONFERENCES PRESENTATIONS PRODUCED TO DATE 203
6.4.1. Papers 203
6.4.2. Conferences presentations 202

REFERENCES 203

APPENDICES 231

APPENDIX 1: TGA GRAPHS OF CO_2 ADSORPTION FOR DRY ADSORBENTS WITH 100% CO_2 232

APPENDIX 2: TGA GRAPHS OF N_2 ADSORPTION FOR DRY ADSORBENTS WITH 100% N_2 246

APPENDIX 3: TGA GRAPHS OF O_2 ADSORPTION FOR DRY ADSORBENTS WITH 100% O_2 250

APPENDIX 4: TGA GRAPHS OF O_2 ADSORPTION FOR MOIST ADSORBENTS WITH 100% O_2 254

LIST OF FIGURES

Figure 1.1: CO_2 emissions reduction option, 2005-2050. Source: IEA-2008; Energy Technology Perspectives, scenarios and strategies to 2050. 3

Figure 2.1: CO_2 emissions by U.S. power plants by major fuel groups, 2003-2007 11

Figure 2.2: Different categories of biomass conversion 13

Figure 2.3: A visual sketch of the petrochemical value chain and application 18

Figure 2.4: Carbon dioxide separation methods 20

Figure 2.5: Typical schematic of CO_2 compression process 22

Figure 2.6: The pressure drop in fluid flow 37

Figure 2.7: Three fixed beds operating in TSA system for CO_2 capture 46

Figure 2.8: A fixed bed with two different types of adsorbent for specific adsorption 47

Figure 2.9: Circulating adsorbent–Continuous Counter-Current 48

Figure 2.10: Fluidized bed reactors (FBRs) 49

Figure 2.11: Polyethylenenimine structure 54

Figure 2.12: Chemical structure of polymer grafted with amine and CO_2 in reaction 55

Figure 2.13: Structure of coating of CNTs with polymer 55

Figure 2.14: Polycondensation of aspartic acid for poly-DL-succinimide (PSI) synthesis 57

Figure 2.15: PSI grafted to diamine for polyaspartamide synthesis 57

Figure 3.1: Thermogravimetry analyzer of type TA-Q600 68

Figure 3.2: Structure of polyamide - type carrier 70

Figure 4.1: ^1H NMR spectra showing protons in chemical structure of PSI 83

Figure 4.2: FTIR showing necessary peaks in structure of PSI 83

Figure 4.3: TGA mass loss curve showing the temperature stability of PSI 84

Figure 4.4: Reaction for PSI-EDA formation showing the chemical structure 85

Figure 4.5: ^{1}H NMR spectra showing protons in the chemical structure of PSI-EDA 86

Figure 4.6: FTIR showing necessary peaks in PSI-EDA 86

Figure 4.7: TGA showing the stability of PSI-EDA with temperature 87

Figure 4.8: Reaction for PSI-PDA formation showing the chemical structure 88

Figure 4.9: ^{1}H NMR according to PSI-PDA chemical structure 88

Figure 4: 10: FTIR showing the necessary peaks for the chemical structure of PSI-PDA 89

Figure 4.11: TGA showing the stability of PSI-PDA with temperature 89

Figure 4.12: Reaction for PSI-MEA formation showing the chemical structure 90

Figure 4.13: ^{1}H NMR showing protons relevant to PSI-MEA chemical structure 91

Figure 4.14: FTIR showing the necessary peaks for the chemical structure of PSI-MEA 91

Figure 4.15: TGA showing the stability of PSI-MEA with increasing temperature 92

Figure 4.16: CO_2 adsorption capacity of different polyaspartamides at 25 ℃ 94

Figure 4.17: CO_2 adsorption rate of all polyaspartamides at 25 ℃ 95

Figure 4.18: TEM showing the nanostructure image of MWNT 98

Figure 4.19: Raman spectra (MWNTs) 99

Figure 4.20: TGA showing weight degradation of MWNTs with temperature 99

Figure 4.21: TEM showing the nanostructure image of the MWNT-PSI 101

Figure 4.22: Raman spectra (MWNT-PSI) 101

Figure 4.23: TGA showing weight degradation of MWNT-PSI with temperature 102

Figure 4.24: TEM showing the nanostructure image of MWNT-PAA 103

Figure 4.25: Raman spectra (MWNT-PAA) 103

Figure 4.26: FTIR for MWNT-PAA identification 104

Figure 4.27: TGA showing the weight stability of MWNT-PAA with temperature 105

Figure 4.28: The growth of D and G bands from MWNT to the *f*-MWNTs 106

Figure 4.29: TGA for all adsorbents showing the weight stability with temperature 107

Figure 4.30: CO_2 adsorption isotherm at 25◦C using a flue gas of 100% CO_2 108

Figure 4.31: CO_2 adsorption isotherm at 35◦C using a flue gas of 100% CO_2 111

Figure 4.32: CO_2 adsorption isotherm at 45◦C using a flue gas of 100% CO_2 113

Figure 4.33: CO_2 adsorption isotherm at 55◦C using a flue gas of 100% CO_2 114

Figure 4.34: CO_2 adsorption isotherm at 65◦C using a flue gas of 100% CO_2 116

Figure 4.35: CO_2 adsorption isotherm at 75◦C using a flue gas of 100% CO_2 117

Figure 4.36: CO_2 adsorption isotherm at 85◦C using a flue gas of 100% CO_2 118

Figure 4.37: Temperature effects on CO_2 adsorption capacity for all adsorbents 120

Figure 4.38: The adsorption of N_2, O_2 and CO_2 using PAA at 25◦C 122

Figure 4.39: The adsorption of N_2, O_2 and CO_2 using MWNT-PAA at 25◦C 123

Figure 4.40: The adsorption of N_2, O_2 and CO_2 using PAA at 35◦C 124

Figure 4.41: The adsorption of N_2, O_2 and CO_2 using MWNT-PAA at 35◦C 124

Figure 4.42: The adsorption of N_2, O_2 and CO_2 using PAA at 45◦C 125

Figure 4.43: The adsorption of N_2, O_2 and CO_2 using MWNT-PAA at 45◦C 126

Figure 4: 44: The adsorption of N_2, O_2 and CO_2 using PAA at 55◦C 127

Figure 4.45: The adsorption of N_2, O_2 and CO_2 using MWNT-PAA at 55◦C 127

Figure 4.46: Adsorption using 100, 40 and 14% CO_2 onto PAA at 25◦C 131

Figure 4.47: Adsorption using 100, 40 and 14% CO_2 onto MWNT-PAA at 25◦C 132

Figure 4.48: Adsorption using 100, 40 and 14% CO_2 onto PAA at 35◦C 134

Figure 4.49: Adsorption using 100, 40 and 14% CO_2 onto MWNT-PAA at 35◦C 135

Figure 4.50: Adsorption using 100, 40 and 14% CO_2 onto PAA at 45◦C 137

Figure 4.51: Adsorption using 100, 40 and 14% CO_2 onto MWNT-PAA at 45◦C 137

Figure 4.52: Adsorption using 100, 40 and 14% CO_2 onto PAA at 55◦C 139

Figure 4.53: Adsorption using 100, 40 and 14% CO_2 onto MWNT-PAA at 55◦C 139

Figure 4.54: CO_2 adsorption from 100% CO_2 onto moist PAA at 25◦C 147

Figure 4.55: CO_2 adsorption from 100% CO_2 onto moist MWNT-PAA at 25◦C 147

Figure 4.56: CO_2 adsorption from 100% CO_2 onto moist PAA at 35◦C 149

Figure 4.57: CO_2 adsorption from 100% CO_2 onto moist MWNT-PAA at 35◦C 149

Figure 4.58: CO_2 adsorption from 100% CO_2 onto moist PAA at 45◦C 151

Figure 4.59: CO_2 adsorption from 100% CO_2 onto moist MWNT-PAA at 45◦C 159

Figure 4.60: CO_2 adsorption from 100% CO_2 onto moist PAA at 55◦C 152

Figure 4.61: CO_2 adsorption from 100% CO_2 onto moist MWNT-PAA at 55◦C 153

Figure 4.62: CO_2 adsorption from 14% CO_2 onto moist PAA at 25◦C 154

Figure 4.63: CO_2 adsorption from 14% CO_2 onto moist MWNT-PAA at 25◦C 155

Figure 4.64: CO_2 adsorption from 14% CO_2 onto moist PAA at 35◦C 156

Figure 4.65: CO_2 adsorption from 14% CO_2 onto moist MWNT-PAA at 35◦C 157

Figure 4.66: CO_2 adsorption from 14% CO_2 onto moist PAA at 45◦C 158

Figure 4.67: CO_2 adsorption from 14% CO_2 onto moist MWNT-PAA at 45◦C 158

Figure 4.68: CO_2 adsorption from 14% CO_2 onto moist PAA at 55◦C 160

Figure 4.69: CO_2 adsorption from 14% CO_2 onto moist MWNT-PAA at 55◦C 160

Figure 4.70: Adsorption (25◦C)-desorption (90◦C) cycle for PSI 166

Figure 4.71: Adsorption (25◦C)-desorption (90◦C) cycle for MWNT 166

Figure 4.72: Adsorption (25◦C)-desorption (90◦C) cycle for PAA 167

Figure 4.73: Adsorption (25◦C)-desorption (90◦C) cycle for MWNT-PAA 167

Figure 4.74: Adsorption (25◦C)-desorption (100◦C) cycle for PSI 169

Figure 4.75: Adsorption (25◦C)-desorption (100◦C) cycle for MWNT 169

Figure 4.76: Adsorption (25◦C)-desorption (100◦C) cycle for PAA 170

Figure 4.77: Adsorption (25◦C)-desorption (100◦C) cycle for MWNT-PAA 170

Figure 4.78: Heat flow from DSC-TGA for a cycle adsorption –desorption using PAA 174

Figure 4.79: Heat flow from DSC-TGA for a cycle adsorption-desorption using MWNT-PAA 174

LIST OF TABLES

Table 2.1: Energy content of fuels 10

Table 2.2: General types of chemical fuels 11

Table 2.3: Cost of electricity and CO_2 avoidance 29

Table 2.4: Estimates of CO_2 storage costs 30

Table 3.1: List of adsorbents 72

Table 4.1: BET analysis showing surface area, pore volume and pore size of adsorbents 84

Table 4.2: CO_2 adsorption capacity of PAAs at 25◦C in 100% CO_2 as flue gas 96

Table 4.3: CO_2 adsorption isotherm at 25◦C 108

Table 4.4: CO_2 adsorption capacity corresponding to the first 10 minutes 109

Table 4.5: CO_2 adsorption isotherm at 35◦C 110

Table 4.6: CO_2 adsorption isotherm at 45◦C 113

Table 4.7: CO_2 adsorption isotherm at 55◦C 114

Table 4.8: CO_2 adsorption isotherm at 65◦C 115

Table 4.9: CO_2 adsorption isotherm at 75◦C 117

Table 4.10: CO_2 adsorption isotherm at 85◦C 118

Table 4.11: Temperature effects on CO_2 adsorption capacity and isothermal time 119

Table 4.12: Adsorption capacity using 100% CO_2, 100% O_2 and 100% N_2 122

Table 4.13: Adsorption capacity and selectivity for CO_2 over (O_2 + N_2) at 25◦C 130

Table 4.14: Adsorption capacity and selectivity for CO_2 over (O_2 + N_2) at 35◦C 133

Table 4.15: Adsorption capacity and selectivity for CO_2 over (O_2 + N_2) at 45◦C 136

Table 4.16: Adsorption capacity and selectivity for CO_2 over (O_2 + N_2) at 55◦C 139

Table 4.17: O_2 adsorption capacity for dry and wet adsorbents at variable temperatures 145

Table 4.18: CO_2 adsorption using 100% CO_2 for moist adsorbents 146

Table 4.19: Moisture effects on CO_2 adsorption using a gas stream of 14% CO_2 at 25◦C 154

Table 4.20: Moisture effects on CO_2 adsorption using a gas stream of 14% CO_2 at 35◦C 156

Table 4.21: Moisture effects on CO_2 adsorption using a gas stream of 14% CO_2 at 45◦C 157

Table 4.22: Moisture effects on CO_2 adsorption using a gas stream of 14% CO_2 at 55◦C 159

Table 4.23: Moisture effects on CO_2 adsorption capacity from gas stream of 100% CO_2 162

Table 4.24: Moisture effects on CO_2 adsorption capacity from gas stream of 14% CO_2 163

Table 4.25: Capacity of CO_2 desorption at 90◦C after adsorption at 25◦C 165

Table 4.26: Capacity of CO_2 desorption at 100◦C after adsorption at 25◦C 168

Table 4.27: Heat flow relevant to the sweeping process 172

Table 4.28: Heat flow relevant to adsorption process 175

Table 4.29: Heat flow relevant to desorption process 177

Table 4.30: Heat flow for a cycle with variable adsorption isothermal times 179

Table 4.31: The length of heating and cooling time in a sweeping process 180

Table 4.32: The length of heating and cooling time with 30 minutes of desorption process 180

Table 4.33: Integration of numbers of beds for a TSA system at 25◦C 183

Table 4.34: Integration of numbers of beds for a TSA system at 35◦C 184

Table 4.35: Integration of numbers of beds for a TSA system at 45◦C 185

Table 4.36: Integration of numbers of beds for a TSA system at 55◦C 186

Table 5.1: CO_2 adsorption capacity and CO_2 purity in adsorbed gas for PAA 189

Table 5.2: CO_2 adsorption capacity and CO_2 purity in adsorbed gas for MWNT-PAA 191

LIST OF ABBREVIATIONS

BET: Brunauer, Emmett, and Teller

BOF: Basic oxygen furnace

CCS: Carbon capture and storage

CNG: Combined natural gas

CNTs: Carbon nanotubes

COP: Conference of the parties

COS: Carbonyl sulfide

CS_2: Carbon disulphide

DCC: Dicyclohexylcarbodiimide

DMF: Dimethylformamide

DSC: Differential scanning calorimetry

EAF: Electric arc furnace

EC: Electrical conductivity

ECBM: Enhanced coal bed methane

ESA: Electric swing adsorption

ESP: Electrostatic precipitor

FBRs: Fluidized bed reactor

FGD: Flue gas desulphurization

FTIR: Fourier transform infrared

GAC: Granular activated carbon

GHG: Greenhouse gas

1H NMR: Hydrogen magnetic resonance

HR-TEM: High resolution transmission electron microscope

IEA: International energy agency

IEAGHG: International energy agency greenhouse gas

IGCC: Integrated gasification combined cycle

IPCC: Intergovernmental Panel on Climate Change

LPG: Liquefied petroleum gas

LUB: Length of the unusable (or unused) bed

MEA: Monoethanolamine

MOFs: Metal-organic frameworks

MTZ: Mass transfer zone

MWNTs: Multi-walled carbon nanotubes

NCA: N-carboxyanhydride of α-amine acid

NMR: Nuclear magnetic resonance

OECD: Organization for Economic Co-operation and Development

O/N: Overnight

OOIP: Original oil in place

PAA: Polyaspartamide

PEI : Polyethylenenimine

PSA : Pressure swing adsorption

PDA: 1,3 propanediamine

PS : Pore size

PSI: Polysuccinimide

PV: Pore volume

RT: Room temperature

SA: Surface area

SCR: Selective catalytic reduction

SNCR: Selective non-catalytic reduction

SSA: Specific surface area

SWNTs: Single-walled carbon nanotubes

Syngas: Synthesis gas

TEPA: Tetraethylenepentamine

TGA: Thermogravimetric analyzer

TMS: Tetramethylsilane

TSA: Thermal swing adsorption

UCG: Underground coal gasification

VSA: Vacuum swing adsorption

Wits: Witwatersrand

NOMENCLATURE

A: bed surface

A_p: bed and particle surface area

C: tracer concentration in the bulk fluid

C_{ad}: adsorption capacity

C_{eff}: effluent CO_2 concentration

C_{in}: influent CO_2 concentration

C_p: heat capacity

D_{ax}: axial dispersion coefficient of the adsorbing species

D_e: intraparticle effective diffusivity

D_P: particle diameter

f: dimensional friction factor

K_A: adsorption equilibrium constant

Ka: adsorption rate constant

K_f: particle-to-fluid mass transfer coefficient

L: length of packed column

$M_{ads:}$ adsorbed gas

N_{ads}: adsorbed N_2

O_{ads}: adsorbed O_2

p: pressure

Q: heat flux

Q_{st}: isosteric heat

r: radial distance variable

R: particle radius

R_{ad}: adsorption rate

S_i: number of sites

T: temperature

T_0: ambient temperature

T_{ad}: adsorption temperature

t_{ad}: adsorption temperature

T_{des}: desorption temperature

T_s: sweeping temperature

U: interstitial fluid velocity

V_m: number of molecule

w: work

X_{CO2}: selectivity for CO_2

LIST OF GREEK SYMBOLS

α: thermal diffusivity

δC: variation of cancentration

δt: variation of time

ΔG: free energy charge

ε_b: bed void fraction

ε_p: intraparticle void fraction

λ: excess air ratio

ρ_f: fluid density

ρ_p: particle density

v_c: fluid velocity

Φ: interaction energy potential

Φ_D: dispersion energy

Φ_{FQ}: interaction between field gradient (F) and a quadrupole (with quadrupole moment Q)

Φ_{FU}: interaction between electric field (F) and a permanent dipole

Φ_{ind}: induction energy

Φ_R: close-range repulsion energy

CHAPTER ONE

INTRODUCTION

1.0. INTRODUCTION

In the 19th century, scientists realized that gases in the atmosphere cause a "greenhouse effect" which controls the planet's temperature. These scientists were interested chiefly in the possibility that a lower level of atmospheric CO_2 gas might explain the ice ages of the distant past [1]. At the turn of the century, Svante Arrhenius calculated that emissions from anthropogenic industries might someday bring about a global warming [2]. Other scientists dismissed his idea as faulty.

In 1938, G.S. Callendar declared that the level of CO_2 was climbing and raising global temperatures [3]. He found that a doubling of atmospheric CO_2 concentration resulted in an increase in the mean global temperature of 2 ˚C, with considerably more warming occurring at the poles. However, most scientists found Callendar's arguments improbable [4]. In the 1950s, few researchers joined him by discovering that global warming truly was possible. In the early 1960s, C.D. Keeling measured the level of CO_2 in the atmosphere: it was rising fast [5]. This raised the big debate for researchers seeking to understand the cause of changing levels of CO_2 in the past, and how the chemical and biological forces could be impacted by changing levels. Researchers have concluded that gas plays a crucial role in global warming, and that the rising level of CO_2 due to anthropogenic emissions seriously affects the future. Indeed, Keeling (1998), found the CO_2 growth from less than 1 ppm/yr in the 1960s to about 2 ppm/yr after 2000 [6] decreased the ability for the terrestrial biosphere and ocean to take up CO_2 [7, 8]. The Intergovernmental Panel on Climate Change (IPCC) has assessed, from present levels, a 50-85% reduction in emission would be required by 2050 in order to limit the global temperature to less than 2 ˚C by 2100 [9], and thus preventing major climate change.

1.1. BACKGROUND OF STUDY

Global warming is caused by the enhancement of the greenhouse effect, a phenomenon due to the thin layer of mixed gas which surrounds the Earth, trapping some of the solar radiation. In general, the gases present in the atmosphere convert radiation energy into thermal energy by absorption of electromagnetic radiation, and vice versa by radiation. The mechanism for the absorption of radiation in a gas is that the gas molecules absorb the radiation energy by increasing its kinetic energy through molecular translation, rotation, and vibration, as well as electron translation and spin, and nuclear spin. The longer the radiation travels through a gas, the more energy is converted. Water vapor (H_2O) and carbon dioxide (CO_2) are the two main gases responsible for the greenhouse effect. The other "natural" greenhouse gases are: methane (CH_4), nitrous oxide (N_2O), halocarbons (gases containing fluorine, chlorine and bromine), and ozone (O_3). Their presence is beneficial since, without them, the temperature on Earth would not exceed -18 ˚C [10]. The two most abundant gases in the atmosphere – N_2 and O_2 – contribute almost nothing to the greenhouse effect as homonuclear diatomic molecules (such as N_2, O_2, and H_2) neither absorb nor emit infrared radiation.

At present, carbon-based fossil fuels provide ~80% of the world's energy needs [11]; CO_2 is generated by these energy producing processes. Due to increasing anthropogenic emissions of CO_2 and other greenhouse gases, climate change has become a major concern. Many solutions can be given to the question: how to reduce CO_2 emissions?; but an efficient solution requires special attention for specific approaches. The CO_2 emission reduction strategies can be divided into five broad categories [12], as shown in Figure 1.1:

1) Control of energy consumption by: (a) improving the energy efficiency of automotive vehicles, (b) limiting the use of vehicles (development of public transport, teleworking, etc.), and (c) improving the energy performance of buildings (insulation, low-consumption equipment, etc.).
2) Renewable energies which include the use of hydroelectric, wind, solar and biomass energy [13].
3) Enhancement of natural CO_2 sequestration in order to limit the increase of CO_2 concentration in the atmosphere by feeding the soils or forests with CO_2 [11].

4) Nuclear power can produce electricity with zero greenhouse gas (GHG) emissions, but it needs more development for safety improvement and waste disposal [12, 11].

5) Management of fossil energies which can be completed either by change in the fossil energy mix; for example, the coal-fired power plant can be substituted for natural gas-fired power plant to reduce CO_2 emissions; or the incorporation of CO_2 Capture and Storage.

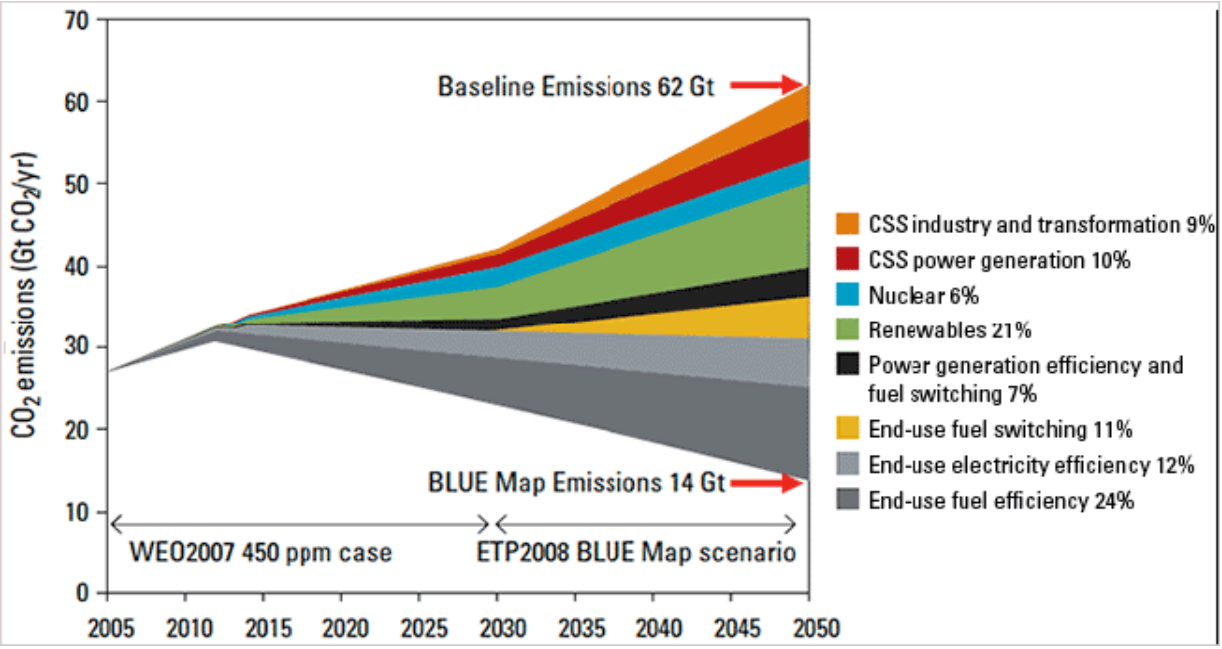


Figure 1.1: CO_2 emission reduction option, 2005-2050. Source: IEA-2008, Energy Technology Perspectives, Scenarios and Strategies to 2050 [14].

It is obvious that fossil fuel utilization, due to large CO_2 emissions amongst other pollutants, is of big concern to the environment. The suppression of fossil fuel utilization will be, on the one hand, a rapid solution to reduce CO_2 emissions in the atmosphere, on the other hand, a breakdown of industrial development and world economic growth. Fossil fuel energy will continue to play a central role over the next few decades due to the increase of world population going hand-in-hand with increased energy demand per inhabitant. Thus, there is a need to reduce CO_2 emissions, and carbon capture and storage (CCS), is a widely accepted selected track towards sustainable application of fossil fuels.

With regard to coal, South Africa is a major consumer of coal, mainly for power generation. Eskom and Sasol convert coal for electricity and chemical fuel production respectively. An

investigation conducted in 2010 stated that Eskom emits 225 Mt of CO_2 per annum, and Sasol emits 72.7 Mt of CO_2 equivalent per annum [15]. South Africa is the largest producer of CO_2 in Africa and 13th in the world; the annual quantity of CO_2 emitted in South Africa can be estimated to 350Mt [16]. South Africa is ranked among the top 20 countries measured by absolute CO_2 emissions, with emissions per capita in the region of 10 metric tons per annum. This shows why South Africa is counted amongst countries which must be bound to the international agreements/obligations to reduce their GHG emissions via the Kyoto protocol or other mechanisms. During the 17th Conference of the Parties (COP 17) hosted by South Africa, the country reaffirmed its commitment to voluntarily reduce its GHG emissions to below the business-as-usual trajectory by 34% by 2020, and 42% by 2025 [17]. Thus, CCS, via the capture of CO_2 from power plants and its transportation after compression to geologic sinks for storage, presents a viable approach of reducing CO_2 emissions in South Africa. There is a need to develop safe and economical CCS technologies that will make deep cuts in South Africa's GHG emissions.

1.2. PROBLEMS STATEMENT

Carbon dioxide must be isolated from the other gases in the flue gas stream produced following coal conversion in order to be diverted from large point sources of generation to storage in geologic sinks. Effluent flue gas from power generation typically contains CO_2 in dilute concentrations (3-15% mol). It is impractical to store flue gas effluent with all its constituents, because of costs associated with transportation and compression, in addition to storage space considerations. The theoretical minimum energy cost for compressing the entire flue gas stream from a coal fired plant to 100 atm is about 18% of energy released from the combustion per unit of flue gas [18]. With a theoretical separation energy of 110 kJ/kg CO_2 for a 14% mole fraction CO_2 stream at atmospheric pressure [19] and 200 kJ/kg CO_2 for compression [20], the minimum energy requirement for reversible separation and compression of only the CO_2 component is about 4% of the energy released. For these reasons, an efficient method of separating CO_2 from the flue gas and producing a pure CO_2 stream would greatly enhance the potential for CO_2 storage to make an impact on global CO_2 emissions.

Capture technologies are well defined, and their efficiencies, cost and energy penalties are estimated [21]. However, the efficiency penalty induced by CO_2 capture within energy

conversion systems poses a threat to the economic viability of these systems. Moreover, coal-fired power generation where average net efficiency penalties for post-and oxy-combustion capture are 10 percentage points relative to a pulverized coal plant without capture, and 8 percentage points for pre-combustion capture, compared to an integrated gasification combined cycle (IGCC) [22]. Therefore, the need to develop efficient and cost-effective resources for CO_2 capture is pressing in order to enhance the outlook for commercial application.

The treatment of flue gas for the capture of relatively pure CO_2 requires identification of impurities in the flue gas that otherwise affect the transport and the storage of CO_2. Separating the low concentrations of CO_2 from an exhaust stream, especially from pulverized coal-fired power stations is a complex and, even with today's technologies, expensive process which results in a high energy penalty and high cost. The CO_2 must be separated to achieve plus 95% purity. Other components, which include CH_4, N_2, O_2, NO_x, SO_x and Ar, and some particulates in the flue gas stream could have different impacts in the transportation and storage processes need to be minimized in the CO_2 stream. An advanced technology will separate CO_2 from the flue gas, aiming to minimize the risk, to simplify the technology, and to reduce the cost for capture as well as transportation and storage. As CO_2 capture will require particulate control and flue gas desulphurization prior to the capture plant, it is hoped at least most SO_x and particulates will be removed prior to CO_2 separation, as well as any moisture in the gas stream (if required by the technology). A good adsorbent will operate to separate CO_2 at an efficient selectivity from the other components that remain in the flue gas after SO_x and particulate removal.

The existing commercial separation technologies include the use of alkanolamines (Monoethanolamine, Diethanolamine and Triethanolamine) and ammonia[23, 24], which all have presented significant concerns due to their limited effectiveness of capturing CO_2 at the concentration above 90%, as well as cost and environmental issues [25]. Thus, alternative technologies for capturing CO_2 are constantly being sought, with lower cost, higher efficiency, and lower environmental impact.

1.3. RESEARCH AIMS AND OBJECTIVES

Within the framework of CCS research in the School of Chemical Engineering, University of the Witwatersrand (Wits), the present project presents a contribution to CO_2 mitigation. It is the project's primary aim to address the problem of inefficiency of CO_2 capture by providing an alternative separation method for improved CO_2 capture. Using various strategies, the aim is to capture CO_2 through the development of an adsorbent synthesized from carbon nanotubes (CNTs) bound to a polyaspartamides surfactant. This method could be a suitable competitor in CO_2 capture technologies when trapping a large quantity of CO_2 during the adsorption process, leading to the formation of carbamate group ($-COO^-$). The proposed approach is instrumental in fulfilling the project's specific objectives, viz.,

1) to design an adequate hydrophobic and biodegradable sorbent for CO_2 capture;
2) to test the adsorbent performance for CO_2 capture under variety conditions by using thermogravimetry;
3) to investigate the differential heat flow of the adsorbent operating in thermal swing adsorption (TSA) systems;
4) to elaborate the possibility of implementing TSA systems operating in continue under optimum conditions.

1.4. RESEARCH HYPOTHESIS AND QUESTIONS

An amine polymer has a potential to form carbamate in the presence of CO_2 where the length of polymer limits the quantity of CO_2 uptake. The carbon nanotubes generally present good mechanical properties, and can be used for the improvement of potential interaction between adsorbent and adsorbate in the adsorption process. Therefore, carbon nanotubes with long chain polyasprtamide surfactants are expected to be highly suitable for CO_2 capture.

The energy penalty and economical cost have been common concerns for the existing technologies capturing CO_2 from power plants: the energy input for regeneration is one of the key factors in determining the efficiency and cost. A key question is how to develop efficient and cost-effective means for CO_2 capture, taking into account the technical and economic consideration of processes for both adsorption and desorption for adsorbent regeneration? Knowing that the capture cost is related to the performance of adsorbents, the following questions were addressed during this work:

1) Can nanotubes with polyaspartamide surfactant be used to capture CO_2?
2) The diamine used to synthesize polyaspartamide is more reactive due to two amine groups, which also pose a risk of being bound to the polymer and cause cross linking. The question is: how to provide one amine group to react with the polymer and the other group to be available to capture CO_2?
3) If the adsorbent can capture a large quantity of CO_2, how can the CO_2 be stripped from the adsorbent with limited energy impacts, and at a low cost?
4) What is the advantage of using nanotubes with polyaspartamide to capture CO_2 over the other techniques currently available?

1.5. RESEARCH TECHNIQUES

The technique of this work consists in the design of adsorbent with specific chemical surface having large available sites for CO_2 anchoring and good geometry/structure which can provide high potential interaction. A long chain polymer named polysuccinimide was grafted to amine in order to produce a polyaspartamide with primary amine as terminal group. In varying the amines used as CO_2 anchors, many polyaspartamides were synthesized; the best was selected for coating of multi-walled carbon nanotubes (MWNTs) in order to enhance the geometry/structure of the adsorbent.

1.6. EXPECTED CONTRIBUTION TO KNOWLEDGE

This work is introducing a novel technology which an efficient evaluation requires deep understanding of the performance standard of CCS technology which is still in development.

- A series of novel sorbent systems with high selectivity for CO_2 capture was synthetically and analytically developed as a contribution to the national and worldwide CCS management programs.
- Varying the amines as CO_2 anchoring to make specific polyaspartamides, the best performing amine was selected for effective surface modification of adsorbent in advanced adsorption technology for CO_2 capture.
- The CO_2 adsorption properties were highly enhanced through the use of multi-walled carbon nanotubes with polyaspartamide surfactant. Non-covalent functionalization process was preferentially chosen to preserve the functionalities required for CO_2 capture enhancement and environmental safety.

- It is hoped that this work has provided adequate information on the developed CO_2 adsorption technology operating in thermal swing adsorption (TSA) systems with efficient energy.

1.7. ORGANIZATION OF THE THESIS

A general introduction of the study, background, problems, aims and objectives of the research, techniques and expected contribution to knowledge are presented in **Chapter One**. **Chapter Two** contains literature review of the basic concepts and on previous and recent work relating to this study. The methodology which includes equipment, chemicals and procedures for adsorbent characterization and adsorbent synthesis were found in **Chapter Three**. **Chapter Four** was relative to the results and discussion where reasonable scientific approaches were developed for the sustainability of this work. The summary of the study, conclusions and recommendations were presented in **Chapter Five**. The contribution of the work to scientific advancement and achievements were found in **Chapter Six**. Lastly, a comprehensive list of all referred materials to this thesis and appendices are given.

Thus, more information about CCS has been of great importance to elaborate a work with conventional scientific standard.

CHAPTER TWO

LITERATURE REVIEW

2.0. INTRODUCTION

The increase of industrial and population energy demands requires high energy production by fossil fuels. Fossil fuels are packed with high potential energy, but the release thereof causes an increase in anthropologic CO_2 emissions in the atmosphere. It is imperative to reduce CO_2 emissions into the atmosphere in order to reduce the threat to mankind in terms of global climate change. Huge quantities of fuel, composed of solid, liquid and gaseous fuels, are in use on this planet to support the essential life activities of human beings. The capturing of CO_2 is a promising solution for fossil fuel power plant emission reduction. The CO_2 diverted from the atmosphere must be led elsewhere with the objective of minimizing the risk of global climate change. CCS contains three parts as follow: (a) firstly the capturing of CO_2, (b) secondly the transport of CO_2, and (c) finally the long term storage of CO_2. Valuable advanced CO_2 capture technologies with the possibility to retrofit combustion plants which include post-combustion, pre-combustion and oxy-fuel combustion, are intended to reduce significant anthropogenic CO_2 emissions.

CO_2 capture technologies, including absorption, adsorption, membrane separation, and cryogenics, are being used or investigated for the implementation of advanced technologies required for large scale CO_2 uptake with high purity production, high energy efficiency for regeneration or CO_2 recovery, and low economic cost. The transport of CO_2 to a storage location must be done without any technical problems. The storage of CO_2 requires adequate geological sites able to keep large quantities of CO_2 for the indefinite future.

With regard to the adsorption technology for CO_2 capture, much research done with existing natural adsorbents (such as activated carbon, silica gel and zeolites) have shown the inefficiency relative to CO_2 purity production, regeneration and moisture tolerance. The art of improving the chemical surface of adsorbents has been exploited for many years, and today the adsorption technology for CO_2 capture is taking the rise. However, chemical surface

modification and geometry/structure improvements through polymer grafted with amine and MWNTs for CO_2 uptake enhancement still in its infancy. Therefore, investigation of the sources of CO_2 emissions is very important in order to assess the scale of CO_2 separation technology in a given source.

2.1. CO_2 EMISSION SOURCES

2.1.1. Fuel and Fuel production

Fossil fuel is packed with high potential energy that is needed for work or heat energy. The use of fossil fuel increases with the world development, which goes together with high energy consumption. The fuel releases heat that can be used for warmth, cooking, or industrial processes. The development of engine technology has impacted further on the use of fuel, through which the heat energy is harnessed into mechanical energy via an engine. Though many substances, which include radioactive metals and cells of organisms, are also utilized; hydrocarbons are the most common source of fuel used by humans. Frequently heat is released after specific reaction or combination of substances. Table 2.1 shows energy content values of different fuels with mega Joule [MJ] as the energy scale unit.

Table 2.1: Energy content of fuels [26]

Energy carrier, 1 kg of fuels	Energy content [MJ]
Brown coal	9.0
Wood	14.7
Hard coal	29.3
Natural gas (1 m^3)	31.7
Crude oil	42.6
Fuel oil, light	42.7
Gasoline	43.5

The increase of industrial and population energy demands in the world results in high energy production by fuel which consequently goes with the increase of anthropogenic CO_2

emissions in the atmosphere. The largest fuel groups which include coal, natural gas, and propane accounted for 94% of total CO_2 emissions in 2007, where coal alone represented 78% of all CO_2 emissions by electric power plants (Figure 2.1) [27, 28].

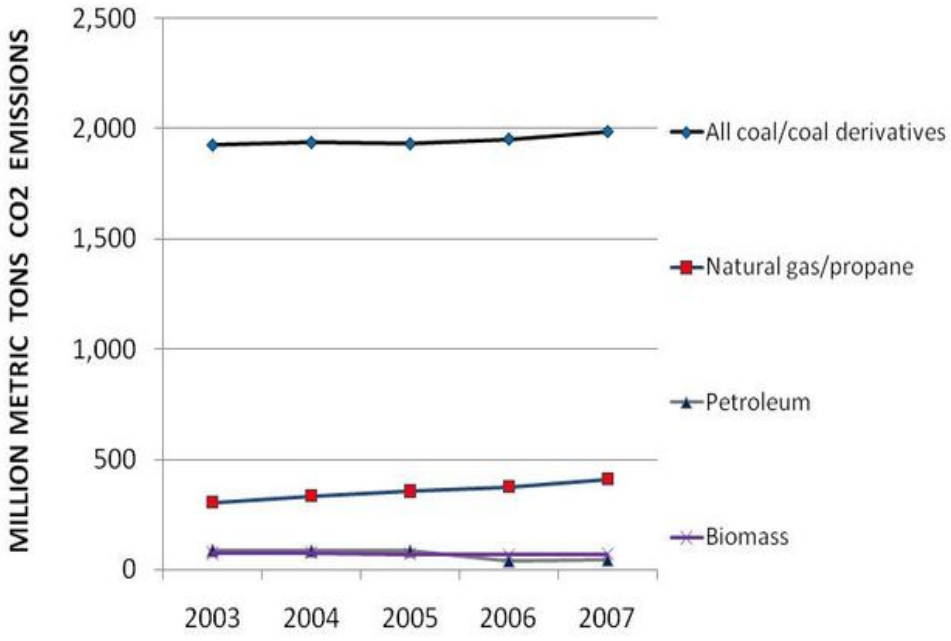


Figure 2.1: CO_2 emissions by U.S. power plants by major fuel groups, 2003-2007 [29]

All substances able to release heat through oxidation process or combustion are considered as chemical fuels. The chemical fuels are divided in physical properties as solid, liquid and gas, occurring as natural or artificial fuels as shown in Table 2.2.

Table 2.2: General types of chemical fuels

	Primary (natural)	**Secondary (artificial)**
Solid fuels	Wood, coal, peat, dung, etc.	Coke, charcoal103
Liquid fuels	petroleum	Diesel, gasoline, kerosene, LPG, coal tar, naptha,ethanol
Gaseous fuels	Natural gas	Hydrogen, propane, coal gas, water gas, blast furnace gas, coke oven, CNG

2.1.1.1.Solid fuel

Solid fuel includes all wood, charcoal, peat, coal, hexamine fuel tablets, and pellets from wood that are used as fuel to produce energy and provide heating. Combustion is the technology utilized for solid fuel conversion to release energy and heat. Solid fuels were used early in the existence of human beings, since the primitive epochs, to create fire. This started with the use of wood as solid fuel which does not require tools, especially when picking up dead wood for fire production. However, nowadays special tools such as skidders and hydraulic wood splitters have been developed to industrialize the production of wood for fuel. In the photosynthesis cycle, trees take in CO_2 and release O_2, balancing carbon cycle. Furthermore, the burning of trees under O_2 reaction converts the carbon to CO_2, which is released again into atmosphere. Despites the release of CO_2, the photosynthesis cycle [30] works to reduce GHG emissions for climate change mitigation. The photosynthesis cycle has given more importance to the use of biomass, which includes wood, and all plant and plant-derived materials as well as animal matter and animal manure, for combustion.

Wood remains the largest biomass energy source to date. In addition, biomass has shown the ability to produce fuels and chemicals that are often produced in petroleum resources [31, 32]. The use of biomass is more environmental friendly compared to other fossil fuels by the fact that it leads to net CO_2 emission reductions [33]; it also contains negligible amounts of sulfur and nitrogen. Consequently, the CO_2, SO_2 and NO_x emissions are extremely low compared to conventional fossil fuels. Biomass contains moisture; the high moisture content is not feasible for combustion unless the biomass is pre-dried. Though high moisture content biomass is intended for suitable biological conversion process, a content < 50% is required for efficient biomass combustion [34]. According to US statistics 190 million dry tons of biomass is consumed per year, which is equivalent to 3% of current energy consumption [35]. Variables methods have been developed to convert chemical energy present in biomass to useful heat energy. These conversion methods can be summarized as shown in Figure 2.2.

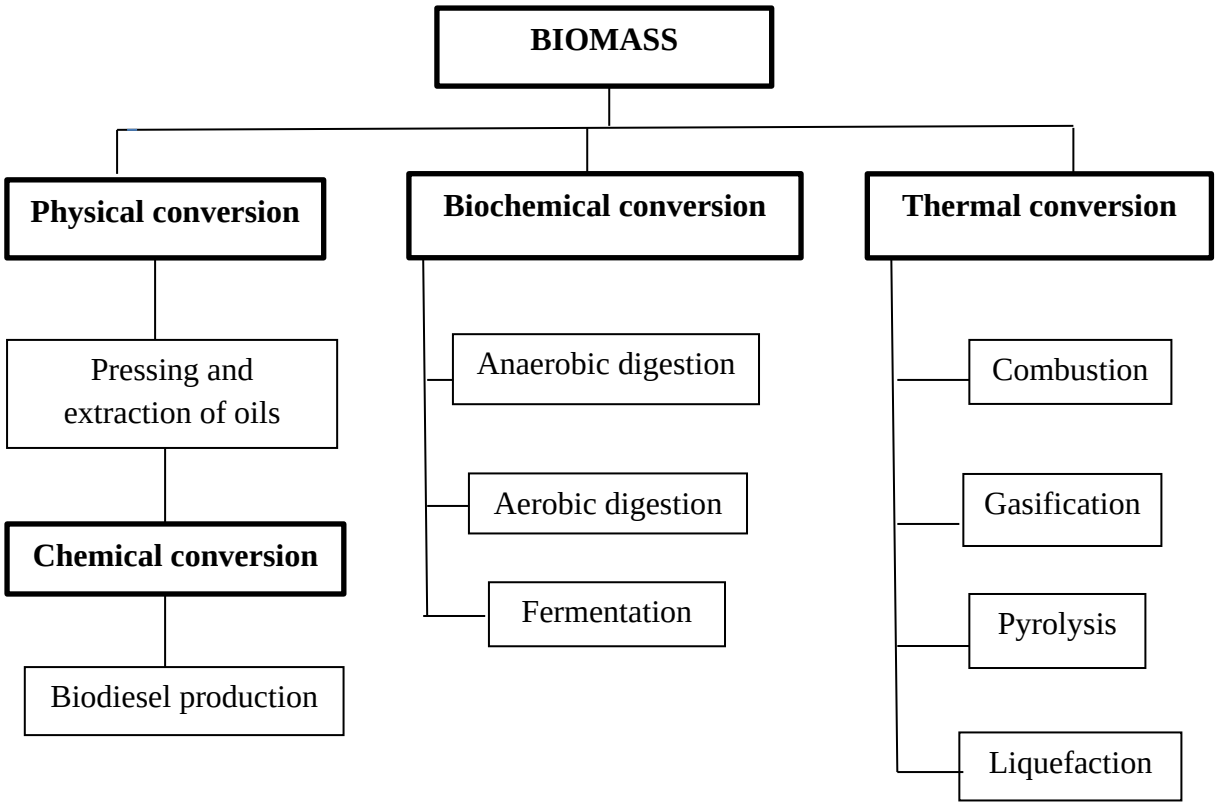


Figure 2.2: Different categories of biomass conversion [36]

Due to the low-cost and high energy production, coal has been a large source of energy for power regeneration worldwide. The coal-fired plants (via combustion + gasification) in South Africa actually generate more than 93% of local electricity, demand 70% of primary energy consumption, and 30% of petroleum liquid fuels [5]. Thus, there is necessity of either substituting the coal-fired plants with other feedstocks or renewable power plants or retrofitting with CO_2 capture plants. This will result in CO_2 emissions mitigation and prevent further disaster changes in the environment. Coal is a solid fuel which enabled the industrial revolution, from furnaces, to running steam engines. However, coal is the dirtiest fossil fuel which contributes to high CO_2 emissions. Nowadays, an enormous quantity of coal is burnt every day for energy and electricity generation. Coal, essentially fossilized vegetation, has generally a high carbon contain which is converted to CO_2 during the combustion or oxidation process.

In an anaerobic medium and under the influence of pressure and moderate temperature, fossilized vegetation is converted into peat, low-grade fuel, brown coal, lignite, sub-bituminous, bituminous, semi anthracite or finally anthracite coal (increasing rank). These types of coal are useful according to the specific application. Higher-rank coal is defined as

coal with a higher heating value of more than 24MJ/kg on moisture and ash-free basis, and low-rank coal below 24MJ/kg [37]. High-rank coals, including bituminous and anthracite coals, contain more carbon than lower-rank coals, which results in a much higher energy content. Anthracite, a hard coal with high luster, has the highest carbon content between 92.1% and 98% [38, 39, 40]. Industrial and the population growth have influenced the release of huge quantities of CO_2 from coal combustion due to the high demand for electricity. According to international information, in 1999, the CO_2 emissions were estimated to 8666 million tonnes [41], and an increase of 66% was recorded in 2011 [42]. Compared to natural gas, a coal-fired electric power generation emits around 900kg of CO_2 for every megawatt-hour generated, while natural gas-fired electric plant emits 495kg of CO_2 for every megawatt-hour generated [43]. Thus, the reduction of coal and the increase of natural gas generation have been considered as an approach to mitigate climate change [44].

2.1.1.2. Liquid fuel

Liquid fuels consist mainly of hydrocarbons, which are combustible or energy-generating molecules that can be harnessed to create mechanical energy. Most liquid fuels used currently are produced from petroleum. Petroleum oils consist almost entirely of hydrocarbons, with some impurities including S and N_2 in small quantities. There are three types of liquid fuels classified according to the chemical structure of hydrocarbons, namely: aliphatic hydrocarbons, aromatic hydrocarbons and naphthene hydrocarbons [45].

- Aliphatic hydrocarbons are constituted of carbon atoms in straight chains, branched chains, or non-aromatic rings. The aliphatic hydrocarbons are divided into two series. These are saturated and cannot adsorb hydrogen, or the paraffins, and these are unsaturated and can still adsorb hydrogen, or the olefins.
- Aromatic hydrocarbons are constituted of carbon atoms in aromatic compounds attached to each other in the form of rings.
- Naphthene hydrocarbons, sometimes called naphthenic compounds, cycloparaffins or hydrogenated benzenes are type of organic compound of carbon and hydrogen that contains one or more saturated cyclic (ring) structures, or contains such structures as a major portion of the molecule.

Hydrogen compounds dominate the liquid fuels, while O_2 and N_2 compounds are usually present to very small extent in refined products, and in unrefined petroleum products [46].

Crude petroleum, from whatever source, contains S compounds which are generally undesirable constituents of liquid fuels and considered as impurities in petroleum, shale oil, and coal-tar products.

In the combustion process of hydrocarbon, the C is converted to CO_2 and the H_2 to steam according to the chemical equation shown in Equation 2.1:

$$C_nH_m + \lambda\left(n+\frac{m}{4}\right)(O_2 + 3.78N_2) \rightarrow nCO_2 + \frac{m}{2}H_2O + (\lambda - 1)\left(n+\frac{m}{4}\right)O_2 + 3.78\left(n+\frac{m}{4}\right)N_2 \qquad (2.1)$$

The fuel molecule parameters *n* and *m* are numbers respective to the nature of hydrocarbon, while the parameter λ is excess air ratio to make available the total conversion of carbon to carbon dioxide. Additionally high hydrogen content in the liquid fuels results in release of large quantity of steam.

2.1.1.3. Gaseous fuels

All hydrocarbons in the form of gas are a potential source of energy to generate heat or electricity; referred to as gaseous fuels. The fuel gases are classified in to natural gas and manufactured gas.

Natural gas, found in deep underground rock formations, is the result of fossil fuel formation exposed to intense heat and pressure over thousands of years. It is primarily composed of CH_4 including some alkanes in varying amount, and lesser percentage of CO_2, N_2, and H_2S [47]. As an energy source for heating and electricity generation, natural gas is also used as a chemical feedstock in the manufacture of plastics and other commercially important organic chemicals. According to the different sources of fossil fuels and process of formation, there are many types of natural gas, which includes: shale gas [48], hydrate gas [49], town gas [50], and biogas [51, 52]. With regard to CO_2 emissions, natural gas releases less CO_2 into the atmosphere than oil and coal conversion. The IPCC Fourth Assessment Report[53] stipulates that natural gas produced about 5.3 billion tons a year of CO_2 emissions, while coal and oil produced 10.6 and 10.2 billion tons respectively. Other pollutants in very small quantity release in the atmosphere through the combustion of natural gas are: CO, SO_2, NO, and particulates at 40 ppm, 1 ppm, 92 ppm, and 7 ppm respectively.

Manufactured fuel gases are produced through an artificial or gasification process, usually from coal or oil, resulting in gases which include coal gas, water gas, producer gas, syngas, wood gas, biogas, and blast furnace gas [54]. The technology relevant to the gasification of coal as well as gasification of other hydrocarbon resources such as biomass or oil residues, is flexible with flexible conversion. In a gasification reactor, the hydrocarbons in the feedstock are transformed into a synthesis gas (syngas), basically a mixture of H_2, CO and CO_2, which can be used for energy generation, heat production and other chemical synthesis.

Coal gasification is the incomplete combustion of coal, and operates at specific condition of temperature and pressure with deficiency of air in order to produce a syngas composed primarily of H_2 and CO [55]. For the purpose of power generation (created by turbines under steam pressure) the CO is converted to CO_2 and H_2, or CO_2 only, dependent on the air feed (H_2O, O_2). The gas product is composed of CO_2 and H_2 and CO_2 is captured prior to the production of steam through synthetic gas combustion. The presence of H_2O to convert CO to CO_2 has an advantage of increasing the yield of H_2, resulting in large steam generation for high power generation. Coal gasification in integrated gasification combined cycles (IGCC) plants has the ability to render CCS easy and offers the lowest cost of CO_2 capture compare to any fossil-fuel-based power plant [56]. In case of underground coal gasification (UCG), the CO_2 emissions are drastically minimized because UCG can be directly coupled to CCS in order to contribute to a sustainable future [57]. Most CO_2 sequestration investigation are done on considering depleted oil and gas reservoirs or geologically-similar deep saline aquifers, while UCG operations create voids that offer further possibility for CO_2 storage [58]. In addition, UCG process avoids the need for coal mining, transportation, preparation, gasification equipment and the transportation as well as disposal of ash, which has cost, labor and environmental benefits.

2.1.2. Other industrial sources of CO_2

2.1.2.1. Cement production

Cement is an important construction ingredient produced in large quantity throughout world. However, the process of cement production results in significant CO_2 emissions. Investigations done have shown that 2.4% of global CO_2 emissions are released from cement plants [59]. CO_2 is released as a by-product during the calcination of $CaCO_3$ in the temperature

range 600 - 900 ◦C. In the production of cements, Portland cement is made with addition of gypsum, resulting in no additional emissions; while Masonry cement requires addition of lime resulting in large CO_2 emissions.

2.1.2.2. Refineries

Refineries are production facilities to convert crude oil into finished petroleum products. Refineries can operate with fractioned distillation process of petroleum to give different finished products such as propane, butane, natural gas, refinery fuel gas, gasoline, solvent, kerosene, chemical precursor (plastic, rubber, etc.), diesel, heating oil, lube oil, greases, asphalt, pitch, coke and byproducts, respective to the temperature limit of volatility [60]. It is obvious that the combustion of refinery products results in CO_2 emissions into the atmosphere, but the concentration of CO_2 emissions from the refineries process of petroleum is relatively low. Emissions from the petroleum refining sector, classified by the IPCC (2006) code 1A1b, cover all combustion activities required to support the refining of petroleum products, including burning the site to generate electricity for own use [61].

2.1.2.3. Iron and steel industry

Crude iron is obtained from the reduction of iron oxide performed in a blast furnace through CO provided by the combustion of coke, petroleum coke, or coal. The process operates with the addition of heat in order to melt the iron and elimination impurities. However, the CO_2 emissions occur through the calcination of carbonate fluxes; the oxidation of coal/coke leads to the production of CO_2. The produced crude steel has 0.5 to 2 percent of C content by weight, which is the cause of CO_2 emissions in the production of the steel. The steel can be produced in a basic oxygen furnace (BOF) or an electric arc furnace (EAF). As the EAF requires graphite electrodes, additional CO_2 emissions occur as these electrodes are consumed [62].

2.1.2.4. Petrochemical industry

Basically the petrochemical industry treats the outputs from crude oil refineries to produce petrochemical products that are gathered in three groups as follow: olefins, aromatics and

synthesis gas. These petrochemical products are utilized to make a wide range of chemicals as shown in Figure 2.3.

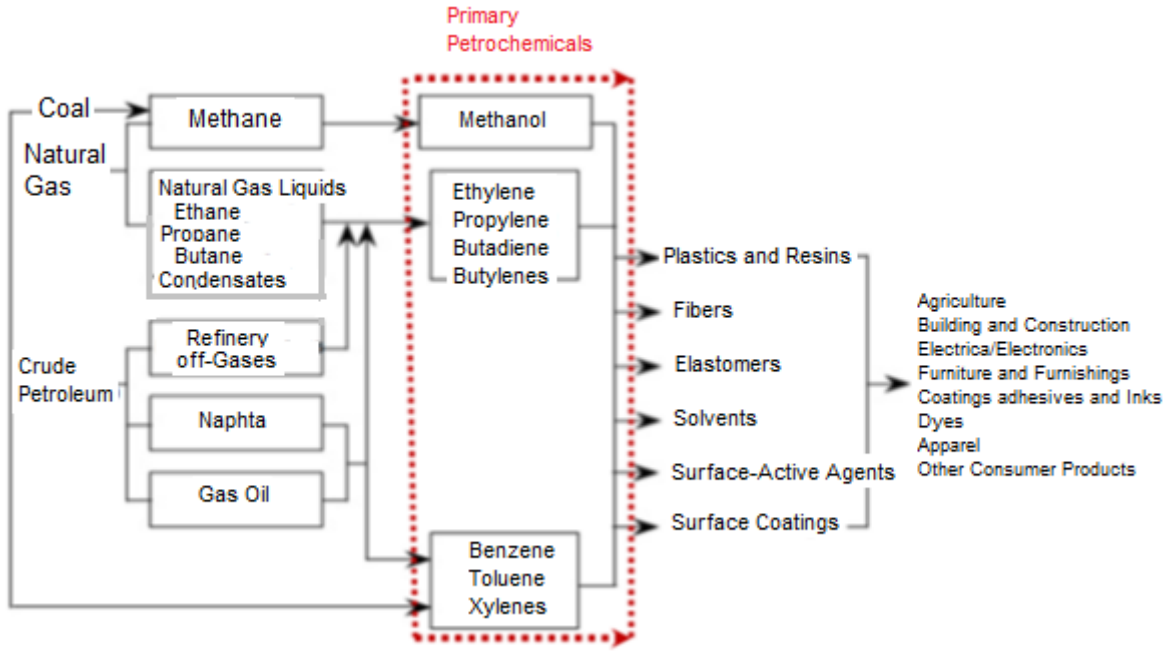


Figure 2.3: A Visual Sketch of the Petrochemical Value Chain and Applications [63]

The IEA (2006) report stated that the chemical and petrochemical industry is the third largest source of CO_2 emissions after the iron/steel and cement industries [64]. The CO_2 emissions in a petrochemical plant come from three sources: (a) large CO_2 emissions come from the fuel combustion used to heat the steam cracker furnaces; (b) other energy (electricity) generation; and (c) feedstock or process gas losses from cracker operations.

2.2. CO_2 CAPTURE, TRANSPORT AND STORAGE

2.2.1. CO_2 capture

Carbon dioxide as a gas contributes largely to the greenhouse gas effect, because large quantities of CO_2 is produced from the combustion of fossil fuels such oil, natural gas or coal, for energy production or heating, and in industrial processes. The capture of CO_2 is a huge challenge which needs the implementation of advanced technologies able to significantly reduce anthropogenic CO_2 emissions. Combustion plants have three methods for separating concentrated streams of CO_2 [65] as depicted in Figure 2.4.

- Post-combustion: Separation of CO_2 from N_2, O_2, H_2O. In this method, the flue gas stream from the combustor is subjected to CO_2 separation anywhere along the path

before effluent exhaust. In general, the concentration of CO_2 is rarely above 15% mole fraction and requires concentration to 95% after separation. Thus, the post-combustion CO_2 capture is characterized by: (a) low CO_2 concentration (10-15% CO_2), 4.4%O_2, 6.2% H_2O, 73-74% N_2, 50ppm CO, 420ppm NO_x and 420ppm SO_2 [66]; (b) large volumes, where 600MW coal-fired power station produces ~10,000 tonnes CO_2 per day; and (c) elaborate low pressure. Post-combustion facilities can be retrofitted to existing power plants [67] or provided as a feature of new plants in the future, but there is a need to bring down costs considerably. Despite the existing cost barrier, post-combustion capture is receiving increased attention, because of the realization that many existing coal-fired power stations will continue to operate for 30 years or more. In addition, post-combustion capture can be used to treat flue gases from a range of industries including cements or iron and steel plants, not just fossil fuel power plants.

- Pre-combustion: this is the separation of carbon in the form of CO_2 from a resource after the energy content of the resource is transferred to a carbon-free carrier. An alternative approach, pre-combustion capture, involves IGCC. In this type of plant, the fuel is not burnt, but is reacted at high pressure and temperature to form a synthesis gas containing CO, CO_2 and H_2. The CO_2 is then removed and the H_2 is burnt to produce power, leaving H_2O (vapor) as the main exhaust to the atmosphere. The flue gas composition is 7.4-7.7% CO_2, 14.6% H_2O, ~4.45% O_2, 200-300ppm CO, 60-70 ppm NO_x, and 73-74% N_2. The advantage of this approach is that it is much less expensive than the post-combustion capture process. The disadvantages are that there are only a few IGCC plants in the existing coal fleet and IGCC plants are more expensive to construct + operate than PC plants when costs of CO_2 capture are not included.
- Oxy-fuel combustion: the nitrogen-free oxidizer stream is used for combustion in order to produce a stream with composition: 3-4% O_2, 0-10% N_2, 60-70% CO_2, 20-25% H_2O, 60-85 ppm (NOx + SO_2). This results in a flue gas with high CO_2 concentrations (greater than 80% by volume). The water vapor is then removed by cooling and compressing the gas stream.

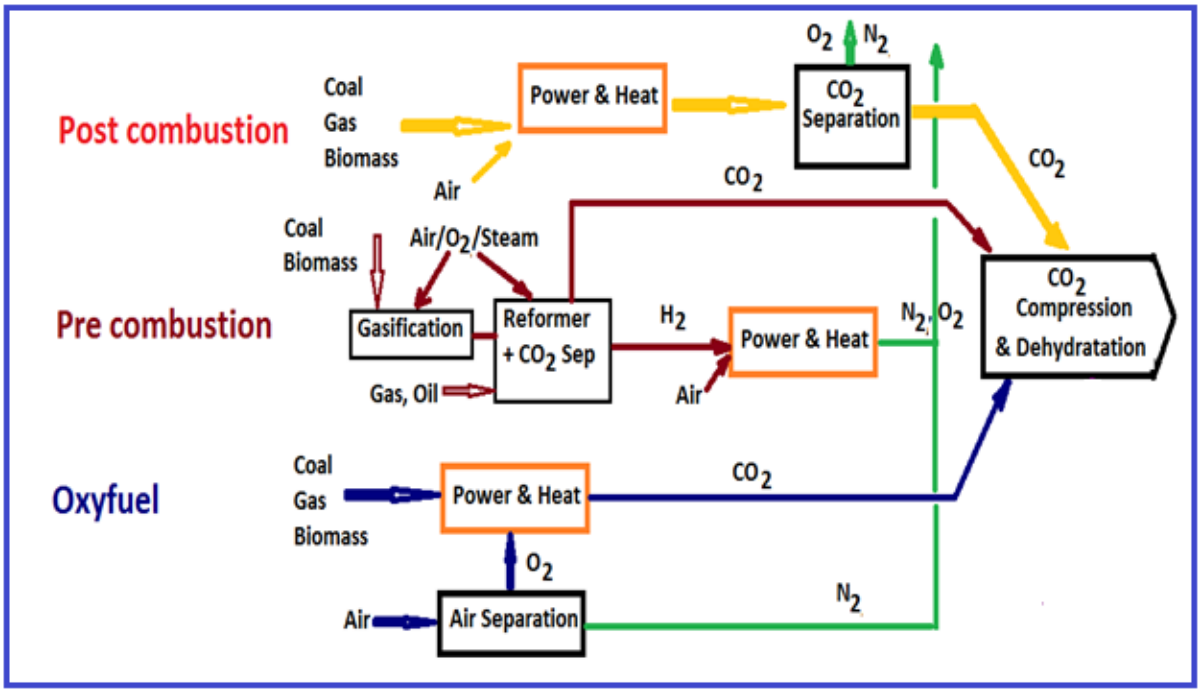


Figure 2.4: Carbon dioxide separation methods [65]

All coal-fired electricity is currently produced by direct combustion of coal with air in a boiler, whilst gasification and oxy-fuel processes present good perspective for clean and efficient energy production. Regarding the technology efficiency, the separation of CO_2 with low partial pressure in the flue gas is more challenging. However, post-combustion offers the advantages to be incorporated into existing combustion technologies without radical changes to them. The power plants using pulverized coal systems can be more practically retrofitted with CO_2 capture plants than the IGCC power plants; this makes post-combustion capture easier to implement as a retrofit option to existing plants. IGCC power plants will require certain modifications for the implementation of the CO_2 capture plant. In pre-combustion capture, CO_2 found at much higher pressure is separated from gasified coal syngas (largely H_2 and CO) prior to the gas going to a combustion turbine. While in the post-combustion capture, CO_2 is at low partial pressure in flue gas from combustion and must be separated from flue gas (mostly N_2). Finally, for oxy-combustion, coal is burned in nearly pure oxygen separated from air to generate a flue gas that has a high concentration of CO_2 and almost ready for sequestration, but O_2 separation is costly.

Progress towards more efficient and lower carbon capture from large point sources is constrained primarily by technological progress in gas separation. The theoretical minimum

energy of 200kJ/kg CO_2 is required for CO_2 capture plant technology to be approved performant regarding the significant progress on energy penalty [19]. An optimum design of the process will provide the necessary equipment able to ensure good separation when considering different factors that include selectivity, capacity, and regeneration. Therefore, three factors will be important in achieving the design of the equipment: 1) flue gas specification, 2) CO_2 product specifications, and 3) constrains that include flow rate of the flue gas, product specification as defined in the scope of work, minimum harmful emission to air or environment. Another factor that affects system design is the equipment's pressure drop gradient or required operating power. The equipment must be efficiently selected in order to yield over 90% of CO_2 with other gases and trace of elements [68, 69]. The maximum impurity levels in captured CO_2 are as follow: H_2S 3.3%, SO_2 2.5%, O_2 1.8%, H_2 1.7%, CO 0.2%, NO_x, 0.15%; and maximum levels of trace elements are follow: Hg 0.14mg/kg, As 9.8 mg/kg, Se 3.5 mg/kg, Cd 0.2 mg/kg, Pb 1.7 mg/kg Sb 0.74 mg/kg, Cr 22mg/kg, Ni 279 mg/kg, 1560mg/kg [69].

The purity of CO_2 concentration influences the efficiency of further operations which includes compression and transportation, and storage.

2.2.2. CO_2 compression and transport

The CO_2 separated from flue gases comply with transportation requirements for injection in the appropriate storage site. The CO_2 can be transported by either ship or pipeline (onshore or offshore) without any particular technical problems, and has been done so far many years. The big challenge is to design an advanced CO_2 transport technology able to carry highly volumes of CO_2 form CO_2 capture plant to storage site after minimizing possible risks. In transport by pipeline, the CO_2 must be carried under supercritical condition at a pressure over 74 bars [70, 71, 72]. To bring the CO_2 to supercritical stage requires combination of technique processes in four stages, which include: compression, intercooling, dehydration, and compression for supercritical CO_2, as shown in the Figure 2.5. The dehydration stage operates for liquid knockout in order to prevent the material of the CO_2 pipeline from being attacked by moisture. The supercritical CO_2 is discharged to the storage site at appropriate delivery pressure through multistage CO_2 pump/compressors, depending on the distance [72]. The possibility of transporting CO_2 by pipeline in liquid state under suitable conditions of temperature and pressure (for example -40 °C and 10 bars), is still under investigation [72]. For

the long distance, in particular, for offshore storage, the use of ship with tankers is more advantageous to transport CO_2 than pipeline. The transport of CO_2 by ship requires less energy, because the CO_2 is transported in liquid phase at moderate pressure and low temperature (about 20 bars and -20 °C) [72].

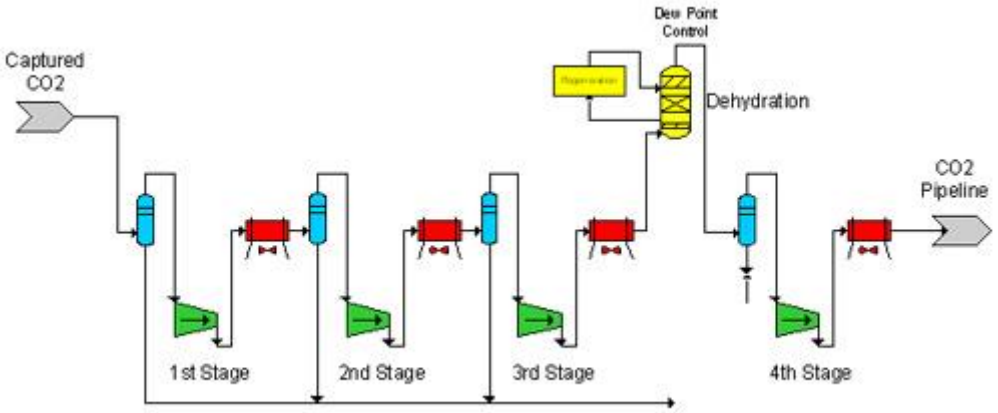


Figure 2.5: Typical Schematic of CO_2 Compression Process [73]

2.2.3. Storage

The question about the place where CO_2 can be stored is fundamental, and must be answered before capturing of CO_2. The technology relevant to the geological storage of CO_2 requires deep understanding and integration of basic principles of earth sciences, petroleum geology, geophysics, geochemistry and engineering [74]. If a 600 – 1000 MW power plant can release about 10,000 tonnes of CO_2 per day [75], it is really a huge task to find geologic sinks and trapping mechanisms able to confine safely the injected CO_2 for eras. Small quantities of essentially pure CO_2 can be used for industrial applications including carbonated beverages, and urea + EOR [76], but the large quantities require a permanent sequestration in order to reduce significant CO_2 emissions in the atmosphere. The exploration of efficient storage site leads to different studies which include:

- Site selection and characterization giving a guarantee of leaktight storage about 0.01% per year [77], because the leakage of CO_2 could release the CO_2 back to the atmosphere and may present the potential for health problems other than global warming.
- Storage capacity and injectivity where a specific depth must be above 800m for CO_2 injection in order to reach the pressure and temperature conditions respective to CO_2 transition to supercritical state [78].

- Containment able to encourage the geochemical reactions over time between the injected CO_2 and the minerals in the rocks without any undesirable geomechanical consequences. In addition, the planning and geologic analysis of the storage requires safe operation through careful monitoring of the CO_2 during the injection and a long time afterwards.

Underground and ocean CO_2 storage, mineral carbonation and industrial use of CO_2 are briefly discussed.

2.2.3.1. Underground Storage

Several data sources have confirmed that underground CO_2 storage is feasible as a CO_2 emission mitigation option due. The capacity, structure, seals, porosity and other properties are assessed, that make underground storage safe to store CO_2 for decades or centuries; the longer the CO_2 remains underground, the more securely it is stored. After injection, the CO_2 enters the storage rock through tiny pores and, over time, dissolves into the water already in the rock formation. Chemical combinations with the rocks will then occur for the trap pines of CO_2 even more securely. The assessment of seismic activity of the underground storage area is very important in order to prevent potential fractures in the rocks. Otherwise the rocks will no longer act as a seal or cap rocks, but will allow the stored CO_2 to return to the atmosphere thus potentially causing disaster to all surrounding life (life scale rupture) and ultimately rendering the storage unsuccessful [79].The CO_2 may be stored in depleted oil and gas reservoirs, possibly deep coal formations, and particularly saline formations (deep underground porous reservoir rocks saturated with brackish water or brine) [80].

In depleted oil and gas field, CO_2 is injected for enhanced oil recovery (EOR) or enhanced gas recovery (EGR), where the injection of CO_2 could lead to greater production of oil or natural gas due to changes in viscosity + pressure. The geology of hydrocarbon source rocks is general well understood, and hence the reason why this option is nowadays extensively use for CO_2 sequestration. The mechanism of EOR is that CO_2 as a solvent mixes with the oil, causing oil expansion, oil viscosity reduction, and interfacial tension disappearance [81]. The produced oil comes out with about 50-67% of the injected CO_2 which must be captured in order to be recycled to the oil reservoir [82]. In United States, about 30 to 50 million metric tonnes of CO_2 is re-injected into declining oil fields [83]. The experience from the USA is that

EOR with CO_2 gives an incremental oil recovery of 7-23% (average 13.2%) of the original oil in place (OOIP) (IPCC-CCS 2005) [84].

With regard to CO_2 storage in coal formation, it is important to note that coal presents the affinity for gas adsorption. Gas adsorption is the main mechanism of gas storage in coal seams, geological factors such as pressure, temperature, moisture content and rank (including lignite, sub-bituminous, bituminous and anthracite) play an important role in defining reservoir capacity for CO_2 storage. Working on investigation of factors which influence the CO_2 adsorption in coal seams, Ceglarska-Stefanska et al (2002) [85] found that capillarity structure or maceral composition could act to reverse the usual trend and result in preferential desorption of CO_2. Likewise, Bustin *et al* (2000) [86] concluded that the presence of moisture has the effect of decreasing the amount of gas absorbed and the selectivity of CO_2. Moreover, the pore structure of coal is highly heterogeneous, with the pore size varying from a few Angstroms to frequently over a micrometer in size [87]. One advantages of using coal seams for CO_2 storage resides on the possibility of displacing the CH_4 in the coal by CO_2 injection into deep unmineable coal seams. Injection of CO_2 enables more CH_4 to be extracted, while at the same time sequestering CO_2. Thus, the balance of CO_2 storage cost and the cost of produced CH_4 results in low storage cost. However, CO_2 from the combustion of CH_4 and the reinjection of CO_2 into coal seams, the coal bed can still provide net storage of CO_2, because coal can adsorb twice as much CO_2 by volume as CH_4 [88].

The Norwegian research community will contribute in developing the knowledge and technology necessary to enable large-scale storage of CO_2 (>10 Mt CO_2/year) on the Norwegian shelf by 2018. Particular attention is put on the use of CO_2 for EOR, harvesting from the Norwegian petroleum expertise and business opportunities related to CO_2 storage [89].

Although the presence of water limits the storage capacity, deep saline formations are more widespread and have the largest potential volumes for geological storage of CO_2 with fewer well penetrations to reduce the risk of leak paths [90].

2.2.3.2.Ocean storage

As 70% of the Earth's surface is comprised of oceans (with an average depth of about 3,800 m), deep oceans contain large spaces to isolate unlimited quantities of CO_2 from the atmosphere for a very long time; probably several hundreds of years. The injection of CO_2 in the ocean can be done into the saline water, where the CO_2 will dissolve and be diluted in large volumes of seawater, or beneath the ocean floor (if injected). The CO_2 injected into the oceans at great depth can take millennia to balance with the same quantity of CO_2 as it is ultimately rereleased into the atmosphere. As the reaction of water with CO_2 converts to carbonic acid, the CO_2 dissolves in the upper ocean layer in order to be mixed further with deep ocean waters. However, despite there being virtually no change in acidity in the deep ocean, the increase of CO_2 in the atmosphere has caused not only the climate change, also a decrease of 0.1 in pH on the upper layer of oceans [91]. The investigation done showed 30-40% of anthropogenic CO_2 found in the atmosphere dissolves into oceans, rivers and lakes [92, 93]. With regards to 1300Gt CO_2 released over the past 200 years into atmosphere by human activities, the oceans have taken up about 500 $GtCO_2$ [94].

The CO_2 ocean storage technology is under investigation and can be feasible after fulfilling certain criteria that include [95]: a) storage technology at effective cost; b) acceptable environmental impact; c) politically and legally viable methods, and 4) the increase of scientific certainty for safe CO_2 storage.

2.2.3.3.Mineral carbonation

The reaction of CO_2 with metal oxide bearing metals is a mineral carbonation process; the formation of insoluble carbonates occurs where calcium, magnesium and iron are the most attractive metals. The chemistry of mineral carbonation is completed with the release of heat at suitable temperature and pressure levels, according to the following chemical reaction:

$$MO + CO_2 \longrightarrow MCO_3 + \text{heat.} \quad (2.2)$$

In the case of metal silicates, metal carbonate is produced with the silica in an exothermic reaction, according to the following chemical reaction:

$$\text{Olivine: } Mg_2SiO_4 + 2CO_2 \longrightarrow 2MgCO_3 + SiO_2 + 89\ KJ\ mol^{-1}\ CO_2 \quad (2.3)$$

$$\text{Serpentine: } Mg_3Si_2O_5(OH)_4 + 3CO_2 \longrightarrow 3MgCO_3 + 2SiO_2 + 2H_2O + 64\ KJ\ mol^{-1}\ CO_2 \quad (2.4)$$

Wollastonite: $CaSiO_3 + CO_2 \longrightarrow CaCO_3 + SiO_2 + 90\ KJ\ mol^{-1}\ CO_2$ (2.5)

The reaction of solid and gas is too slow to be practical in the case of unrefined material [96] unless the reaction is done at reasonable pressure, especially for the refined materials like oxides or hydroxides of calcium and magnesium [97, 98, 99]. Mineral carbonation with refined materials can be also used for the CO_2 capture in case of pressurized CO_2 rich gases from IGCC plants.

2.2.3.4. Industrial use — products

The production of chemicals through the industrial use of CO_2 as gas or a liquid or as feedstock is an approach of mitigating climate change by keeping captured CO_2 out of the atmosphere in order to store it in anthropogenic carbon products. Currently, CO_2 is used at a rate of approximately 110 Mt CO_2/yr (33 Mt C/yr) worldwide, excluding the use for EOR [29]. The industrial production of urea requires two third of this quantity of CO_2, while the one third is shared by different carbonate products, such as methanol and salicylic acid [100, 101]. Nowadays, the development of technology has given more influence to the industrial use of CO_2 for the production of fine and commodity chemical productions, fuel, plastics and beverage. The greatest challenge for the industrial use of CO_2 is the storage life-time; the limited cycle time of the industrial products enacts either the recycle of the products into a new or different industrial product, or the disposal of the products as a waste. Thus, an efficient CO_2 storage system will require the increase of amount of carbon in industrial production or the increase of amount of industrial waste.

2.2.4. CO_2 capture economic cost evaluation

Regarding the impact of carbon constraints on different sectors of the economy, it is important to set specific environmental and economically sensible approaches to controlling GHG emissions, the primary driver of global warming. The government has to elaborate policies relevant to the pricing CO_2 emissions through a carbon tax in order to encourage companies and households to pollute less by investing in cleaner technologies and adopting greener practices [102]. A carbon tax is a fee placed on GHG pollution, mainly from burning fossil fuels. The carbon fee or tax must be set with the strategy of making polluting activities more expensive in order to render the green technologies more affordable. With the strategy to reinforce the fight against global warming, Tokyo Metropolitan Assembly passed the bill

to take effect in fiscal 2010 with the introduction of Japan's first cap-and-trade emissions trading program [103]. The 2010 carbon tax discussion paper proposes three options for implementing comprehensive carbon price through the carbon tax, and defines the following tax bases [104]:

a) Carbon pricing will encourage a shift in production patterns towards low-carbon and more energy-efficient technologies by altering the relative prices of goods and services based on their emissions intensity, and by encouraging the uptake of cost-effective, low-carbon alternatives.
b) The carbon-intensive factors of production, products and services are likely to be replaced with low-carbon-emitting alternatives. In order to achieve the extent of emissions reduction committed to under the Copenhagen Accord, the consumption of certain carbonintensive products (e.g. cement, steel and aluminium) need to be reduced and/or the production technologies have to become less carbon intensive. Given that these industries are important for the country's proposed infrastructure building programme, appropriate policies are required to ensure that mitigation and adaptation strategies are taken into account in investment decisions with long-term lock-in effects.
c) A carbon price will create dynamic incentives for research, development and technology innovation in low-carbon alternatives. It will help to reduce the price gap between conventional, carbon-intensive technologies and low-carbon alternatives.

Regarding the carbon cost, it is obvious to say that CCS in power plants makes sense economically only for large, highly efficient plants. Thus, the evaluation of CCS economic cost is very important in order to determine from the project technical specifications, an estimation of the investment required, the operating costs, and the possible revenues. A fairly wide range of costs has been reported by literature for employing CCS systems with fossil-fired power production and various industrial processes [105]. It is estimated that the investment cost of a demonstration power plant with CCS ranges from US $0.5 to 1 billion, 50% of which covers the CCS equipment [106]. The economic evaluation of CCS takes into account the extra cost required for CO_2 capture, transport and storage divided by the quantity of CO_2 stored in order to give the cost per tonne of CO_2. The requirement on the CO_2 purity (e.g. CO_2 concentration above 90%), the type of transportation (pipe or ship), and the storage generally makes the cost per CO_2 to be high. The capture section, which includes the CO_2 compression to a pressure, (typically about 14 MPa) suitable for pipeline line transport, is

always very expensive compared to transport and storage costs. This is due to the energy requirement for capture and compression. Today's typical cost CCS in power plants may range from US \$30 to \$90/tCO_2. The cost includes capture at \$20-80/t; transport \$1-10/t per 100km; storage and monitoring \$2-10/t [107, 108]. It is obvious that the increase of CCS cost per tonne of CO_2 will increase also the cost of electricity, especially when the electricity is generated by the fossil fuel power plants.

New or improved technologies for CO_2 capture have to be investigated with aims to reduce significantly the cost of CO_2 capture in the future. An advanced technology must be able to capture large quantities of CO_2 at record time with efficient energy and low economic cost. Assuming the reasonable rates of technology learning, the total CCS cost is expected to fall by at least 20-30%, while new technologies currently under development may allow for more substantial cost reductions in the future [109]. In case of EOR or ECBM, the CO_2 storage is beneficial to the oil or CH_4 production respectively. The additional tonne of oil or CH_4 produced per amount of CO_2 allows the deduction of storage cost per tonne of CO_2 to low cost or no cost.

The majority of the operating costs are based on the consumption of utilities, including steam and electricity. Other costs including chemical consumption, insurance and taxes, and labor associated with the operation and maintenance along with overhead costs. Since the concentration of CO_2 must be raised to above 90%, the more dilute CO_2 in the flue gas generally more expensive the capture section. Making a comparison study of cost between post-, pre-, and oxy-combustion, the average net efficiency penalties for post- and oxy-combustion capture are 10 percentage points relative to a pulverized coal plant without capture, and eight percentage points for pre-combustion capture. The costs of CO_2 avoided are on average \$58/tCO_2, but vary between \$40/tCO_2 and \$74/tCO_2 for case studies across OECD region. Costs of CO_2 avoided for China are estimated \$42/tCO_2 [107]. Davidson (2006) [110] has investigated the performance cost of power plant with capture (Table 2.3).

The CO_2 transport cost depends on the distance of the location storage site and the type of transport used (includes pipe and ship). The transport of CO_2 through pipelines is the most economical method able to carry large amounts of CO_2. The cost of pipelines can be affected by the distance and geographical location between the capture location and the storage site. A normal terrain presents generally low cost, when compared to the more mountainous and

densely populated areas. For a longer distances at sea, the use of ship will requires large tankers in order to carry large amount of CO_2. Ship transport will be preferred to the pipeline especially for the long distance beyond 1000 km.

In the storage section of CO_2, the expectation of finding a safe and permanent CO_2 storage plays a significant role in CO_2 storage cost. The specific reservoir depth and the geological characteristics of the storage formation (e.g., permeability, thickness, porosity, etc.) are major factors that will influence a significant range and variability of costs of CO_2 storage, which include onshore and offshore locations. Table 2.4 depicts the estimation costs for CO_2 storage, excluding monitoring costs in different geological sites, with offshore transportation costs evaluated for a distance range and depth of 100-500 km and 3000 m respectively.

Table 2.3: Cost of electricity and CO_2 avoidance [110]

Fuel	**Power generation technology**	**CO_2 capture technology**	**$1.1/GJ coal, $3.9/GJ gas**		**$2.2/GJ coal, $7.8/GJ Gas**	
			c/kwh	**$/t CO_2 avoided**	**c/kwh**	**$/t CO_2 avoided**
Coal	Pulverised fuel	None	4.46		5.36	
		Post-combustion Fluor	6.34	30	7.34	34
		Post-combustion MHI	6.27	28	7.40	31
		Oxy-combustion	6.63	33	7.76	36
	IGCC (Shell)	None	4.88		5.81	
		Pre-combustion, Selexol.	6.52	33	7.68	39
	IGCC (GE)	None	4.55		5.60	
		Pre-combustion, Selexol	5.66	20	6.94	27
Gas	Combined Cycle	None	3.70		6.23	
		Post-combustion, Fluor	5.07	44	8.03	58
		Post-combustion, MHI	4.93	39	7.76	48
		Oxy-combustion	6.84	85	9.98	102

As shown in Table 2.4, unlike geological and ocean storage, mineral carbonation requires significant energy inputs equivalent to approximately 40% of the power plant output.

Table 2.4: Estimates of CO_2 storage costs [110]

Option	Representative Cost Range (US$/tonne CO_2 stored)	Representative Cost Range (US$/tonne C stored)
Geological - Storage	0.5-0.8	2-29
Geological - Monitoring	0.1-0.3	0.4-1.1
Ocean		
Pipeline	6-31	22-114
Ship (Platform or Moving Ship Injection	12-16	44-59
Mineral Carbonation	50-100	180-370

2.3. CO_2 CAPTURE TECHNOLOGY

The focus in this research will be post-combustion CO_2 capture technology. A number of separation technologies could be used with post-combustion capture. These include: (a) absorption; (b) membranes; (c) cryogenics separation, and (d) adsorption.

2.3.1. Absorption

Absorption is a separation method based on Henry's Law in which atoms, molecules or ions enter some bulk phase – gas, liquid or solid material. With all the available CO_2 capture technologies, chemical absorption of CO_2 is utilized as the most efficient technology for capturing CO_2 [111]. The absorption is rendered possible through the use of solvent and advanced studies have been done in order to find a number of properties that contribute to determine if a solvent can be applied economically at an industrial scale for CO_2 capture.

Recent investigations by Eirik Falck da Silva [112] have suggested that chemical absorption of CO_2 is likely to remain a highly competitive technology for CO_2 capture in the future. All absorption processes are a continuous processes, which include an adsorption step where the CO_2 present in the flue gas is selectively absorbed by the solvent, and a solvent regeneration step where the CO_2 is extracted from CO_2 rich solvent (desorption) under specific conditions of pressure and temperature. The absorption process becomes a big challenge especially when chemical solvents are used for high-volume gas flows. The effectiveness requires large amounts of material resulting in high investment costs and energy consumption. In addition, degradation and oxidation of the solvents over time produces products that are corrosive and may require hazardous material handling procedures [113]. Among the solvents, alkanolamines are divided into three groups, which are primary, secondary and tertiary amines, as well as ammonia. Amine-based chemical absorbent is today the favorite chemical solvent technology for CO_2 capture. Monoethanolamine (MEA) relatively cheap, and with the lowest molecular weight [114], has been used as amine for CO_2 separation from natural gas streams. However, this also has showed some ineffectiveness related to the energy regeneration, loss of solvent due to high vapor pressure, and irreversible reactions with minor impurities such as carbonyl sulfide (COS) and Carbon disulphide (CS_2).

2.3.2. Adsorption

Adsorption is a separation method based on adhesion of atoms, ions, or molecules from gas, liquid, or dissolved solid to a surface of porous materials [115]. Porous adsorbents with large CO_2 capture and desorption capacity under PSA or TSA conditions are currently under investigation to overcome the disadvantages of amine aqueous solutions. However, the separation of CO_2 from a diluted solution is more challenging; the adsorption technology has the ability to treat diluted solution. The most important characteristics of an adsorbent to achieve efficient CO_2 capture from CO_2 diluted in the flue gases are: capacity, selectivity, regenerability, kinetics, compatibility, and cost. For several economic, environmental, and technical reasons, the adsorbent should not be discarded, after one use, but should regenerate have crossed this out so many times.

In the process of CO_2 capture, the flue gas from coal-fired power plant must be cleanup prior to CO_2 adsorption process. After leaving the boiler, the hot flue gas contains particulates and certain gases including SO_2, and NO_x which can affect the performance of the CO_2

adsorption process. These components must be removed from the flue gas prior to CO_2 adsorption. SO_2 removal is usually achieved in a Flue Gas Desulphurization (FGD) unit. The investigation by Davidson [116] shows that SO_2 concentrations of less than 10ppm are recommended in the flue gas prior to CO_2 capture. NO_x is removed using Selective Catalytic Reduction (SCR), Selective Non-catalytic Reduction (SNCR) or low NO_x burners during combustion. Particulate matter such as fly ash is removed by either electrostatic precipitators (ESP) or bag house filters [117]. This "clean" flue gas will flow to the CO_2 capture plant for CO_2 separation.

2.3.3. Membranes

Membrane is a selective barrier based on the permeation of atoms, ions and molecules in diffusion from bulk gas, liquid and solid [118]. The absorption process has been improved with the application of membrane systems with thin barriers that, due to the high surface area, allow selective permeation of certain gases; one component in a gas stream can pass through faster than the others [119]. Permeation rates will be related to the sizes of the molecules or diffusion coefficients in the membrane material. The driving force for the permeation is the difference in partial pressure of the components either side of the membrane. However, though an extra energy requirement, the ineffectiveness due to the direct contact between the liquid solvent and gas mixture could be circumvented. It is noticeable that a membrane with efficient permeation allows a higher uptake of absorbate in the liquid solvent compared to the absorption where the gas mixture and solvent are in direct contact. The varying rates of gas transport cause inherent difficulty to most membranes in achieving high degrees of gas separation. In addition, the process must operate in recycling stream where the selectivity is enhanced by refeeding the membrane with the previous refusal gas or multiple stages of membranes to achieve CO_2 concentrations for geologic storage [120]. This requires, of course, an increase in energy consumption.

2.3.4. Cryogenic separation

Cryogenic technology consists at creating different phases allowing easy separation of components. When gases have different freezing temperatures, they can be separated by cooling them until they separate into different phases. Carbon dioxide can be frozen at 195 K and atmospheric pressure, and pressurized past its critical point at about 304 K and 74 bars to

form a liquid. The cryogenic separation technology for CO_2 is beneficial for oxyfuel combustion where the flue gas contains 60-70% CO_2 with 20-25% H_2O. The application of cryogenic technology in post-combustion capture where the concentration of CO_2 is very low (3-13%) in the flue gas, will require a theoretical energy requirement of 1.9MJ/kg CO_2[121] to bring the CO_2 diluted in flue gas to the critical point. With real equipment, this could represent a significant energy penalty, unless liquid CO_2 is already required for transport.

2.4. ADSORPTION TECHNOLOGY

2.4.1. Introduction

The adsorption technology has been booming in chemical industry, also in the fields of environmental pollution control and energy utilization. Adsorption is classed among practicable separation methods for purification or bulk separation in newly developed material production processes of, for example, high-tech materials and biochemical and biomedical products [122]. Adsorption is usually described through isotherms, that is, the amount of adsorbate on the adsorbent as a function of its pressure (if gas) or concentration (if liquid) at constant temperature. The quantity adsorbed is nearly always normalized by the mass of the adsorbent to allow comparison of different materials [123].

Adsorption takes place at the surface of the adsorbent where the solid and gas come in contact with each other, i.e. at the interface between the phases. This is rendered possible through self-distribution of molecules of adsorbate between the gas phase and the adsorbed phase (almost instantaneously in some cases, in others at a measurable rate) until a state of equilibrium is reached. Various forces are operative in holding together the atoms or molecules constituting the solid. Regardless of the nature of the predominating forces, a molecule in the body of the solid is subjected to unbalanced forces, the inward pull being greater than the outward force [124]. Gases are adsorbed on solids by the saturation of the unsatisfied forces of the surface atoms of the solids by the force of the gas molecules striking the solid surface. Thus, the reduction of the surface tension of the solid substance is obvious. This process tends spontaneously to the decrease of surface energy, which is a function of surface area and surface tension. Therefore, all adsorption phenomena are spontaneous [125] and result in a decrease of the free energy of the system.

Adsorption, being an exothermic process, decreases with a rise in temperature. The adsorption process is thermodynamically exothermic with heat release. Therefore, the heat from external source decreases in order to balance with the heat release in the system as the adsorption temperature is intended to be constant for an isothermal operation. Thus, physical adsorption and chemisorption will be relevant to the nature of the forces involved through the evolution of the general magnitude heat. Indeed, physical adsorption named physisorption takes place where the fundamental interacting force is caused by Van der Waals forces as reversible force. Working in certain conditions, including high pressure, through weak interactions such as van der Waals forces, adsorbents can separate CO_2 from a stream by preferentially attracting it to the material surface. Upon changing the conditions to remove the CO_2, adsorbents can be regenerated with the ability to reverse the chemical potential adsorbed phase. The challenge in adsorption is to improve the efficiency by working with limited temperature changes that require a time cycle due to the heat capacity of adsorbent material. The central advantage of physical adsorption methods is the possibility for low energy requirement to regenerate the sorbent material, and the quick regeneration time associated with changing the pressure [126]. The forces operative at high temperatures for primary chemical valence forces occurrence results in chemisorption. With regards to chemisorption, gas molecules can chemically bond to the surface of some materials. The molecule will be either totally bound to the surface as associative process, or the gas molecule will break up as dissociative process, forming a bond. This, most of the time, requires the sorbent to be composed of an active surface layer supported by an inert substrate.

2.4.2. Fundamental factors for designing adsorbents

Surface characteristics and pore structures of adsorbents are the main properties in determining the performance of adsorption, based on equilibrium and rate properties as factors needed for plant design. A high surface area to volume ratio will determine a successful adsorbent as adsorption is a surface phenomenon. Large adsorption capacity as a property for characterizing adsorptivity of adsorbents is an important aspect, which requires understanding factors for adsorption efficiency, including large specific surface area and the pore size distribution of micropore. The amount of gas adsorbed per gram of the adsorbent at equilibrium is dependent upon the temperature, the pressure, and the nature of the adsorbent, the preparation and history of the adsorbent and the adsorbate. The quantity of a gas adsorbed by a given weight of adsorbent varies greatly from one adsorbing solid to another, as well as

from different adsorbents of the same apparent chemical composition. It is not the most porous adsorbent which adsorbs the most gas; the shape of the pores is an important consideration. The pore structure of the adsorbent plays a part in unimolecular adsorption only if an appreciable portion of the surface is comprised of pores that are not more than one or two molecular diameters wide. In such narrow pores the heat of adsorption is greater than on a plane surface, since the adsorbate is subjected to greater attractive forces. This results in an increase in the amount of gas adsorbed. If the pores are too narrow, the molecules may not be able to penetrate them. This may result in a considerable decrease in the amount of gas adsorbed or an entire elimination of adsorption. Very fine pores act as molecular sieves, allowing the penetration of smaller molecules and shutting out the larger ones. The adsorbability of gas, i.e., the amount taken up by a given adsorbent at a fixed temperature and pressure, depends upon the nature of the adsorbed gas. However, no simple quantitative relationships have been advanced to express adsorption as a function of the nature of the adsorbate.

Small particles as substrates are beneficial to providing large surface area. This gave raise to nanotechnology, where a particle is defined as a small object that behaves as a whole unit in terms of transport and properties. The physical adsorption and chemical adsorption occurrence during the adsorption process depend on the surface characteristic of adsorbents and their affinity with the adsorbate.

The selection of a proper sorbent for a given separation is a complex problem. The predominant scientific basis for sorbent selection is the equilibrium isotherm. Diffusion rate is generally secondary in importance. The equilibrium isotherms of all constituents in the gas mixture, in the pressure and temperature range of operation, must be considered. The adsorption isotherm is generally based on: (1) interaction potentials, and (2) geometry/structure of the adsorbent. This shows the importance of physical and chemical investigations on the bonding state and the reactivity of the functional groups on the surface of an adsorbent [127]. Thus, a specific tailoring of pore size and the surface of adsorbents will certainly affect the surface area and the interaction between adsorbate-adsorbent interactions respectively. The adsorption is then the phenomenon adsorbate-adsorbent interactions depending on dispersion, electrostatic and chemical bond [128]. Weak chemical bonds involving π electrons or π -complexation may be a good factor of designing new and highly selective adsorbents.

Based on adsorption isotherms, the following factors are important to the design of the separation process can be estimated [113]:

a) Capacity of the sorbent, in the operating temperature and pressure range.
b) The method of sorbent regeneration— for example, temperature or pressure swing— and the magnitude of the required swing.
c) The length of the unusable (or unused) bed (LUB).
d) The product purities.

An adsorbent will face fluid flow in order to yield its efficiency during the adsorption process; however, all factors to the design the adsorbent can be suitable. Therefore, the deep knowledge of fluid flow is of major importance for the effective adsorption.

2.4.2.1. Fluid flow through packed bed

The adsorption process is the contact between adsorbent and fluid in packed bed causing the pressure drop during the fluid flow through the packed column, as shown in Figure 2.6. The pressure drop depends on variables, which include particle size, fluid velocity and bed dimension. The pressure is determined by the following equation [129, 130]:

$$\Delta p = f(\frac{L}{D_p})\rho_f (v_c)^2 \quad (2.6)$$

Where:

f: a dimensional friction factor
L: length of packed column
ρ_f: fluid density
v_c: fluid velocity
D_P: particle diameter

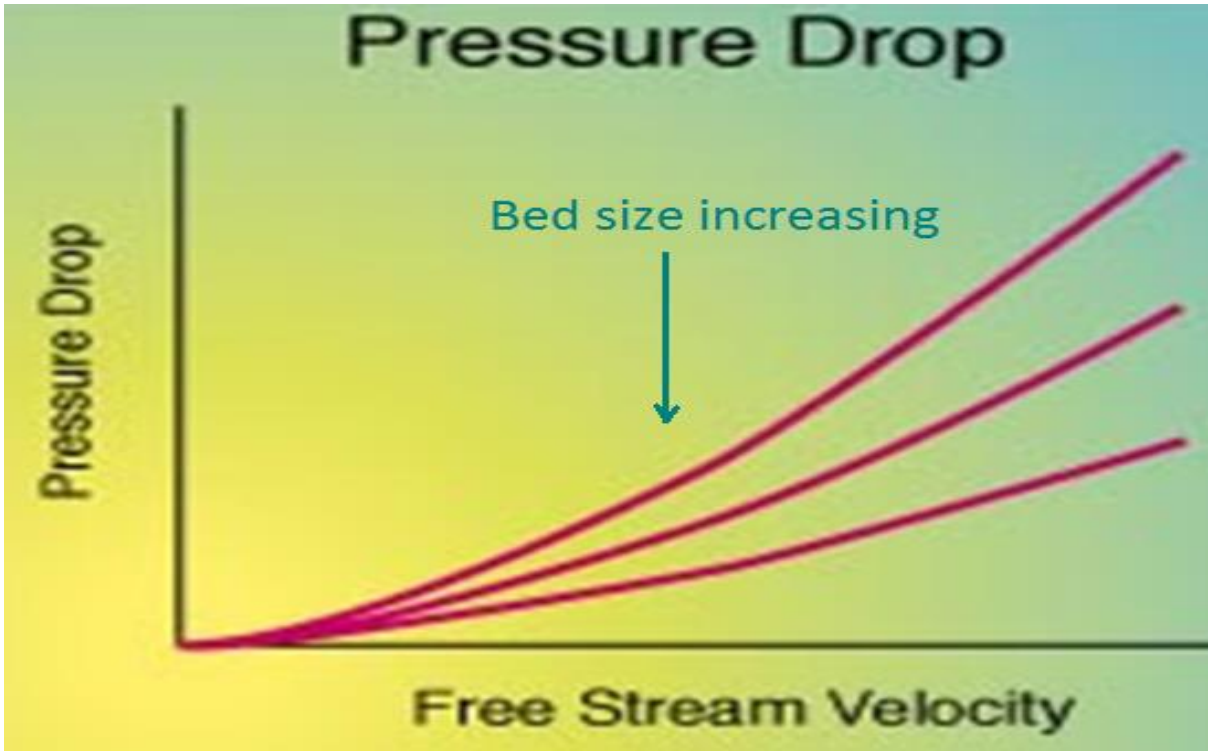


Figure 2.6: The pressure drop in fluid flow [131]

2.4.2.2. Mass transfer and adsorption kinetics

Mass transfer of gas depends on the adsorption isotherms, flow rate (i.e. residential time), and mass residence. Throughout the adsorption process there is occurrence of mass transfer zones (MTZ) where the length of bed is involved in the adsorption process, and adsorption moves along the bed from the inlet to the outlet point during the operation time. As an adsorbent becomes exhausted in the zone where it reaches the equilibrium capacity, the MTZ will travel further through the adsorbent. Thus, the MTZ length is a function of the influent rate and adsorption rate. In the MTZ, the diffusion of adsorbate from the bulk toward the adsorption site occurs in both axial and radial directions depending on the geometry/structure of the adsorbent, the potential interaction between adsorbate and adsorbent[132], the velocity and viscosity of the bulk fluid. Therefore, an efficient adsorption bed design will need adequate length and velocity of MTZ in order to enhance the capacity of the bed. Minimizing the MTZ length increases the capacity of the bed. Breakthrough point occurs when the front edge of the MTZ reaches the end point of the bed. The breakthrough curves depend on bed geometry, operating conditions, transport properties, heat effects, and equilibrium adsorption isotherm(s).

The adsorbate molecules transfer between the fluid and adsorbents through three stages in packed beds [133, 134]:

a) External transport: First molecules transfer occurs via convection from the bulk flow in the bed to the laminar film adjacent to the particle [135].
b) Internal transport: the penetration of the gas molecules into the porous structure and the adsorbed on the internal surface of the pellet. Thus, the diffusion phase occurs through pore diffusion and surface diffusion in parallel [136, 137].
c) Adsorption: the attachment of the adsorbate molecules with the adsorbent via physical or chemical adsorption. This phenomenon occurs on the interface between the gas phase and the solid phase, either at the external surface or within the pores of the particles [138, 139].

Adsorption is complex; therefore, requires experiment for the understanding of the principle relevant to it. It is difficult to utilize completely the maximum capacity of an adsorbent, because of the involvement of the mass transfer effects in actual fluid-solid contacting processes. The elaboration of model mathematics has been rendered possible when considering that the mass transfer takes place from the fluid surrounding a particle into the particle or vice versa, with the alternative that the intraparticle concentration of the mass transferring species is concentric (the same as radial symmetry or center symmetry). Then the physical adsorption in a packed bed with an imposed signal is described by the following equations [140, 141]:

$$\frac{\partial C}{\partial t} = D_{ax}\frac{\partial^2 C}{\partial x^2} - U\frac{\partial C}{\partial x} - \frac{a}{\varepsilon_b}D_e\left(\frac{\partial c}{\partial r}\right)_R \tag{2.7}$$

$$\varepsilon_p\frac{\partial c}{\partial t} = D_e\frac{1}{r^2}\frac{\partial}{\partial r}\left(r^2\frac{\partial c}{\partial r}\right) - \rho_p\frac{\partial c_{ad}}{\partial t} \tag{2.8}$$

and when $C = c = c_{ad} = 0$ at $t=0$; $\frac{\partial c}{\partial r} = 0$ at $r=0$; the above equation at $r = R$ becomes:

$$D_e\frac{\partial c}{\partial r} = k_f\left(C - c\right) \tag{2.9}$$

Where

a = particle surface area per unit volume of packed bed; with $a = 3(1-\varepsilon_b)/R$ for spherical particles

C = tracer concentration in the bulk fluid

c = tracer concentration in the intraparticle pore volume

c_{ad} = amount adsorbed in the particle

D_{ax} = axial dispersion coefficient of the adsorbing species

D_e = intraparticle effective diffusivity

K_f = particle-to-fluid mass transfer coefficient

R = particle radius

r = radial distance variable

U = interstitial fluid velocity

ε_b = bed void fraction

ε_p = intraparticle void fraction

ρ_p = particle density.

When c is small, the physical adsorption rate is assumed to be first-order

$$\frac{\partial c_{ad}}{\partial t} = k_a\left(c - \frac{c_{ad}}{K_A}\right) \tag{2.10}$$

Where K_A = adsorption equilibrium constant and k_a = adsorption rate constant.

Thus, Equation (2.10) results in Langmuir's adsorption isotherm model, where the adsorption is developed in a unimolecular layer from the stand point of the equilibrium between gas molecules striking the surface, and those which evaporate after the lapse of a certain time. When taking the concentration, c, to the partial pressure, p, of the gas, at the equilibrium, the rate of adsorption is equal to the rate of desorption.

$$K_{-a}\,p(1-c_{ad}) = k_a c_{ad} \tag{2.11}$$

Assume that $K = k_{-a}/k_a$

hence,

$$c_{ad} = \frac{Kp}{1-Kp} \tag{2.12}$$

Chungsying Lu et al. have found model mathematics to determine the amount of CO_2 on adsorbents (q, mg/g) at a certain time (t, min) by the following relation [142]:

$$q = \frac{1}{m}\int_0^t Q\left(C_{in} - C_{eff}\right)dt \tag{2.13}$$

where m is the weight of virgin adsorbents (g); Q is the influent flow rate (L/min); C_{in} and C_{eff} are the influent and effluent CO_2 concentrations (mg/L), respectively.

2.4.2.3. Potential Energies for adsorption

Selection or synthesis of adsorbents for a target adsorbate molecule is based on the adsorption isotherm. The interaction potentials and geometry/structure of the adsorbent are factors which influence the adsorption isotherms. Work (W) must be done in order to take a gas molecule to the adsorbed stage. Thus, the adsorption occurs when Φ (Interaction Energy Potential) = W. Considering the first adsorbed state approximately at the saturated vapour pressure P_0, the adsorption pressure P for the given Φ, and ΔG the free energy change [128]. Hence:

$$-\Phi = -\Delta G = \int_{P}^{P_0} VdP = RT \ln \frac{P_0}{P} \tag{2.14}$$

$$\Phi_{total} = \Phi_{adsorbate-adsorbate} + \Phi_{adsorbate-adsorbent} \tag{2.15}$$

If $\Phi = \Phi_{adsorbate\text{-}adsorbent}$

$$\phi = \phi_D + \phi_R + \phi_{Ind} + \phi_{F\mu} + \phi_{FQ} \tag{2.16}$$

Where

Φ_D = dispersion energy,

Φ_R = close-range repulsion energy,

Φ_{Ind} = induction energy (interaction between electric field and an induced dipole),

$\Phi_{F\mu}$ = interaction between electric field (F) and a permanent dipole (μ),

$\Phi_{\dot{F}Q}$ = interaction between field gradient (Ḟ) and a quadrupole (with quadrupole moment Q).

($\Phi_D + \Phi_R$) are nonspecific, which are operative in all sorbate-sorbent systems.

While ($\Phi_{Ind} + \Phi_{F\mu} + \Phi_{\dot{F}Q}$) arises from charges (which create electric fields) on the solid surface.

2.4.2.4. Heat of adsorption

Adsorption is accompanied by the evolution of heat, and temperature changes affect the adsorption equilibrium relation and, in some cases, adsorption rate. The achievement of the adsorption involves mechanical work, because the adsorption goes with evolution of heat. Thus, the important definitions of heat of adsorption are differential heat of adsorption and isosteric heat of adsorption. However, Enthalpy and internal energy state variables depend on the initial and the final states: the definition of different thermodynamics paths will be necessary for evaluation of the energy balance in adsorption process. As the adsorption process is exothermic heat is released along the adsorption. A high heat release in an adsorption isotherm will require a temperature controller in order to maintain the temperature by regulating the external source of heat. This is beneficial for energy conservation which results in low cost of energy expenditure. Conversely, in the desorption process, the external source of energy operates to compensate the desorption heat which is absorbed by the system due to endothermicity of the desorption reaction. A competitive adsorbent must be able to release more heat during the adsorption than to absorb heat during desorption process. The adsorption heat implies advection heat, diffusion heat and isosteric heat occurring according to the following process [143]:

a) The fluid is preheated and the transfer heat is done by advection due to bulk motion

$$Q = Av\rho C_p \Delta T \tag{2.17}$$

b) In interface fluid-solid the heat is transferred by diffusion

$$Q = A_P \rho C_p \left(\frac{\partial T}{\partial t} - \alpha \frac{\partial^2 T}{\partial x^2}\right) \tag{2.18}$$

c) In adsorption isotherm: Isosteric Heat Q_{st}

$$\frac{Q_{st}}{RT^2} = \left(\frac{\partial \ln P}{\partial T}\right)_{n_a} \tag{2.19}$$

Where

Q: heat flux (w); A and A_p: bed and particle surface area (m^2) respectively; v: fluid velocity (m/s); ρ: density; α: thermal diffusivity; T: temperature (K); C_p: heat capacity (J/kg ◦C)

2.4.3. Adsorption separation process

The adsorption separation process is based on uptake and release phenomenon, where the efficiency depends on the conditions of operation including temperature, pressure and medium pH. The regeneration of spent adsorbent is necessary because the low economic cost, reduced environmental space for disposal and continuous operation.

2.4.3.1. Regeneration of spent adsorbent

Adsorption is an unsteady process which operates with different conditions for the completion of specific stages. The regeneration of adsorbents is used on the one hand to restore the adsorption capacity of exhausted adsorbent, and on the other hand to recover valuable components present in the adsorbed phase, if any. As the sorbent has to be regenerated for most commercial applications, the adsorption operations are necessary cyclic. Therefore, adequate investigation is required to state the efficiency and cost of regeneration which play important roles in the overall feasibility of adsorption process.

2.4.3.2. Regeneration methods

There are several methods in application for the regeneration of spent adsorbents:

a- Thermal swing adsorption (TSA)
b- Pressure swing adsorption (PSA)
c- Vacuum swing adsorption (VSA)
d- Electrical swing adsorption (ESA)

A. Thermal swing adsorption

In a thermal swing adsorption (TSA) process cycle, the elevation of temperature is required to regenerate the bed. Thus, the decrease of temperature promotes the adsorption while the

increase of temperature promotes the regeneration or desorption. The suitable way for raising the temperature is to preheat the gas in order to purge the bed. This process is important for the sweeping of the adsorbent, with the intention to remove the gas or water previously incorporated in the lattice of pores, in order to provide more available sites for adsorption. The greatest challenge in adsorption processes using TSA is the heating and the cooling times, which generally lengthen each cycle usually from several hours to over a day. To circumvent this challenge requires a specific internal heat-exchanger able to collect the heat released from the processes, including adsorption and cooling, to heat up the adsorber for desorption process [144, 145]. Therefore, specific numbers of beds must be arranged in order to synchronize the TSA system with efficient timing for the multiplication of cycles resulting in higher daily adsorption. Since the TSA operates with a complete cycle of adsorption and desorption, dual-bed systems are most commonly used for TSA. The dual-bed systems will then operate continuously in such way that when one bed is adsorbing, simultaneously the other is desorbing. To circumvent certain unexpected problems in the operation of TSA system, a third bed was found appropriate to operate as a guard bed [146]. A large number of beds to assure the TSA system to operate continuously will increase the daily adsorption rate; but will be a drawback due to large space, high energy cost and high equipment cost.

The TSA system is good for strong adsorbed species [147] and a small change of temperature has the advantage of increasing significantly the adsorption capacity. In addition, the desorbate is recovered at high concentration. However, the thermal aging of the adsorbent is one of disadvantages in TSA system. Also, the heat loss causes the inefficiency in energy usage [148, 149]. Furthermore, the TSA system is unsuitable for rapid cycling due to inability for the adsorbent to be used for maximum efficiency.

In carbon capture technology, the TSA system is suitable for post-combustion capture where the gas mixture is supposed to be at low pressure and most of the time low temperature. The process of preparation is not so significant than it could be for pre-combustion capture where the gas is released from the power plant to the capture plant at high temperature and high pressure.

B. Pressure swing adsorption

Pressure swing adsorption (PSA) is an unsteady technology for separation and purification of gas mixtures. The increase of pressure promotes the adsorption while the decrease of pressure promotes the regeneration or desorption. PSA is favorable for high purity of species; therefore it is good when the adsorption is weak. The cyclic operation relative to adsorption desorption is rapid and efficient in PSA system; however the process requires high mechanical energy which is more expensive than heat and also the desorbate is recovered at low purity. A conventional PSA method involves a usual cycle of four steps ranked as follow compression (pressurization), high pressure production (i.e. feed), decompression (i.e. blowdown), and low pressure purge [150].

C. Vacuum swing adsorption

Vacuum swing adsorption (VSA) operates at low temperature; therefore requires less energy. VSA is more efficient and requires less maintenance than TSA and PSA. The main difference between PSA and VSA is that in PSA the feed gas is compressed substantially above atmospheric pressure and the recovery is done at atmospheric pressure. While in VSA, the feed is only "slightly" compressed (up to 1.5 atm at most), and the recovery is performed under vacuum conditions [151].

D. Electrical swing adsorption

Electrical swing adsorption (ESA) applies an electric field to drive the cycle adsorption-desorption with a basic switch able to be turned on/off for gas separation. This results in instantaneous modification of thermodynamics of adsorbent/adsorbate interaction with the external field. The complete realization of ESA to its fullest potential has the advantage of increasing the efficiency of overall energy production [152]. Moreover, the ESA system is very fast because the temperature of the adsorbent is rapidly increased through the application of a low voltage electric current by the direct Joule effect [153, 154, 155, 156] and requires less energy.

One of the disadvantages in using ESA system is that the electric power is used to raise the temperature compared to TSA system where the waste heat is used to increase the temperature [157].

2.4.4. Adsorption technology for CO_2 Capture

Adsorption technology for CO_2 capture separates CO_2 from flue gas from fossil fuel power plants. CO_2 adsorption is based on a cyclical process in which CO_2 is adsorbed from a gas stream on to the surface of solid called adsorbent. The gas stream, with most of the CO_2 removed, is then emitted to the atmosphere. The adsorbent is then regenerated using differences in either pressure or temperature to remove CO_2 and compress it for storage. In both pre-combustion and post-combustion capture, the flue gases are hot and wet and require pretreatment specific to the adsorbent or bed. But most of the time the flue gas from post-combustion is pre-treated through the desulphurization process, and therefore meet the CO_2 adsorption requirements. Developing an adsorbent based system for CO_2 capture requires a material that is cheap, environmentally friendly, impurity and water tolerant, and has a good thermal stability.

The adsorption technology for CO_2 capture uses different types of bed (namely fixed bed, moving bed and fluidized bed) where the efficiency is of importance.

2.4.4.1. Adsorption technology for CO_2 capture using fixed bed

A fixed bed packed bed reactor consists of a compact, immobile stack of catalyst pellets within a generally vertical vessel [158]. In the technology of fixed bed adsorption the adsorbent is usually in a vertical cylindrical bed, where the gas is injected from downstream to upstream in case of low pressure or from upstream to downstream in case of significant or high pressure. One of advantages of the fixed bed is that the attrition is minimized therefore the adsorbent has a long life. Figure 2.7 shows three beds operating in a TSA system, where a complete cycle occurs in the following stages [159]:

1) Feed: the flue gas goes into the adsorption bed, CO_2 is adsorbed and N_2 flows through.
2) Purge: CO_2 is pumped back into the adsorption bed to flush out impure nitrogen trapped in spaces between the granules of the adsorbent.
3) Evacuate: the vacuum pump lowers the pressure and CO_2 is removed from the chamber.
4) Repressurise: N_2 flows back into the adsorption bed to re-pressurise the adsorption bed.

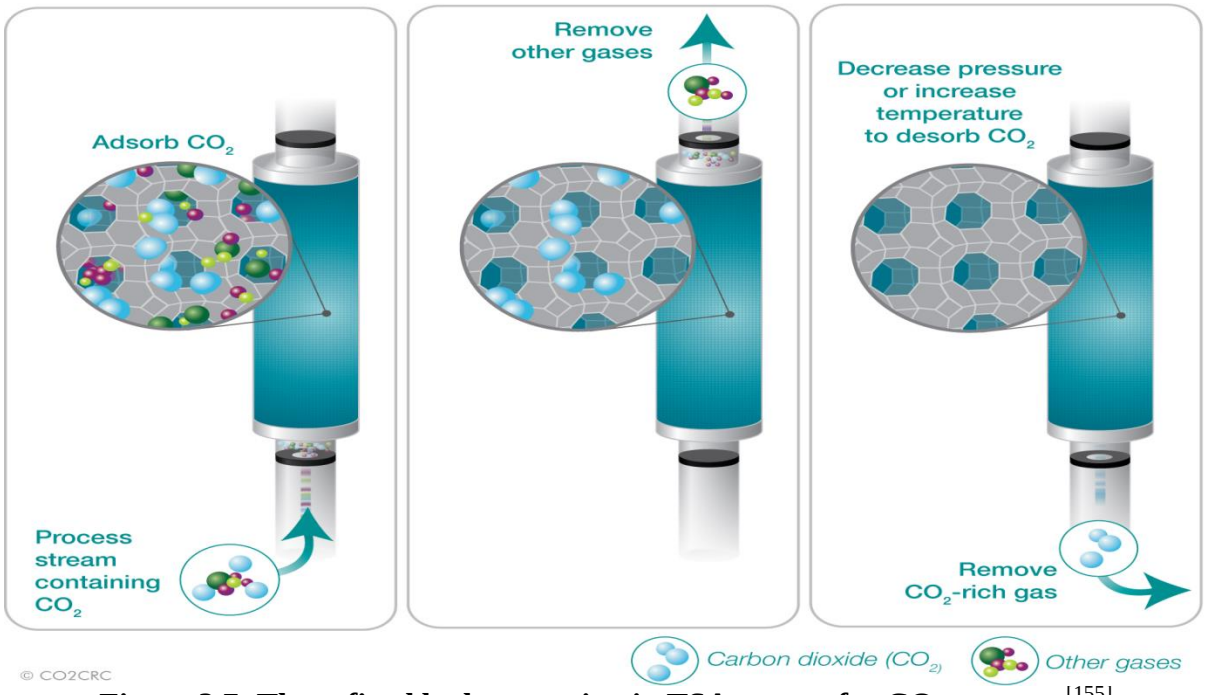


Figure 2.7: Three fixed beds operating in TSA system for CO_2 capture [155]

Figure 2.8 shows use of a TSA system technology where a fixed bed contains two types of adsorbent. The flue gas is injected where the lower adsorbent operates to capture SO_X, NO_X and water. The flue gas, devoid of SO_X, NO_X and water, continues its path upward into the upper adsorbent, where the CO_2 is captured. The two kinds of adsorbent must have different condition of adsorption and desorption. Therefore, these adsorbents are designed in such a way that CO_2 is not supposed to be adsorbed at the lower adsorbent, likewise SO_X, NO_X and water at the upper adsorbent; however they can pass through to be removed for adsorbent regeneration.

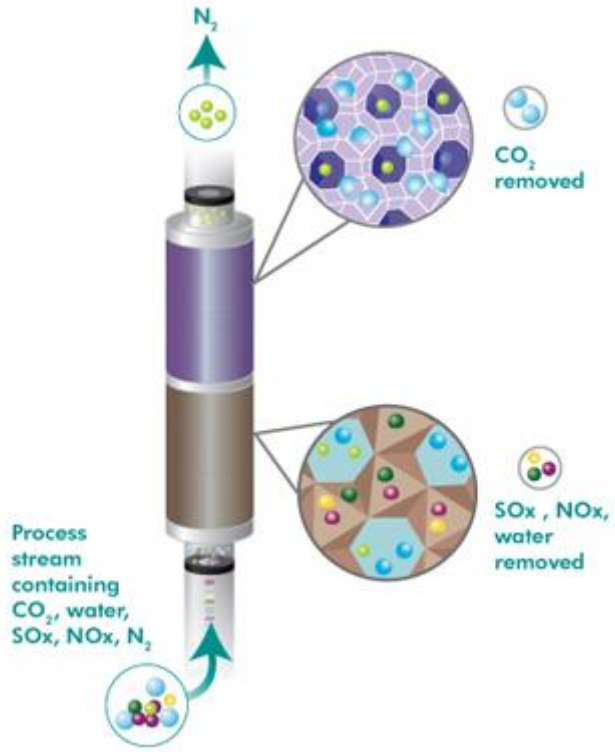


Figure 2.8: A fixed bed with two different types of adsorbent for specific adsorption [160]

Compared to other reactor types or designs utilizing heterogeneous catalysts, the fixed packed bed reactors are preferred because of simpler technology and ease of operation [154].

2.4.4.2. CO_2 adsorption technology using moving beds

The CO_2 adsorption technology using moving beds (Figure 2.9) consist of the circulation of solids as adsorbents from adsorber to regenerator and vice versa. During the adsorption process, the flue gas and the steam at low pressure are injected counter current to the adsorber, and to the regenerator for the capture and release of CO_2 respectively. The moving bed has the advantage of rapid generation after adsorption completion and the heat transfer is better than in fixed beds. The technology of moving bed is more expensive as it is a more complex piece of equipment compared to fixed beds. Moreover, inevitable attrition of the adsorbent occurs, with the equipment. This requires more attention on the selection of equipment.

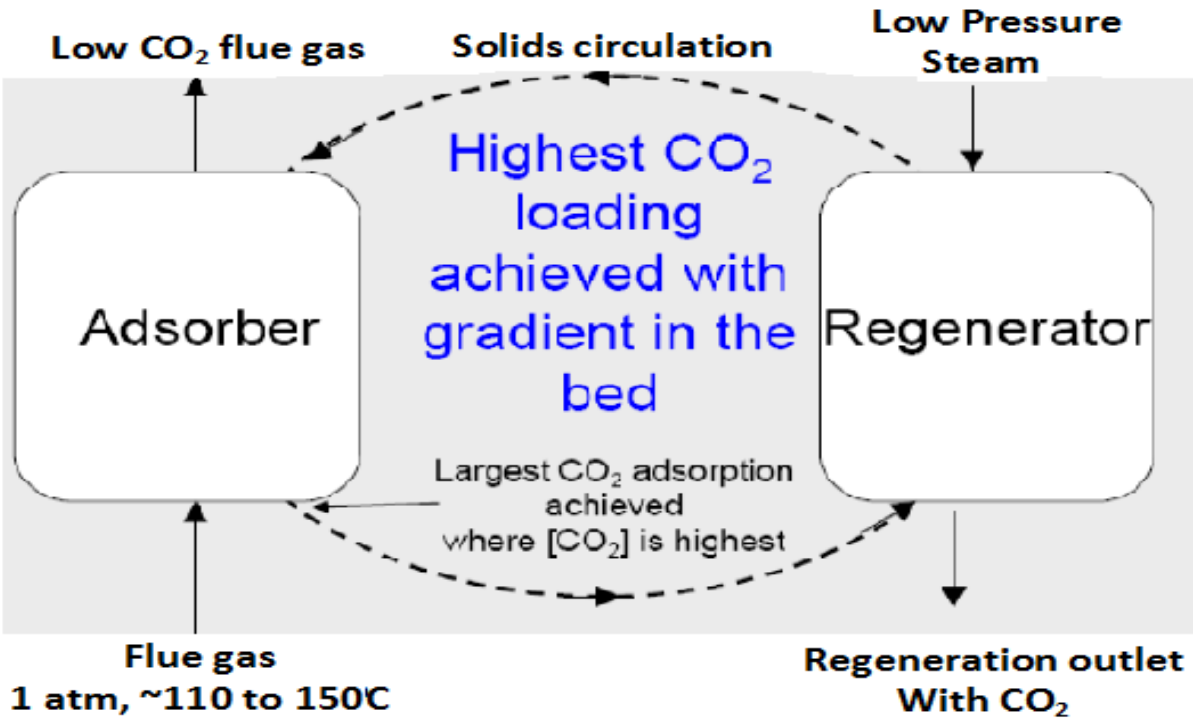


Figure 2.9: Circulating Adsorbent –Continuous Counter-Current [161]

2.4.4.3. CO_2 adsorption technology using fluidized bed reactors (FBRs)

The technology of fluidized bed (Figure 2.10) consists of a suspension of solid particles in an ascending circulation of flue gas under pressure, making a bed for CO_2 adsorption. A limited velocity of the fluid is required to avoid random movement of particles caused by the circulation of fluids with excess of upward velocity [162]. The solid particles saturated with CO_2 are recovered by overflow for further regeneration.

The advantages of using a fluidized bed are as follows. [163]:

a) Good thermal transport inside the system and good heat transfer because the contact of the solid particles with the fluidization medium is greatly enhanced. Thus, the FBR system is beneficial for large-scale operations

b) Uniform particle mixing resulting in elimination of radial and axial concentration gradients.

c) Uniform Temperature Gradients leading to exothermic reactions.

d) Ability to operate reactor in continuous state

The disadvantages of using a fluidized bed are as follow [164]:

a) Increased reactor vessel size causing the expansion of the bed materials in the reactor

b) Pumping requirements and pressure drop resulting in higher fluid velocity for solid suspension.

c) Particle entrainment requires extra unit for the separation of fine particles entrained in the fluid.

d) Lack of current understanding because it is very difficult to predict and calculate the complex mass and heat flows within the bed.

e) Erosion of internal components cause possible wear of the reactor vessel

f) Pressure loss scenarios leads to sudden loss of fluidization pressure causing sudden surface area reduction and runaway reaction.

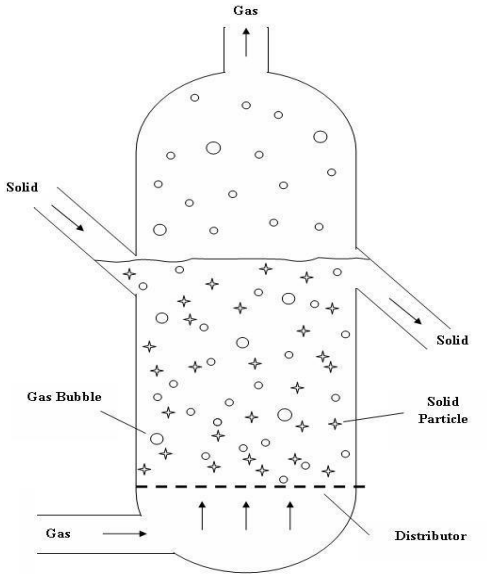


Figure 2.10: Fluidized bed reactors (FBRs) [165]

2.4.5. Adsorbent materials for CO_2 capture

Suitable adsorbents for CO_2 capture from flue gas should satisfy several important criteria to compete with the present technologies, including:

a) The solid sorbent for CO_2 must be cost effective and energy-efficient where a highly exothermic adsorption reaction will prevent heat from generated source. [166]
b) High adsorption capacity and high selectivity for CO_2
c) Adequate adsorption/desorption kinetics and high rate of adsorption under the operating conditions.
d) The stability during repeated ad/desorption cycling for adsorbents life time and replacement frequency.
e) Mechanical strength: stable microstructure and morphology under several operating conditions which include high volumetric flow rate of the flue gas, vibration, and temperature.
f) Good performance in the presence of moisture and impurities in the feed (i.e. water vapor, O_2 and SO_2)
g) Low operating cost

Among prospective materials for the gas separation processes are: activated carbons [167, 168], silica gel, zeolites [169,170], and metal-organic frameworks (MOFs); and related compounds [171,172] are currently receiving preferential attention.

2.4.5.1. Activated carbon

Activated carbon is prepared at high temperature from carbon containing source materials such as coal (anthracite or brown coal), lignite, wood, nutshells, petroleum, and sometimes synthetic high polymers, which are commercially available for different actions including gas purification, and removal of organic pollutants from water [173]. The huge advantage over other adsorbents is the temperature stability over 500 ◦C and low cost of the raw materials. Activated carbon as a non-polar adsorbent provides the larger micropores preferable for the adsorption of larger molecules. With larger micropores, this method will be inefficient for CO_2 capture and gas separation, because the molecule gases in flue gas have generally small sizes: 3.3, 3.5 and 3.6 Angstroms for CO_2, O_2, and N_2 respectively [174]. The adsorption is

more efficient when there is good contact between the adsorbent and the adsorbate. Therefore, the yield of activated carbon from raw materials is, in most cases, less than 50%, and sometimes 10% [175].

2.4.5.2. Silica gel

Silica gel, another type of adsorbent, is a dehydrated adsorbent with nanopores, generally obtained through coagulation of colloidal solution of silicic acid. Possessing a highly porous form of silica, with an extremely large internal surface area, silica gel is non-corrosive, odourless, tasteless, non-toxic, and chemically inert [117]. Silica gel has a very strong affinity for water; this enables its use in numerous applications, including dehumidification of gases such as air and hydrocarbons, chromatographic separation, and removal of impurities in adsorption. Silica gel can be used to capture CO_2, but, as it is also a good adsorbent for N_2, the adsorption process will be more selective in oxyfuel separation methods. Hyun-Kon Song et al. [176] chemically modified the surface of silica gel at 700 °C in order to increase the adsorptivity for CO_2. However, the adsorption process, requiring large energy consumption, operates at 100 – 250 °C.

2.4.5.3. Zeolites

A third adsorbent is natural zeolite, an aluminosilicate mineral, composed of SiO_4 and AlO_4, tetrahedra with shared O_2 atoms with various regular arrangements in order to form an open crystal lattice containing pores of molecular dimensions into which molecules can penetrate. This form of structure gives zeolite the characteristic of a polar adsorbent. Zeolite as an adsorbent is used for drying agents, deodorants, adsorbents for air separation, ion exchangers for water purification (especially for removing ammonium ion and heavy metal ions), and for water softening, soil upgrading, and so on [177]. Zeolites are used in the petrochemical and petroleum refining industries as ion exchangers, adsorbents, and selective catalysts [178], and have a high affinity for polar molecules such as H_2O and CO_2. Breck (1974) found at ambient temperature and pressure competitive adsorption using zeolite is typically of the order $H_2O>CO_2>N_2>O_2$ [179]. Thus, it is more challenging to separate CO_2 from flue gas containing water by the use of zeolite as adsorbent.

2.4.5.4. Metal Organic Frameworks

Metal-organic frameworks (MOFs) are easy to synthesize and have permanent porous structures able to operate as a molecular sieve or as a storage device for some gases [180]. Thus, MOFs are developing rapidly as materials for selectivity adsorbing CO_2 [181]. MOFs are highly porous[182], and thermally stable. [183] Also they can be made in large quantities from low-cost ingredients. In addition, they can be designed for a specific pore size, and functionality can be added to the pores [184]. MOFs exhibit higher CO_2 adsorption capacities than traditional zeolites and other porous material reported [185]. Some MOFs can selectively adsorb CO_2 from mixture with N_2 or CH_4 at both sub-atmospheric pressures and high pressures [186]. Yazaydin *et. al* (2009) through the presence of water molecules coordinated to metal sites in the framework, have shown that CO_2 adsorption in $Cu_3(btc)_2$ (HKUST-1 or Cu-BTC, btc-1,3,5-benzenetricarboxylate) was significantly high. [187]

2.4.6. Modification of surface characteristic of adsorbents

Most physical CO_2 adsorbents such as 13X zeolite,[188, 189] activated carbons, [190, 191] unmodified periodic mesoporous silicas, [192] and metal-organic frameworks (MOFs)[193] present a drawbacks according to the conditions of adsorption operation which require large pressure and/ or temperature gradients between the adsorption and desorption stages in order to perform efficient adsorption and adequate regenerability. Additionally, they display relatively low selectivity toward CO_2 and mostly low tolerance to water vapour in the gas feed, and their CO_2 separation performance decreases significantly at increasing temperature.

The surface characteristics of an adsorbent can be technically subjected to modification in order to improve the affinity or/and the interaction potential between adsorbent and adsorbate for adsorption capacity enhancement. In the mixture of the gas, the adsorbent preferentially adsorbs the molecule where it has greater affinity. The application of chemicals on a given adsorbent will either modify the chemical surface of the adsorbent or/ and change the geometry/structure that includes surface area, pore volume and pore size. Nowadays, with the use of amine, there is a trend of modification of chemical surface of adsorbent for CO_2 capture, due to the fact that the chemical reaction of amine and CO_2 results in carbamate formation which is a reversible bond. However, amine degradation and the energy intensive nature of the regeneration process, motivate alternative approaches; the separation of CO_2

from low pressure stream gases by amines is recognized as an effective technology for CO_2 capture [194, 195, 196]. Monoethanolamine (MEA) has been the most common adsorbent in absorption technology for CO_2 capture plants leading to carbamate formation in aqueous solution. The chemical engineering literature has shown considerable number of publications on carbamate formation [197, 198, 199]. In the prominent mechanism of carbamate formation, Caplow (1968) [200] originnally showed the formation of a zwitterionic form of the carbamate, followed by a slow proton exchange reaction with a base. Furthermore, this carbamate formation mechanism, as showed below, has been used in many instances [201].

$$CO_2 + RNH_2 \leftrightarrow RNH_2^+CO_2^- \quad (2.20)$$

$$RNH_2^+CO_2^- + B \leftrightarrow RNHCO_2^- + BH^+ \quad (2.21)$$

During the reaction amine and CO_2, the amides obtained through carbamate formation cannot protonate easily, because they are very weak bases compared to amine itself. Consequently, the released proton is captured by the amine to form an ammonium complex, according to the following reaction:

$$2RNH_2 + CO_2 \leftrightarrow RNHCO_2^- + RNH_3^+ \quad (2.22)$$

Many types of adsorbents with amine surface modification have been reported, including amine-tethered silica materials [202, 203, 204, 205], activated carbon, zeolite and carbon nanotubes [206]. Chungsying Lu et al. (2008) [142] investigated the adsorption behaviour of zeolite, granular activated carbon (GAC), and carbon nanotubes (CNTs), and also their modified surface in CO_2 capture using 3-aminopropyl-triethoxysilane. Under the same conditions, the modified surface of these adsorbents have shown high CO_2 adsorption capacity, where the modified CNTs possess the greatest followed by the modified zeolites, and then the modified GAC.

A big challenge of the use of amine is related to health risks; the wide-scale deployment of CCS requires that health, safety and environmental risks are identified and minimized [207, 208, 209, 210]. The identification of a risk can lead to the performance of new studies to circumvent the risk in order to design and operate an amine based CO_2 capture plant without any health and environmental risks.

For a long-time, polymers have been used as an adsorbent for volatile organic compounds [211]. While the pores of polymers can range from macro-porous through molecular sizes, the application of polymeric adsorbents has been limited due to the lack of very small micropores. These days researchers focus on polymers containing amine group [212] in order to increase the affinity of the adsorbent with CO_2. Such polymers have a promising potential for large CO_2 capture capacity respective to the large number of amine group in monomer along the polymer intended to be converted to reversible carbamate. Thus, a long chain polymer grafted with an amine group will capture more CO_2 than a short chain polymer. The selection of polymers must be done with the aim to maximize their potential as polymeric adsorbents through the decrease of toxicity, and (or) the increase of adsorptivity index of CO_2. Accordingly, they must meet certain requirements which include biodegradability, biocompatibility, and chemical composition.

The most common polymer with amine group investigated for CO_2 capture is Poly(ethylenenimine) (PEI) [213, 214, 215, 216]; the structure is shown in Figure 2. 11 Eoghan *et al* (2008) [199], by increasing the molecular weight of PEI from 6000, 10000 to 25000, found that the capacity of CO_2 capture increased respectively. However, PEI is extremely toxic [217], due to two different mechanisms [218]: 1) the disruption of the cell membrane leading to necrotic cell death (immediate), and 2) the disruption of the mitochondrial membrane after internalisation leading to apoptosis (delayed). In addition, Yuting, *et al* (2008) [219] showed that the PEI becomes more toxic and non-biodegradable at higher molecular weights.

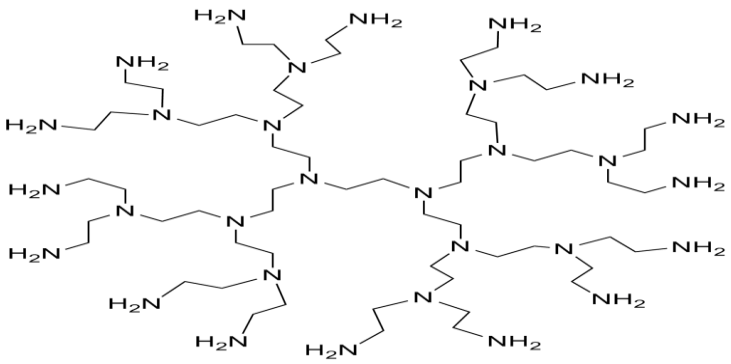


Figure 2.11: Polyethylenenimine structure [220]

Carbon nanotubes (CNTs) have recently gained popularity as potential gas carriers due to their high surface area, enhanced porosity, superior thermal conductivity, and mechanical, and electrical properties [221]. CNTs are categorized as single-walled nanotubes (SWNTs) and

multi-walled nanotubes (MWNTs) with single and multiple rolled layers of graphene respectively. However, due to the hydrophobic and inert nature of the surface of CNTs, modification of the surface is necessary in order to improve the interaction of CNTs and foreign molecules [222]. This manner of modifying the surface of nanotubes results in the functionalization of the CNTs.

The functionalization of MWNTs includes covalent functionalization and non-covalent functionalization. In the covalent functionalization the chemical reactions form bonds on the nanotube sidewalls, resulting sometimes in a change in structure. Non-covalent functionalization of MWNTs can be modified with amphiphilic surfactant molecules or polymers. The non-covalent dispersion of MWNTs in a solution allows preservation of their aromatic structure and thus their electronic characteristics [223]. In addition, the physical properties of MWNTs are essentially preserved by the non-covalent approach.

The functionalization of CNTs with polymers has been beneficial to circumvent the challenge related to polymer macropore capacity, and has extended the application of polymers as adsorbents with micropores. It has been shown that SWNT will be attached by more than two up to five polymers [206], while a polymer grafted with amine can present many available sites for CO_2 trapping, as shown in Figures 2.12 and 2.13. Aiming to trap CO_2, the integration of CNTs with functional groups, specifically amines, has been found to be good for high selectivity toward CO_2. [202]

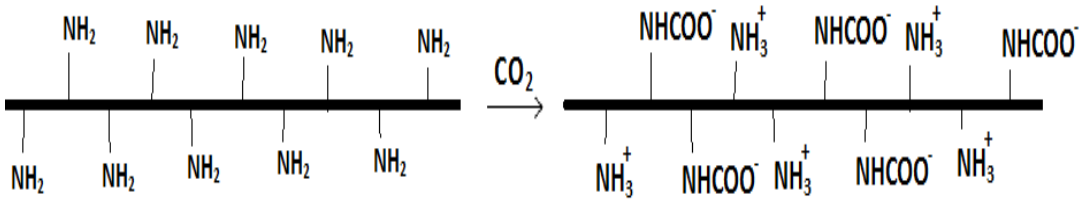


Figure 2.12: Chemical Structure of Polymer grafted with amine and CO_2 in reaction [224]

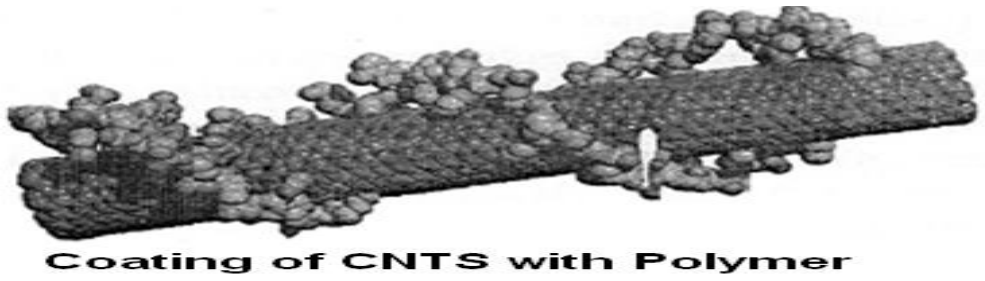


Figure 2.13: Structure of coating of CNTs with polymer [225]

In this work an adsorbent tailor-made will be designed from a long chain polymer (molecular weight > 50000) grafted with amine for CO_2 trapping, covering MWNTs for structure/ geometry enhancement. The synthesized polymer will have high molecular weight, being polysuccinide (PSI) with diamines, resulting in (polyaspartamide) PAA production. The synthesized PAA will cover MWNTs to enhance the adsorbent characteristics. The synthetic polymers, presenting high CO_2 adsorption capacity, are tailor-made in accordance with the general requirement to be fulfilled by any polymer in the attempt to serve in a biological environment with their minimal entire molecular-weight distribution of 50000. These synthetic polymers are categorized according to the chemical nature (*e.g.* polysaccharides, vinylic, acrylic polymers, poly(amino acids), etc.), the stability of the backbone, and the molecular weight. In recent years, intensive studies of poly(amino acids) have been performed, motivated by the definite advantages these polymers have over other macromolecules generally used as drug carriers. The first poly(amino acid) whose plasma expander property was investigated was poly(glutamic acid) [226]. However, the results were not encouraging, the compound proved to be toxic [227, 228]. Therefore, the interest for the preparation of uncharged poly(amino acids) as plasma expander rose. In this respect, the polycondensation of aspartic acid at the temperature range 190 - 250 ˚C was used to synthesize poly(succinimide) (PSI) with high molecular weight (> 640000) [229] and closed ring (Fig. 2.14); this exhibited special properties, such as biocompatibility, biodegradability [230], and non-toxicity [231]. The PSI can be lengthened by the use of Dicyclohexylcarbodiimide (DCC) [232] as a coupling agent. Due to its long chain, ease to open the ring by amine action, and ability to retard renal clearance, PSI has been chosen as the best macromolecular carrier for drug delivery [233, 234, 235]. Moreover, PSI is used in engine oil compositions of various viscosity grades as dispersants, with complementary antifriction efficiency, and some conventional detergent, antioxidant, antiwear, and anticorrosion engine oil additives [236, 237]. Thus highlights the choice made to use PAA a polymer with PSI as the backbone incorporated with diamine (NH_2-R-NH_2), as shown in Figure 2.15; here one amine is grafted to the backbone in order to open the ring for amide formation, and another remains available for CO_2 trapping. The amide group is a biofissionable bond able to be broken under enzymatic or hydrolytic actions. This gives to the PAA the characteristic of biodegradability. In addition, the diamine must be totally fixed in the PAA without excess; excess amine can increase the health and environmental risks, and material corrosion as well.

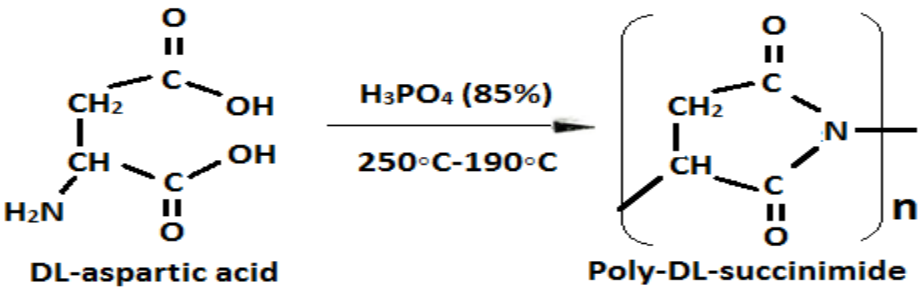


Figure 2.14: Polycondensation of aspartic acid for Poly-DL-succinimide synthesis [238]

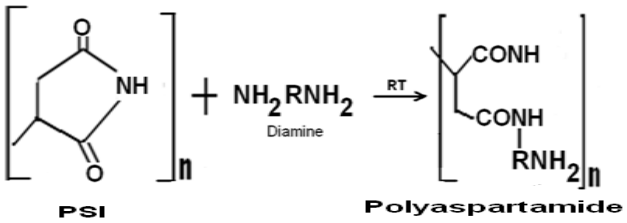


Figure: 2.15: PSI grafted to diamine for Polyaspartamide synthesis [239]

For the choice of diamine, a large commercial availability must be considered in order to enssure continuous operation of the adsorption unit. Ethylenediamine (EDA), an organic compound with the formula $C_2H_4(NH_2)_2$, is the most commercialized diamine with a worldwide yearly production of approximately 0.5 Mt [240]. EDA has large applications that include bleach activator, chelating agents, corrosion inhibitors, elastomeric, fibbers, fungicides, fuel additives, mineral processing aids, pharmaceutical intermediate, plastic lubricants, polyamide, resins and rubber processing additives, textile additives, and urethane chemicals [241]. The choice of 1,3 propanediamine (PDA), an organic compound $[C_3H_6(NH_2)_2]$ was beneficial in order to investigate the behaviour of polyaspartamide using diamines with variable alkanes for CO_2 capture. Monoethanolamine (MEA), having both amine and phenol groups, is used in aqueous solutions to remove CO_2 from flue gas.

2.4.7. Moisture effects on adsorbents for CO_2 capture

The flue gas from combustion power plants generally includes some moisture in its composition, originating mostly from the combustion of H_2, or sometimes also from the crude materials containing moisture before combustion. During the combustion process of fossil fuel, carbon and hydrogen are converted to CO_2 and H_2O respectively. The presence of

moisture in the flue gas becomes a challenge for CO_2 adsorption efficiency, due to either the affinity of H_2O over CO_2 for a given adsorbent, or the possible pore blockage preventing the CO_2 from finding available sites for adsorption. Jadhav *et al.* [242] found that hydrophilic materials, such as 13X zeolite, decrease the CO_2 adsorption capacity in the presence of moisture. Su *et al.* [243] stated that hydrophobic materials, such as CNTs, experience an increase of CO_2 adsorption capacity in the presence of moisture.

With regard to amine adsorbents, it is noticeable that the reaction of CO_2 with amine results in carbamate formation, as shown in Equation (2.22) where the stoichiometry gives 0.5molCO_2/mol. Concerning CO_2 in the presence of moisture, there is the formation of carbonate due to the amphoteric aspect of H_2O which behaves as base and acid by releasing OH^- and H^+ to CO_2 and amine in order to make HCO_3^- and RNH_3^+, as shown in Equations (2.23) and (2.24) [244].

$$RNH_2 + CO_2 + H_2O \longleftrightarrow RNH_3^+ + HCO_3^- \quad (2.23)$$

$$R_2NH + CO_2 + H_2O \longleftrightarrow R_2NH_2^+ + HCO_3^- \quad (2.24)$$

Thus, the stoichiometry evaluation of Equations (2.23) and (2.24) show the amount of 1molCO_2/mol. The CO_2 uptake obtained for the flue gas with moisture has doubled compared to the dry flue gas. This shows that the amine adsorbent has the potential to increase the CO_2 adsorption capacity by 100% from dry flue gas to flue gas with moisture content. Peter *et al.* [245] shown the increase of CO_2 adsorption capacity with mesoporous silicas synthesis and triamine silane grafting, in the flue gas with moisture. Huang *et al.* [246] shown that the CO_2 adsorption capacities of monoamine grafted on silica-based and silica xerogel doubled from dry flue gas to a more humid flue gas. Hiyoshi *et al.* [247], studying the effect of amine and moisture on CO_2 adsorption performance for various amines grafted onto SBA-15, found a slight decrease of CO_2 uptake when using monaamino and slight increase when using both diamino and triamino. Thus the statement saying that the CO_2 adsorption performance is relative to amine density. The modification of the chemical surface of Y-type zeolite by the use of tetraethylenepentamine (TEPA) resulted in an increase of CO_2 adsorption capacity from dry flue gas to flue gas containing. [248] Wurzbacher, *et. al.* [249] investigated the adsorbent diamine-functionalized silica gel, and concluded that the CO_2 adsorption capacity is higher in flue gas with moisture content than in dry flue gas.

The adsorbent MWNT-PAA designed in this work presents the potential of hydrophobicity due to combination of MWNT, which is highly hydrophobic, and the polymer PAA, which is water insoluble. Furthermore, the presence of amine in MWNT-PAA procures the ability of carbonate formation in the presence of water. Therefore, it is predictable for the CO_2 adsorption capacity to be higher in the presence of flue gas with moisture content than dry flue gas when using the adsorbent MWNT-PAA for CO_2 adsorption.

2.4.8. Specific Characterization for adsorbents evaluation

2.4.8.1. Nuclear magnetic resonance spectroscopy

Nuclear magnetic resonance spectroscopy (NMR) is an analytical technique which provides information on the magnetic properties of the center of an atom (nucleus) which contains protons and neutrons. The principle of NMR is based on specific resonance that an intramolecular magnetic field around an atom in a molecule can change in order to give access to details of the electronic structure of a molecule [250]. Therefore, NMR is used to determine the content and purity of a sample, as well as its molecular structure. Through the NMR, it is possible to qualitatively analyse mixtures containing known compounds. The NMR is active in the magnetic field of ^{1}H (proton) or ^{13}C (carbon) where electromagnetic radiation can be absorbed at a frequency characteristic of the isotope. [251]

2.4.8.2. Fourier transform infrared spectroscopy and Raman spectra

Fourier transform infrared spectroscopy (FTIR) and Raman spectra both probe molecular vibrations, and they are often used for similar analytical problems, with FTIR being more commonly used.

FTIR is an analytical technique which provides information for a solid, liquid or gas through infrared spectrum captured by absorption, emission, or photoconductivity [252]. It is noticeable

that every atom or molecule vibrates at a specific frequency which is related to a wave number. Thus, the principle of FTIR analysis is based on the absorption of infrared of matter, causing the increase of vibration energy in atoms or molecules within the matter. Consequently, the link between atoms will be excited and stretched in a certain band or region with emission of infrared respectively [253]. FTIR analysis is helpful for the identification of the molecules or atoms in substance. The advantages of FTIR spectroscopy are as follows: spectra provide much information; the analysis is relatively fast and easy; it is relatively inexpensive and sensitive [254]. However, FTIR cannot detect some molecules, including sp^2-hybidized carbons, and finds challenges for mixtures with water.

2.4.8.3. High resolution transmission electron microscope

High resolution transmission electron microscope (HR-TEM) enables straightforward imaging of the atomic structure of the sample [255.] HR-TEM is intended to study nanomaterials; therefore it operates at a high-magnification in order to analyse the nanomaterial by imaging on the atomic scale. The HR-TEM has an advantage of analysing crystal structures and lattice imperfections in different types of advanced materials on an atomic resolution scale and can characterize point defects, dislocations, and surface morphology [256, 257, 258].

2.4.8.4. Brunauer, Emmett, and Teller

The surface area, pore volume and pore size of adsorbents were determined by using the Brunauer, Emmett, and Teller (BET) equation (3.1). BET have proposed the theory of multilayer which is adsorption applied principally to physical adsorption isotherms. The BET equation is recognized as an excellent method of estimating surface areas [259].

$$V/V_m = \sum_0^\infty iS_i \Big/ \sum_0^\infty S_i \qquad (3.1)$$

Where V is the number of adsorbed gas molecules, V_m the number of molecules required to form a monolayer, and S_i is the number of sites covered with stacks *i* molecules high.

2.4.8.5. Thermogravimetric analyser

Thermogravimetry analysis (TGA) is a domain of thermal analysis which gives information on the mass change of a sample versus temperature in the scanning mode or versus time in the isothermal mode, and therefore operates to provide information on the decomposition and thermal stability of materials. Thermal events including desorption, sorption, sublimation, vaporization, oxidation, reduction and decomposition bring about a change in the mass of sample [260]; conversely, the thermal events including melting, crystallization or glass transition are not associated with a change in the mass of the sample [261]. TGA curves are produced relating the unique sequence of the physicochemical processes, dependent on the molecular structure of the sample, that occurs over specific temperature ranges and heating rates. TGA curves are normally plotted with the mass change (Δm) expressed as a percentage on the vertical axis and temperature (T) or time on the horizontal axis.

Several research projects were successfully done on the evaluation of CO_2 adsorption capacity and the regenerability of the adsorbents using TGA [262, 263, 264]. In addition, Heydari-Gorji *et al.* (2011), using the TGA for the investigation of CO_2 adsorption through polyethylenimine (PEI)-impregnated mesoporous silica, found that at low temperature the adsorbent with relatively low PEI contents are more efficient than their highly loaded counterparts[265]. Xu *et al.* (2004), operating at 75 °C for CO_2 adsorption using the TGA through the mesoporous molecular sieve MCM-41 loaded with PEI, found that the CO_2 adsorption capacity was higher when using linear PEI than branch PEI [266]. The regenerability of the adsorbent ethylenediamine-modified SBA-15 was investigated by Zeng *et al.* (2004) using TGA [267].

2.5. SUMMARY

Large quantity of CO_2 is emitted principally from the burning of fossil fuels and from some industrial and resource extraction processes. In all fossil fuels, the burning of coal is the most generating CO_2 emissions in the atmosphere; however, coal has the advantage of low-cost and high energy production [28]. Biomass contains negligible amounts of sulphur and nitrogen, and it can be used for energy production with reduced CO_2 emissions. Though, the combustion is not feasible for biomass containing moisture. Increased moisture means less energy available for the boiler [268].

Carbon dioxide capture and storage (CCS), is one of approaches for reducing anthropogenic CO_2 emissions in the atmosphere. The application of CCS to large point sources of CO_2, such as power plants or large industrial processes is the most preferentially developed approach to accelerate the mitigation of climate change caused by enormous CO_2 emissions in the atmosphere. CCS involves the use of technology, first to capture large quantity of CO_2 at the concentration above 90% [25], to transport it after compression to a suitable storage location where it will stay away from the atmosphere for a long period of time. The economy evaluation of CCS includes the cost relevant to the CO_2 capture, transport and storage taking into account all requirements to achieve advanced technologies with minimum risk and suitable energy penalty.

The CO_2 capture technologies using absorption, adsorption, membranes and cryogenic are intended to be efficiently applied in post-combustion, pre-combustion and oxy-fuel combustion. Using absorption technology, MEA is the chemical solvent mostly utilised for CO_2 capture [114]; however, more investigations are being done to improve its efficiency due to oxidation degradation, material corrosion and high energy for regeneration. The adsorption technology with the property of purification or bulk separation is still in development for CO_2 capture. Thus, the CO_2 adsorption requires specific adsorbents operating preferentially in fixed, moving or fluidized bed with efficient regeneration respective to the system operating in TSA, PSA, VSA or ESA.

The existing adsorbents including activated carbon, silica gel, zeolites and MOFs have been found inefficient regarding the capturing of CO_2 at the threshold limit requirement. Therefore, the design of specific adsorbents for CO_2 capture has been of great importance. This requires good potential interaction through good geometry/structure and adequate chemical surface. The application of nanotechnology through the use of carbon nanotubes is the most investigated to improve the mechanical and electronic properties including geometry/structure (surface area, pore volume and pore size) of solid materials. The amine has the potential to form a reversible carbamate or a reversible carbonate when reacted with CO_2 or moist CO_2 respectively. Consequently, the grafted of amine to the solid has been investigated as a good alternative to improve the chemical surface of the adsorbents which are intended to capture CO_2.

Amine polymers have a promising potential for large CO_2 capture which increases with the longest chain polymer [210]. The use of polysuccinimide grafted with amine to give a polyaspartamide presents an amide bond as biodegradable potential and a primary amine as CO_2 anchoring site potential.

Furthermore, it has been investigated that amine adsorbents have the potential of doubling the CO_2 adsorption capacity when the CO_2 is mixed with water compared to the dry CO_2 [194, 234]. Because, the water and CO_2 will lead to carbonate formation which in stoichiometric evaluation requires one mol of amine for one mol of CO_2. While for carbamate occurrence one mol of amine captures half mol of CO_2.

Thus, the implementation of adequate adsorbent for CO_2 capture needs the experimental to investigate the improvement of factors such as geometry/structure and chemical surface modification resulting in biodegradability, large CO_2 adsorption capacity, efficient adsorption kinetics, effective regeneration and efficient energy for the overall adsorption system.

CHAPTER THREE

METHODOLOGY

3.0. INTRODUCTION

This work presents the development of a novel adsorbent for CO_2 capture adsorption technology. The methodology has been set out with the intention to provide specific data for the achievement of the objectives provided in Chapter 1. The design of an adequate hydrophobic and biodegradable adsorbent required specific material with appropriate equipment design for chemical reaction and purification, resulting in MWNTs covered, via a non-covalent functionalization process, by a water insoluble polymer with a biofissionable bond. The testing of the performance of the adsorbents for CO_2 adsorption was achieved through the evaluation of factors which include CO_2 adsorption capacity, selectivity for CO_2, adsorption kinetics, water tolerance and regenerability using thermogravimetry analyser at different temperatures and constant pressure of 110 kPa (1.1 bar). Gases with different compositions of air with CO_2 at variable proportions (100, 40 and 14%) were fed through the TGA using dry and wet adsorbents. Furthermore, pure O_2 and N_2 were fed through the TGA at the same conditions in order to evaluate the selectivity for CO_2 over other gases. The regenerability efficiency of the adsorbent was evaluated through the percentage of CO_2 recovery, which is the ratio of the desorption curve and the adsorption curve. The evaluation of heat flow for a complete cycle of TSA systems, which includes sweeping, adsorption and desorption processes, was achieved after considering the differential heat of the segment and/or section making a loop as the output of heat flow versus temperature from the DSC. Finally, the evaluation of timing relevant to the sweeping, adsorption and desorption processes was a major factor to optimize the number of beds for the synchronization of TSA system.

The technique of designing the enhanced adsorbent was completed in three stages: 1) the synthesis of polysuccinimide (PSI) as the backbone, 2) the grafting of the amine onto the backbone to make polyaspartamide (PAA), and 3) the coating of the MWNT by PAA. Three amines, namely 1) ethylenediamine (EDA), 2) 1,3 propanediamine (PDA), and 3) monoethanolamine (MEA) were separately grafted to the PSI to produce different PAAs.

With the objective to enhance the CO_2 adsorption capacity, the PSI was grafted to amine to produce PAA with the requirement to have higher CO_2 adsorption capacity than PSI.

The designed adsorbents were tested using the necessary characterizations: 1) nuclear magnetic resonance spectra (NMR), 2) Fourier transform infrared (FTIR), 3) high resolution transmission electron microscope (HRTEM), 4) Brunauer, Emmett, and Teller (BET), and 5) thermogrametric analyser (TGA).

3.1. EQUIPMENT AND CHEMICALS

3.1.1. Equipment

The chemical reactions were performed in a laboratory fumehood (Mode: LA1500EFC & Serial No: 2511008-E) in the School of Chemical and Metallurgical Engineering at the University of the Witwatersrand (Wits). A Rotavapor R-114 & heater vessel was used for polycondensation to produce the polymer, and Rotavapor R-210 for the evaporation to eliminate solvent in the compound. The chemical reactions to produce PAAs and MWNT-PAAs were done in a reactor with a magnetic bar inside a flask placed on a plate heater with a magnetic stirrer. An Oven LabCon (EGO4 (50 - 300 °C)) was used for routinely drying samples.

3.1.2. Chemicals

Commercially available MWNTs with a diameter of < 8 nm (purchased from Cheap Tubes: www.cheaptubes.com) were used as the basis chemical product. The length of MWNTs was in the range of 10-30 μm, the purity > 95wt%, Ash < 1.5wt%, SSA > 500m^2/g, EC >10^2-s/cm and SKU 030101. This data was provided by the manufacturer.

The hydroxyamines and amines were of analytical grade obtained from Aldrich Chemie, Fluka AG, South Africa. These included: D,L aspartic acid, ethylenediamine (EDA), 1,3 diaminopropane (PDA), monoethanolamine (MEA) and dicyclohexylcarbodiimide (DCC).

Different bases and acids including ammonium hydroxide, sodium hydroxide, sodium bicarbonate, sodium carbonate, hydrochloric acid, glacial acetic acid, phosphoric acid, sulphuric acid and nitric acid were occasionally used for the cleaning of the products.

Distilled water was used for preparative work. All reactions were run in the solvent, N,N-dimethylformamide (DMF) with 99.8% purity. All other solvents, Diethyl ether (Et_2O), hexane, acetone and toluene, were of laboratory grade, received from unit 11 Fedsure Park Midrand South Africa.

3.2. CHARACTERIZATION

In this work the following characterization was found necessary for sample evaluation:

- Proton nuclear magnetic resonance (^{1}H NMR) spectra performed in the School of Chemistry at Wits were recorded on a Bruker AVANCE III 500 at 500.13 MHz. These spectra were used in order to gain information about the purity of PSI and PAA where excess of amine was avoided. ^{1}H NMR spectra were recorded on a Bruker AVANCE III 500 at 500.13 MHz. Spectra were recorded in deuterium oxide (D_2O) solution. The chemical shifts, δ in ppm, were referenced against sodium 3-(tetramethylsilane)-2, 2, 3, 3-d_4 propionate (TMS), which occurs at zero ppm for ^{1}H NMR. The pH values of the sample in D_2O solution were adjusted to 10-11 by adding sodium hydroxide in order to eliminate potential protonation effect.
- Fourier transform infrared (FTIR) was used in order to prove the presence of the primary amine group (NH_2) and amide (CONH) as CO_2 anchoring site and biodegradable bonds respectively in the synthesized adsorbents. Solid-state FTIR spectra were recorded with KBr pellets over the region of 4000-600 cm^{-1}. Only the significant bands were considered. The Raman spectra were used to identify the

integrity of sp^2-hybridized carbon atoms and the existence of carbon containing defects of the MWNTs. FTIR and Raman spectrometry were performed in the Schools of Chemistry and Physics at Wits.

- The morphology of adsorbents was analysed using a High resolution transmission electron microscope (HR-TEM), model JEM-100S, in the School of Biology at Wits.
- The geometry/structure which includes surface area, pore volume and pore size was analysed using Brunauer, Emmet, and Teller (BET) in the School of Chemistry at Wits.
- The thermal stability, the adsorption and desorption capacities, and the thermodynamic studies of the samples, were determined by the use of a Simultaneous DSC-TGA Q Series instrument, or SDT Q600 (Fig. 3.1), housed in the School of Chemical and Metallurgical Engineering at Wits. The SDT Q600 is an analysis instrument capable of performing both differential scanning calorimetry (DSC) and thermogravimetric analysis (TGA) at the same time. The SDT Q600 has an advantage of furnishing data about the heat flow and weight changes associated with transitions and reactions in materials over the temperature range ambient to 1500 °C. The data provided by the SDT Q600 are beneficial for the thermodynamic studies of the material through the knowledge of endothermic and exothermic events regarding the physicochemical process of the material. This information helps the scientist or engineer to identify processing and end-use performance. Furthermore, performing both DSC and TGA measurements at the same time, on the same instrument and same sample, offers greater productivity and removes experimental and sampling variables as factors in the analysis of data [269]. The simultaneous DSC-TGA works in conjunction with a controller and associated software.

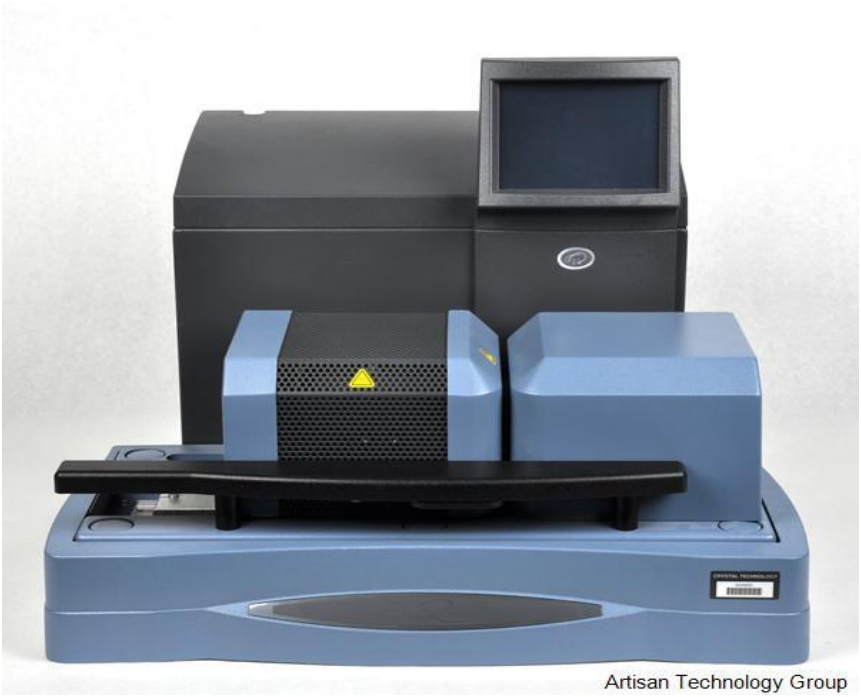


Figure 3.1: Thermogravimetry analyzer of type TA-Q600 [270]

3.3. EXPERIMENTAL PROCEDURE

The synthesis of adsorbents started by the preparation of the polysuccinimide (PSI) which was made through polycondensation of aspartic acid in a phosphoric acid medium, resulting in a short chain PSI. A long chain PSI as backbone will provide large number of monomers with NH_2 when grafted to amine; leading to high potential CO_2 anchoring. Therefore, a coupling agent named dicyclohexylcarbodiimide (DCC) was necessary in order to lengthen the polymer chain through the attachment of a minimum of two PSI short chains together, resulting in a long chain PSI. The anhydrous hydrophobic and biodegradable PSI long chain, henceforth named PSI, was used as a CO_2 adsorbent, and was further subjected to treatment for the production of different adsorbents to enhance CO_2 uptake. The grafting of amine to the PSI is a delicate process which can lead to the polymer crosslinking when the amine used contains more than one amine group. Therefore in the grafting process of amine to PSI the conditions of operation are very specific for EDA and PDA, which are diamines; MEA is a monoamine which requires less attention. The polymer crosslinking must be avoided, because the presence of NH_2 as potential available site for CO_2 uptake is reduced. The process of polymer crosslinking synthesis is deliberately used to obtain a plastic structure as nonporous materials taking the form of a crystalline, rigid unit in a glassy state [271]. These

materials are not favourable for any adsorption process. The crosslinking occurs when both right and left extreme primary amines of NH_2-R-NH_2 react with the PSI. An unreacted diamine (NH_2-R-NH_2) is always more reactive than the reacted one (-NH-R-NH_2). This means that the next reaction is always an opportunity for an unreacted diamine to become reacted. Consequently, the following conditions must be respected during the reaction:

a) Considering that –NH-R-NH_2 (after reaction) is less reactive than NH_2-R-NH_2, excess diamine is required to prevent the reaction between the polymer and –NH-R-NH_2.

b) A low temperature is needed in order to promote a slow reaction between the polymer and diamine. This will allow the unreacted diamine (NH_2-R-NH_2) to control the reaction over the reacted diamine (-NH-R-NH_2).

c) The polymer solution must be released dropwise into the solution for the limitation of available sites that NH_2-R-NH_2 should totally hold by prevailing over –NH-R-NH_2.

d) In addition, the reaction must be performed under strictly anhydrous conditions in order to avoid unwanted hydrolytic ring opening, resulting in the generation of free carboxylic side group.

Three types of polyaspartamide (PAA) were synthesized from EDA, PDA and MEA.

In the process of enhancing the adsorptivity of the adsorbents, PSI and PAA were both used to coat MWNTs in a non-covalent functionalization process for the preserve of the functionality, which includes the biodegradability and the CO_2 anchoring sites.

Following the adsorbent selection, all types were tested under 100% CO_2 using the TGA at 25 °C and 1.1 bar. Successful adsorbents were subjected to further tests. The adsorbent synthesis is discussed in further detail below.

3.3.1. Detailed description of adsorbents synthesis

3.3.1.1. Design of polyaspartamides (PAAs)

With the objective to elaborate the adsorbent models for CO_2 capture, an attempt was made to

use tailor-made adsorbent through the design and derivation of several synthetic polymeric structures. This possibly will prevent the destruction of polymer and provide an adequate adsorption of CO_2 in flue gas with high selectivity and efficient regenerability. Note that the synthesis by biodegradable conjugation of selected adsorbent models with hydrophobicity, and CO_2 affinity evaluation of the resulting adsorbents, are two objectives to be fulfilled in respect of necessary prerequisites for any polymer intended to serve in CO_2 adsorption technology. The polymeric adsorbents used for the anchoring of CO_2 fell into the wide aliphatic polyamide type (schematized below) with subunits randomly distributed along the chain. F represents the extra functional group capable of reversible CO_2 anchoring and y represents the degree of polymerization (Fig.3.2).

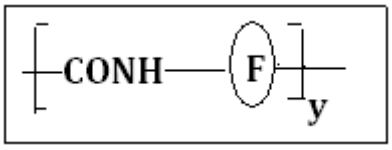


Figure 3.2: Structure of polyamide-type carrier

In this study, to provide an access to the polymer-CO_2 binding via carbamate bond formation, a primary amino group was found important. The most important point is that the amide bond performs the ability to develop biofission, which results in enzymatic activity in the internal structure of the polymer, causes the polymer release from the cleavage space. The incorporation of subunits of the preset structures, by the use of multi-walled carbon nanotubes (MWNTs), will be necessarily important to afford tailor-made adsorbents that are equipped with all required functions. This allows efficacious adsorption properties including geometry/structure, and enhanced selectivity for CO_2. Thus, a non-covalent functionalization of the MWNTs by the designed polymer is necessary in order to conserve the functionality of the polymer. The adsorbents were designed to be hydrophobic with the amine grafted totally on the long chain polymer to provide high selectivity for CO_2.

The polyamide conforming to the basic adsorbent models (Figure 2.10), namely Polyaspartamide (PAA) was used for CO_2 conjugation by carbamate bond formation. The primary amine functional groups of these polymers were introduced as terminals in component **F** (Figure 4.1). With the recognition of the incorporation of CO_2 from **F**-labeled subunits of the primary-amine, the polymer containing larger mole percentages of **F**-labeled

subunits will be needed for utilization of an unduly large excess of CO_2 to provide high CO_2 adsorption capacity. The purification of polymeric adsorbents was completed by water, toluene and acetone to remove the excess of aspartic acid, amine and solvent respectively.

3.3.1.2. Preparation of poly-αß-DL-succinimide (PSI)

The preparation of PSI, a long chain polymer, used as backbone in PAAs required efficient method assessed to be viable in terms of simplicity of technology, energy efficiency and economy cost for the achievement of favorite product.

The polymerization of N-carboxyanhydride of α-amino acid in general (NCA method) [272] and thermal phosphoric acid-catalyzed polycondensation of aspartic acid (Neri method) [273] are two different methods that occur in literature for the synthesis of polysuccinimide (PSI). The protection of the pendent reactive groups carried by the amino acid and their disclosure under harsh consideration as required in the NCA method in order to produce poly (amino acid) are very challenging. This will need large amounts of phosgene, disphosgene or triphosgene, as reagent widely used for the synthesis of N-carboxyanhydride. This raised complex safety problems in large-scale plants. Thus, the NCA method has been found disadvantageous both in cost and production. On the contrary, the Neri method has an advantage of producing high molecular weight PSI in one step [274]. Therefore, this approach was adopted for the synthesis of poly-DL-succinimide (PSI) from DL aspartic acid as shown in Figure 2. 9. A coupling agent dicyclohexylcarbodiimide (DCC) was added to the crude polymer for further chain extension purposes. A representative polymer had a relative viscosity of 36 mL g-1 in DMF at 30 ºC, which corresponds to a weight-average molecular weight of 32000.

The PSI was therefore synthesized according to the following stages:

1) A mixture of D.L. aspartic acid (50 g) and H_3PO_4 (25 g) was homogenized in a 2 L round-bottom flask, and the flask was placed in an oil bath at 250 ˚C. During polymerization, the expansion of the mixture was controlled by nitrogen. The reaction was allowed to proceed at 250 ˚C until the end of expansion. Note that during the expansion, the polymer spreads around the round flask reactor. Thereafter, the temperature was reduced to 190 ˚C for another 2 hours. The resultant product, being

very acid, was washed with water until 6 < pH < 7, and dried in an oven for 72 hours, thus producing a PSI, a short chain polymer.

2) In order to obtain a long chain PSI polymer, an appropriate coupling agent was applied to the short chain polymer, under specific conditions. Therefore, 15 g of PSI short chain polymer was dissolved in 60 ml of DMF and stirred overnight (O/N). The brownish solution obtained was stirred again for 1 hour in an ice bath, and 2.0 g of DCC added while the solution was stirred for another 4 hours in the ice bath. The solution was allowed to continue at room temperature (RT) O/N. The solution was centrifuged to give a clear solution, which was precipitated with distilled water. The precipitate was filtered, and kept in an oven for 48 hours, producing a brittle solid PSI long chain polymer reported as adsorbent in Table 3.1.

Table 3.1: List of adsorbents

Adsorbents Chemical composition
PSI
PSI-EDA
PSI-PDA
PSI-MEA
MWNT
MWNT-PSI
MWNT-PSI-EDA
MWNT-PSI-PDA
MWNT-PSI- MEA

3.3.1.3. PAA synthesis with PSI- EDA

As stated in Section 2.4.6, EDA as a diamine was used, because of its large commercial availability. Thus, the PSI (2.95 g; 30 mmol) was dissolved in DMF (37 ml). The resultant

solution was added dropwise to EDA (6.67 g; 45 mmol) in DMF (20 ml). The reactor was cooled in an ice bath to control the temperature below 5 °C. The solution was flushed with nitrogen gas and stirring continued for 20 hours in the ice bath, and for another 5 hours at 27 °C as room temperature. The solution was then concentrated on the roti-evaporator at 60 ˚C to reduce the volume by half. The polymer was precipitated out with a mixture of diethylether-hexane (2:1), and washed with hot toluene, followed by hot acetone several times to eliminate the excess of EDA and solvents respectively. After filtration, the precipitate was dried for 24 hours in the oven at a moderate temperature (40 °C) to give the final product PSI-EDA, a polysapartamide reported as adsorbent in Table 3.1.

3.3.1.4. PAA synthesis with PSI- PDA

PDA is a diamine with alkane which has more number of carbons than EDA. The reason why PDA was chosen is started material in Section 2.4.6; the purpose is to evaluate the behaviour of diamine with variable alkane radicals for CO_2 adsorption when grafted on PSI. Thus the PSI (2.95 g; 30 mmol) was dissolved in DMF (37 ml). The resultant solution was added dropwise to PDA (3.33 g; 45 mmol) in DMF (10 ml). The reactor was cooled in an ice bath to control the temperature below 5 °C. The solution was flushed with nitrogen gas and stirred continuously for 20 hours in the ice bath and for another 5 hours at room temperature. The solution was then concentrated on the roti-evaporator at 60 ˚C to reduce the volume by half. The polymer was precipitated with a mixture of diethylether-hexane (2:1). The precipitate was washed several times with hot toluene, followed by hot acetone to eliminate the excess of PDA and solvents. After filtration, the precipitate was dried for 24 hours in the oven at moderate temperature of 40 °C to give the final product PSI-PDA, a polysapartamide reported as adsorbent in Table 3.1.

3.3.1.5. PAA synthesis with PSI- MEA

Compared to the previous diamines, MEA is a monoamine and it was selected due to its large utilization for CO_2 adsorption technology, as discussed in Section 2.4.6.

The PSI (2.95 g; 30 mmol) was dissolved in DMF (37 ml), and MEA (2.5 g; 41 mmol) was added to the resultant solution at 27 °C at room temperature and stirred for 20 hours. The solution was then concentrated using the roti-evaporator at 60 °C to reduce the volume by half. The polymer was precipitated with diethylether, and washed several times with hot toluene, followed by hot acetone to eliminate the excess of MEA and solvents respectively. After filtration, the precipitate was dried for 24 hours in the oven at a moderate temperature of 40 °C to give the final product PSI-MEA, a polysapartamide reported as adsorbent in Table 3.1.

3.3.1.6. Coating MWNTs by PSI to give MWNTs-PSI

Using the commercial MWNTs discussed in Section 3.1.2, identified as in Table 3.1, 300 mg was dispersed by sonication in DMF (10 ml) for 15 minutes and mixed with 3 g of PSI dissolved in DMF (15 ml). After 3 days of stirring, the resultant solution was filtered and washed several times with hot toluene and acetone. The solid product was then dried at 40 °C in an oven for 24 hours, to give MWNTs-PSI as reported in Table 3.1.

3.3.1.7. Coating of MWNTs covered by PAA to give MWNT-PAA

The commercial MWNTs (300 mg) were dispersed by sonication in DMF (10 ml) for 15 minutes and mixed differently with 3 g of Polyaspartamides as follow: PSI-EDA, PSI-PDA and PSI-MEA respectively dissolved in DMF (15 ml). After 3 days of stirring, the resultant solution was filtered and washed several time with hot toluene and acetone. Solid product was then moderately dried at 40 °C in an oven for 24 hours to give MWNTs-PSI-EDA, MWNTs-PSI-PDA and MWNTs-PSI-MEA as reported in Table 3.1.

3.3.2. Adsorption experiments

3.3.2.1. CO_2 adsorption using the TGA

Adsorption tests were carried out using a TGA connected to an external mass flow controller, used to evaluate flow rate. For all the runs were performed flow rate was kept at a constant pressure of 1.1 bars (110 kPa). The first adsorption tests were run at the temperature of 25 °C using 100% CO_2 and the results obtained were used for the selection of polyaspartamides produced from EDA, PDA and MEA. Thus, a sample was swept in flowing N_2 (60 mL/min) at 110 °C for an isothermal time of 30 minutes, before the temperature was cooled to 25 °C as the desired adsorption temperature, and then exposed to flowing CO_2 (60 mL/min) isothermally for 180 minutes. The adsorption isothermal curve obtained was used to evaluate the CO_2 adsorption capacity, the CO_2 adsorption rate, and the adsorption kinetics.
Variable runs were used for the achievement of the adsorption experiments:

- Investigating the influence of temperature on CO_2 adsorption capacity for different adsorbents, N_2 (60 mL/min) was done by sweeping gas at 110 °C isothermally for 30 minutes, before the temperature was cooled to the desired temperatures: 25, 35, 45, 55, 65, 75, and 85 °C. The adsorbent was exposed to flowing CO_2 (60 mL/min) isothermally for 180 minutes. The different adsorption isothermal curves produced respective to the change of temperature were used to evaluate CO_2 adsorption capacity with regards to temperature.
- Regarding the selectivity for CO_2 over other gases, after sweeping with N_2 (60 mL/min) at 110 °C for 30 minutes, the adsorbents were exposed to pure N_2 (60 mL/min) and pure O_2 (60 mL/min) at different adsorption temperatures (25, 35, 45 and 55 °C) for 150 minutes. The N_2 and O_2 adsorption isothermal curves obtained were compared to CO_2 adsorption isothermal curves in order to evaluate the affinity of each gas on the different adsorbents.
- To test the efficiency of selected adsorbents in different CO_2 concentrations, the adsorbents were exposed simultaneously to the flow rates 14 mLCO_2/min and 86mLair/min to make a flue gas of 14% CO_2, and 40 mLCO_2/min and 60 mLair/min to make a flue gas of 40% CO_2. The adsorption tests were carried out at various temperatures: 25, 35, 45 and 55 °C, for 180 minutes. The purity of CO_2 after

adsorption was calculated according to the CO_2 concentration as the mathematic relationship below:

$$\%CO_2 = \frac{M_{Ads} - (N_{Ads} + O_{Ads})}{M_{Ads}} 100 \quad (3.2)$$

Where M_{Ads} is the adsorbed gas obtained from the adsorption using the gas mixtures of 14% CO_2 and 40% CO_2 with air. N_{Ads} and O_{Ads} are N_2 and O_2 adsorbed from pure N_2 and O_2 respectively. The purity of CO_2 was considered as minimum due to the following reasons: (a) the adsorbents were exposed to pure N_2 and O_2, because N_2 and O_2 are likely to occur in flue gas from power plants; (b) when an amine adsorbent is exposed to the flue gas mixture with CO_2, N_2 and O_2, CO_2 is expected to be captured preferentially to N_2 and O_2, due to its (CO_2) high affinity for amines.

- To evaluate water tolerance, the adsorbents were swept with N_2 as previously, and the run was interrupted in order to incorporate the moisture into the adsorbents. The quantity of water incorporated was 20% and 40%, calculated from the quantity of adsorbent remaining after the sweeping process. The wet adsorbent was exposed to pure O_2, 100% CO_2 and a gas mixture of 14% CO_2 with air, at various temperatures: 25, 35, 45 and 55 °C for 180 minutes. The adsorption isothermal curves were subjected to evaluation of selectivity for CO_2 as stated previously.

3.3.3. Desorption experiments

The regenerability testing of adsorbents was rendered possible through desorption process with the use of the TGA. Thus, the adsorbent was swept with N_2 (60mL/min) at 110 ◦C for 30 minutes. The temperature was cooled to 25 °C as a desired adsorption temperature where the adsorbent was exposed to CO_2 (60 mL/min) for 60 minutes. Afterwards, the CO_2 adsorbed was stripped from the adsorbent using N_2 (60 mL/min) as a purge gas at desired desorption temperatures, which varied as 90 °C and 100 °C. This operation of CO_2 adsorption and desorption was then repeated ten times in order to confirm the regenerability of the adsorbent. The isothermal curves were used for: (a) the evaluation of the percentage of CO_2 recovery obtained from the ratio of CO_2 desorbed and CO_2 adsorbed, considering the minimum and maximum of each isothermal curve; (b) the evaluation of differential heat flows of the different paths include in sweeping, adsorption and desorption processes for the

TSA system with variable adsorption temperatures (ranging from 25 to 55 °C); (c) finally the optimization of TSA systems for continued operation after evaluation of the heating and cooling times for possibly integration of the number of adsorption beds.

3.4. SUMMARY

The achievement of this work required specific chemicals and appropriate equipment for the design of hydrophobic and biodegradable adsorbent with a geometry/structure and chemical surface suitable for high potential interaction between the adsorbent and the adsorbate (CO_2). Different characterizations were applied to the adsorbents in order to predict the adsorptivity characteristic of the specimen prior to adsorption. The synthesis of PAA was obtained through the polycondensation of aspartic acid in phosphoric acid medium which, resulting in PSI, was grafted to amine. Three amines, being EDA, PDA and MEA were used to synthesize PAAs which include PSI-EDA, PSI-PDA and PSI-MEA respectively. The ^{1}H NMR was beneficial to evaluate the proportion of incorporation of amine in PAA. The FTIR was applied for the confirmation of the chemical structure of PAAs, including the presence of NH_2 group as CO_2 anchoring and CONH a biofissionable bond for biodegradability. The BET was necessary for the evaluation of the geometry/structure which includes surface area, pore volume and pore size. The TGA was used on one hand to evaluate the thermal stability for the operational temperature range of the adsorption. On the other hand the TGA was used for the adsorption with 100% CO_2 as gas steam at 25 °C and 1.1 bar in order to select the best PAA which should have a higher CO_2 adsorption capacity compared to PSI.

To improve the geometry structure, the selected PAA was applied for non-covalent functionalization with MWNT to give MWNT-PAA with the aim to preserve the functionality. Besides the FTIR and BET applied to MWNT-PAA with the same objective as done previously for PAA, more attention was given to the HRTEM to confirm the structure of MWNT, and to Raman spectra to confirm the coating of MWNT by PAA with the increase of carbon containing defect. Besides the thermal stability which was analysed through the TGA, both selected PAA and MWNT-PAA were exposed to the flowing of different gas stream of 100% CO_2, 100% N_2 and 100% O_2 in temperature range 25 – 55 °C at 1.1 bar for the evaluation of the affinity of each single gas to these adsorbents. To evaluate the influence of gas mixture with variable CO_2 concentration on CO_2 adsorption capacity, both selected PAA and MWNT-PAA were exposed through TGA to flowing of gas stream composed of

14% CO_2 and 40% CO_2 with air as balance. The adsorption was then performed in the same condition of temperature and pressure as done previously for the single gas.

The moisture test was rendered possible through the wettability of both PAA and MWNT-PAA at the proportion of 20 and 40%, which was further exposed to the flowing of different gas stream of 100% O_2, 100% CO_2 and gas mixture composed of 14% CO_2 with air as balance. The adsorption was run using TGA in the same condition of temperature and pressure as previously.

The regeneration of MWNT, PSI, PAA and MWNT-PAA was completed with the use of TGA for the 10 cycles adsorption-desorption for the adsorption temperature of 25 ℃ and desorption temperature of 90 and 100 ℃.

Using the simultaneous DSC-TGA it was possible to evaluate differential heat flows and the optimization of continuous TSA with integration of adsorption bed

CHAPTER FOUR

RESULTS AND DISCUSSION

4.0. INTRODUCTION

After adsorbent synthesis, the manufactured adsorbents were characterized to predict the adsorbents efficiency, taking into account factors relevant to the adsorptivity, which include: surface modification and geometry/structure improvement, solidity which includes thermal stability, and biodegradability. Therefore the information obtained through ^{1}H NMR, FTIR, BET, TEM, Raman spectra and TGA was beneficial for the establishment of different approaches relevant to the performance of the adsorbents developed.

In recapping the reasons for the selection of the various analytical techniques prior to the detailed discussion pertinent to the adsorbents developed, the following is provided:

- ^{1}H NMR spectra were necessary to evaluate the efficiency of the experimental method according to the model of chemical structure of the adsorbent. The interpretation of ^{1}H NMR results were rendered possible through the knowledge of chemical structure of the compound, which gives information regarding the protons expected in proportion to the protons obtained from the integration of the corresponding peaks. Thus, ^{1}H NMR spectra were used as quantitative analysis for the evaluation of amine incorporation in the polymer where the excess of amine reveals the unsuccessful cleaning process. As the amine was previously used in excess over polysuccinimide, this excess was meant to be removed during the cleaning process.
- FTIR analysis was useful in the adsorbent design, as the surface modification was supposed to show the presence of primary amine (NH_2) and amide (CONH) groups as CO_2 anchoring and biodegradable sites respectively. This was rendered possible through FTIR analysis where the bonds relevant to primary amine and amide groups were stretched in appropriate regions.

- BET analysis was necessary for the evaluation of the geometry/structure of adsorbent in order to insure adequate adsorptivity for the adsorbent. Therefore, the use of BET analysis provided information on surface area, pore volume and pore size, with a discussion to predict the performance of each adsorbent.
- TEM analysis was useful for the verification of the MWNTs structure and the functionalized MWNTs with the polymer, providing information on the diameter of MWNTs, as well as the position of polymer on the MWNTs. Due to the coating of the MWNT by the polymer the aim was to conserve the polymer functionality, which includes primary amine and amide groups.
- Raman spectra were able to show the peaks of graphitized carbon and carbon contain defects of MWNTs and the functionalized MWNT with the polymer. This was helpful to know the increase of carbons contain defect after functionalization with the polymer, since a large quantity of polymer versus small quantity of MWNT in a ratio of 1/30 was used to synthesize the adsorbent.
- TGA was useful to evaluate the thermal stability of adsorbents, their CO_2 adsorption capacity, adsorption kinetics and their regenerability efficiency. The DSC-TGA could evaluate heat flow for each adsorbent during CO_2 adsorption. A possible integration of the number of beds for the continuous synchronization of TSA was discussed through the knowledge of time variance in order to set the optimum conditions.

In this work, the chemical surface modification and the improvement of geometry/structure of the adsorbents were principally developed for the enhancement of CO_2 adsorption in temperature range 25 – 100 °C which includes the adsorption and desorption temperatures at 1.1 bar.

Regarding the chemical surface modification, after the design of PSI, three amines which are EDA, PDA and MEA were differently grafted to PSI in order to produce PSI-EDA, PSI-PDA and PSI-MEA as PAAs respectively. The PAAs obtained show for PSI-EDA and PSI-PDA the presence of NH_2 as CO_2 anchoring sites which was not the case for PSI-MEA, because EDA and PDA are diamines, and MEA is a monoamine as stated in Section 2.4.6. However, the grafting of amine was a drawback to the geometry/structure and thermal stability for all PAAs. Consequently, the interaction potential between the adsorbent and the adsorbate was

weak to produce a higher CO_2 adsorption capacity especially for PSI-PDA which was classified in macroporous category and for PSI-MEA which does not have NH_2 group as CO_2 anchoring sites. The PSI-PDA and PSI-MEA were deselected as their CO_2 adsorption capacities are lower compared to PSI.

The improvement of geometry/structure was rendered possible through the non-covalent functionalization of MWNT with PSI and PAA resulting in MWNT-PSI and MWNT-PAA. The geometry/structure was enriched from PSI to MWNT-PSI and from PAA to MWNT-PAA. However, the CO_2 adsorption capacity of MWNT-PSI was almost the same compared to the CO_2 adsorption capacity obtained for PSI.

The CO_2 adsorption capacity increased significantly from PSI to PAA and from PAA to MWNT-PAA; however, PAA has poor geometry/structure. The evaluation of selectivity for CO_2 on N_2 and O_2 was rendered possible with the use of 100% CO_2, 100% N_2 and 100% O_2. Thus, both PAA and MWNT-PAA showed high selectivity for CO_2 due to the presence of NH_2 as CO_2 anchoring site.

The result obtained with the moisture testing showed the possibility of increasing the CO_2 adsorption capacity for both PAA and MWNT-PAA in the presence of flue gas with moisture content. This becomes more significant with MWNT-PAA which has high potential interaction due to geometry/structure improvement.

Regarding the result on the cycle adsorption-desorption, the regeneration of adsorbents PAA and MWNT-PAA was successfully achieved. This led to the thermodynamic study through the evaluation of heat flow which resulted in very high heat release in adsorption process and very low heat absorbed in desorption process.

Finally, the evaluation of the number of beds for TSA systems was rendered possible through the results of CO_2 adsorption capacity, adsorption kinetics, the adsorption time, and the heating and cooling times.

4.1. POLYASPARTAMIDES (PAAs)

The adsorbents, being PAAs, include PSI, PSI-EDA, PSI-PDA, PSI-MEA, and the functionalized MWNTs which include MWNT, MWNT-PSI and MWNT-PAA were subjected to characterization in order to evaluate their performance as adsorbents for CO_2 capture.

4.1.2. Characterization of PAAs

4.1.1.1. Polysuccinimide (PSI)

The production yield was used to assess the efficiency of the synthesis process. The process of PSI synthesis included two steps: 1) the preparation of PSI short chain and 2) the use of a coupling agent in order to lengthen the PSI chain. In the first step 35 g of crude PSI was collected from the polycondensation of 50 g of aspartic acid where 25 g of phosphoric acid was used as catalyst; this resulted in a yield of 70%. After investigation, the following causes justify the loss of 30%: (a) the washing of the crude PSI for pH adjustment (6-7) using distilled water to remove unreacted aspartic acid; (b) raising the pH from the range 2-3 to the range 6-7 required several washing steps resulting in product loss. Thus, the improvement of washing process will certainly enhance the yield of production. The second step relevant to the extension of the chain using DCC as coupling agent resulted in a yield of 38 g or 95%, with the loss of 5% possibly due to the separation process which includes centrifugation and precipitation.

The ^1H NMR spectrum (Fig. 4. 1) of PSI in oxide deuterium (D_2O) showed a broad resonance in the spectra range 4.4 - 4.8 ppm, corresponding to the methine proton (NCO-CH) where the integration of the relevant peak was 0.49 compared to 0.5 as expected. Accordingly, another resonance was shown in spectra range 2.4 - 3.0 ppm corresponding to the methylene protons

(-C**H₂***-CH). The peak was used as a reference in order to evaluate the synthesized PSI, according to the structure presented in Figure 4.1.

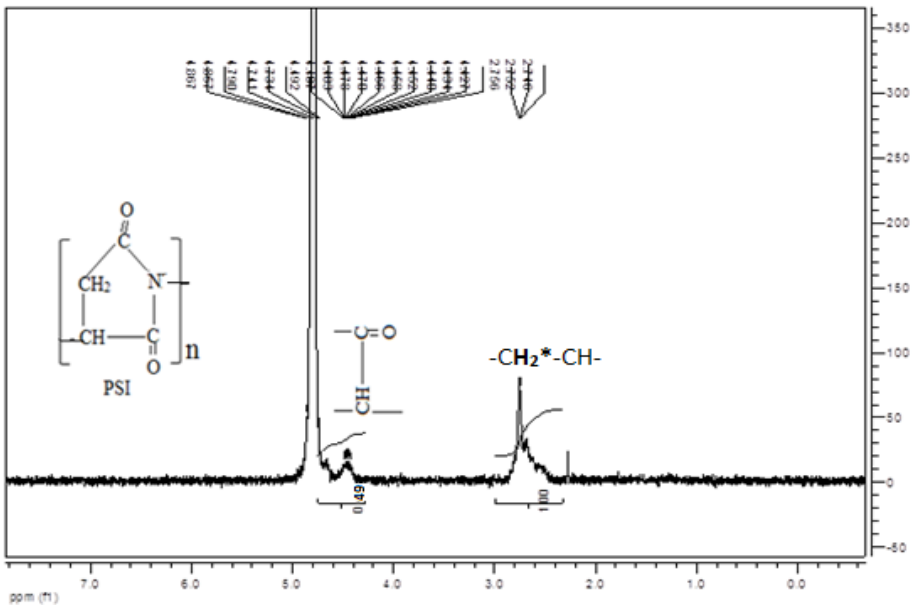


Figure 4.1: ^{1}H NMR spectra showing protons in the chemical structure of PSI

The presence of the imide group (-CON-) as depicted in the structure of PSI in Section 2.4.6 (Fig. 2.14) is the key component to prove biodegradability of the synthesized PSI. The analysis done with FTIR shows in Figure 4. 2 the peak C=O stretched at 1710 cm^{-1} in the region 1680-1720 cm^{-1} and the peak C-N stretched in the region 1436.3 cm^{-1}. This confirms the imide group (-CON-) in the chemical structure of the synthesized PSI as a biodegradable bond which can be potentially cleaved under hydrolytic, enzymatic or biological actions.

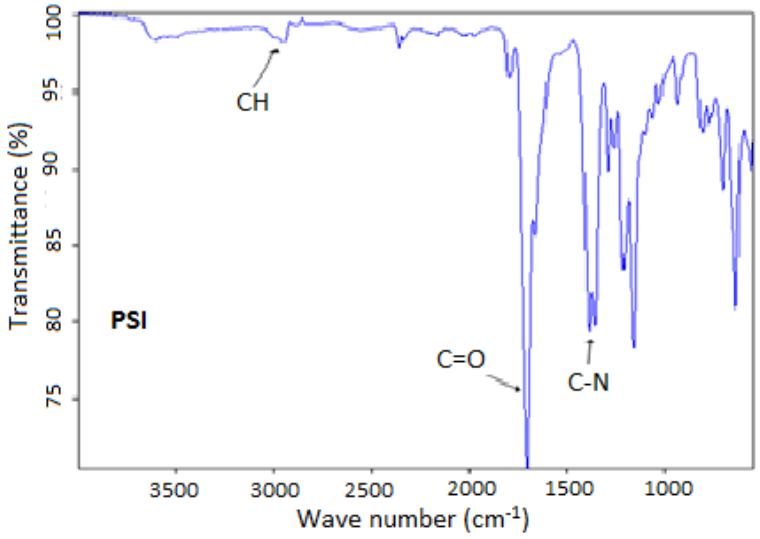


Figure 4.2: FTIR showing necessary peaks in chemical structure of PSI

The synthesized PSI was stable with an increase of temperature up to 400 ˚C as depicted in Figure 4. 3. The loss of 8% below 200 ˚C was due to water elimination. A suitable drying device after production will prevent the sample from this loss. Thus, the PSI has the ability to operate below 400 ˚C without being subjected to destruction or combustion.

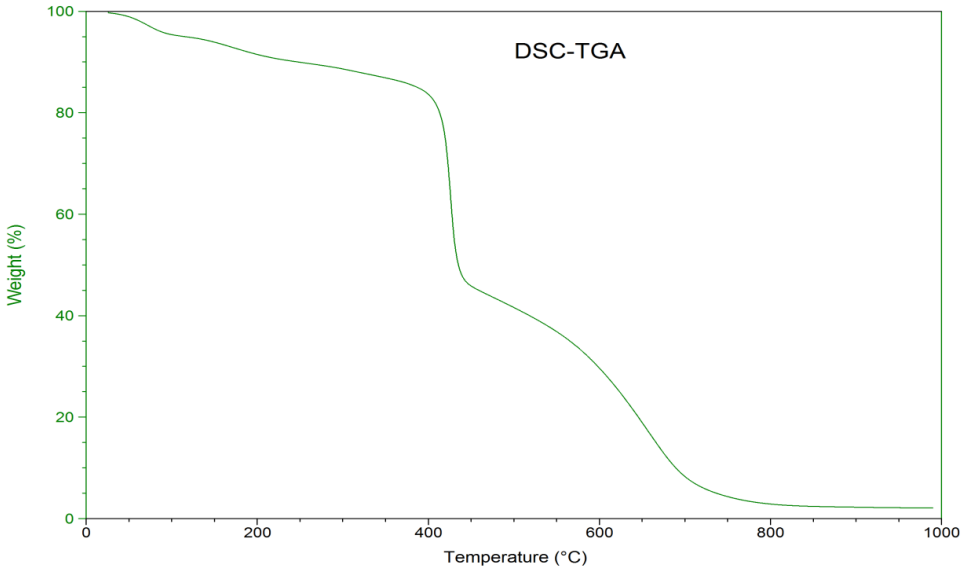


Figure 4. 3 : TGA mass loss curve showing the temperature stability of PSI

The BET analyses for PSI shows the results of surface area, pore volume and pore size (Table 4.1). According to IUPAC [275] the classification of an adsorbent is as follows: micropore for pore size < 2 nm, mesopore for pore size in the range 2 – 50 nm and macropore for pore size > 50 nm. The synthesized PSI is mesoporous.

Table 4.1: BET Analysis showing surface area, pore size and pore volume of adsorbents

Sample ID	Surface area (m^2/g)	Pore Volume (cm^3/g)	Pore size (nm)
PSI	42.99	0.3808	35.43
PSI-EDA	1.93	0.0100	20.63
PSI-PDA	1.02	0.0099	122.92
PSI-MEA	5.56	0.0501	12.87
MWNTs	452.69	0.7441	6.56
MWNT-PSI	305.76	0.6699	8.44
MWNT-PAA	60.44	0.4043	13.76

4.1.1.2. PAA using EDA to produce PSI-EDA

The production of PSI-EDA resulted in a yield of 4.30 g, corresponding to a recoverable yield of 76% from the reaction of 2.95 g (30 mmol) of PSI with 2.7 g (45 mmol) of EDA. Since the reaction was operated with an excess of 50% EDA to prevent polymer crosslinking, the maximum yield could not exceed 83% due to the removal of unreacted EDA during the cleaning process.

The chemical structure of PSI-EDA (Fig. 4.4) shows the presence of significant elements including primary amine (NH_2) and amide groups (-CONH-) as devices for CO_2 anchoring and biodegradability respectively. Thus, the identification of these elements in the synthesized PSI-EDA by the use of ^{1}H NMR and FTIR were necessary to prove the structure of the resultant product. The integration of peaks in the ^{1}H NMR spectra (Fig. 4.5) for the chemical shift (-CONH-C**H$_2$**-C**H$_2$**-NH_2) in the range 2.5-2.9 ppm was evaluated (4H), and CH-C**H$_2$**-CONH- in the range 3.2-3.3 ppm (2H), and yielded the expected values. This shows that the reaction between PSI and EDA was successfully completed with 100% EDA incorporation in PAA. The purification process for the removal of free EDA to obtain clean PAA was complete. Likewise, the FTIR analysis (Fig. 4.6) shows the NH_2 peak in the region 3300 - 3500 cm^{-1} and the NH peak in the region 3100 - 3200 cm^{-1}. The peaks C=O and C-N stretched in regions 1680 - 1720 cm^{-1} and 1436.3 cm^{-1} respectively. These confirm the possibility of CO_2 attachment at primary amine groups for carbamate formation. Also, the amide group in the chemical structure of the synthesized PSI-EDA confirms a potential biodegradable bond which can be cleaved under hydrolytic, enzymatic or biological actions.

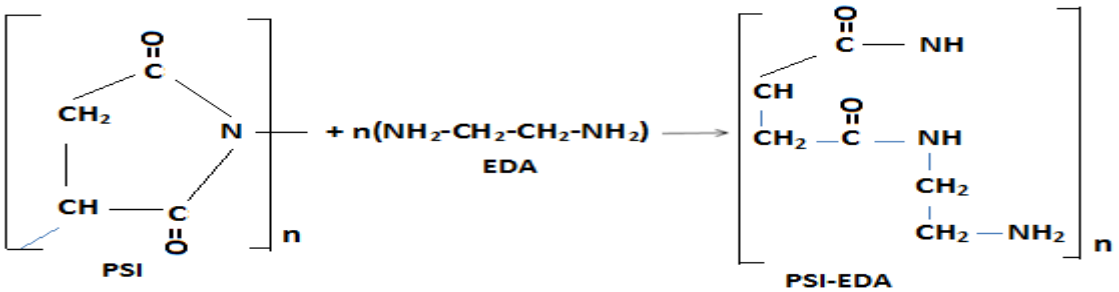


Figure 4.4: Reaction for PSI-EDA formation showing the chemical structure.

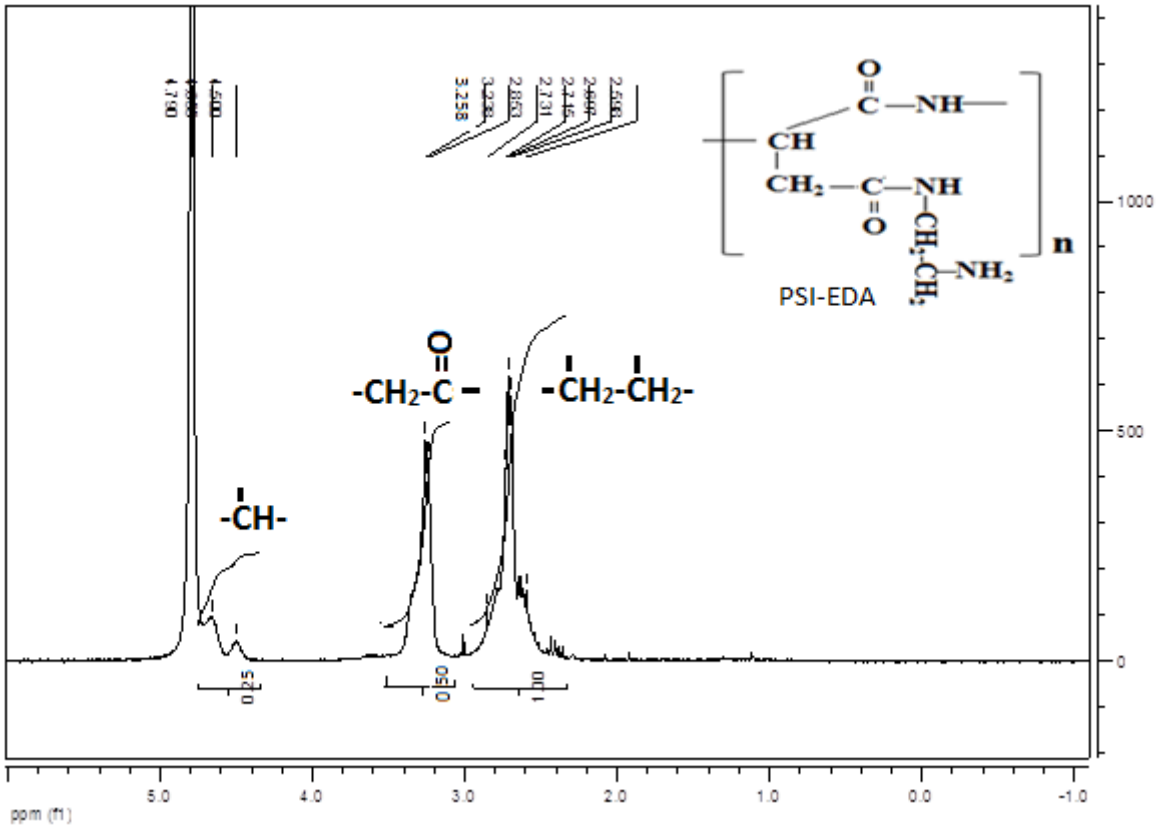


Figure 4.5: ^{1}H NMR spectra showing protons in the chemical structure of PSI-EDA

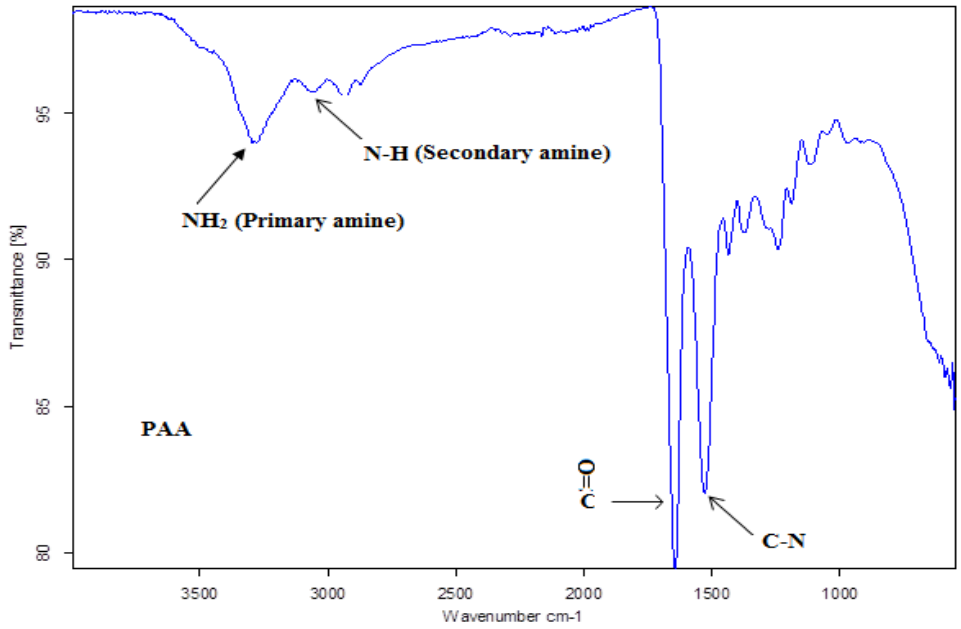


Figure 4.6: FTIR showing necessary peaks in PSI-EDA

Regardless of the decreased weight (< 5%) due to water elimination (Fig. 4.7), the TGA results show that the PSI-EDA was stable up to 200 ˚C. A large destruction of PSI-EDA was

observed after 200 ˚C where the weight loss increased significantly, indicating possible combustion of the sample. While PSI could be stable until 400 ˚C, the stability of PSI-EDA was reduced to 200 ˚C. This is because the incorporation of EDA into PSI for PAA formation opens the ring of the polymer. Thus, regarding the thermal stability, the opened ring has a drawback.

The BET analysis for PSI-EDA (Table 4.1) classify the pore size in the mesoporous category according to IUPAC rules [264]. The geometry/structure of PSI-EDA was poor compared to PSI.

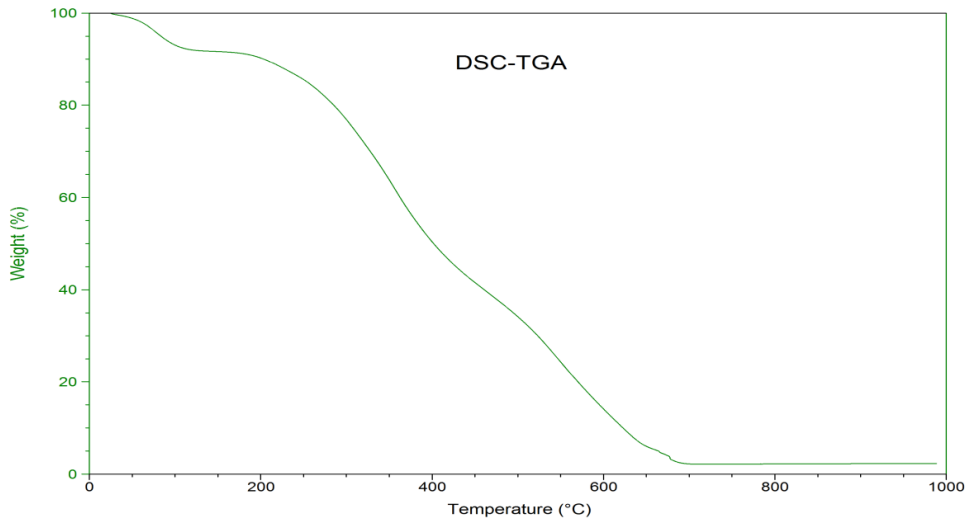


Figure 4.7: TGA showing the stability of PSI-EDA with temperature

4.1.1.3. PAA using PDA to produce PSI-PDA

The production of PSI-PDA resulted in a yield of 4.74 g, corresponding to 75.5%. In order to prevent polymer from crosslinking that could occur due to the simultaneous reaction between crude PSI and both terminal primary amine groups in PDA, the inhibition of the primary amine group was necessary. This was rendered possible through the use of 50% excess of PDA in the reaction. Therefore, the maximum yield could not go beyond 83%.

The structure of PSI-PDA (Fig. 4.8) shows the presence of significant elements including primary amine (NH_2) and amide groups (-CONH-) as devices for CO_2 anchoring and biodegradability respectively. Thus, the identification of these elements in the synthesized PSI-PDA by the use of ^1H NMR and FTIR was necessary to prove the validity of resultant product. The integration of peaks in the ^1H NMR spectra (Fig. 4.9) for the chemical shift (-CONH –CH_2-C**H_2**-CH_2-NH_2) in range 1.4 - 1.8 ppm was evaluated respective to 2H and (-C**H_2**-CONH-, -NH-C**H_2**, and CH_2-N**H_2**) in the range 2.2-3.4 ppm. This shows 92% PDA incorporation in PAA with 8% of loss most likely due to the purification stage. Likewise, Figure 4.10 shows all expected peaks including NH_2 between 3300 – 3500 cm^{-1}, to confirm the presence of primary amine as CO_2 anchoring site. NH at 3100 - 3200 cm^{-1}, C=O at 1650 - 1740 cm^{-1} and C-N between 1430 – 1530 cm^{-1} confirm the amide group as the potential biodegradable bond.

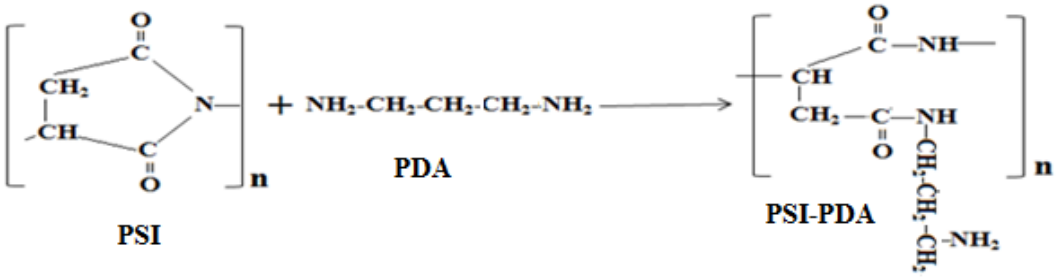


Figure 4.8: Reaction for PSI-PDA formation showing the chemical structure.

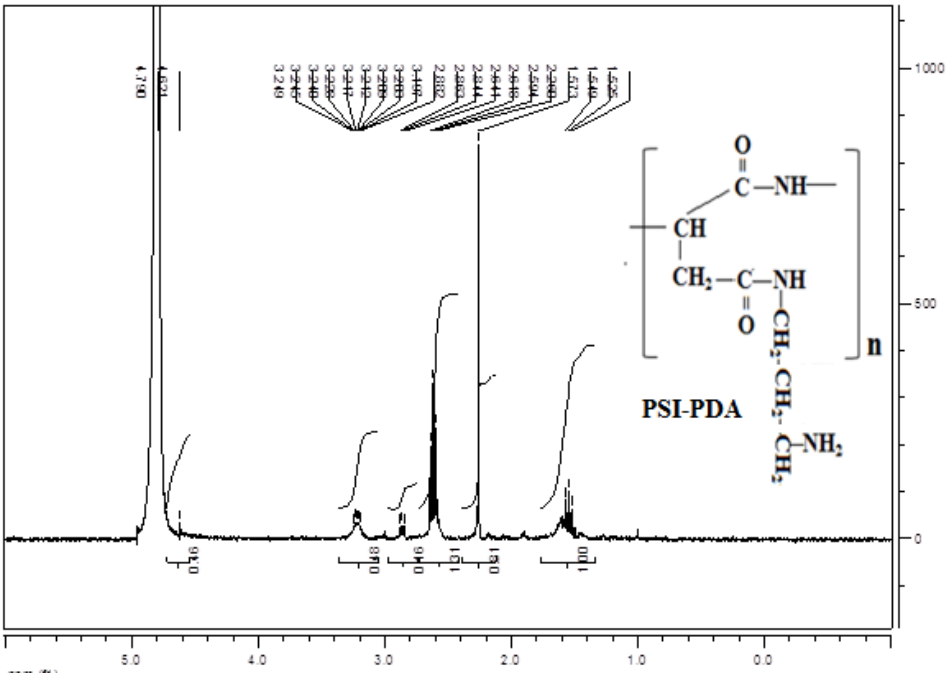


Figure 4.9: ^1H NMR according to PSI-PDA chemical structure.

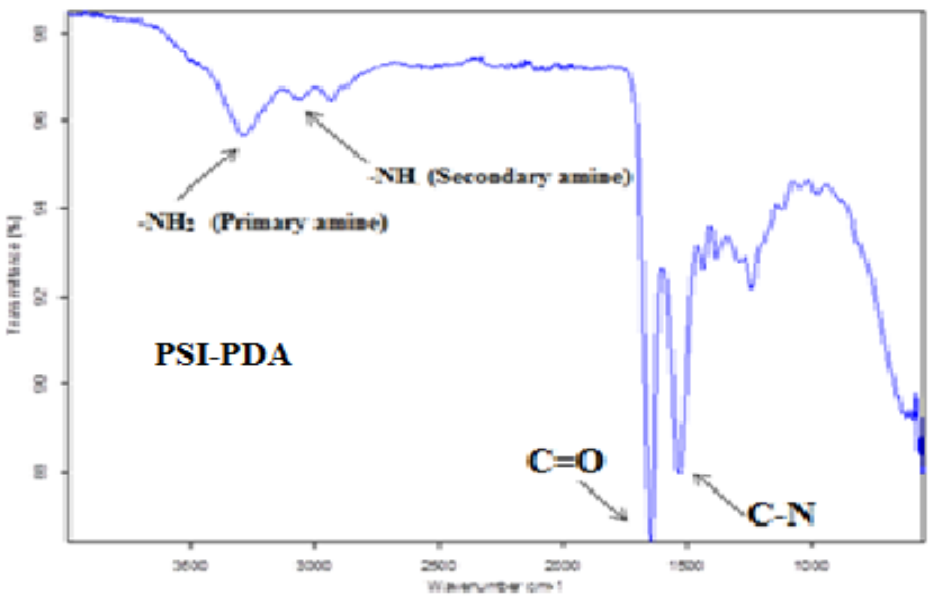


Figure 4.10: FTIR showing the necessary peaks for the chemical structure of PSI-PDA

Regardless of the decrease of weight (< 8%) due to water elimination, the TGA results (Fig. 4.11) show that the PSI-PDA was stable with the increase of temperature up to 200 ˚C. However, the PSI showed reasonable stability with the increase of temperature up to 400 ℃. This confirms the statement that the opening of the polymer ring renders the polymer more combustible compared to the crude polymer.

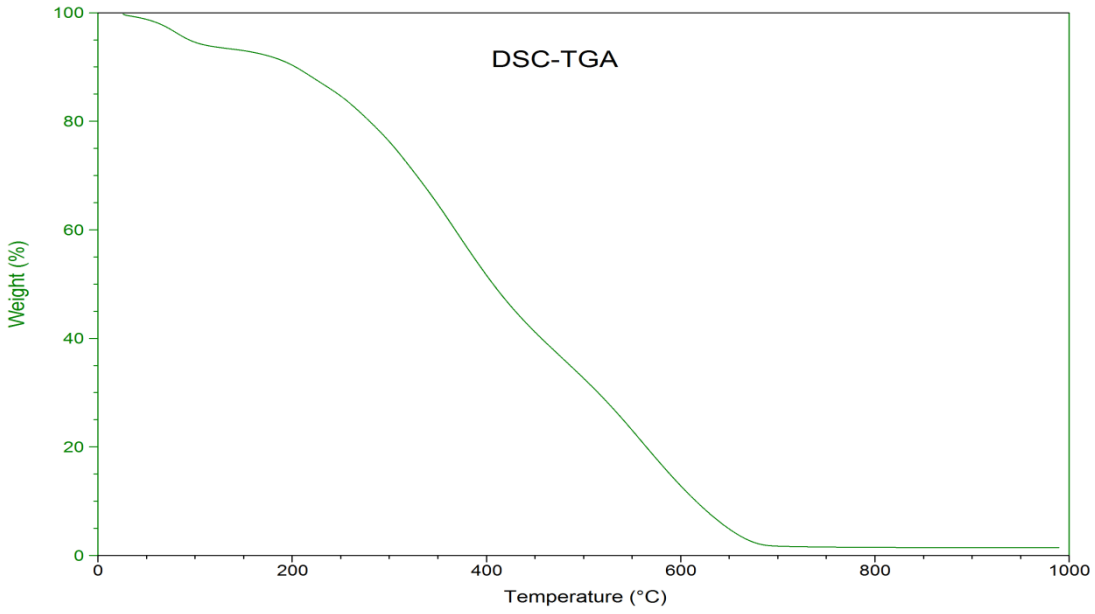


Figure 4.11 TGA showing the stability of PSI-PDA with increasing temperature

The BET analysis (Table 4.1) shows that the PSI-PDA has a very poor geometry/structure and was classified in the category of macroporous due to the broad pore size.

4.1.1.4. PAA using MEA to produce PSI-MEA

The production of PSI-MEA resulted in a yield of 4.60 g, corresponding to 93%. Compared to the diamines EDA and PDA, which were used in excess in order to prevent polymer crosslinking, an excess was not required with MEA as a monoamine which was added to PSI in a stoichiometric ratio. Therefore, a higher yield was recorded for PSI-MEA due to the simple purification process.

The chemical structure of PSI-MEA (Fig. 4.12) does not show the presence of a primary amine (NH_2) as potential device for CO_2 anchoring, because the single NH_2 found in MEA as monoamine has previously reacted with PSI in order to open the ring of PSI during the reaction. However, the amide group (-CONH-), a chemical bond use to predict the potential biodegradability, was confirmed in the chemical structure of PSI-MEA. Thus, the integration of peaks in ^1H NMR spectra (Fig. 4.13) for the chemical shift (-CH-C**H**$_2$-CONH-) in range 3.5 - 3.6 ppm was evaluated as 2.13 respective to a theoretical value of 2H. The integration for chemical shift (-C**H**$_2$-OH-) in the range 3.8 - 4.0 ppm was 2.10, which is equivalent to 1.97H against an expected theoretical 2H. This shows 98.6% MEA incorporation in the PAA. The FTIR analysis (Fig. 4.14) shows all necessary peaks expected according to the chemical structure depicted in Figure 4.12. Thus, the following peaks were observed in Figure 4.14: OH stretching peaks in range 3250-3300cm^{-1}, the secondary amine NH stretching peaks in range 2850 – 3100 cm^{-1}, C=O and C-N stretching peaks in range 1650 – 1700 cm^{-1} and 1100 – 1200 cm^{-1} to confirm the amide group.

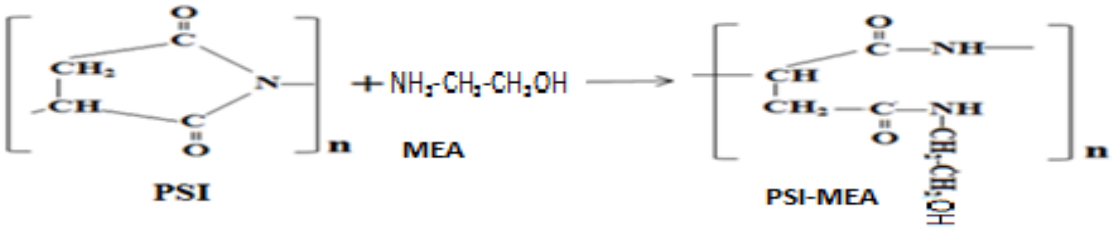


Figure 4.12: Reaction for PSI-MEA formation showing the chemical structure.

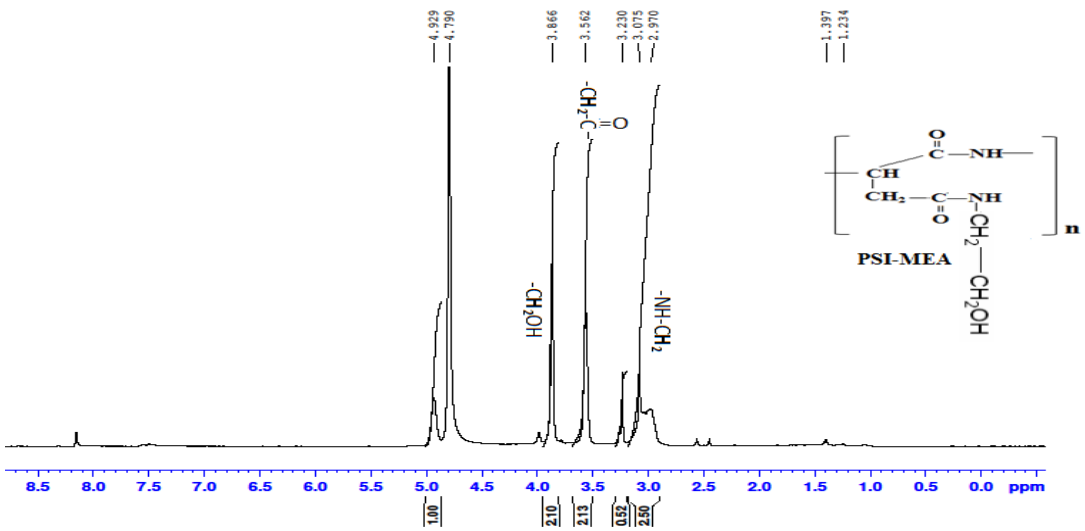


Figure 4.13: ^{1}H NMR showing protons relevant to PSI-MEA chemical structure.

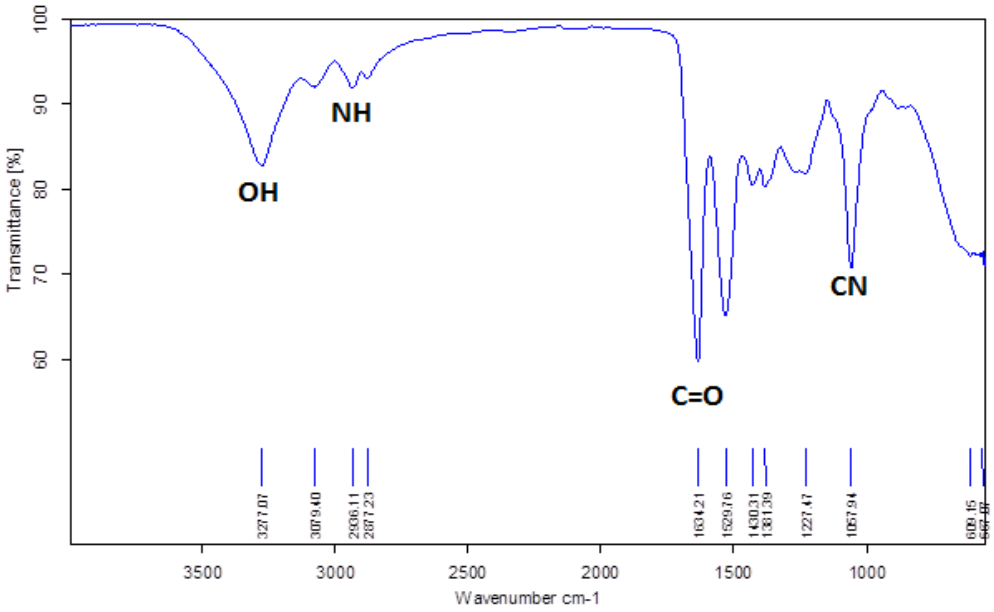


Figure 4.14: FTIR showing the necessary peaks for the chemical structure of PSI-MEA

Regardless of the decrease of weight (< 8%) due to water elimination shown by the TGA results in Figure 4.11, the PSI-MEA was stable with an increase of temperature up to 200 ˚C. The stability of PSI-MEA has dropped to 200 ℃ due to the opening of the rings of polymer compared to PSI where the thermal stability was up to 400 ℃.

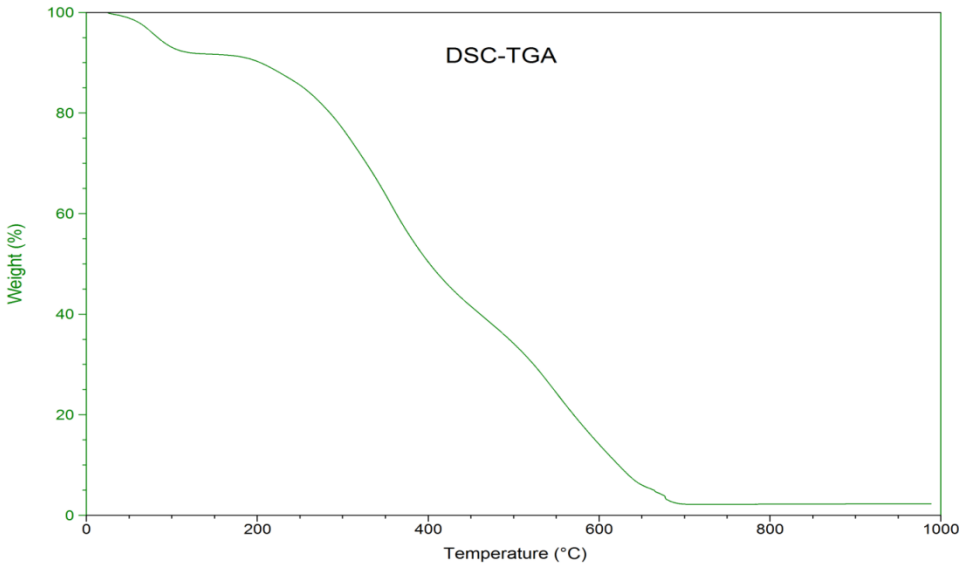


Figure 4.15: TGA showing the stability of PSI-MEA with increasing temperature

The BET analysis shows (Table 4.1) the surface area, pore volume and pore size respectively. Compared to the crude PSI, the pore size is improved.

4.1.1.5. Comparison of PAAs

PSI as an adsorbent presents adequate characteristics, which include biodegradability, thermal stability and geometry/structure; however the PSI does not possess NH_2, as an available site for CO_2 anchoring. The use of diamines (which include EDA and PDA) to produce PAA through PSI was on one hand beneficial to provide a terminal primary amine group as potential CO_2 anchoring point in the resultant polymer. On the other hand, the thermal stability and geometry/structure were less than ideal. The ability of the primary amine group (NH_2) to form a carbamate through CO_2 chemisorption is a determining factor to provide large CO_2 adsorption capacity. Otherwise, the adsorption properties are likely to be poor when predicting large adsorption capacity through physisorption.

The synthesized PSI-MEA has shown an acceptable surface area, pore volume and pore size compared to the PAAs obtained through the use of EDA and PDA. However, the surface area and pore volume compared to PSI are lower. The pore size predicts a good potential for interaction between CO_2 and PAA if should there be a possibility of CO_2 uptake. Conversely,

the lack of a terminal primary amine group (NH_2) could be an obstacle for carbamate formation, and can negatively affect the CO_2 adsorption capacity, unless physisorption is the determining mechanism in the adsorption process.

4.1.2. Adsorption at 25◦C for PAA selection

The evaluation of the adsorption capacity PAA was done using PSI as reference. It is noticeable that the PAA was deliberately designed with the objective to obtain improved CO_2 adsorption capacity compared to the crude PSI. Otherwise the process to synthesize PAA from PSI would be meaningless. Thus, four adsorbents namely PSI, PSI-EDA, PSI-PDA and PSI-MEA were subjected to pure CO_2 at a flow rate of 60 mL/min to measure the CO_2 adsorption process using the TGA at 25 °C and 1.1 bars.

4.1.2.1. PSI

Figure 4.16 shows a CO_2 adsorption capacity of 25 mg-CO_2/g after an adsorption time (t_{ad}) of 60 minutes (min) when using the adsorbent PSI. It is observed that the kinetics of CO_2 adsorption was very fast in the first 10 minutes of adsorption, within which 21 mg-CO_2/g was adsorbed at an adsorption rate of 2.1 mg-CO_2/g min, as showed in Figure 4.17. This shows that within the first 10 minutes, PSI as an adsorbent was able to take up 84% of the total adsorption capacity over the 60 minutes of adsorption time. In the last 50 minutes a slow kinetic adsorption with a low adsorption rate: 0.08 mg-CO_2/g-min is observed, within which only 4 mg-CO_2/g was adsorbed (Fig. 4.16).

4.1.2.2. PAA of the type PSI-EDA

With regards to the adsorbent PSI-EDA, Figure 4.16 shows a CO_2 adsorption capacity of 52 mg-CO_2/g after t_{ad} = 180 min. The high adsorption capacity of PSI-EDA in spite of the poor geometry/structure confirms the prevalence of chemisorption during the adsorption process. Within the first 10 minutes of the adsorption process, PSI-EDA adsorbed 24 mg-CO_2/g with a

CO_2 at an adsorption rate of 2.4 mg-CO_2/g min, which is more or less the same as the total CO_2 adsorption capacity recorded for PSI. This shows that 46% of the total adsorption capacity was achieved during the first 10 minutes. More importantly, a large CO_2 adsorption capacity occurred during the first 30 minutes, within which the CO_2 adsorption for PSI-EDA was 34 mg-CO_2/g, corresponding to 65.4% of the total CO_2, adsorption capacity achieved in 180 minutes. This means that after adsorbing 34 mg-CO_2/g in the first 30 minutes, 18 mg-CO_2/g more was adsorbed; over the remaining 150 minutes to achieve the CO_2 adsorption capacity of 52 mg-CO_2/g (Fig. 4.16). Thus, the adsorbent PSI-EDA could capture an acceptable quantity of CO_2 if the capture plant is deliberately designed with a number of beds integrated to operate with short adsorption time (< 30 min). As the CO_2 adsorption rate decreases with the increase of adsorption time (Fig. 4.17), a lengthy CO_2 adsorption period is not beneficial.

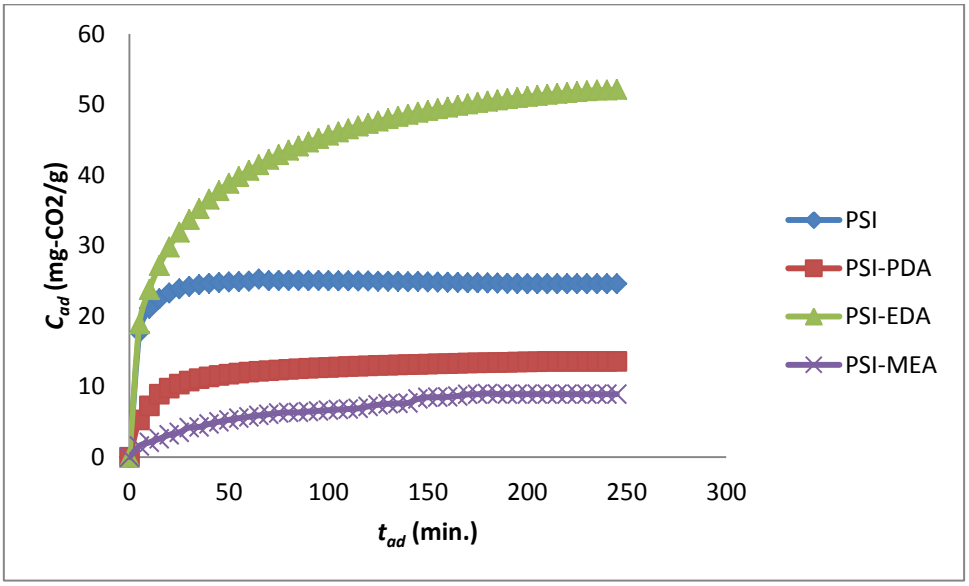


Figure 4.16: CO_2 adsorption capacity of different Polyaspartamides at 25 °C

4.1.2.3. PAA of the type PSI-PDA

A CO_2 adsorption capacity of 13.5 mg-CO_2/g was achieved after t_{ad} = 180 minutes when using PSI-PDA (Fig. 4.16). The poor geometry/structure was not able to promote adequate interaction that could allow chemisorption between CO_2 and NH_2 for carbamate formation. However, the surface modification did confirm the presence of a NH_2 groups. The CO_2

adsorption capacity is very low compared to the CO_2 adsorption capacity of PSI. Thus, CO_2 capture using PSI-PDA as adsorbent is inefficient.

4.1.2.4. PAA of the type PSI-MEA

After 180 minutes of the adsorption process, the use of PSI-MEA as adsorbent has resulted in a very low CO_2 adsorption capacity of 9.0 mg-CO_2/g, as shown by the results presented in Figure 4.16. Compared to the PSI where it derived from, this is much reduced and lower. The trend of adsorption kinetics was so slow (Fig. 4.16) that the prediction of the use of PSI-MEA in large scale for a capture plant is simply not feasible.

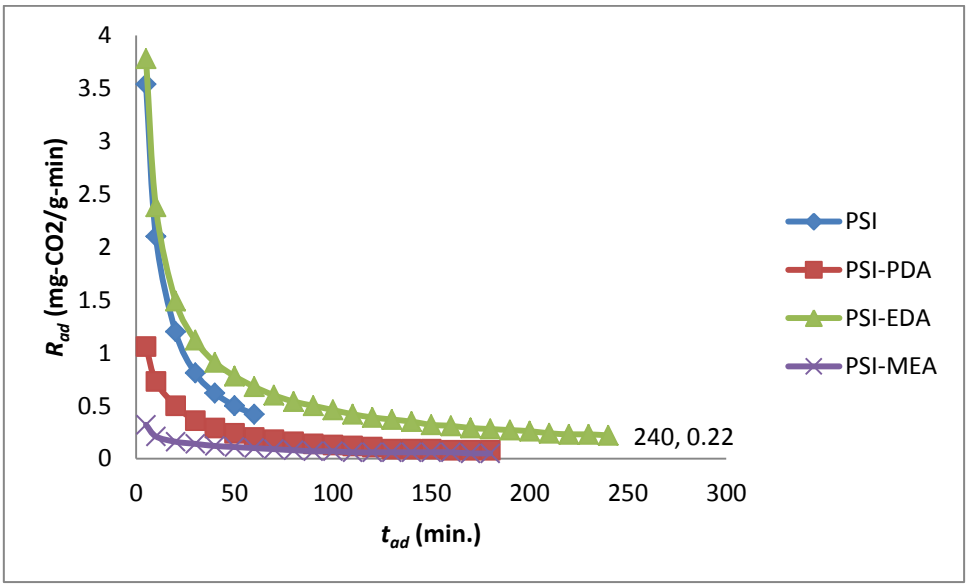


Figure 4.17: CO_2 adsorption rate of all Polyaspartamides at 25 °C

4.1.2.5. Comparison and PAA selection

After grafting the PSI with amines, the results in Table 4.2 show a higher CO_2 adsorption capacity for PSI-EDA and lower CO_2 adsorption capacity for PSI-PDA and PSI-MEA. The PAAs produced through the reaction of PSI with amine were unfavorable regarding surface

area (SA), pore volume (PV) and pore size (PS), as depicted in Table 4.1. The CO_2 adsorption capacity and the CO_2 adsorption kinetics were improved for PAA corresponding to PSI-EDA, as shown in Figures 4.16 and 4.17. The high CO_2 adsorption capacity of crude PSI prior to chemical surface modification is due to the good geometry/structure with regard to SA, PV and PS, that allowed rapid physisorption to occur, as shown in Figure 4.17. The surface modification of PSI by the use of EDA to give PSI-EDA, resulted in a dominant chemisorption process, which yielded high CO_2 adsorption capacity and high adsorption kinetics in spite of poor geometry/structure.

Table 4. 2: CO_2 adsorption capacity of PAAs at 25 ◦C in 100% CO_2 as flue gas

Adsorbents	**CO_2 C_{ad}[1] (mg-CO_2/g)**
PSI	25.0
PSI-EDA	52.0
PSI-PDA	13.5
PSI-MEA	9.0

The chemical surface modification of PSI by the use of PDA to produce PSI-PDA resulted in a low CO_2 adsorption capacity; however PSI-PDA demonstrated the presence of a NH_2 group necessary to form a carbamate group. This shows that the geometry/structure was so poor; the chemisorption expected through carbamate formation was a failure, while the physisorption could not occur as the adsorbent PSI-PDA is macroporous in size.

With regard to PSI-MEA, where the CO_2 adsorption capacity and kinetics of adsorption (R_{ad}: adsorption rate) were very low compared to PSI and other PAAs, the amine group that was intended to form carbamate has previously reacted as part of the opening of the polymer rings. However, despite the acceptable geometry/structure in PSI-MEA was achieved compared to other PAAs. The lack of a primary amine group as an available CO_2 anchoring site was a disadvantage for PSI-MEA. In addition, physisorption was not able to provide enough CO_2 adsorption in order to overcome the absence of chemisorption. While the CO_2

[1] *C_{ad}: adsorption capacity*

adsorption capacity of PSI-EDA increased by 108% compared to the crude PSI, the CO_2 adsorption capacity of PSI-PDA and PSI-MEA decreased by 46% and 64% respectively. Consequently, it is more beneficial to use PSI as adsorbent for CO_2 capture than PSI-PDA and PSI-MEA, which, instead of improving CO_2 capture, rather decreased it.

Thus, PSI and PAA synthetized with the use of EDA were selected for further test work as adsorbents, where the improvement of geometry/structure was made possible with the use of MWNTs. Hence forth, PSI-EDA is named PAA. Whenever PAA will be stated subsequently, it is referred to PSI-EDA.

4.2. NON-COVALENT FUNCTIONALISATION OF MULTI-WALLED CARBON NANOTUBES WITH POLYASPARTAMIDE (MWNT-PAA)

The advantage of the non-covalent functionalization process on the design of an adsorbent is started in Section 2.4.6. Therefore, the non-covalent functionalization of MWNTs with polyaspartamide was deliberately preferred in this work over the covalent functionalization, for CO_2 adsorption applications.

The PAA coated MWNT have the following characteristics: 1) the coating molecules should be biodegradable and nontoxic; 2) the coating should be sufficiently stable to resist detachment from the nanotubes surface in CO_2 adsorption and desorption process; 3) the coated molecules should have a functional groups which are available for CO_2 anchoring.

4.2.1. Characterization of MWNT with PAA

4.2.1.1. Multi-walled carbon nanotubes (MWNTs)

A commercial MWNT, as described in Section 3.1.2, was used to improve the adsorption properties of the adsorbent respective to CO_2 adsorption. A diameter size of 8nm was determined by TEM result (Fig. 4.18).



Figure 4.18: TEM showing the nanostructure image of MWNT

The Raman spectra of the MWNTs show two peaks located at ~1350 and ~1580 cm^{-1} (Fig.4.19). The peak near 1580 cm^{-1} is the G band with intensity I_G which is related to graphite E_{2g} symmetry of the interlayer mode reflecting structural integrity of sp^2-hybridized carbon atoms of the nanotubes. There is also a prominent band around 1350 cm^{-1}. This band is known as a hybridized vibration mode associated with graphene edges and it indicates the presence of some disorder to the graphene structure [276]. The band D is known to be typically very weak in graphite and typically weak in graphene as well. If the D-band is significant, it indicates that there are a lot of defects in the material [277]. This band is often referred to as the disorder band or the defect band and its intensity relative to that of the G band is often used as a measure of the quality with nanotubes [278]. Hence, the extent of carbon containing defects of MWNTs can be evaluated by intensity ratio of D band to G band ((I_D/I_G). The I_D/I_G ratio of MWNTs was evaluated to 0.667. This value is recorded for MWNTs without being functionalized. Thus, the I_D/I_G ratio of all functionalized MWNTs (*f*-MWNTs) made from these MWNTs will be compared to that value of 0.667 to evaluate the growth of carbons contain defect in the *f*-MWNTs which is intended to increase.

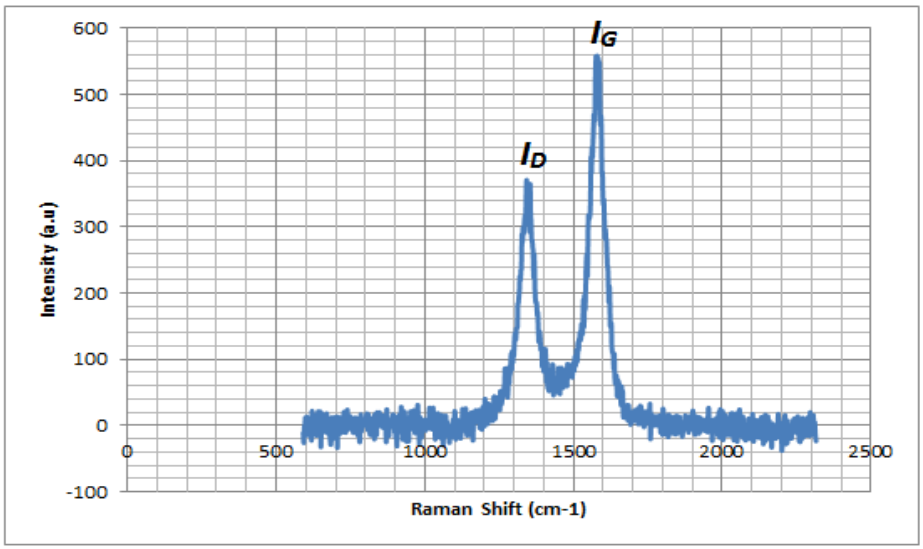


Figure 4.19: Raman Spectra (MWNTs)

The commercialized MWNT was stable at up to 500 ˚C, as determined using the TGA (Fig. 4. 20). Thus, the MWNT has the ability to operate below 500 ˚C without being subjected to destruction or combustion.

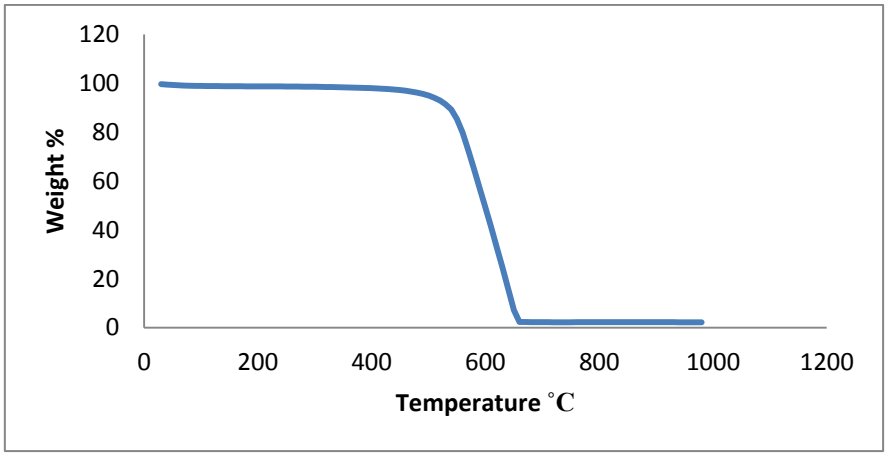


Figure 4.20: TGA showing weight degradation of MWNTs with temperature

The BET analysis (Table 4.1) classified the MWNT as a mesoporous adsorbent from the evaluation of SA, PV and PS. The MWNTs used present good adsorbent characteristics which can be used to enhance the adsorptive properties of PAA, which has previously showed a suitable chemical surface for CO_2 anchoring.

4.2.1.2. Multi-walled carbon nanotube with polysuccinimide (MWNT-PSI)

The investigation of MWNT-PSI was found necessary in order to justfy the reason for using PSI-EDA (PAA) instead of PSI alone, because an extra-process corresponding to extra-cost is required to PSI synthesis to get PAA. Therefore MWNT-PSI was used for CO_2 adsorption in comparison to MWNT-PAA.

A mixture of 100 mg MWNTs and 3 g PSI resulted in the production of 2.8 g MWNT-PSI, corresponding to a yield of 90%. The loss of 10% is due to the cleaning and fitration processes.

Evaluation using TEM indicates a 10 nm diameter for the MWNT-PSI product (Fig. 4.21). The microscope image shows that the PSI, as a long chain polymer, has tightly twisted around the MWNT during the coating process. This shows that the PSI possess enough strain able to compress around the MWNTs through the coating. Consequently, the diameter size has not changed significantly between the MWNT and MWNT-PSI (8-10nm respectively).

The Raman spectra of the MWNT-PSI shows two peaks located at ~1350 and ~1580 cm^{-1} (Fig. 4.22). The higher disorder in graphite results in a larger G band with higher intensity, as well as a D band with relative average intensity [279, 280]. The evaluation of the extent of carbon containing defects of MWNT-PSI was done by considering the intensity ratio of D band to G band, which is I_D/I_G= 0.532.



Figure 4.21: TEM showing the nanostructure image of the MWNT-PSI

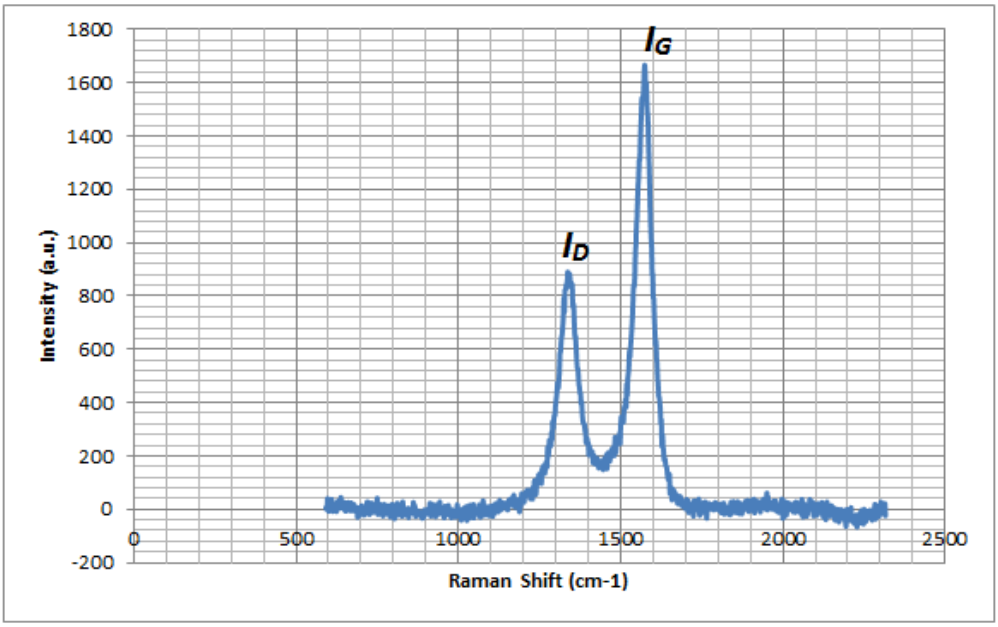


Figure 4.22: Raman Spectra (MWNT-PSI)

The TGA curve (Fig. 4.23) shows 3 stages of weight change with the increase of temperature as follow: a) the first stage is the 5% of weight degradation in the temperature range 100 - 150 °C due to water elimination and other gases that were infused in MWNT-PSI; (b) in the second stage, about 10% of sample was degraded in the temperature range 350 - 400 °C; this is related to the temperature limit of PSI stability as shown in Figure 4.3; (c) finally, a broad weight degradation after 600 °C, related to the combustion temperature of MWNTs, is shown in Figure 4.20. Since the PSI and MWNT were mixed with a ratio 1:30 to produce MWNT-

PSI, a broad weight degradation should appear due to the large quantity of PSI, which degrades at 400 °C. Instead, broad weight degradation was observed after 600 °C, a temperature beyond the pure MWNT temperature degradation. This shows that PSI has tightly coated the MWNT, resulting in MWNT-PSI with a high thermal stability.

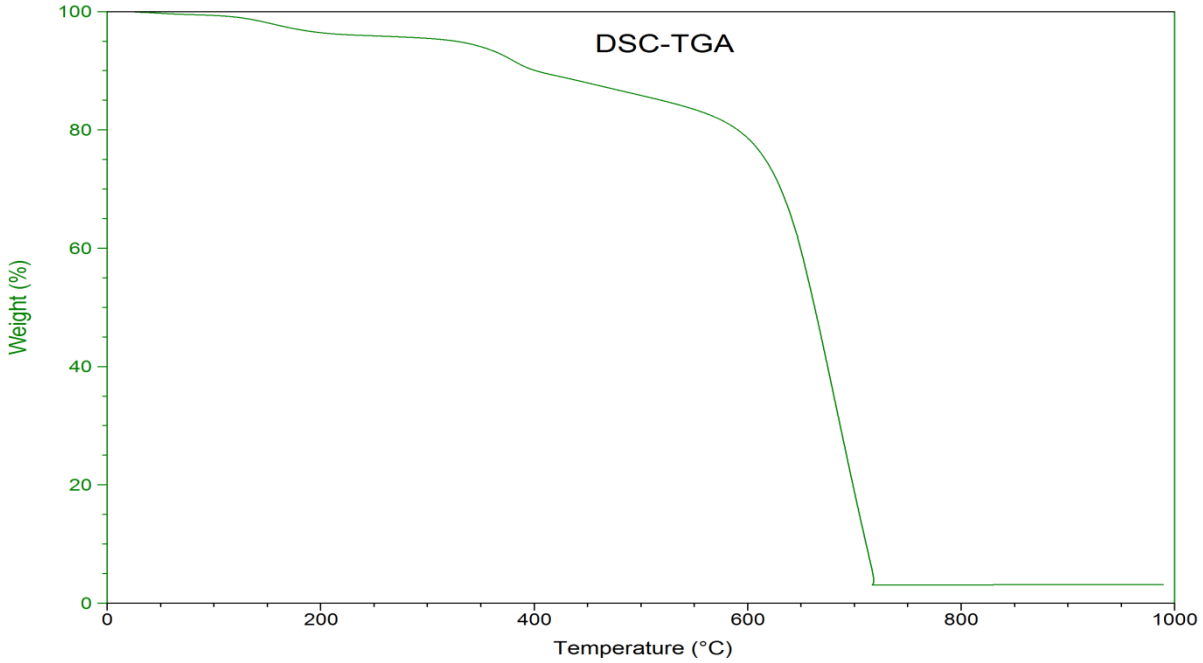


Figure 4.23: TGA showing weight degradation of MWNT-PSI with temperature

The BET analysis (Table 4.1) shows that the MWNT improved the geometry/structure of the adsorbent MWNT-PSI compared to PSI alone. The MWNT-PSI is classified in the mesoporous category adsorbent according IUPAC statement.

4.2.1.3. Multi-walled carbon nanotube with polyasparatmide (MWNT-PAA)

The TEM analysis (Fig. 4.24a) confirmed the nanotube structure of 15 nm diameter size with the presence of transversal dark line related to the coating of MWNTs by PAA. Figure 4.24b shows the growth of PAA rolling over the MWNTs in multi-layers following the nanotube shape.

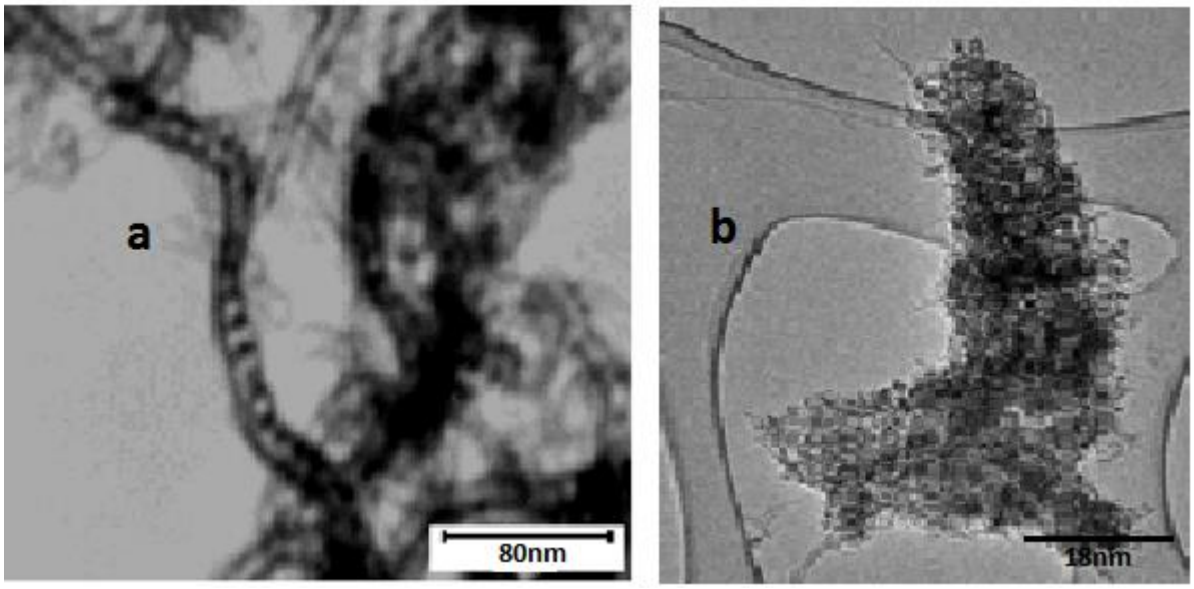


Figure 4.24: TEM showing the nanostructure image of MWNT-PAA:

a) Coating of MWNT showing PAA in tranvesal lines and b) Multilayer of PAA on MWNT growing in path of nanotubes

The Raman spectra for the MWNTs-PAA (Fig. 4.25) show the D band for graphitized carbon in range 1300 – 1400 cm^{-1}, while the G relevant to carbon contains defects occur in the range 1500 – 1600 cm^{-1}. Thus, the coating of MWNTs by PAA resulted into I_D/I_G ratio = 0.375.

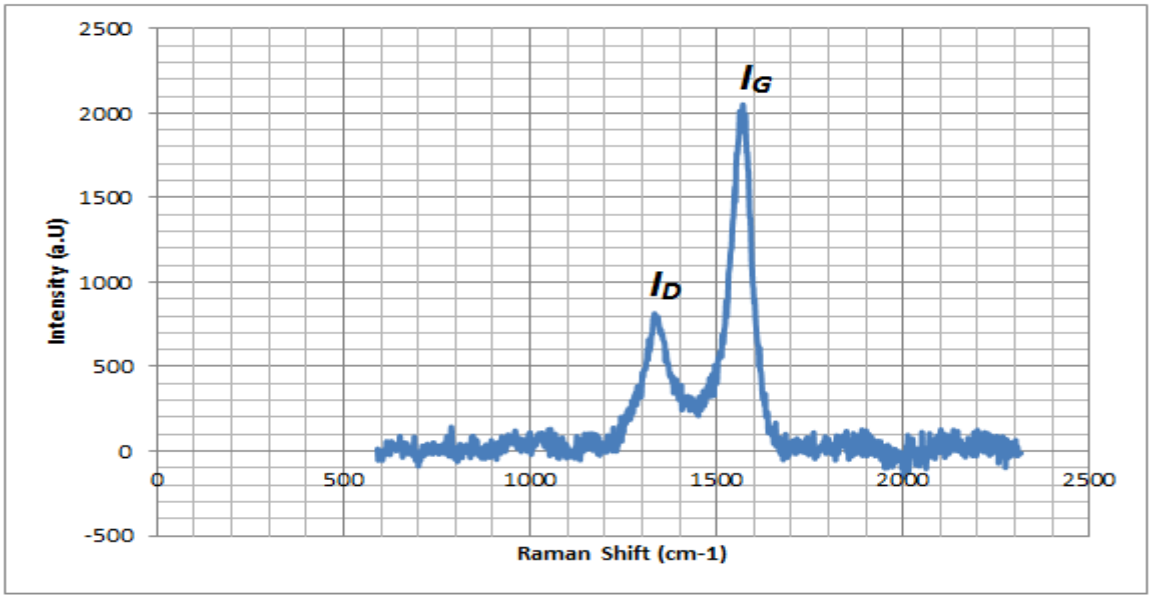


Figure 4.25: Raman Spectra (MWNT-PAA)

The use of MWNTs to improve the adsorption properties of the adsorbent has resulted in the conservation of the functional group. The MWNT-PAA shows through FTIR analysis in Figure 4.26 the primary amine group (NH_2) stretched in the wavenumber range 3000 - 3500 cm^{-1}, confirming the CO_2 anchoring site for carbamate formation. The biodegradable bond (the amide group CONH) was apparent through the CN, C=O and NH stretches in the wavenumber ranges 1500 – 1600 cm^{-1}; 1650 – 1800 cm^{-1}; and 2800 – 3000 cm^{-1}, respectively.

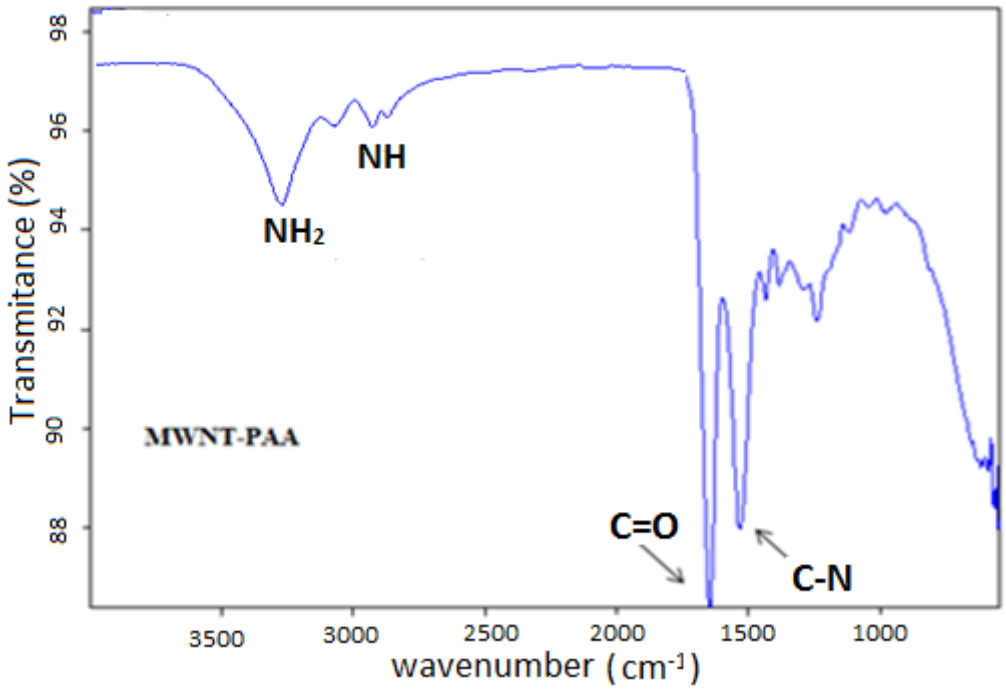


Figure 4.26: FTIR for MWNT-PAA identification

The TGA curve (Fig. 4.27) shows a 3 stages of weight degradation with the increase of temperature as follows: (a) the first stage is the 8% of weight degradation below 110 °C due to water elimination and other gases that were infused in MWNT-PAA; (b) in the second stage, a large degradation about 42% occurred in the temperature range 200 - 400 °C; this may be the destruction of the major part of the PAA coating on the MWNTs; (c) Finally, the remaining part of the adsorbent was totally destroyed in temperature range of 400 - 650 °C. Thus, the adsorbent MWNT-PAA produced from the mixture of MWNT and PSI-EDA has weight stability up to a temperature of 200 °C.

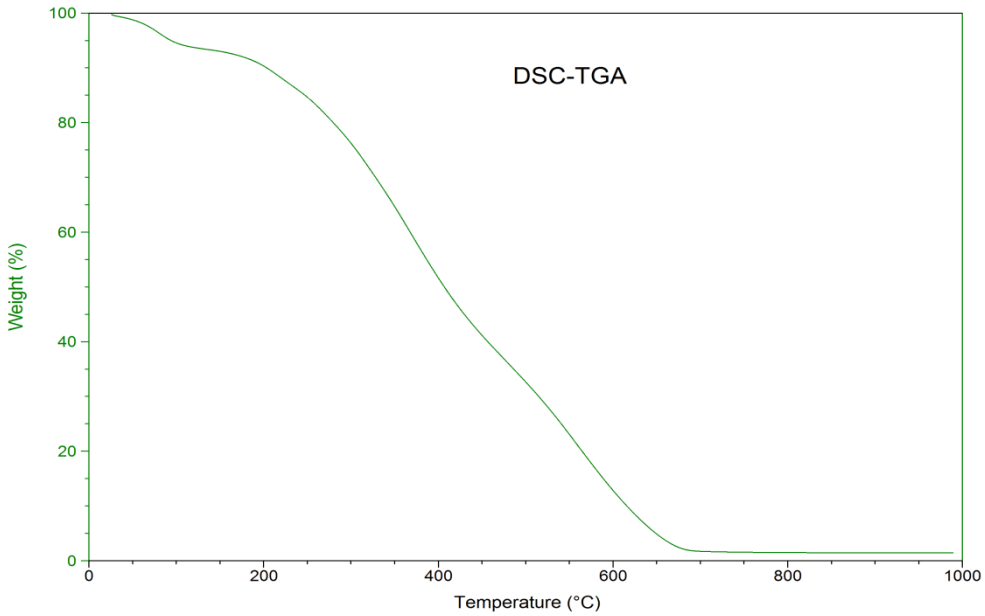


Figure 4.27: TGA showing the weight stability of MWNTs-PAA

The BET analysis (Table 4.1) shows that the use of MWNT to make MWNT-PAA has resulted in an improvement of the geometry/structure. The SA, PV and PS for MWNT-PAA were improved by 31.3, 40.5 and 1.5 times compared to PAA. Thus, the adsorbent MWNT-PAA is classified as a mesoporous material.

4.2.2. Comparison study of growth of adsorbent characterization

PSI was enhanced chemically and physically to produce MWNT-PAA with the aim of enhancing its CO_2 adsorption properties. The chemical surface modification with a primary amine group (NH_2) as the CO_2 anchoring sites was achieved by making PSI-EDA as PAA part of the structure. The enhancement of the physical structure was achieved by the use of the MWNT's. The FTIR results (Figs 4.2, 4.6, 4.26) show the growth of NH_2 in the MWNT-PAA, as expected. The SA and PV for the PAA were poor, but for the MWNT-PAA, these values were significantly increased.

The Raman spectra in Figure 4.28 show the growth of D and G bands respective to graphitized carbon intensity and carbon containing defects intensity from MWNT, MWNT-

PSI to MWNT-PAA. The ratio I_D/I_G has decreased from MWNT, MWNT-PSI to MWNT-PAA at the value of 0.667, 0.532 and 0.375, respectively. This showed that the carbon containing defects increased more in the functionalized MWNTs (*f*-MWNTs) than in MWNT. With regard to *f*-MWNTs, which comprise MWNT-PSI and MWNT-PAA, it is clear that MWNT-PAA showed high carbon containing defects due to the presence of the encapsulated carbon chain in the structure of PAA (Fig. 4.4), while PSI has a ring structure (Fig 2.14). Thus, MWNT-PAA is more functional and predicted to be more unstable compared to MWNT-PSI.

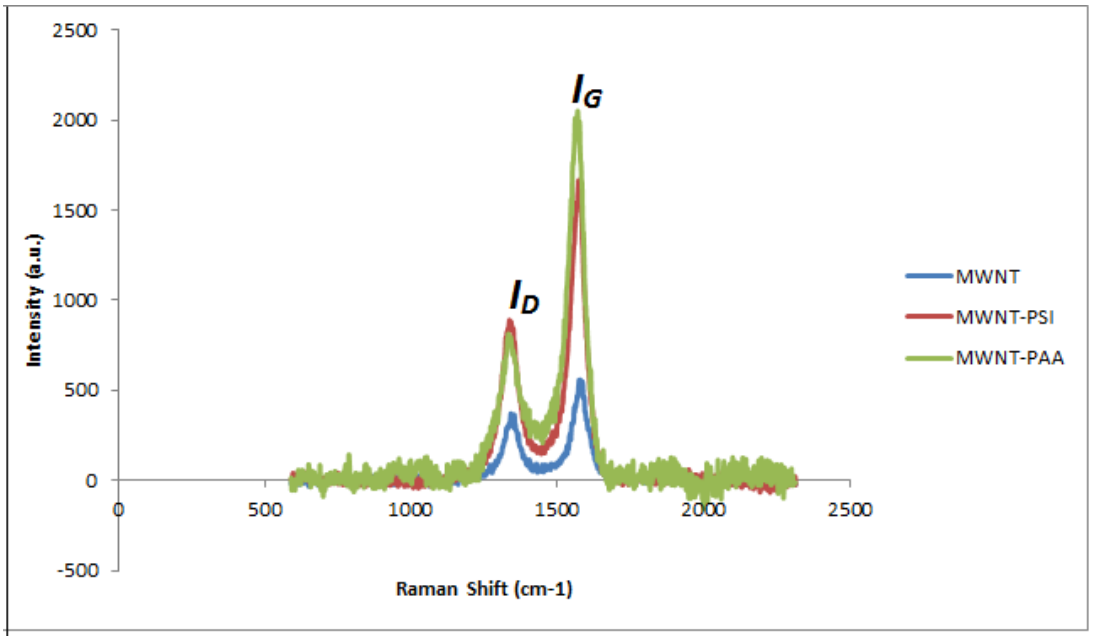


Figure 4.28: The growth of D and G bands from MWNT to the *f*-MWNTs

The adsorbent stability with the increase of temperature in the TGA was proportional to the composition of the structure of the adsorbent. Figure 4.29 shows a high mass stability with temperature in MWNT-PSI, followed by MWNT. The nanostructure of MWNT-PSI (Fig. 4.21) shows that the PSI twisted tightly around the MWNT, resulting in high weight stability with the increase of temperature (T < 600 °C). Due to the chain formation in the structure of PAA, a low weight stability was observed for the MWNT-PAA and PAA where the curve overlaps to confirm the same weight stability (T < 200 °C).

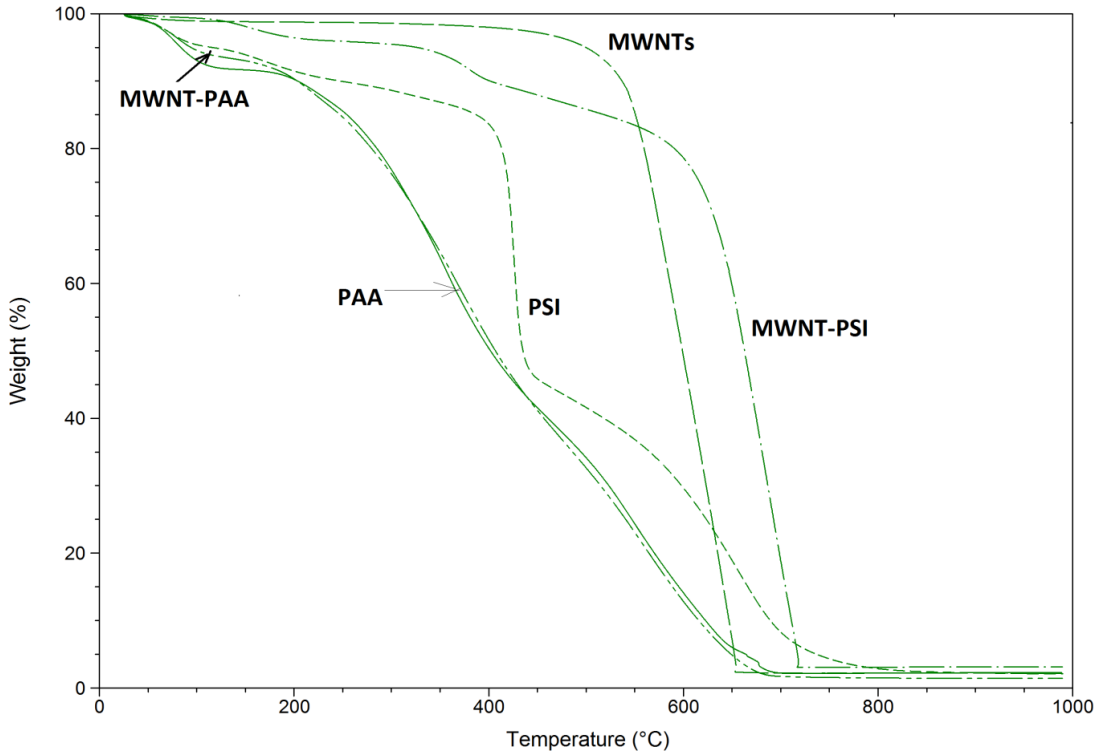


Figure 4.29: TGA for all adsorbents showing the weight stability with temperature

4.3. TEMPERATURE EFFECTS ON CO_2 ADSORPTION USING 100% CO_2

Each adsorbent (PSI, PAA, MWNT, MWNT-PSI, MWNT-PAA) was subjected to CO_2 adsorption tests in 100% CO_2 at 1.1 bar, and a flow rate of 60 mL/min at temperatures varying from 25 to 85 °C in intervals of 10 °C, using the TGA.

4.3.1. CO_2 adsorption at 25 °C

The CO_2 adsorption capacities of the 5 adsorbents with the complete adsorption time are shown in Table 4.3 and Figure 4.30.

Table 4.3: CO_2 adsorption isotherms at 25 °C

Adsorbents	C_{ad} (mg-CO_2/g)	t_{ad}[2] (minutes)	R_{ad}[3] (mg-CO_2/g-min)
PSI	25	50	0.5
PAA	52	180	0.29
MWNT	12.2	27	0.45
MWNT-PSI	23	39	0.59
MWNT-PAA	70	155	0.45

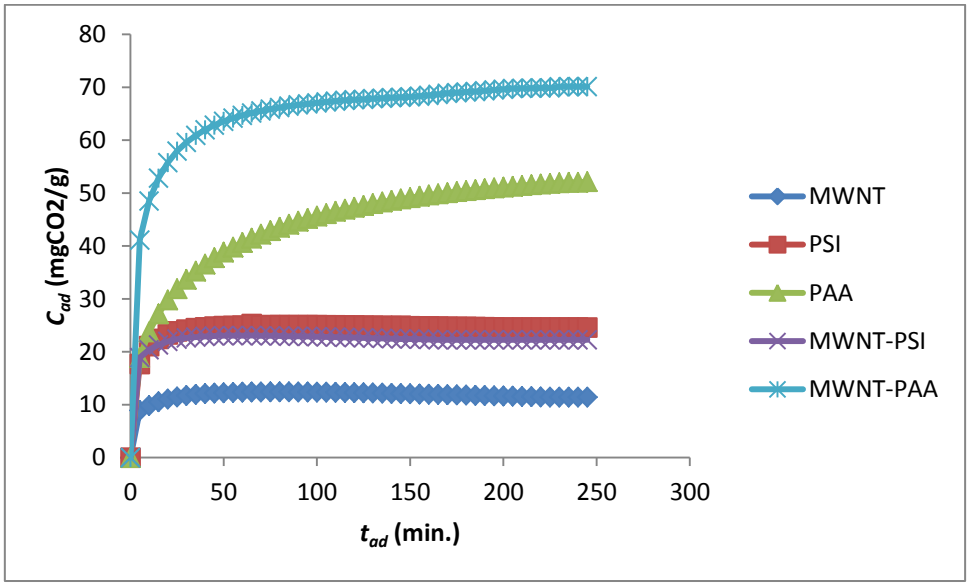


Figure 4.30: CO_2 adsorption isotherm at 25 °C using 100% CO_2

Considering the adsorption isotherm curves in Figure 4.30, the adsorption kinetics is generally high for the first 10 minutes and decreases afterward, as the curves become flatter and correspond with Langmuir models.

Thus, the first 10 minutes the adsorption was marked by high adsorption rates, as shown in Table 4.4. Apart from PAA, which has poor geometry/structure, the rest of adsorbents have high adsorption kinetics, where more or less 70% of CO_2 adsorption capacity was achieved

[2] *t_{ad}: adsorption time*
[3] *R_{ad}: adsorption rate*

during the first 10 minutes. This shows that a good geometry/structure in an adsorbent has the advantage of improving the adsorption properties. As the CO_2 adsorption capacity for PAA is 52 mg-CO_2/g over 180 minutes, the 23.8 mg-CO_2/g achieved in the first 10 minutes compared to 28.2 mg-CO_2/g over the remaining 170 minutes is important information for technology design.

Table 4.4: CO_2 adsorption capacity corresponding to the first 10 minutes

Adsorbents	**CO_2 uptake (mg-CO_2/g)**	**CO_2 uptake/CO_2 C_{ad} (%)**
MWNT	10	75
PSI	21.1	85
PAA	23.8	45.8
MWNT-PSI	20.4	89
MWNT-PAA	48.5	70.3

The large CO_2 adsorption with high adsorption kinetics within the first 10 minutes of the adsorption process shows that the possible combination of broad available sites produce high attraction forces able to capture large quantities of CO_2. The faster the adsorption occurs, the more the available sites decrease, resulting in a reduction of attraction forces to capture CO_2. Accordingly the driving force for CO_2 adsorption decreases in intensity over time.

The lack of the CO_2 anchoring site to form carbamate on MWNT, PSI, and MWNT-PSI has limited the CO_2 adsorption capacity to physisorption occurrence. Further, on adsorption PAA shows high adsorption capacity compared to MWNT, PSI and MWNT-PSI which have rather good geometry/structure properties. This shows that the improvement of chemical surface through PAA synthesis with the presence of NH_2 as CO_2 anchoring site was an efficient route to allow chemisorption over carbamate occurrence. However, the adsorption process took 180 minutes to allow a large quantity of CO_2 adsorption at 25 °C.

Thus, the surface modification done of PSI using EDA was beneficial to increase the CO_2 adsorption capacity by 108%. Similarly, the improvement of geometry/structure of PAA using MWNT to produce MWNT-PAA was beneficial to increase the CO_2 adsorption capacity by 35% (Table 4.2).

4.3.2. CO_2 adsorption at 35 °C

Considering the CO_2 adsorption isotherms at 35 °C (Fig. 4.31), the adsorbent MWNT-PAA shows a higher CO_2 adsorption capacity (60 mg-CO_2/g) compared to the others, shown in Table 4.5. All adsorbents, excluding PAA which remains stable, showed a decrease of CO_2 adsorption capacity at 35 °C (Fig. 4.31) compared to 25 °C. This confirms the predominance of physisorption, which is known to decreases with an increase of temperature. PAA alone shows a predominance of chemisorption for carbamate formation was more favorable at 35 °C. The poor geometry/structure of the adsorbent PAA was a drawback for the physisorption occurrence. When the chemisorption determines the adsorption process, the increase of adsorption capacity with the increase of temperature is possible in a certain temperature range. Also, the adsorption process of a gas at low temperature with the physisorption occurrence can change into chemisorption at higher temperatures.

Table 4.5: CO_2 adsorption isotherm at 35 °C

Adsorbents	C_{ad} (mg-CO_2/g)	t_{ad} (minutes)	R_{ad} (mg-CO_2/g-min)
PSI	20	38	0.53
PAA	52	113	0.46
MWNT	11	39	0.30
MWNT-PSI	20	38	0.53
MWNT-PAA	60	120	0.50

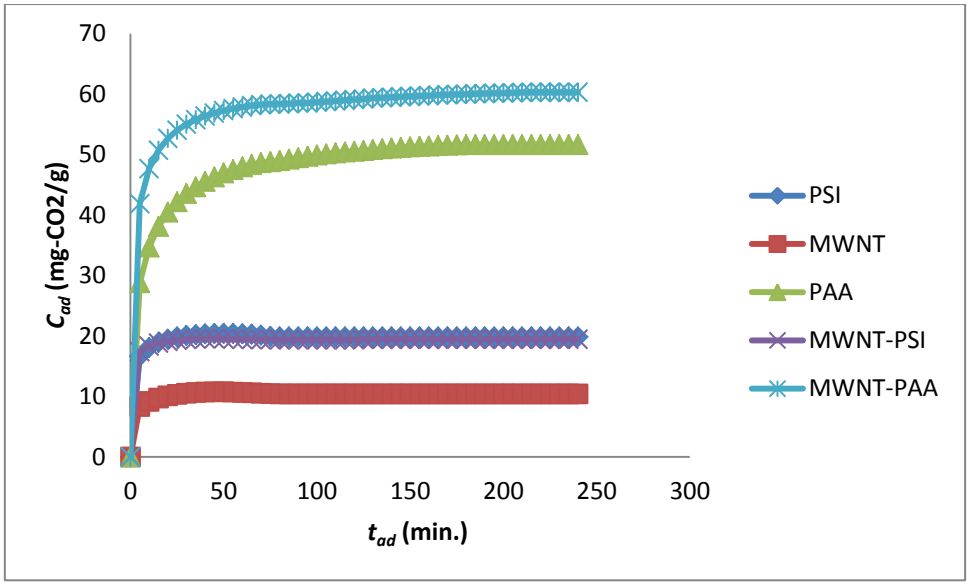


Figure 4.31: CO_2 adsorption isotherm at 35 °C using 100% CO_2

The chemical surface modification of the adsorbent PSI to produce PAA has resulted in an increase of CO_2 adsorption capacity by 160% from PSI to PAA for the adsorption performed at 35 °C. Similarly, the geometry/structure improvement of the adsorbent PAA to produce MWNT-PAA has resulted in an increase of CO_2 adsorption capacity by 16%. The adsorbent MWNT was purposely used to improve the geometry/structure in order to produce the adsorbent MWNT-PAA with higher CO_2 adsorption capacity. However, the adsorbent MWNT always had a lower adsorption compared to all other adsorbents. The CO_2 adsorption capacity of the adsorbent MWNT-PSI was not favorable compared to PSI; however the MWNT-PSI shows the improvement of geometry/structure through the coating of MWNT by PSI. The same phenomenon was observed on the reduced CO_2 adsorption capacity for MWNT-PSI at 25 °C as was reproduced at 35 °C. It was stated previously that the PSI has tightly twisted over the MWNT, keeping the diameter of the resultant product constant (Fig. 4.21). This can significantly shrink the pore size, resulting in the restriction of CO_2 to migrate towards available sites. Consequently, the adsorbent MWNT-PSI was found less suitable for CO_2 capture since it does not demonstrate the CO_2 adsorption capacity improvement when compared to PSI.

The CO_2 adsorption rate has generally increased at 35 °C compared to the adsorption rate obtained at 25 °C. This is obvious according to the Arrhenius equation (Eq. 4.1), which

shows clearly that the increase of temperature causes the entropy of the system to increase as well. Consequently, the adsorption rate increases, leading to higher energy of adsorption.

$$\ln k = \ln A - \frac{E_a}{RT} \qquad \text{Equation 4.1}$$

where k is the rate constant, E_a is the activation energy, R is the gas constant, T is temperature in Kelvin and A is frequency factor constant or also as pre-exponential factor or Arrhenius factor.

Thus, the adsorbents MWNT and MWNT-PSI were found less important due to their low CO_2 adsorption capacity compared to PSI; MWNT-PAA performed the best overall at 35 °C. Going forward PSI, PAA and MWNT-PAA were tested.

4.3.3. CO_2 adsorption at 45 °C

The adsorbent MWNT-PAA again has the highest CO_2 adsorption capacity of the 3 samples (PSI, PAA and MWNT-PAA), with a maximum of 56 mg-CO_2 at 45 °C (Fig. 4.32). There is an increase of adsorption rate and the adsorption kinetics as the temperature increases from 35 to 45 °C, which is in agreement with the Arrhenius equation (Eq. 4.1). The adsorbents MWNT-PAA and PAA perform best within the first 5 minutes, where 79 and 90% of the maximum of CO_2 adsorption capacity was achieved (Fig. 4.33). The first 30 minutes were marked with very high adsorption kinetics for all three adsorbents where 95, 93 and 97% of the maximum CO_2 adsorption capacity was achieved (Fig. 4.32).

Thus, as observed at previous temperatures (25 and 35 °C), the surface modification of PSI using EDA to produce PAA was beneficial to increase the CO_2 adsorption capacity by 120% for the adsorption performed at 45 °C. Similarly the improvement of geometry/structure done on PAA by using MWNT to produce MWNT-PAA was beneficial to increase the CO_2 adsorption capacity by 48% compared to PAA alone.

Table 4.6: CO_2 adsorption isotherm at 45 °C

Adsorbents	C_{ad} (mg-CO_2/g)	t_{ad} (minutes)	R_{ad} (mg-CO_2/g-min)
PSI	17.0	30	0.57
PAA	38	65	0.58
MWNT-PAA	56	90	0.62

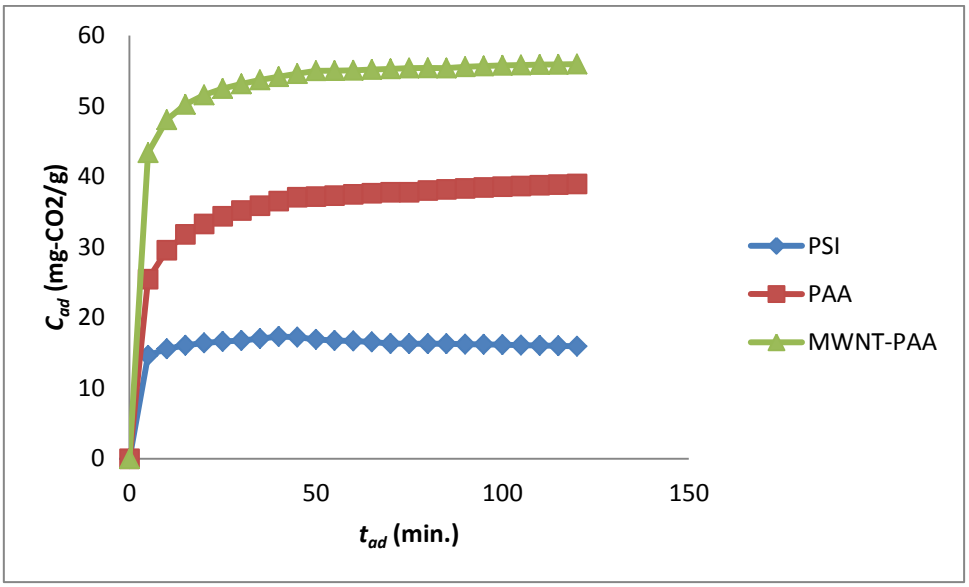


Figure 4.32: CO_2 adsorption isotherm at 45 °C using 100% CO_2

4.3.4. CO_2 adsorption at 55 °C

The adsorbent MWNT-PAA again shows a higher CO_2 adsorption capacity at 55 °C compared to PAA and PSI (Table 4.7). In contrast to the adsorbents MWNT-PAA and PSI, the adsorbent PAA showed an increase of CO_2 adsorption capacity from 45 °C (Fig. 4.32) to 55 °C (Fig. 4.33). This shows that at 55 °C the CO_2 adsorption using the adsorbent PAA was controlled mostly by chemisorption. The chemical surface modification using EDA to produce PAA has been beneficial to increase the CO_2 capacity by 181% from PSI. Similarly, the improvement of geometry/structure using MWNT to produce MWNT-PAA has been beneficial to increase the CO_2 adsorption capacity by 7% from PAA. The increase of CO_2

adsorption capacity from PAA to MWNT-PAA was not significant at 55 °C, as the isotherm curve for PAA is very close to the isotherm curve for MWNT-PAA (Fig. 4.33).

Table 4.7: CO_2 adsorption isotherm at 55 °C

Adsorbents	C_{ad} (mg-CO_2/g)	t_{ad} (min.)	R_{ad} (mg-CO_2/g-min)
PSI	15.4	25	0.62
PAA	43.3	25	1.73
MWNT-PAA	46.4	35	1.33

With regards to the adsorption kinetics, a higher adsorption rate was observed in the first 5 minutes of the adsorption time where 90% of CO_2 adsorption capacity was achieved for PAA and 81% for MWNT-PAA, and PSI (Fig.4.33). However, the adsorption time was reduced to complete the total CO_2 adsorption capacity (Table 4.7) due to the increase of adsorption rate with the increase of temperature (Eq. 4.1).

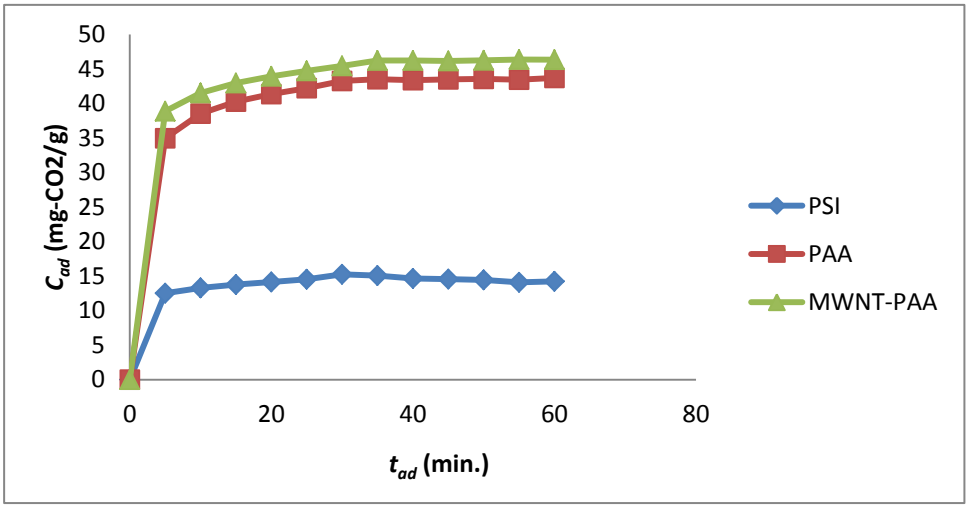


Figure 4.33: CO_2 adsorption isotherm at 55 °C using 100% CO_2

4.3.5. CO_2 adsorption at 65 °C

The decrease of CO_2 adsorption for all the adsorbents was not so significant at 65 °C compared to the CO_2 adsorption obtained at 55 °C. The adsorbent MWNT-PAA shows a higher CO_2 adsorption capacity compared to PAA and PSI (Table 4.8). The chemical surface modification using EDA to produce PAA has been beneficial to increase the CO_2 adsorption capacity by 213% from PSI. Similarly, the geometry/structure improvement using MWNT has been beneficial to increase the CO_2 adsorption capacity by 12% from PAA.

Table 4.8: CO_2 adsorption isotherm at 65 °C

Adsorbents	C_{ad} (mg-CO_2/g)	t_{ad} (min.)	R_{ad} (mg-CO_2/g-min)
PSI	13.1	20	0.66
PAA	41	21	1.95
MWNT-PAA	46	25	1.84

The first 5 minutes of the adsorption times were noticeable, with a high CO_2 adsorption rate, where 82%, 88% and 87% of the maximum of CO_2 adsorption capacity was achieved for PSI, PAA and MWNT-PAA, respectively. However, the adsorption time for complete CO_2 adsorption capacity was short compared to the previous temperatures. This still confirms that the increase of temperature causes the increase of molecular entropy relevant to the increase of kinetic energy, which results in high adsorption kinetics according to the Arrhenius equation (Eq. 4.1).

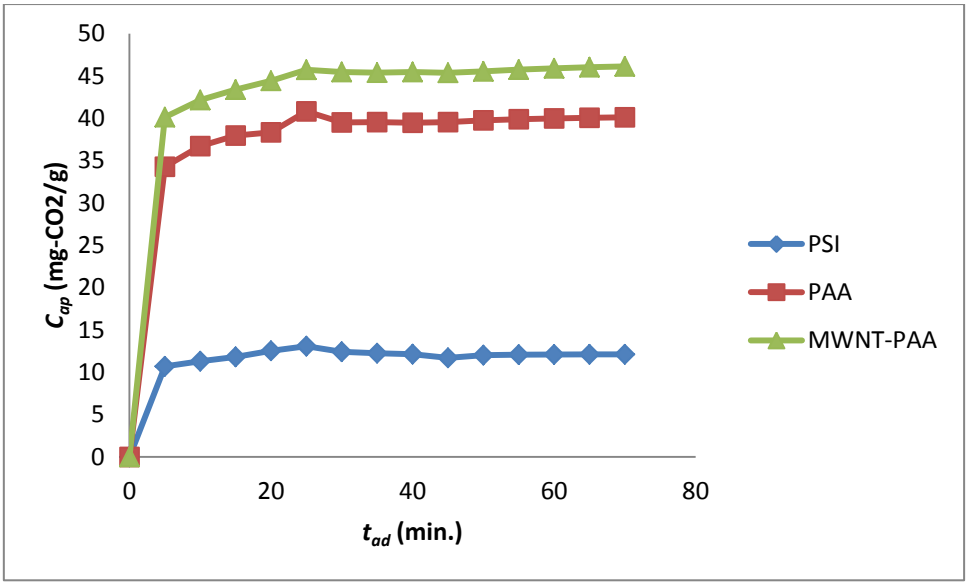


Figure 4.34: CO_2 adsorption isotherm at 65 °C using 100% CO_2

4.3.6. CO_2 adsorption at 75 °C

.

The adsorbent MWNT-PAA shows a higher CO_2 adsorption capacity compared to PAA (Table 4.9) at 75 °C. The CO_2 adsorption capacity for all adsorbents decreased with the increase of temperature from 65 to 75 °C. The chemical surface modification using EDA to produce PAA has been beneficial for the CO_2 adsorption capacity which increased by 230% compared to PSI at 75 °C. Similarly the improvement of geometry/structure using MWNT to produce MWNT-PAA has been beneficial to increase the CO_2 adsorption capacity by a further 27.3% from PAA. The beginning of adsorption was marked with a higher adsorption rate where 82% and 88% of the total CO_2 adsorption capacity was achieved during the first 5 minutes of adsorption process for PAA and MWNT-PAA, respectively. However, the adsorption time to complete the maximum CO_2 adsorption capacity kept decreasing with the increase of temperature to 75 °C (Fig. 4. 35).

Table 4.9: CO_2 adsorption isotherm at 75 °C

Adsorbents	C_{ad} (mg-CO_2/g)	t_{ad} (min.)	R_{ad} (mg-CO_2/g-min)
PSI	10	15	0.67
PSI-EDA	33	20	1.65
PSI-EDA-MWNT	42	20	2.10

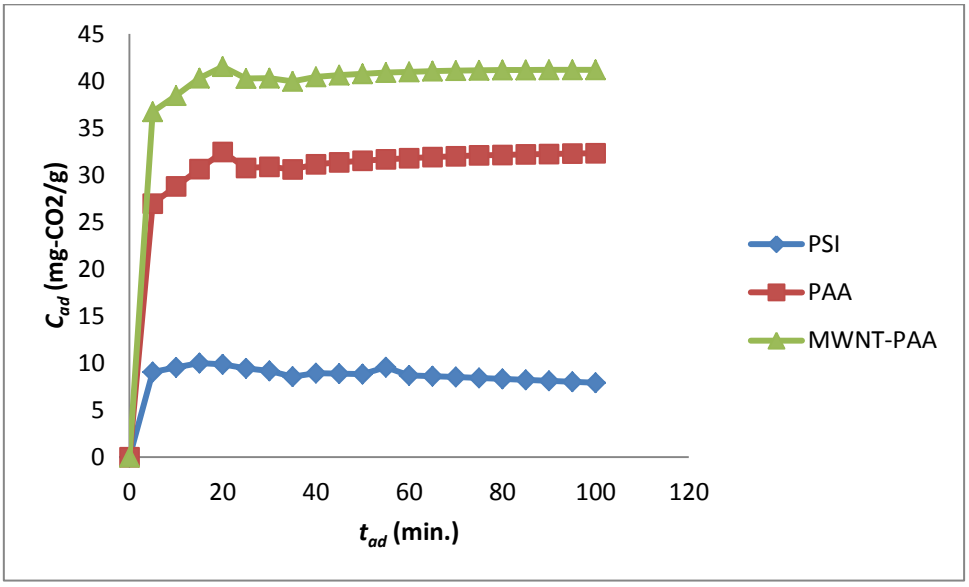


Figure 4.35: CO_2 adsorption isotherm at 75 °C using 100% CO_2

4.3.7. CO_2 adsorption at 85 °C

The last temperature tested was at 85 °C. The decrease of CO_2 adsorption capacity was observed at 85 °C for the adsorbents PSI, PAA and MWNT-PAA as shown in Figure 4.36. Compared to the CO_2 adsorption capacity obtained at 75 °C, the increase of temperature to 85 °C was marked with the decrease of CO_2 adsorption capacity by 10, 15 and 21% for PSI, PAA and MWNT-PAA, respectively. Within the first 5 minutes, 82, 80 and 88% of the maximum CO_2 adsorption capacity was achieved for PSI, PAA and MWNT-PAA, respectively. However, the time to complete the maximum CO_2 adsorption capacity was 10, 15 and 12 minutes for PSI, PAA and MWNT-PAA respectively, as depicted in Table 4.10. The CO_2 adsorption time at 85 °C was very short compared to the CO_2 adsorption time at

previous temperatures. The increase of adsorption kinetics with the increase of temperature was continuously observed at all temperatures, as well as at 85 °C.

Table 4.10: CO_2 adsorption isotherm at 85 °C

Adsorbents	C_{ad} (mg-CO_2/g)	t_{ad} (min.)	R_{ad} (mg-CO_2/g-min)
PSI	9	10	0.9
PAA	28	15	1.87
MWNT-PAA	33	12	2.75

Thus, EDA has been beneficial for chemical surface modification as the CO_2 adsorption capacity of PAA has increased by 211% from PSI at 85 °C. Also the production of MWNT-PAA through geometry/structure improvement using MWNT has been beneficial to increase the CO_2 adsorption capacity by 18% from PAA.

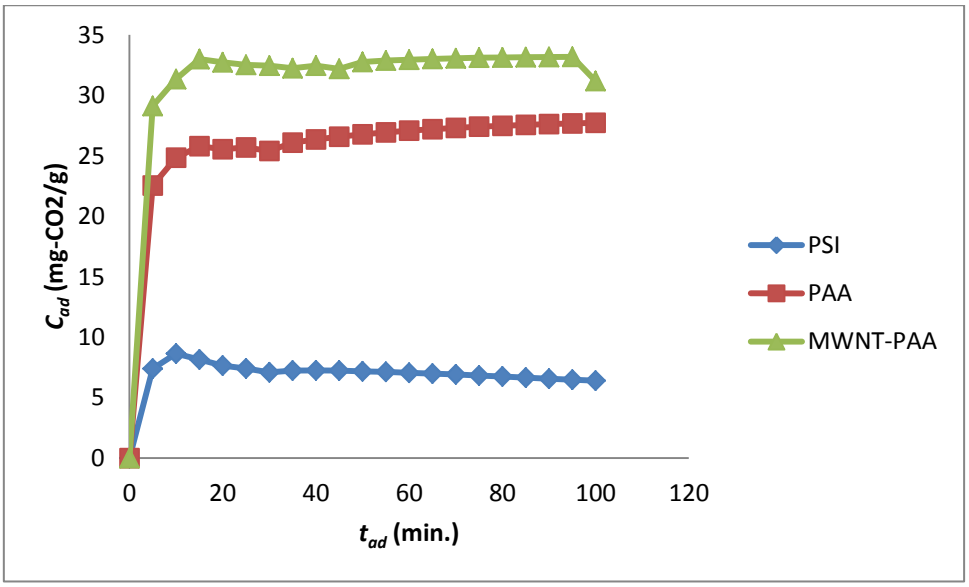


Figure 4.36: CO_2 adsorption isotherm at 85 °C using 100% CO_2

4.3.8. Conclusion of effect of increasing temperature on adsorbents in 100% CO_2

The experiments conducted with the use of the TGA at variable temperatures in the range 25-85 °C and at a constant pressure of 1.1 bars where the adsorbents were exposed to the flowing of 100% CO_2 with a flow rate of 60 mL/min for the CO_2, led to the results presented in Table 4.11 and the following conclusions.

Table 4.11: Temperature effects on CO_2 adsorption capacity and adsorption time

Ads.	25 °C	35 °C	45 °C	55 °C	65 °C	75 °C	85 °C
	C_{ad} t_{ad}	C_{ad} t_{ad}	C_{ad} t_{ad}	C_{ad} t_{ad}	C_{ad} t_{ad}	C_{ad} t_{ad}	C_{ad} t_{ad}
PSI	25mg/g 50 min	20mg/g 38 min	17.3mg/g 30 min	15.4mg/g 25 min	13.1mg/g 20 min	10mg/g 15 min	9mg/g 10 min
PAA	52mg/g 180 min	52mg/g 113 min	38mg/g 65 min	43.3mg/g 25 min	41mg/g 21 min	33mg/g 20 min	28mg/g 15 min
MWNT-PAA	70mg/g 155 min	60mg/g 120 min	56mg/b 90 min	46.4mg/g 35 min	46mg/g 25 min	42mg/g 20 min	33mg/g 12 min

a) In the adsorption process, the first few minutes are marked by high CO_2 adsorption rates, which resulted in high adsorption kinetics, according to the Langmuir models.
b) The increase of temperature leads to high CO_2 adsorption kinetics, in agreement with the Arrhenius equation. Therefore, the higher the temperature, the shorter the time is to achieve the maximum CO_2 adsorption capacity (Table 4.11).
c) However, the total CO_2 adsorption capacity decreases with the increase of temperature, when physisorption is the predominant adsorption process.
d) It is possible to increase the CO_2 adsorption capacity with an increase of temperature when chemisorption is the predominant adsorption process. This was observed for the adsorbent PAA in temperature range 25 - 35 °C and 45 - 55 °C, where the CO_2 adsorption capacity was constant and increased with the increase of temperature (Table 4.11) respectively.

e) The physisorption and chemisorption in the CO_2 adsorption process are related to an adequate geometry/structure and specific chemical surface.

f) The use of EDA to produce PAA and the use of MWNT to produce MWNT-PAA are beneficial to enhance the CO_2 adsorption capacity at all adsorption temperatures (25-85 °C) as shown in Figure 4.37 compared to crude PSI and PAA, respectively (Table 4.11).

g) Despite the poor geometry/structure of PAA, the presence of a primary amine was enough to cause chemisorption through carbamate formation, thus leading to high CO_2 adsorption capacity.

h) Using PAA as adsorbent, the highest CO_2 adsorption capacity was 52 $mgCO_2/g$, obtained at 25 and 35 °C.

i) The chemisorption process is more dominant at 35 and 55 °C when using PAA as an adsorbent.

j) The CO_2 adsorption capacity of the adsorbents MWNT-PAA steadily decreases with the increase of temperature to show the predominance of physisorption over chemisorption that should occur due to the presence of the primary amine on MWNT-PAA. 70 mg-CO_2/g achieved at 25 °C is the highest CO_2 adsorption capacity for the MWNT-PAA in the temperature range 25 - 85 °C (Table 4.11).

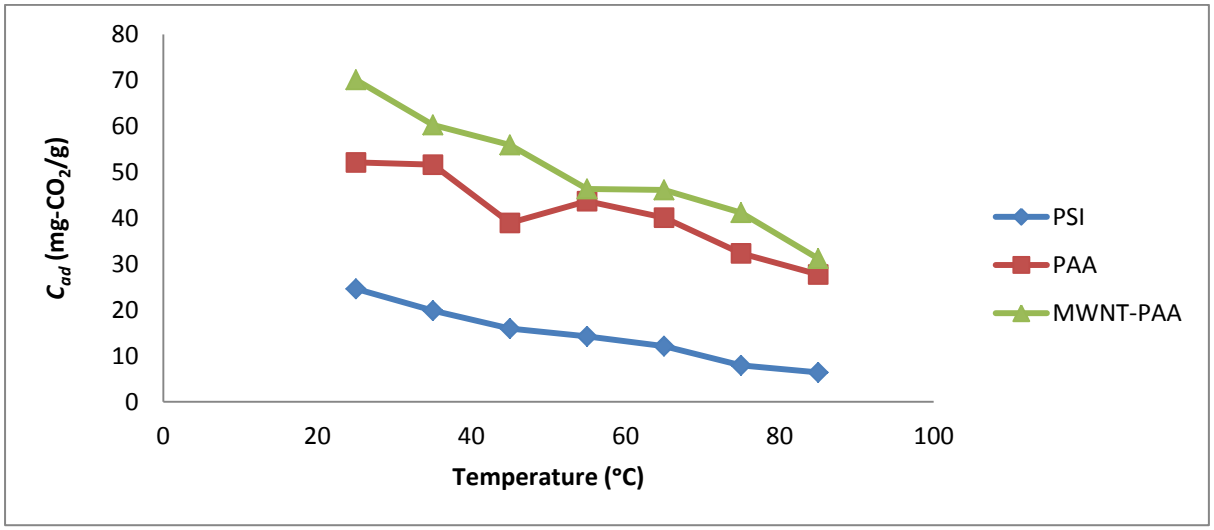


Figure 4.37: Temperature effect on CO_2 adsorption capacity for all adsorbents

The adsorbents PAA and MWNT-PAA have been competitive with respect to adsorption capacity, adsorption rate and kinetics of adsorption. Therefore, further investigation of their selectivity with respect to CO_2 and their ability to adsorb CO_2 diluted in flue gas were necessary for their evaluation and potential application in CO_2 capture technology.

4.4. TEMPERATURE EFFECTS ON CO_2, N_2 and O_2 ADSORPTION

In this section, the adsorbents PAA and MWNT-PAA were exposed to N_2 and O_2 at different temperatures in the range 25-55 °C with increasing temperature intervals of 10 °C using TGA at a pressure of 1.1 bars and a flow rate of 60 mL/min. This was necessary for clarity of the selectivity for CO_2 over N_2 + O_2, flue gas effluent from fossil fuel power plants will contain predominantly N_2, with same O_2 + CO_2, amongst other gases. The activity of O_2 and N_2 is intended to decrease in the presence of CO_2 when using an amine adsorbent.

4.4.1. N_2 and O_2 adsorption at 25 °C compared to CO_2 adsorption

The adsorbent PAA shows very low affinity for N_2 and O_2 at 25 °C compared to CO_2 (Table. 4.12). Therefore, the adsorption of N_2 and O_2 were insignificant when using 100% N_2 and 100% O_2 compared to the adsorption of CO_2 when using 100% CO_2 at 25 °C (Fig. 4.38). As the chemisorption could not occur with N_2 and O_2, only physisorption could occur to a limited extent due to the poor geometry/structure of the adsorbent PAA. This indicates a high selectivity for CO_2 when using the adsorbent PAA for CO_2 captured at 25 °C and 1.1 bar from a mixture of gas containing CO_2, N_2 and O_2 contents.

Table: 4.12: Adsorption capacity using 100% CO_2, 100% O_2 and 100% N_2

Adsorbent	25 °C			35 °C			45 °C			55 °C		
	C_{ad} (mg/g)			C_{ad} (mg/g)			C_{ad} (mg/g)			C_{ad} (mg/g)		
	CO_2	O_2	N_2	CO_2	O_2	N_2	CO_2	O_2	N_2	CO_2	O_2	N_2
PAA	52	1.4	2.8	52	1.3	1	38	0.97	0.78	43.4	0	0
MWNT-PAA	70	2.1	2	60	12.5	1.1	56	3.18	0.88	46.4	0.33	0

The adsorption of pure N_2 and pure O_2 using MWNT-PAA as adsorbent shows a low adsorption capacity of 2 mg/g for both N_2 and O_2 after 150 minutes as compared to CO_2 adsorption capacity that was 70mg/g (Table 4.12). The adsorbent MWNT-PAA has adequate geometry/structure for good adsorption, yet the N_2 and O_2 adsorption was insignificant at 25 °C (Fig. 4.39). This shows that the presence of amine could inhibit the adsorption of N_2 and O_2 to occur through either chemisorption or physisorption at 25 °C. Thus, high selectivity for CO_2 is predicted when using MWNT-PAA as adsorbent for CO_2 which has to be separated from a mixture of gas which includes N_2 and O_2 at 25 °C.

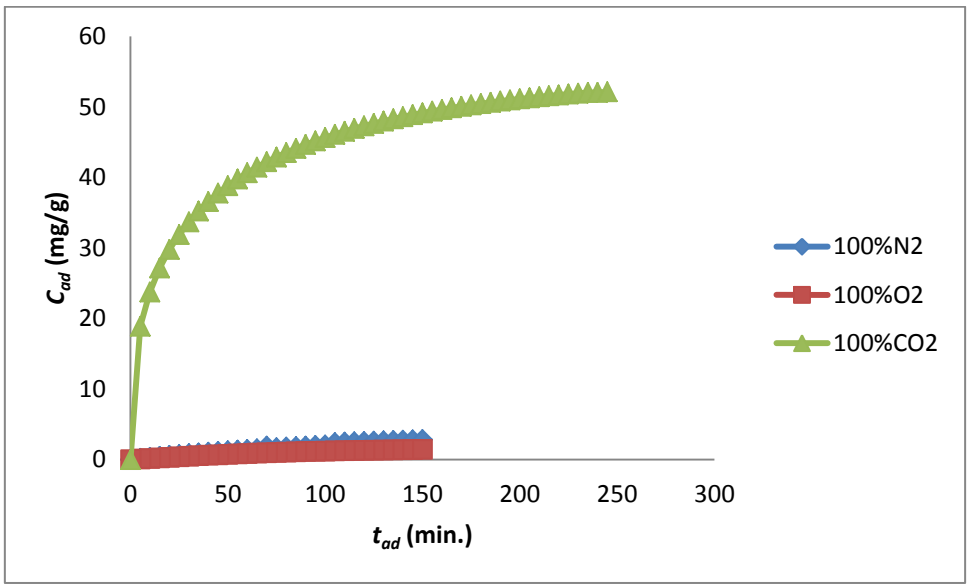


Figure 4.38: The adsorption of N_2, O_2 and CO_2 using PAA at 25 °C

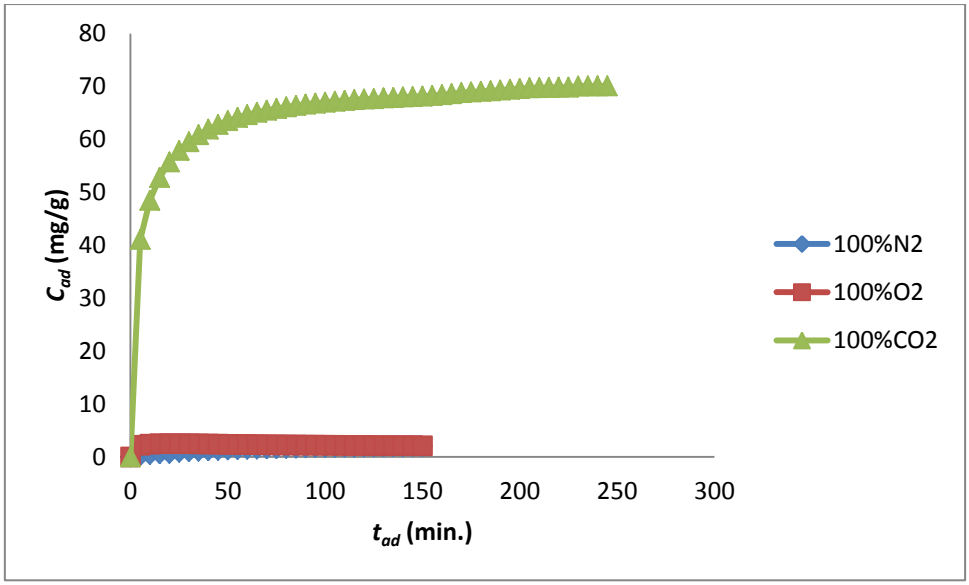


Figure 4.39: The adsorption of N_2, O_2 and CO_2 using MWNT-PAA at 25 °C

4.4.2. N_2 and O_2 adsorption at 35 °C compared to CO_2 adsorption

The adsorbent PAA shows a very low adsorption capacity of 1.3 mg/g for both N_2 and O_2 after 150 minutes of adsorption, compared to the CO_2 adsorption capacity which was 52 mg-CO_2/g at 35 °C (Table 4.12). The adsorption isotherm curves for N_2 and O_2 are very close to zero adsorption at 35 °C (Figure 4.40), confirming the predominance of CO_2 chemisorption occurring at 35 °C as stated previously. Obviously the primary amine group found on the PAA was specific for CO_2 adsorption. This shows the potential high selectivity for CO_2 when CO_2 has to be captured from flue gas with CO_2, N_2 and O_2 contents.

The adsorbent MWNT-PAA shows an increase of O_2 adsorption capacity at 35 °C, while the N_2 adsorption capacity remains low (Table 4.12 and Fig. 4.41). Despite the increase of O_2 uptake with the increase of temperature, it is unlikely that the selectivity for CO_2 will be detrimentally affected as the O_2 levels in the flue gas are typically between 4.6-7.1% [281]. In the case of oxyfuel combustion, the selectivity for CO_2 may be slightly more challenging due to the enhance O_2 content, approximately 30% [282].

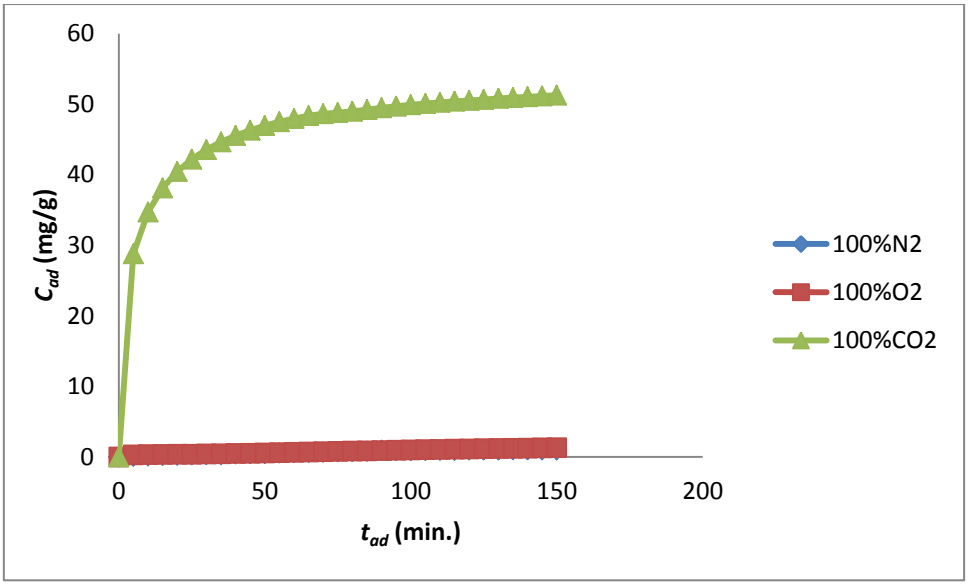


Figure 4.40: The adsorption of N_2, O_2 and CO_2 using PAA at 35 °C

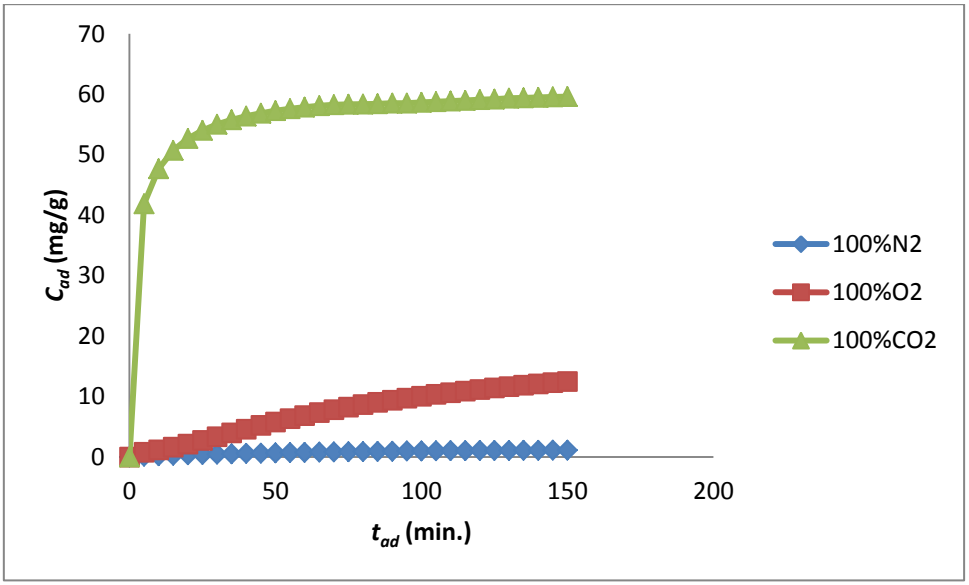


Figure 4.41: The adsorption of N_2, O_2 and CO_2 using MWNT-PAA at 35 °C

4.4.3. N_2 and O_2 adsorption at 45 °C compared to CO_2 adsorption

At 45 °C the PAA adsorption capacity has decreased in the 100% CO_2 stream, the same trend that was reported in Section 4.3. The N_2 and O_2 gases have very low adsorption potential at

this temperature, as shown in Table 4.12. A high selectivity for CO_2 is predicted since the isothermal adsorption curve for CO_2 is much higher compared to the isothermal adsorption curves for N_2 and O_2 (Fig. 4.42).

Figure 4.43 indicates a rapid O_2 uptake by the MWNT-PAA adsorbent in the first 5 minutes, as previously observed. The selectivity for CO_2 is predicted to be negatively affected by other gases at the very beginning of the adsorption, but it recovers afterward as the adsorption process continues. The CO_2 shows a higher affinity to MWNT-PAA compared to N_2 and O_2 (Table 4.12).

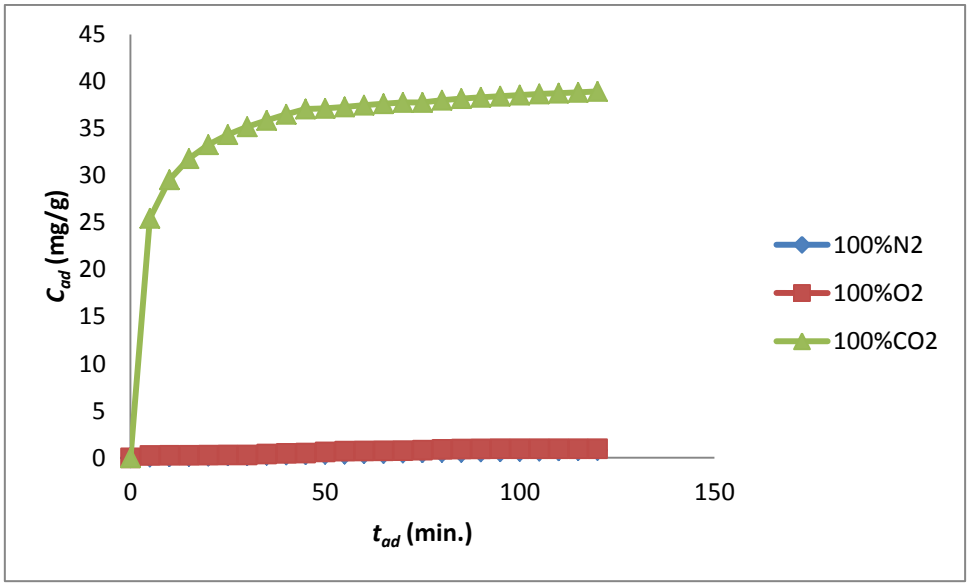


Figure 4.42: The adsorption of N_2, O_2 and CO_2 using PAA at 45 °C

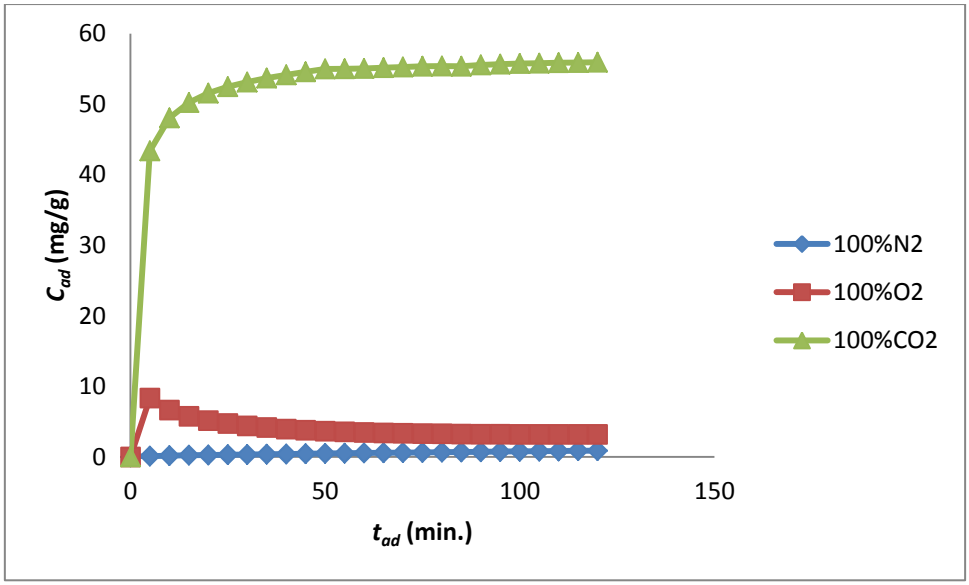


Figure 4.43: The adsorption of N_2, O_2 and CO_2 using MWNT-PAA at 45 °C

4.4.4. N_2 and O_2 adsorption at 55 °C compared to CO_2 adsorption

At 55 °C neither N_2 nor O_2 were adsorbed by the PAA, while a significant amount of CO_2 was adsorbed (Table 4.12). The CO_2 adsorption curve is much more prominent compared to the O_2 and N_2 adsorption curves, which coincide with the zero line of adsorption (Fig. 4.44). This indicates that a maximum selectivity for CO_2 when using a mixture of gas composed with CO_2, O_2 and N_2 for the adsorption performs at 55 °C.

With regard to O_2 adsorption at 55 °C using MWNT-PAA, an insignificant amount of O_2 was adsorbed in the first five minutes, and it dropped to zero after that, while the N_2 adsorption was consistently zero (Fig. 4.45). The higher CO_2 uptake compared to O_2 and N_2 uptake gives maximum selectivity for CO_2 when the flue gas is composed of CO_2, O_2 and N_2.

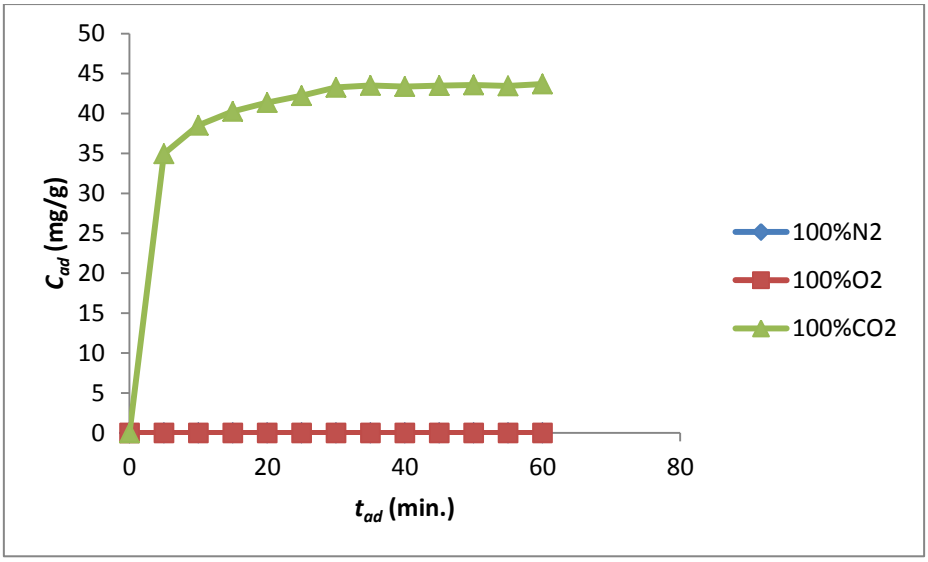


Figure 4.44: The adsorption of N_2, O_2 and CO_2 using PAA at 55 °C

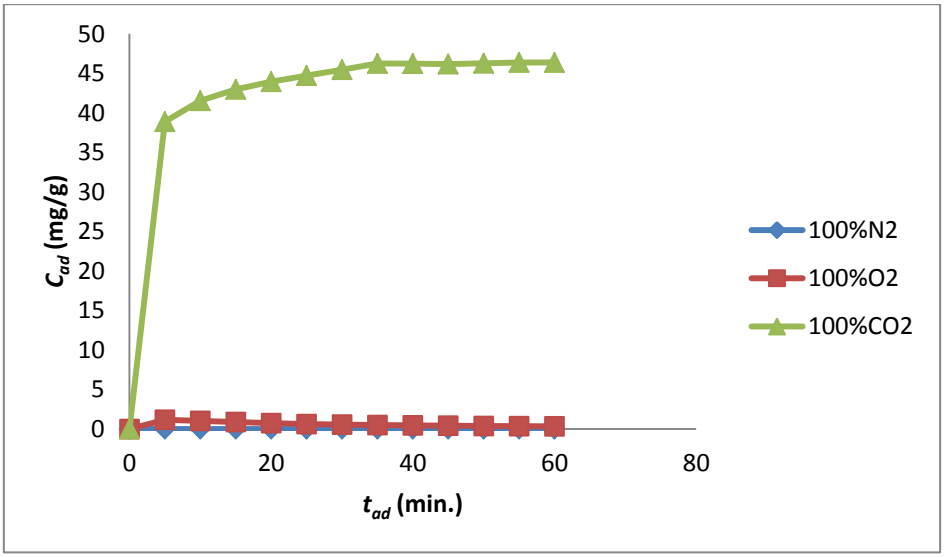


Figure 4.45: The adsorption of N_2, O_2 and CO_2 using MWNT-PAA at 55 °C

4.4.5. Section summary

The selectivity for CO_2 over other gases, in this instance N_2 and O_2, is an important factor to consider when addressing the performance of an adsorbent. The adsorbent PAA showed a high affinity for CO_2 in the temperature range 25 °C and 55 °C, where the chemical surface was essentially unable to attract N_2 and O_2. Thus, PAA could be used for adsorption

technology design after proving its performance for CO_2 capture in flue gas consisting of variable CO_2 and other gas concentrations.

The selectivity for CO_2 over O_2 + N_2 using MWNT-PAA was more challenging in the temperature range 35 – 45 ^oC, where a significant amount of O_2 could be adsorbed. However, the large amount of N_2 in the flue gas composition does not appear to be of any concern, since the N_2 adsorption was almost zero for both PAA and MWNT-PAA in the temperature range tested.

Therefore, it is clear that the PAA and MWNT-PAA would be able to selectively adsorb CO_2 from a CO_2, N_2, O_2 gas mixture in the temperature range 25 - 55 ^oC. The effect of these gas mixtures on CO_2 adsorption capacity are discussed in the following section.

4.5. CO_2 ADSORPTION FROM GAS WITH VARIABLE CO_2 CONCENTRATION

In order to determine the effects of CO_2 adsorption from a gas mixture, the following adsorption tests were performed using the TGA: 1) with a gas mixture containing 14% CO_2 (14 mL/min) and air (86 mL/min); 2) with a gas mixture containing 40% CO_2 (40 mL/min) and air (60 mL/min). The experiments were run at temperatures from 25 to 55 °C with temperature intervals of 10 °C and at a pressure of 1.1 bars to determine how it differs from cases when 100% CO_2 were used.

4.5.1. CO_2 adsorption at 25 °C.

4.5.1.1. PAA

The adsorption performed at 25◦C using the adsorbent PAA shows an increase of adsorption capacity with an increase of CO_2 concentration in a gas stream (Table 4.13 + Fig. 4.46). PAA shows an increase of adsorption capacity by 13% from 14 to 40% CO_2 and by 49% from 40

to 100% CO_2. The dilution of CO_2 in the flue gas resulted in a reduced adsorption of CO_2. As the adsorbent PAA has a poor geometry/structure, which includes large pore sizes, the gas stream could diffuse smoothly while either N_2 or O_2 could interfere with the diffusion of CO_2 toward an available adsorption site. This phenomenon is known as persorption where N_2 and O_2 in air are not held by ordinary valence bonds, but merely fit into the vacant spaces in the lattice of the PAA [283]. It should be born in mind that the adsorption takes place only on the external surface of adsorbent, and not in the fluid surrounding it. In the adsorption process, there is a formation of a film in the vicinity of the spherical [134] pellet of the adsorbent (Section 2.4). The composition of the film depends on the intrinsic rate of adsorption of each gas, which corresponds to the concentration thereof (partial pressure), molecular weight and temperature [284]. Since that film does not define the attachment of the adsorbate on the adsorbent, it can be an obstacle to the adsorbate (CO_2) to reach the available surface of the adsorbent when it is covered by gases such as O_2 or N_2. Thus, the driving force encounters the inertia of the air that is present. This inertia becomes more significant when operating at low pressure and low temperature where the selectivity for CO_2 is supposed to be high, because the N_2 and O_2 in the air could potentially concentrate in the pore without being adsorbed. Consequently, the passage of CO_2 will be slowed down to get to the available adsorption sites. As the adsorption results in carbamate formation through chemisorption, the possibility of increasing the temperature should increase the activity of the CO_2, leading to the activation energy, according to the Arrhenius principle. Thus, the kinetic energy will increase with an increase of temperature, resulting in high convection able to allow a sufficient driving force for the increase of adsorption capacity. Furthermore, the adsorbent PAA has showed in Section 4.4 that the increase of temperature caused a decrease of O_2 and N_2 adsorption. In case of an increase of pressure, the persoption phenomenon will be reduced, because the gases O_2 and N_2, due to very low affinity for the amine, will be driven out, leaving the lattice available for CO_2 adsorption. In addition, the increase of CO_2 concentration can cause the radial dispersion of CO_2 with an increase of driving force toward the available sites, thus resulting in an increase of adsorption capacity.

Table 4.13: Adsorption capacity and selectivity for CO_2 over air (O_2 + N_2) at 25 °C

Adsorbents	14% CO_2		40% CO_2		100% CO_2	
	C_{ad} mg/g	X_{CO2}[4] %	C_{ad} mg/g	X_{CO2} %	C_{ad} mg/g	X_{CO2} %
PAA	31	86	35	87	52	100
MWNT-PAA	47	90	62	92.4	70	100

With regards to the selectivity for CO_2, it can be deduced that the adsorption of N_2 and O_2 in either 14% CO_2 or 40% CO_2 content is probably insignificant, since the adsorption of N_2 and O_2 using 100% N_2 and 100% O_2 by the PAA was very low (Fig. 4.38). Thus, the N_2 and O_2 uptake from 100% N_2 and 100% O_2 was considered as the maximum amount of N_2 and O_2 that PAA can adsorb when exposed to a mixture of gas containing either 14% CO_2 or 40% CO_2. This has allowed the evaluation of a minimum selectivity for CO_2 where, after 150 minutes of adsorption isothermal time, the minimum concentration of CO_2 in the adsorbed gas is shown in Table 4.13.

Considering the adsorption kinetics, it was found that the first 30 minutes was marked by high adsorption kinetics, where 22.5 mg/g and 25 mg/g or 68.2% and 71.4% respectively of the maximum adsorption capacity was achieved for 14% CO_2 and 40% CO_2 gas mixtures (Fig. 4.46). This is beneficial, since Figure 4.38 shows an insignificant adsorption of N_2 and O_2 of 0.5 mg/g in the first 30 minutes. After calculation, the first 30 minutes results in an estimated adsorbed gas with a minimum concentration of 96% CO_2 using both 14% CO_2 and 40% CO_2 in the gas stream respectively. Thus, the selectivity for CO_2 was very high level at the beginning of adsorption and dropped over time.

4.5.1.2. *MWNT-PAA*

Similar comments pertaining to PAA apply to MWNT-PAA, where the adsorption capacity

[4] X_{CO2}: Selectivity for CO_2

increased with the increase of CO_2 concentration in the gas stream at 25 °C (Table 4.13). The MWNT-PAA adsorbent shows a higher adsorption capacity at all concentrations compared to PAA. The improvement of geometry/structure, which includes the smaller pore size, could operate as a sieve to allow more CO_2 to migrate towards available adsorption sites than N_2 and O_2. Therefore, the radial dispersion of CO_2 toward available adsorption sites can become dominant.

With regard to the selectivity for CO_2, it is noticeable that the adsorption of N_2 and O_2 in the mixture of gas containing either 14% CO_2 or 40% CO_2 is undoubtedly insignificant, as the adsorption of N_2 and O_2 from 100% N_2 and 100% O_2 was very low (Fig. 4.39). As with PAA, the minimum selectivity for CO_2 after 150 minutes of isothermal adsorption time when using MWNT-PAA was evaluated, and the minimum concentration of CO_2 in the adsorbed gas is shown in Table 4.13.

The first 30 minutes was marked by a higher adsorption kinetics, where 39 mg/g and 48 mg/g, corresponding to 83% and 77.4% of the maximum adsorption capacity, was reached after 150 minutes from 14 and 40% CO_2 flue gas mixtures, respectively (Fig. 4.47). It was demonstrated that the N_2 and O_2 adsorption was very low within the first 30 minutes when the MWNT-PAA was exposed to 100% N_2 and 100% O_2 (Fig. 4.39). This resulted in the enhancement of selectivity for CO_2 with a minimum CO_2 concentration of 91 and 93% CO_2 adsorbed when using 14 and 40% CO_2 gas mixtures, respectively.

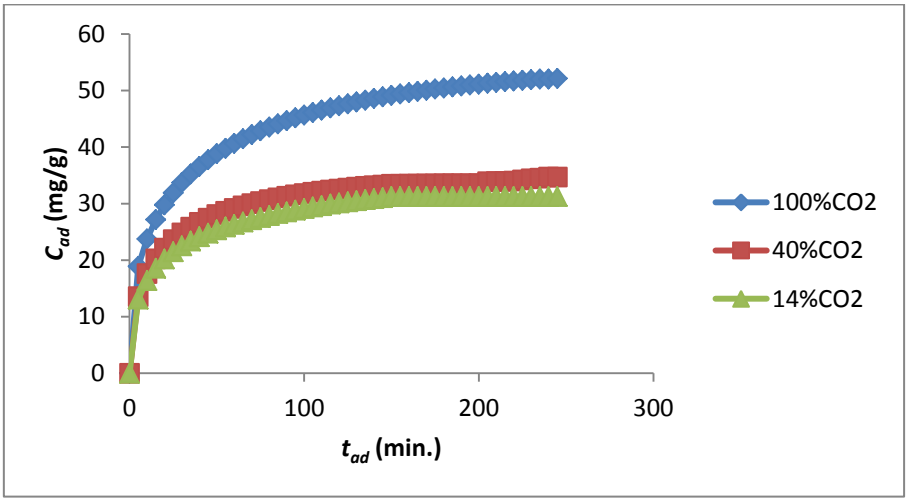


Figure 4.46: Adsorption of 100, 40 and 14% CO_2 onto PAA at 25 °C

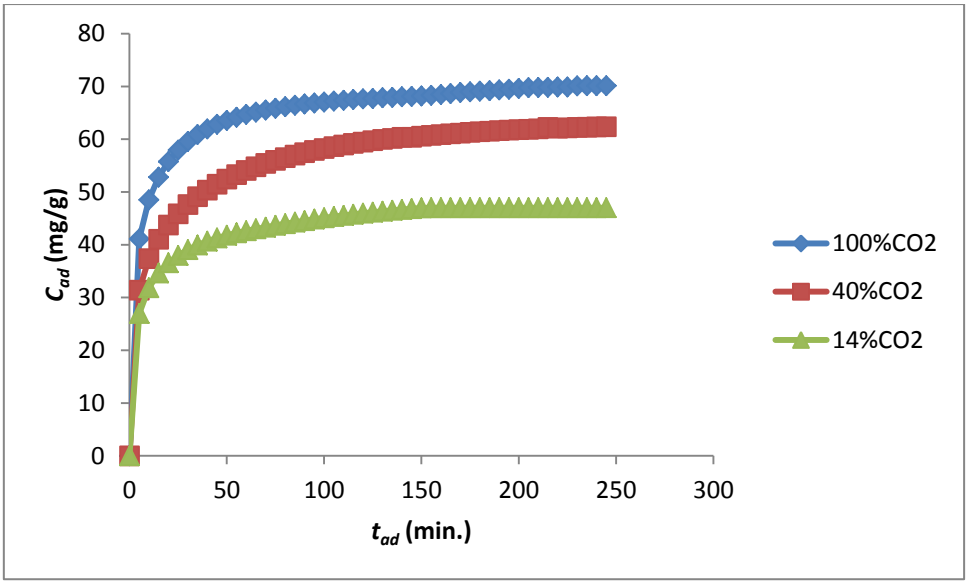


Figure 4.47: Adsorption of 100, 40 and 14% CO_2 onto MWNT-PAA at 25 °C

4.5.2. CO_2 adsorption at 35 °C

4.5.2.1. PAA

The increase of adsorption capacity with the increase of CO_2 concentration in the variable gas stream as stated previously, was also observed at 35 °C for the adsorbent PAA, as shown in Table 4.14. Everything being equal otherwise, the predominance of chemisorption was observed at 35 °C, since the change of adsorption capacity was not significant when the temperature increased from 25 to 35 °C.

With regard to the selectivity for CO_2, it was found that the adsorption of N_2 and O_2 in the gas stream with either 14 or 40% CO_2 content was insignificant since the adsorption of N_2 and O_2 when using 100% N_2 and 100% O_2 was very low, as shown in Figure 4.40. Thus, the minimum CO_2 concentration in the adsorbed gas after 150 minutes of adsorption time was measured as shown in Table 4.14.

Considering the adsorption kinetics, it was found that the first 30 minutes was marked by

higher adsorption kinetics, where 24.3 mg/g and 28 mg/g, corresponding to 78.4% and 82.4% of the maximum adsorption capacity, were achieved. Accordingly, the selectivity for CO_2 was enhanced within the first 30 minutes. A minimum CO_2 concentration of 97% CO_2 was adsorbed using a gas stream with either 14% CO_2 or 40% CO_2. This increase of selectivity for CO_2 is due to the insignificant N_2 and O_2 adsorption for PAA exposed to flowing 100% N_2 and 100% O_2 within the first 30 minutes of adsorption time, as reported in Figure 4.40. Thus, the increase of temperature from 25 to 35 °C for the adsorption using PAA has resulted in an increase of the selectivity to confirm the higher activity for CO_2 due to the chemisorption predominance.

Table 4.14: Adsorption capacity and selectivity for CO_2 over O_2 and N_2 at 35 °C

Adsorbents	14% CO_2		40% CO_2		100% CO_2	
	C_{ad} mg/g	X_{CO2} %	C_{ad} mg/g	X_{CO2} %	C_{ad} mg/g	X_{CO2} %
PAA	31	88	34	92	52	100
MWNT-PAA	45	70	51	74	60	100

4.5.2.2. MWNT-PAA

The CO_2 adsorption capacity for MWNT-PAA to the variable gas composition increased with the increase of the CO_2 concentration in the gas stream, as shown in Table 4.14. The increase of temperature from 25 to 35 °C resulted in a decrease of adsorption capacity. The CO_2 should have been higher to assure good CO_2 radial dispersion in the pores structure due to the good geometry/structure of MWNT-PAA. The radial dispersion is beneficial for CO_2 adsorption, because CO_2 can migrate easily to the vacant pores. This requires a very weak interaction of adsorbent with the flue gas which includes N_2 and O_2. Unfortunately, the adsorption of O_2 was more significant when exposing the MWNT-PAA to 100% O_2 at 35 °C (Fig. 4.41). The adsorption of N_2 could not exceed 1mgN_2/g even though N_2 was found to be in large excess in the gas composed of either 14% CO_2 or 40% CO_2. This observation is due

to the insignificant amount of N_2 adsorption when using 100% N_2 for adsorption at 35 ℃, as shown in Figure 4.41.

The selectivity for CO_2 was slightly hampered due to a large quantity of O_2 in the adsorbed gas. The evaluation of minimum CO_2 concentration in the adsorbed gas after 150 minutes of adsorption time is shown in Table 4.14. The first 30 minutes of adsorption was marked by a higher selectivity for CO_2 due to the slow adsorption kinetics for N_2 and O_2, and the rapid adsorption kinetics for CO_2 (Fig. 4.49). Thus, in the first 30 minutes of adsorption the minimum CO_2 concentration in adsorbed gas was 91% CO_2 and 92% CO_2 for a gas stream with 14% CO_2 and 40% CO_2, respectively. The selectivity for CO_2 at 35 ℃ was lower on MWNT-PAA compared to PAA; however MWNT-PAA has an advantage of large CO_2 adsorption capacity.

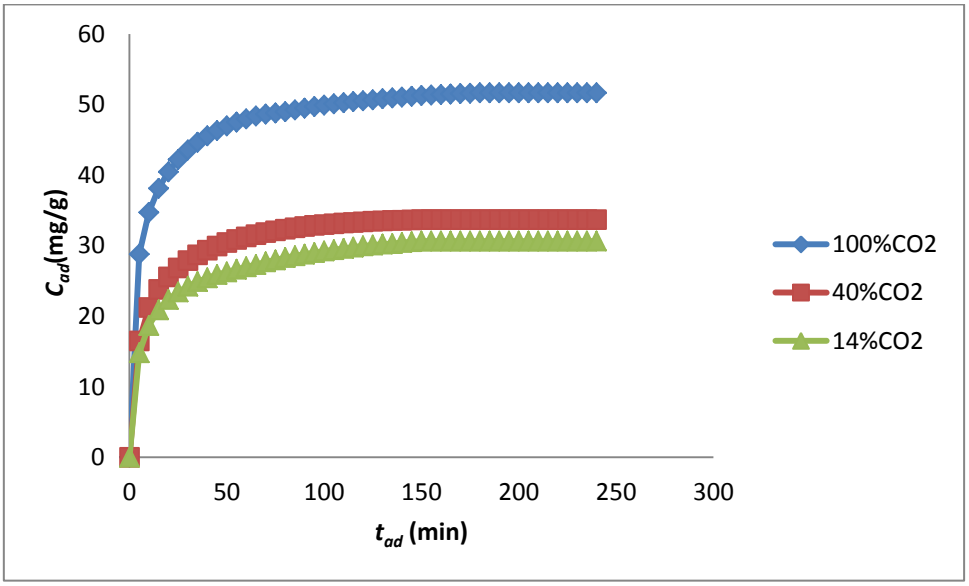


Figure 4.48: Adsorption of 100, 40 and 14% CO_2 onto PAA at 35 °C

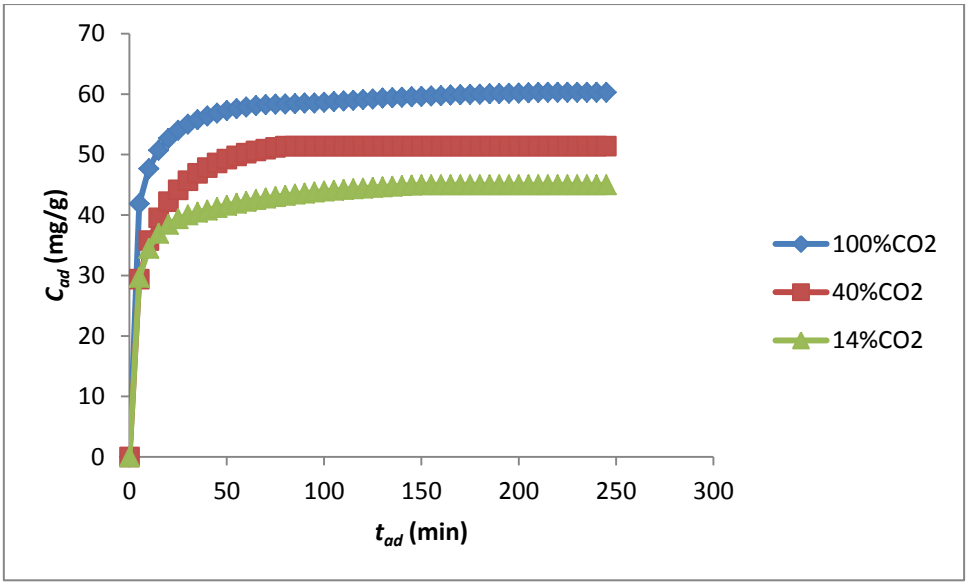


Figure 4.49: Adsorption of 100, 40 and 14% CO_2 onto MWNT-PAA at 35 °C

4.5.3. CO_2 adsorption at 45 °C

4.5.3.1. PAA

At 45 °C, the adsorbent PAA shows an increase of CO_2 adsorption capacity with the increase of CO_2 concentration in the gas stream (Table 4.15). However, due to low adsorption capacity, the selectivity was high due to insignificant adsorption capacity of N_2 and O_2, as evaluated from the N_2 and O_2 adsorption when using 100% N_2 and 100% O_2 at 45 °C (Fig.4.42). The minimum CO_2 concentration in the adsorbed gas is depicted in Table 4.15. The selectivity was enhanced during the first 30 minutes of adsorption, because both O_2 and N_2 demonstrated very low adsorption when using a stream gas of 100% O_2 and 100% N_2. Thus, the minimum CO_2 concentration in the adsorbed gas was approximately 97 and 98% CO_2 for the first 30 minutes of adsorption time when using a flue gas of 14 and 40% CO_2, respectively.

Table 4.15: Adsorption capacity and selectivity for CO_2 over O_2 and N_2 at 45 ◦C

Adsorbents	14% CO_2		40%CO_2		100%CO_2	
	C_{ad} mg/g	X_{CO2} %	C_{ad} mg/g	X_{CO2} %	C_{ad} mg/g	X_{CO2} %
PAA	26	92	32	94	39	100
MWNT-PAA	40	90	50	92	56	100

4.5.3.2. MWNT-PAA

The adsorption at 45◦C using the MWNT-PAA again demonstrated an increase of adsorption capacity with increasing CO_2 concentration in the gas stream; as expected (Table 4.15). Furthermore, the adsorption capacity has decreased with an increase of the temperature from 35 to 45 °C. As mentioned previously, the adsorption of O_2 using 100% O_2 was significant in the first 5 minutes and dropped afterwards, while the adsorption of N_2 was very low during 150 minutes of the adsorption process. Therefore, the selectivity for CO_2 in the gas mixture was negatively affected at the beginning of the adsorption process.

The enhancement of selectivity for CO_2 using the adsorbent MWNT-PAA requires an adsorption process with an isothermal time up to 60 minutes, the O_2 was desorbing while the adsorption process was extended (Fig. 4.43). Therefore, the selectivity for CO_2 evaluated after 120 minutes of adsorption time, shows a higher minimum CO_2 concentration in the adsorbed gas (Table 4.15) compared to the selectivity for CO_2 at a short adsorption time. The shorter the adsorption time, the lower is the selectivity for CO_2. The selectivity for CO_2 in the first 30 minutes of adsorption shows 87 and 90% concentration of CO_2 in adsorbed gas for the feeding gas containing 14 and 40% CO_2 respectively. In the first 5 minutes of adsorption time, the selectivity for CO_2 decreased to 77 and 80% CO_2 concentration in the adsorbed gas.

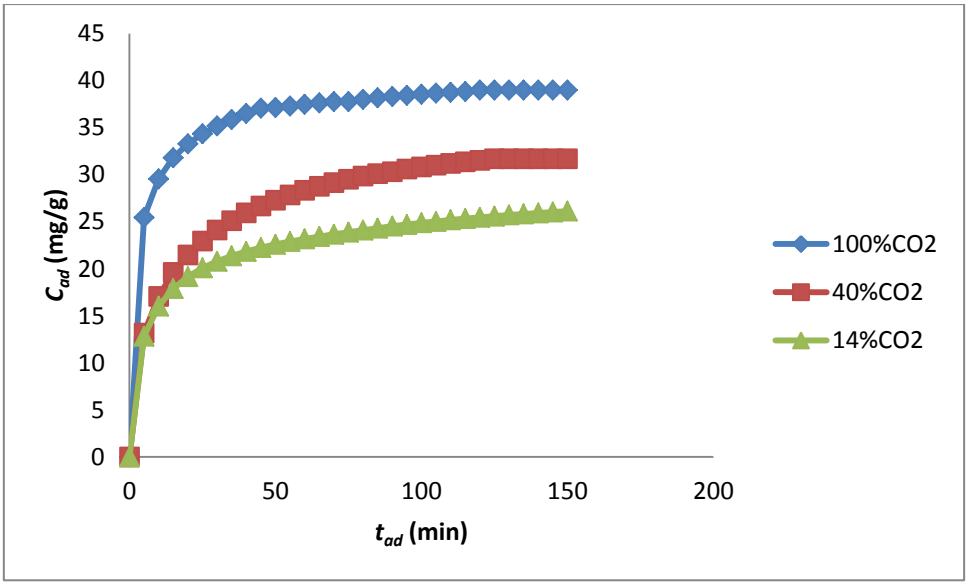


Figure 4.50: Adsorption of 100, 40 and 14%CO_2 onto PAA at 45 °C

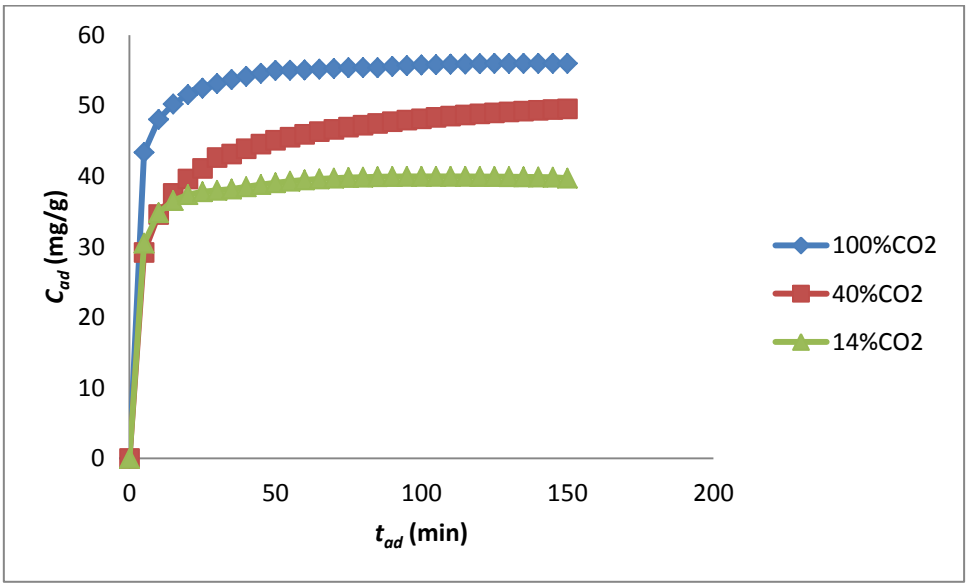


Figure 4.51: Adsorption of 100, 40 and 14%CO_2 onto MWNT-PAA at 45 °C

4.5.4. CO_2 adsorption at 55 °C

4.5.4.1. PAA

The adsorption achieved at 55 °C, the highest temperature tested, again showed that the CO_2

adsorption capacity increase with the increase of CO_2 concentration in gas stream (Table 4.16). The CO_2 adsorption process at 55 ℃ using PAA was more beneficial, because no N_2 and O_2 were adsorbed (Figure 4.44). Thus, the selectivity for CO_2 was at its potential maximum corresponding to 100% CO_2 concentration in adsorbed gas.

The adsorption rate increased significantly at 55 ℃ compared to the adsorption rate at 45 ℃ (Figs 4.52 and 4.51 respectively). The 40% CO_2 gas stream showed a lower CO_2 adsorption in the first 30 minutes compared to the 14% CO_2; however, the CO_2 adsorption for the 40% CO_2 stream was higher afterwards (Fig. 4.52). Thus, the adsorption isotherm curve of flue gas with 40% CO_2 content was less prominent than the adsorption isotherm curve for the 14% CO_2 content during the first 40 minutes of the adsorption process. This contradicts the statement that the CO_2 adsorption increases with the increase of CO_2 concentration in the flue gas; however, the adsorption isotherm curve of flue gas of 40% became more prominent afterwards.

4.5.4.2. *MWNT-PAA*

The adsorption onto MWNT-PAA at 55 ℃ showed an increase of CO_2 adsorption capacity with an increase of CO_2 concentration in the gas stream (Table 4.16). The adsorbent MWNT-PAA showed insignificant O_2 adsorption with no N_2 adsorbed at 55 ℃ (Fig. 4.45). Consequently, the MWNT-PAA demonstrated a potential high selectivity for CO_2, as shown in Table 4.16. The first 5 minutes were marked by a higher CO_2 adsorption rate when using the 14% CO_2 gas than the 40% CO_2 gas stream. The same phenomenon observed previously with PAA was reproduced in MWNT-PAA where the 40% CO_2 adsorption isotherm curve was initially less prominent than the 14% CO_2. In this case the phenomenon corresponded to the first 5 minutes of the adsorption time (Fig. 4.53). This is opposite to what was traditionally observed where the CO_2 adsorption increases with the increase of CO_2 concentration in the flue gas; however, the adsorption isotherm curve of gas of 40% becomes more prominent afterwards.

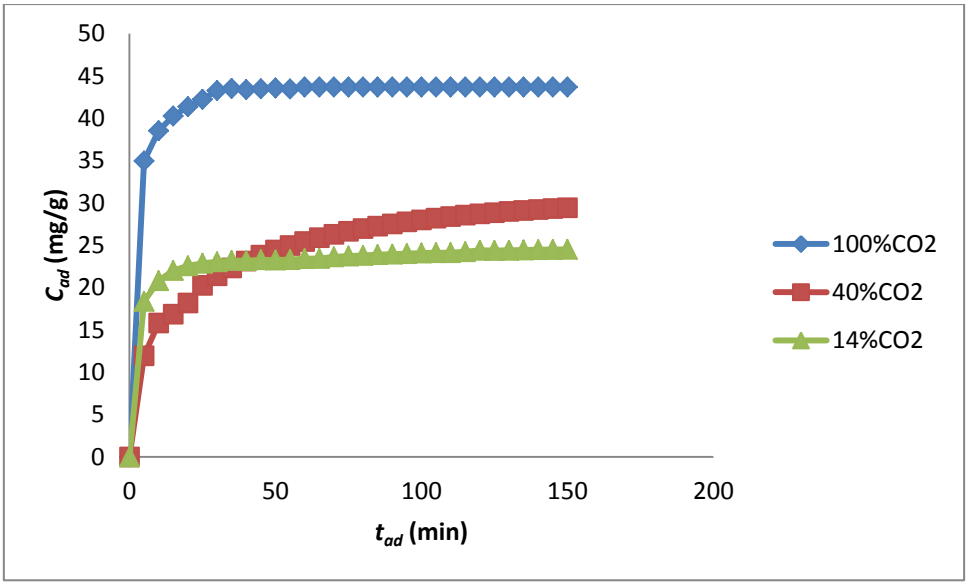


Figure 4.52: Adsorption of 100, 40 and 14%CO_2 onto PAA at 55 °C

Table 4.16: Adsorption capacity and selectivity for CO_2 over O_2 and N_2 at 55 °C

Adsorbents	14% CO_2		40% CO_2		100% CO_2	
	C_{ad} mg/g	X_{CO2} %	C_{ad} mg/g	X_{CO2} %	C_{ad} mg/g	X_{CO2} %
PAA	25	100	29	100	39	100
MWNT-PAA	34	99	43	99	46	100

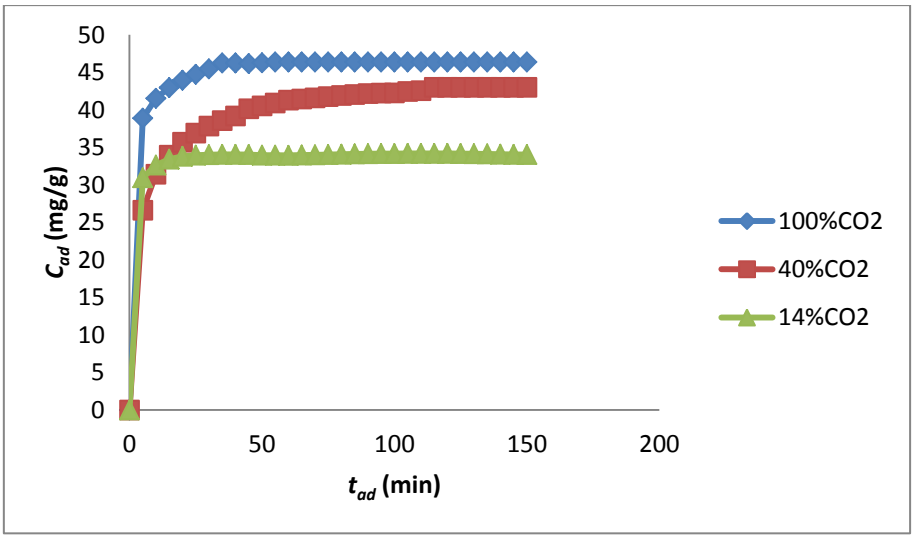


Figure 4.53: Adsorption of 100, 40 and 14%CO_2 onto MWNT-PAA at 55 °C

4.5.5. Discussion of variable CO_2 concentration on adsorption

CO_2 adsorption of a gas stream with variable CO_2 content provided a challenge. The CO_2 adsorption efficiency at the same temperature and pressure is CO_2 concentration dependent. The increase of CO_2 concentration in the gas stream increased the CO_2 adsorption efficiency. Most challenges in adsorption process are related to the fluid flow behavior of the system. Adequate fluid flow must allow good transfer between the adsorbate molecules and adsorbents in packed beds. This requires: (a) good external transport where the molecules transfer via convection from the stream gas in the bed to a laminar film adjacent to the particle surface; (b) good internal transport, where the diffusion occurs through molecules penetrating into the porous structure and adsorbed onto the internal surface of the pellet; and (c) good adsorption through physisorption or chemisorption where the adsorbate molecules reach the interface between the gas phase and the solid phase. The fluid transfer by both convection and diffusion causes radial or axial dispersion of molecules in the fluid flow, which allows the mixing in radial and axial directions respectively.

Generally, for efficient adsorption, the axial dispersion must be minimized for the adsorbate in order to avoid a large quantity of adsorbate content in the breakthrough gas. In the case of axial dispersion, the bed length and the geometry/structure must be designed accordingly in order to assure large adsorption of adsorbate during its path along the axial direction before the gas breakthrough occurs. Since the TGA has a small crucible, axial dispersion is prejudicial for adsorption efficiency. The radial dispersion will be significant when the selectivity for CO_2 is assessed in order to allow good diffusion of CO_2 into available sites. Both radial and axial dispersions are the consequence of convection and diffusion for fluid flow transfer. Therefore, the CO_2 mixed in the gas stream was not easily accommodated in the pore spaces due to the obstacle of air composed of N_2 and O_2. The greater the quantity of air in the gas stream, the greater the CO_2 dilution, and the CO_2 migration toward the available sites becomes more challenging. Even though the radial dispersion is important for good contact between adsorbate and adsorbent, enough driving force is needed for CO_2 to assure rapid CO_2 adsorption kinetics in order to avoid the presence of N_2 and O_2 in the lattice of the adsorbent. This challenge was more significant with PAA due to the poor geometry/structure, including large pore size, than with MWNT-PAA, where the geometry/structure was improved. The location of CO_2 and other gases (N_2 and O_2) are necessary to be considerable

with large pores, because the small pores operate as a sieve, allowing CO_2 migration towards the available sites due to higher affinity to react with the amine to form carbamate. Thus, the increase of CO_2 concentration increases the presence of CO_2 molecules to migrate toward available adsorption sites. The CO_2 adsorption increases as the affinity of CO_2 to react with the amine is considerable. Consequently, the beginning of the adsorption process is marked by the presence of large number of CO_2 available sites which in combination create enough driving force to attract a large quantity of CO_2. The more the CO_2 adsorption is advanced, the more the number of available sites decrease, leading to a flat curve of CO_2 adsorption as observed experimentally.

A circumstantial fluctuation of CO_2 adsorption was observed at 55 °C where during the first 40 minutes the adsorption rate for the gas stream of 14% was larger than the adsorption rate for the gas stream of 40% CO_2 when using the adsorbent PAA. The same phenomenon was repeated with the adsorbent MWNT-PAA, but at very short adsorption time corresponding to the first 5 minutes. This is an exception to the assumption, affirming that the CO_2 adsorption increases with the increase of CO_2 concentration in the flue gas. This phenomenon is random, but can be justified by a possible involvement of an amount of CO_2 in a rapid breakthrough of the gas stream at the beginning of the adsorption where N_2 and O_2 adsorption are almost zero at 55 °C. Since the convection of gas stream occurs more in the breakthrough direction, the flux of gas is more controlled by the axial dispersion than the radial dispersion. Consequently, the driving force decreases with the adsorption kinetics, resulting in a decrease of CO_2 adsorption. This phenomenon was emphasized with the PAA, because of the large pore size where CO_2 could easily be surrounded by other gases, causing the gas stream to flow easily to the down surface edge of the bed, minimizing the potential interaction. It is noticeable that the viscosity of air (79% N_2/21% O_2) is higher than the viscosity of CO_2 [285]; therefore, at higher temperature the air resistance will increase with the possibility to involve easily the CO_2 in its breakthrough lane [286]. A higher CO_2 concentration presents a potential to be packed out by air resistance than a lower CO_2 concentration. Also, at 55◦C, N_2 and O_2 adsorption is close to zero for PAA and very insignificant for MWNT-PAA. This means that the axial dispersion before breakthrough is the only possible path for air (N_2+O_2) due to higher viscosity to interfere/interact easily with CO_2. The availability of adsorption sites could decrease rapidly especially with 14% CO_2 gas stream, causing the decrease of driving force resulting in low CO_2 adsorption. Consequently, after the first 40 and first 5 minutes the

adsorption isotherm curve for 40% CO_2 overtook the adsorption isotherm curve for 14% CO_2 when using the adsorbents PAA and MWNT-PAA at 55 °C respectively.

With regard to the selectivity, PAA generally showed a higher selectivity for CO_2 compared to MWNT-PAA; however, the adsorption for PAA was always low. This is because PAA has a poor geometry/structure; and the adsorption was determined only by good chemical reaction with one primary amine. Therefore, chemisorption was predominant in the adsorption process where N_2 and O_2 adsorption was not favorable. The selectivity for CO_2 using MWNT-PAA faced a competitor – O_2, which was always adsorbed. The O_2 adsorption was more significant at 35 °C and 45 °C. Two explanations can be put forward to justify the O_2 adsorption on MWNT-PAA: (a) the O_2 physisorption occurrence was possible as the adsorbent MWNT-PAA has good geometry/structure; (b) the O_2 chemisorption was possible if the MWNT displayed catalyst behavior between the NH_2 and O_2. Mori *et al.* [287] found that the oxidation of amine by O_2 is more favorable above 100 °C unless an appropriate catalyst is used to lower the activation energy.

One more important thing that must be stated is that the selectivity for CO_2 is time dependent. As the adsorption of the undesirable gas, including N_2 and O_2, increases slowly and becomes significant after a long time of adsorption, it is better to shorten the adsorption time to ensure selectivity for CO_2. This was the case of the adsorption performed with MWNT-PAA at 35 °C, where a significant quantity of O_2 could possibly be adsorbed after 150 minutes. Thus, the selectivity for CO_2 would be a drawback after 150 minutes of adsorption process. The restriction of the adsorption time to 30 minutes would be advantageous to increase the selectivity for CO_2. Conversely, an adsorption process where the adsorption rate of any undesirable gas is high at the beginning, the selectivity for CO_2 will be negatively affected at the beginning and recover later on as the undesirable gas will be desorbing. This corresponded to the case of adsorption performed at 45 °C with the use of MWNT-PAA, where the first 5 minutes was marked by a significant adsorption of O_2.

Furthermore, the CO_2 adsorption using PAA and MWNT-PAA implies adherence to the Langmuir model, where the adsorption rate typically was very high at the beginning of the

adsorption process, and dropped significantly as the adsorption time increased. Therefore, the shortening of the adsorption time will be beneficial when multiplying the cycle adsorption-desorption operation to increase the CO_2 adsorption.

4.6. THE BEHAVIOR OF MOIST ADSORBENTS ON ADSORPTION

Sorbents for CO_2 capture plants (including post-combustion and oxyfuel plants) will inevitably be exposed to certain levels of moisture, especially where predrying of the gas has been avoided to save costs + energy. Therefore, an adsorbent with the ability to tolerate water will be a much sought after, if it has favorable CO_2 adsorption capacity, kinetics, selectivity and regenerability. The flue gas exhausted from different combustion plants generally contains N_2, O_2, H_2O and CO_2. The moisture (H_2O) has an effect on CO_2 and O_2 during the adsorption process, especially in an amine medium. In the presence of CO_2 and amine, H_2O with amphoteric properties behaves as a base and as an acid respectively. The oxidizing action of O_2 becomes more significant in water, which could lead to amine degradation [288]. When O_2 and CO_2 are in the gas mixture, the solubility of O_2 is minimized; therefore the amine degradation is less [289]. As the synthesized adsorbents (PAA and MWNT-PAA) were previously investigated under dry conditions, it is very important to highlight the impact of added moisture in the gas. When the adsorption runs at low temperatures (below 55 °C) the moisture is no longer in a vapor state, but at a liquid state. Consequently, the adsorbents will obviously become wet in the presence of moisture in the flue gas. Thus, the testing of moist PAA and moist MWNT-PAA via the TGA was an effective approach to evaluate the influence of water on the adsorbents. The water content in the wet adsorbents was varied at 20 and 40% moisture with the solid adsorbent the remaining in order to predict the efficiency of the adsorbents as a function of the moisture content.

Firstly, a gas of 100% O_2 was injected into the TGA, passing through the moist or wet adsorbents at different temperatures (25 to 55 °C) to investigate the behavior of O_2 on the moist PAA and moist MWNT-PAA. The results are recorded in Appendix 4 and the outcome can be found in Table 4.17. Table 4.17 depicts the adsorption of O_2 when using moist adsorbents (40% and 20% wet) compared to O_2 adsorption when using dry adsorbents.

Secondly, a flue gas of 100% CO_2 was injected in the TGA passing through the wet adsorbents in the same condition as before. These results are reported in Figures 4.54 to 4.61 (depicting the adsorption of CO_2 using the moist adsorbents (40 and 20% wet) compared to the CO_2 adsorption when using dry adsorbents). Finally, a flue gas containing 14% CO_2 and air was injected in the TGA as previously. The results are reported in Figures 4.61 to 4.69. In Figures 4.54 to 4.69 the symbol dry-P, 40% W-P and 20% W-P are to identify dry PAA, 40% moist PAA and 20% moist PAA respectively. Also dry-M, 40% W-M and 20% W-M identify dry MWNT-PAA, 40% moist MWNT-PAA and 20% moist MWNT-PAA respectively.

4.6.1. The effect of moist adsorbents on O_2 adsorption with change of temperature

Operating in temperature range 25 – 55 ^oC, the adsorbent PAA shows at all temperatures the increase of O_2 adsorption with the increase of moisture (Table 4.17). Since O_2 is soluble in H_2O, the reaction was possible to some extent with the amine in the structure. However, the increase of O_2 adsorption is a drawback to the selectivity for CO_2; it literally shows that the solubility of O_2 in water decreases in the presence of CO_2, which decreases O_2 adsorption. Furthermore, the flue gas from combustion usually contains a low amount of O_2. In the same condition of adsorbent PAA, the O_2 adsorption decreased with the increase of temperature for dry PAA; while the moist PAA shows the increase of O_2 adsorption from 25 °C to 35 °C and decrease afterwards.

The adsorbent MWNT-PAA shows the increase of O_2 adsorption at 25 and 55 ^oC with the increase of moisture concentration. In temperature range 35 – 45 ^oC, the O_2 adsorption decreased with the increase of moisture concentration (Table 4.17). In the same condition of adsorbent, the dry MWNT-PAA shows the increase of O_2 adsorption from 25 °C to 35 °C and decreased afterwards, while the O_2 adsorption was almost the same with moist MWNT-PAA in temperature range 25 – 45 ^oC when minimizing some fluctuation observed. But a significant rise of O_2 adsorption capacity was observed at 55 ^oC.

Compared to PAA, the adsorbent MWNT-PAA showed a higher O_2 adsorption capacity at all temperatures due to its enhanced geometry/structure (Table 4.17). As the purpose is to increase the CO_2 adsorption capacity by using MWNT on PAA, the increase of O_2 adsorption is a drawback, especially in terms of selectivity for CO_2. Nevertheless, the quantity of O_2 in the flue gas from power plant is generally low; moreover, the adsorptivity of O_2 decreases in the presence of CO_2 in cases where amine adsorbents were used. Therefore the investigation of the effect of water on CO_2 adsorption using the adsorbents PAA and MWNT-PAA is important for the evaluation of adsorbents' efficiency.

Table 4.17: O_2 adsorption capacity of dry and moist adsorbents at variable temperatures

Adsorbents	O_2 adsorption capacity mg-O_2/g											
	25 °C			35 °C			45 °C			55◦C		
	% Moisture			% Moisture			% Moisture			% Moisture		
	dry	20%	40%	dry	20%	40%	dry	20%	40%	dry	20%	40%
PAA	1.44	1.84	2.85	1.30	3.78	4.68	0.97	1.71	2.24	0.00	0.64	1.62
MWNT-PAA	2.51	5.02	6.67	12.50	7.17	4.39	8.55	6.03	5.45	1.16	8.03	12.51

4.6.2. The effects of moist adsorbents using variable CO_2 concentration in gas stream at variable temperatures

In this Section, 100% CO_2 at 25, 35, 45, 55 °C is considered for moist PAA and MWNT-PAA, followed by consideration at 14% CO_2 at the same temperatures. Moisture addition is 20 and 40%, indicated as W-P and W-M in the figures to identify moist PAA and moist MWNT-PAA respectively.

4.6.2.1. Gas stream with 100% CO_2 Content

A. CO_2 adsorption at 25 °C

With regards to the water tolerance of the adsorbent PAA, Figure 4.54 and Table 4.18 show a

decrease of CO_2 adsorption at 25 ℃ with an increase of moisture in the adsorbent PA. The presence of moisture in the adsorbent PAA shows broadly a decrease of CO_2 adsorption capacity when the adsorption was done at 25 ℃. This is due to presence of moisture in the lattice pores of the PAA, resulting in the possible blockage of CO_2 from migrating to available sites. If the temperature is not favorable for carbonate formation, the presence of water becomes a resistance to the CO_2 adsorption efficiency. Thus, a flue gas with moisture is predicted to capture less CO_2 at 25 ℃ using PAA and requires pretreatment for moisture removal.

The use of moisture MWNT-PAA for water tolerance evaluation at 25 ℃ with 100% CO_2 as flowing gas is depicted by the results plotted in Figure 4.55. The decrease of CO_2 adsorption with the increase of water concentration is given by the values shown in Table 4.18. The adsorbent MWNT-PAA showed a decrease of CO_2 capture at 25 ℃ when the gas contains moisture. Despite the cost of any flue gas pretreatment for moisture removal, the use of adsorbent MWNT-PAA for CO_2 adsorption at 25 ℃ is very favorable to ensure a high CO_2 uptake when the flue gas is dried.

Table 4.18: CO_2 adsorption using 100%CO_2 for moist adsorbents

Adsorbents	C_{ad} **mg-CO_2/g**			
	25 ℃	35 ℃	45 ℃	55 ℃
Dry PAA	52	52	39	43.7
20% Wet PAA	24.25	46.4	43.5	22
40% Wet PAA	13.67	26.5	47.3	35.7
Dry MWNT-PAA	70	60	56	46.4
20% Wet MWNT-PAA	57.3	57	49.3	46.7
40% Wet MWNT-PAA	43.7	71	70.2	70.9

Considering both MWNT-PAA and PAA under moist conditions, the CO_2 adsorption capacity was higher for MWNT-PAA compared to PAA. At 25 ℃ the adsorbent MWNT-PAA encounters a decrease of CO_2 uptake in the presence of moist gas. Nevertheless this

CO_2 uptake is higher compared to dry gas onto PAA. In the case of moist flue gas the use of MWNT-PAA without gas pretreatment is still better than PAA after gas pretreatment. Even if MWNT-PAA showed significant O_2 adsorption at 25 °C compared to PAA (Table 4.9), which can reduce the selectivity for CO_2, the O_2 adsorption resistance will obviously increase due to the high affinity for CO_2 with the amine adsorbent. Furthermore, the adsorption of O_2 does not affect the selectivity for CO_2 since the quantity of O_2 in the flue gas is not so significant. Also, the preference for CO_2 prevails over O_2 by the amine adsorbent.

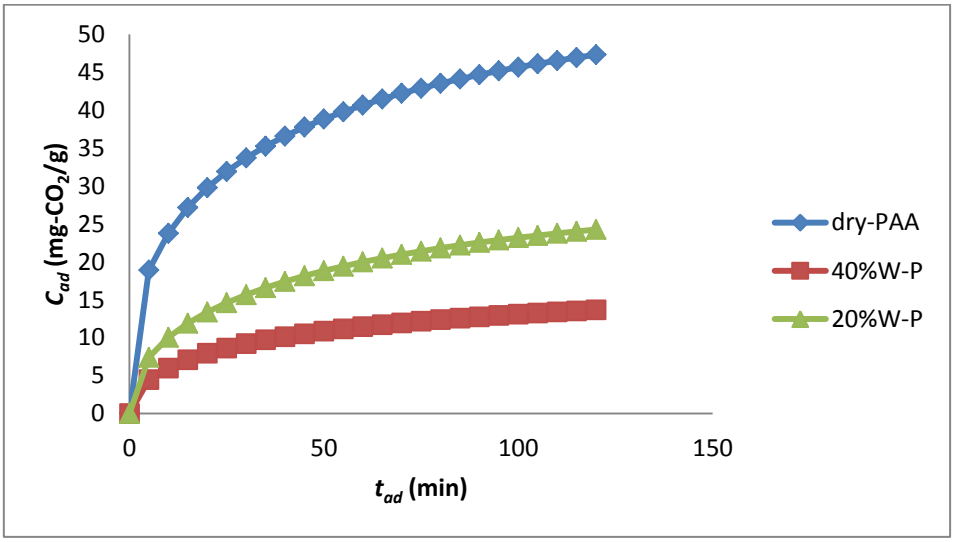


Figure 4.54: CO_2 adsorption from 100% CO_2 onto moist PAA at 25 °C

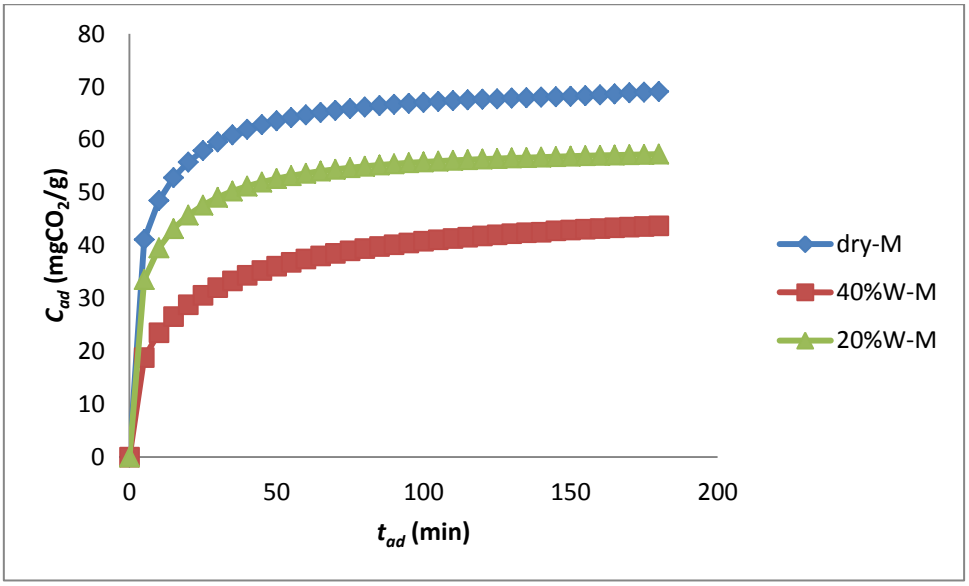


Figure 4.55: CO_2 adsorption from 100% CO_2 onto moist MWNT-PAA at 25 °C

B. CO_2 adsorption at 35 °C

The adsorbent PAA at 35 °C suffered a of CO_2 adsorption capacity with an increase of moisture in the adsorbent (Fig. 4.56). The amount of CO_2 adsorbed by the adsorbent PAA at 35◦C is shown in Table 4.18. The presence of water reduced CO_2 uptake at 35 °C. The effect becomes more significant with a larger quantity of water because the decrease of CO_2 adsorption capacity was not significant from the dry PAA to the 20% moist PAA. Thus, when the flue gas contains a large quantity of moisture, a partial moisture removal will be sufficient, since the difference of CO_2 uptake at 35 °C for dry PAA and 20% moist PAA was not significant. Compared to 25 °C, the CO_2 adsorption has increased at 35 °C for PAA under the same conditions either dry or wet. This shows the predominance of chemisorption for CO_2 adsorption where the increase of temperature was favorable to promote the reaction between CO_2 and amine even if soaked in water.

With regards to the adsorbent MWNT-PAA at 35 °C (Figure 4.57), the CO_2 adsorption capacity decreased slightly from dry MWNT-PAA to 20% moist MWNT-PAA and significantly increased from dry MWNT-PAA to 40% moist MWNT-PAA. The difference of CO_2 uptake between the dry MWNT-PAA and the 20% moist MWNT-PAA was insignificant and could be considered to be approximately the same. Thus, the presence of water does not cause a decrease in CO_2 adsorption capacity, since the CO_2 uptake stayed almost constant from dry MWNT-PAA to 20% moist MWNT-PAA and increase considerably with large quantity of water in MWNT-PAA. This shows that the carbonate occurrence was possible at 35 ◦C when using the adsorbent MWNT-PAA with a high moist content. The use of moist flue gas for CO_2 capture is not impaired when the adsorption has to be performed at 35 °C with MWNT-PAA. Compared to 25 °C (Fig. 4.55), the CO_2 uptake at 35 °C (Fig. 4.57) decreased for the dry MWNT-PAA, stayed constant for 20% moist MWNT-PAA and drastically increased for 40% moist MWNT-PAA.

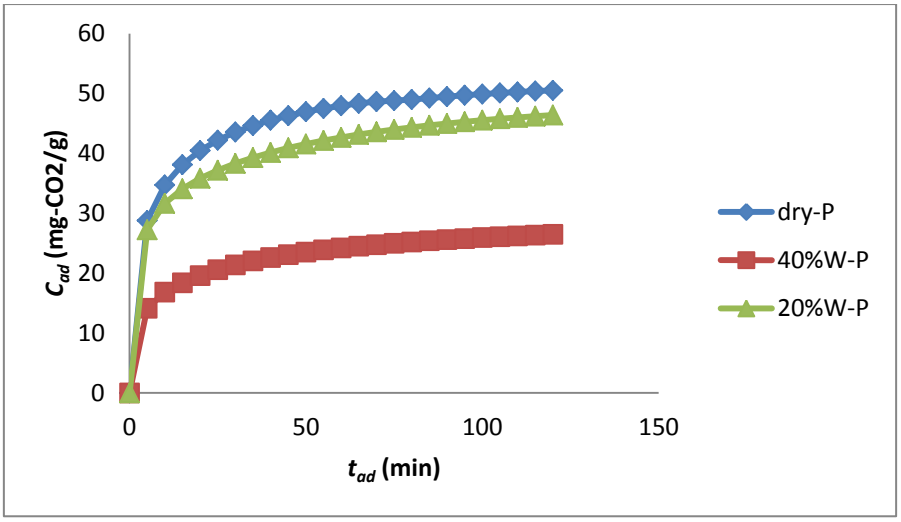


Figure 4.56: CO_2 adsorption from 100% CO_2 onto moist PAA at 35 °C

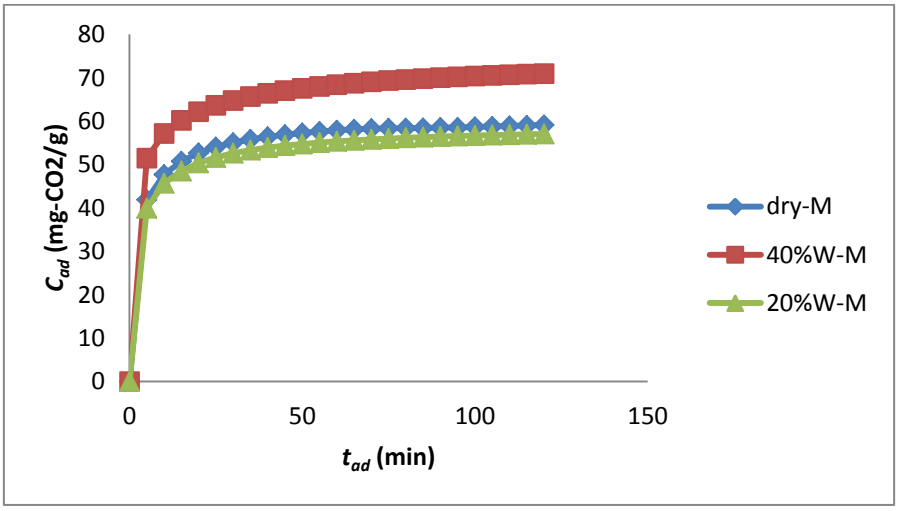


Figure 4.57: CO_2 adsorption from 100% CO_2 onto moist MWNT-PAA at 35 °C

C. CO_2 adsorption at 45 °C

The adsorbent PAA showed an increase in CO_2 adsorption capacity with an increase of moisture in the adsorbent at 45 °C (Fig. 4.58): the amount of CO_2 uptake is noted in Table 4.18. The increase of moisture in PAA for CO_2 adsorption at 45 °C shows the occurrence of carbonate through the increase of CO_2 uptake. This could be due to the presence of water; water, being amphoteric, could possibly react with CO_2 as a base and with amine as an acid.

As flue gas usually contains moisture, pretreatment is unnecessary when the adsorption is done at 45 °C is done with PAA as adsorbent. This results in an increase of CO_2 uptake and energy as well.

Considering the adsorbent MWNT-PAA, a broad increase of CO_2 adsorption capacity was recorded with 40% moist MWNT-PAA compared to dry MWNT-PAA. Under the same conditions 20% moist MWNT-PAA showed a decrease of CO_2 adsorption, as depicted in Figure 4.59. The amount of CO_2 uptake for the adsorption performed at 45 °C after 120 minutes is shown in Table 4.18. The increase of CO_2 adsorption capacity is obviously due to the formation of carbonate which occurred at 45 °C. It is a contrast to see the increase and decrease of CO_2 adsorption capacity with varying moisture contents in MWNT-PAA compared to the dry MWNT-PAA. It is known that the increase of CO_2 uptake in the presence of moisture when using an amine adsorbent is caused by the formation of carbonate, with a stoichiometry reaction showing 1 mol of CO_2 for 1 mol of amine (Section 2.5.7). Carbamate formation requires 2 moles of amine for 1 mol of CO_2 (Section 2.5.6). Moreover, the presence of water in the adsorbent can be very important to promote either carbamate or carbonate formations. When the quantity of water is not enough, it will possibly be incorporated in the lattice of the pores and the CO_2 adsorption will have more chance to occur on the surface of the sorbent particles with amine, resulting to carbamate formation. The temperature of 45◦C was favorable for carbonate formation as a large amount of CO_2 uptake was observed with moist MWNT-PAA. Ogino *et al* (1987), investigating the formation and transformation mechanism of calcium carbonate in water, found that the polymorphs of crystalline $CaCO_3$ are formed at the intermediate temperatures (40 – 60 °C) [290]. At higher temperatures, i.e., above approximately 40 °C, various basic carbonates are usually formed [291, 292, 293, 294]. With more moisture, the CO_2 will form carbonate at the surface of the pellet and continue in the lattice pores. The influence of varying quantities of moisture become more noticeable when the adsorbent has small pores as it is the case of MWNT-PAA compared to PAA.

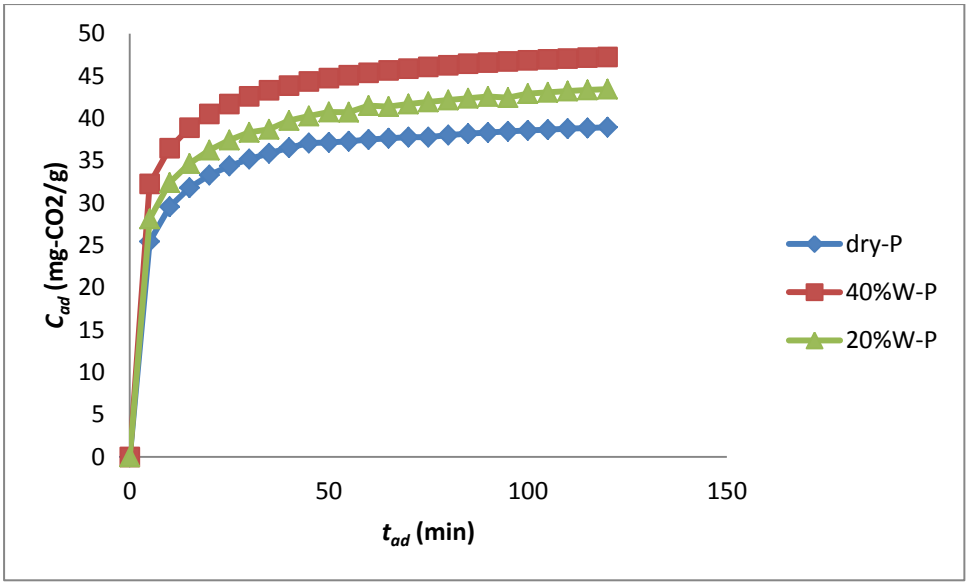


Figure 4.58: CO_2 adsorption from 100% CO_2 onto moist PAA at 45 °C

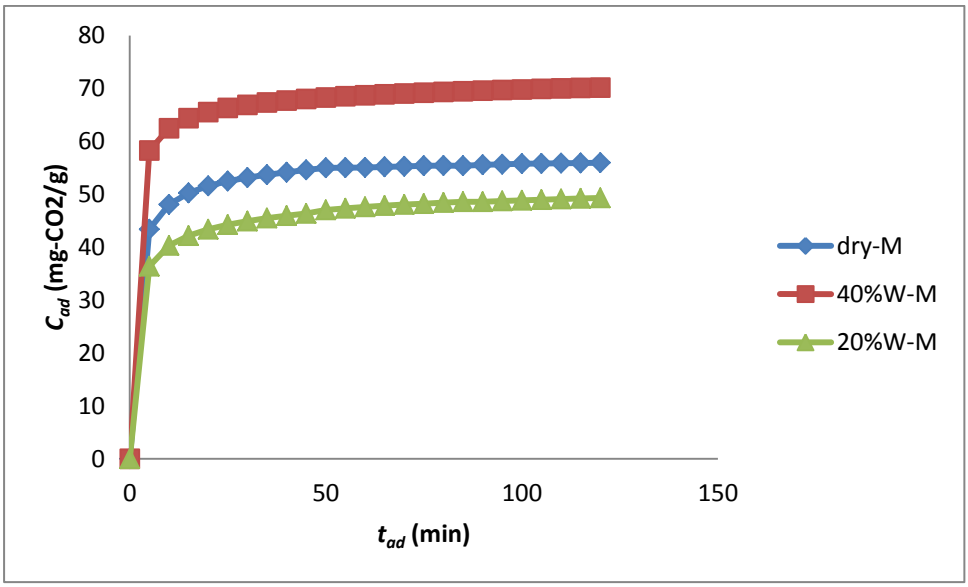


Figure 4.59: CO_2 adsorption from 100% CO_2 onto moist MWNT-PAA at 45 °C

D. CO_2 adsorption at 55 °C

The presence of moisture in the adsorbent PAA really reduced CO_2 adsorption capacity at 55 °C (Fig. 4.60). In contrast to the adsorption at 45 °C where the CO_2 adsorption was increasing with the presence of moisture in PAA, at 55 °C, the CO_2 uptake decreased significantly in the

presence of moisture compared to the dry PAA (Table 4.18). This shows that a large quantity of moisture in PAA could possibly increase the CO_2 uptake compared to the dry condition of PAA. Three possible explanations can justify the phenomenon of decrease of CO_2 adsorption capacity at 55 °C with the presence of moisture in the PAA: (a) firstly the moisture level was not enough to resist the desiccation that was possibly higher at 55 °C; (b) the presence of moisture could possibly prevent the access of CO_2 to the favorable adsorption sites; and (c) finally the resistance to carbonate formation at 55 °C.

With regard to the adsorbent MWNT-PAA, the CO_2 adsorption capacity increased in the presence of moisture. However, the 20% moisture MWNT-PAA shows the same CO_2 adsorption capacity than the dry MWNT-PAA, as depicted in Figure 4.61. The amount of CO_2 adsorption is shown in Table 4.18. Thus, high level of moisture in flue gas has the potential to increase the CO_2 adsorption when the temperature is favorable to carbonate formation.

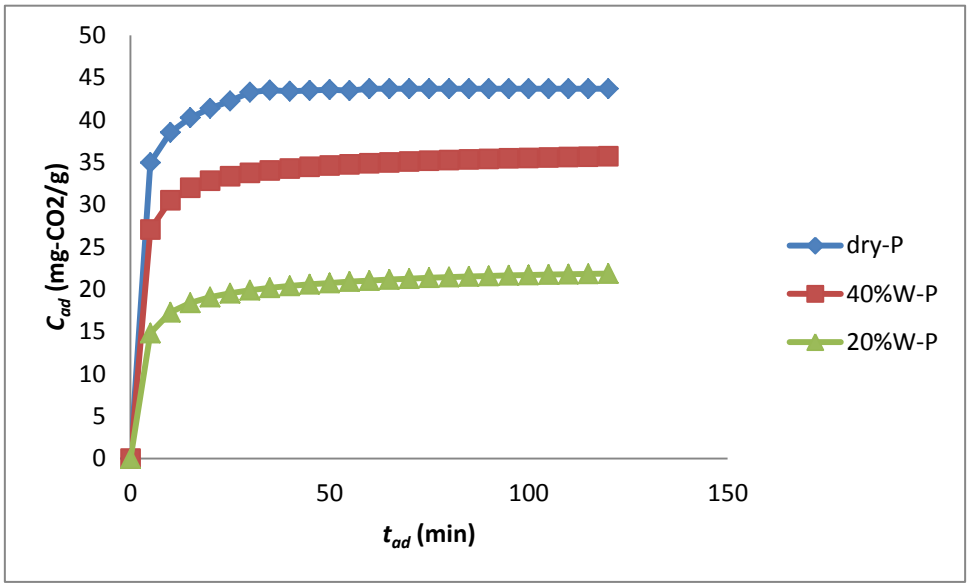


Figure 4.60: CO_2 adsorption from 100% CO_2 onto moist PAA at 55 °C

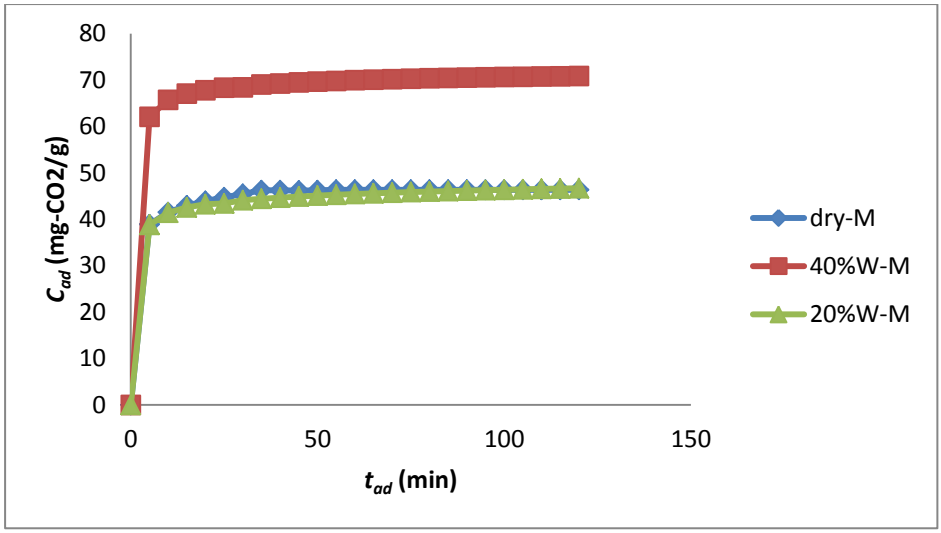


Figure 4.61: CO_2 adsorption from 100% CO_2 onto moist MWNT-PAA at 55 °C

4.6.2.2. Effluent stream gas with 14% CO_2 Content

A. CO_2 adsorption at 25 °C

The presence of water in the adsorbent PAA has reduced CO_2 adsorption capacity at 25 °C when using a flue gas with 14% CO_2 (Fig. 4.62). The amount of CO_2 adsorbed is reported in Table 4.19. This shows that the interaction between the amine and CO_2 was not favorable to form carbonate at 25 °C; dry PAA previously demonstrated the highest CO_2 adsorption at temperatures 25 and 35 °C, with possible carbamate occurrence. Furthermore, the physisorption intended to take over could be hampered by: 1) poor geometry/structure of PAA; and 2) the incorporation of moisture in the pores could prevent CO_2 from diffusion toward available adsorption sites. For post-combustion where the flue gas contains 14% CO_2, the use of PAA for CO_2 capture at 25 °C will require flue gas pretreatment for water removal in order to increase the CO_2 uptake. This will demand an extra energy and equipment costs for desiccation. Since the variation in CO_2 adsorption capacity between dry PAA and 20% moist PAA is not so significant, partial water removal from flue gas will be beneficial. Moisture in PAA reduced the selectivity for CO_2, as the CO_2 adsorption capacity decreased with the increase of water. Under the same conditions the O_2 adsorption capacity increased (Table 4.17).

Table 4.19: Moisture effect on CO_2 adsorption using a flue gas of 14% CO_2 at 25 °C

Adsorbents	C_{ad} mg/g	X_{CO2} %
Dry PAA	31	86
20% Wet-PAA	27.6	83.3
40% Wet-PAA	10.3	58.7
Dry MWNT-PAA	45.9	90
20% Wet-MWNT-PAA	44.5	84.2
40% Wet-MWNT-PAA	46.8	81.5

The adsorbent MWNT-PAA does not show any significant change of CO_2 adsorption capacity between the dry and wet conditions, as shown in Figure 4.63. The adsorption capacity obtained for different conditions of adsorbent was almost the same (Table 4.19). However, the O_2 adsorption increased with the increase of moisture in the MWNT-PAA (Table 4.19), resulting in a decrease of selectivity for CO_2.

Compared to PAA, the MWNT-PAA appears to be more successful in terms of CO_2 adsorption capacity and selectivity at 25 °C. Thus, the use of MWNT-PAA instead of PAA could be advantageous not only to circumvent the cost related to the gas pretreatment process, but also to procure a higher CO_2 adsorption capacity corresponding to 46.8 mg/g for a wet-MWNT-PAA compared to 31 mg/g for a dry PAA (Table 4.19).

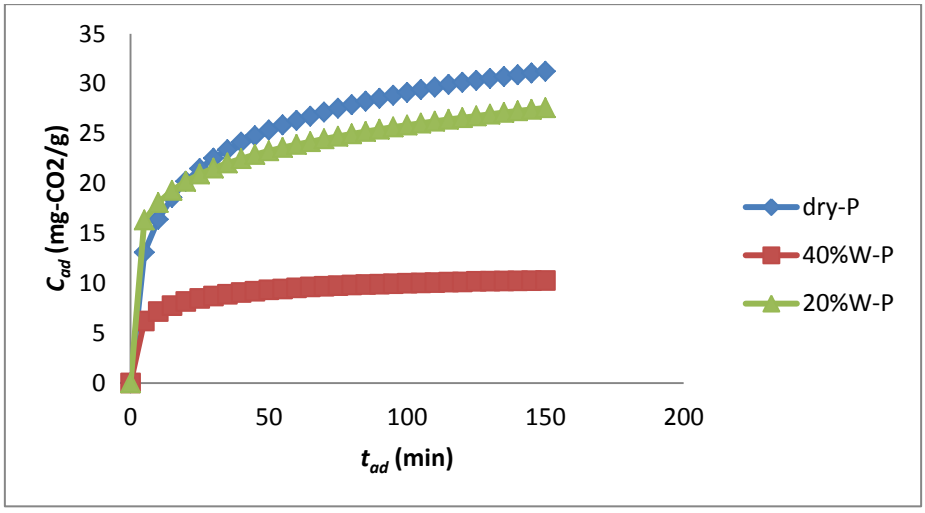


Figure 4.62: CO_2 adsorption from 14% CO_2 onto moist PAA at 25 °C

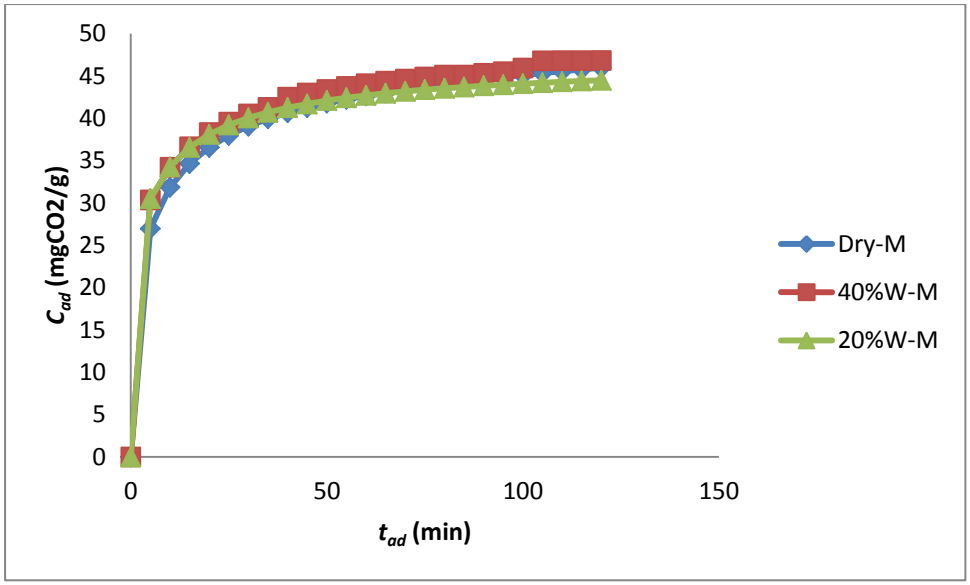


Figure 4.63: CO_2 adsorption from 14% CO_2 onto moist MWNT-PAA at 25 C

B. CO_2 adsorption at 35 °C

The adsorbent PAA continues to show a decrease of CO_2 adsorption capacity with an increase of moisture in the adsorbent (Fig. 4.64 and Table 4.20). A significant decrease of CO_2 uptake was recorded for 40% moist PAA, while the 20% moist PAA and dry PAA showed almost the same CO_2 uptake. Furthermore, the selectivity for CO_2 decreased with the increase of moisture in PAA for the adsorption performed at 35 °C using a gas of 14% CO_2. Thus, a gas pretreatment will improve the adsorption properties, including adsorption capacity and selectivity for CO_2. Even if the flue gas has to be pretreated, a partial water removal will be enough to procure the same amount of CO_2 adsorption compared to dry flue gas.

At 35 °C, the adsorbent MWNT-PAA shows an increase of CO_2 adsorption capacity with an increase of moisture in the adsorbent (Table 4.20); MWNT-PAA at 40% moisture shows a high CO_2 adsorption capacity at 35 °C. The increase of CO_2 adsorption capacity was not so significant between the dry MWNT-PAA and 20% moist MWNT-PAA as the isothermal curves in Figure 4.65 almost coincide. The significant increase of CO_2 uptake with a large amount of water in the MWNT-PAA is possibly due to the carbonate occurrence at 35 °C

enhanced by good geometry/structure in the MWNT-PAA. In addition, the selectivity for CO_2 increased with the increase of water in the MWNT-PAA. Thus, a flue gas with a significant amount of moisture content will increase and ensure high CO_2 adsorption capacity at 35 °C. The humidification of flue gas in order to increase the water content can be an approach to increase CO_2 adsorption capacity when using MWNT-PAA for the adsorption at 35 °C.

Table 4.20: Moisture effect on CO_2 adsorption using a flue gas of 14% CO_2 at 35 °C

	C_{ad} mg/g	X_{CO2} %
Dry PAA	30	88
20% Wet-PAA	28.5	83.2
40% Wet-PAA	16.7	66
Dry MWNT-PAA	41.5	70
20% Wet-MWNT-PAA	44.4	81.4
40% Wet-MWNT-PAA	65	91.6

Compared to PAA where the flue gas pretreatment is required for good adsorption performance, the adsorbent MWNT-PAA presents an enormous advantage which includes high CO_2 uptake and avoiding further cost of gas pretreatment.

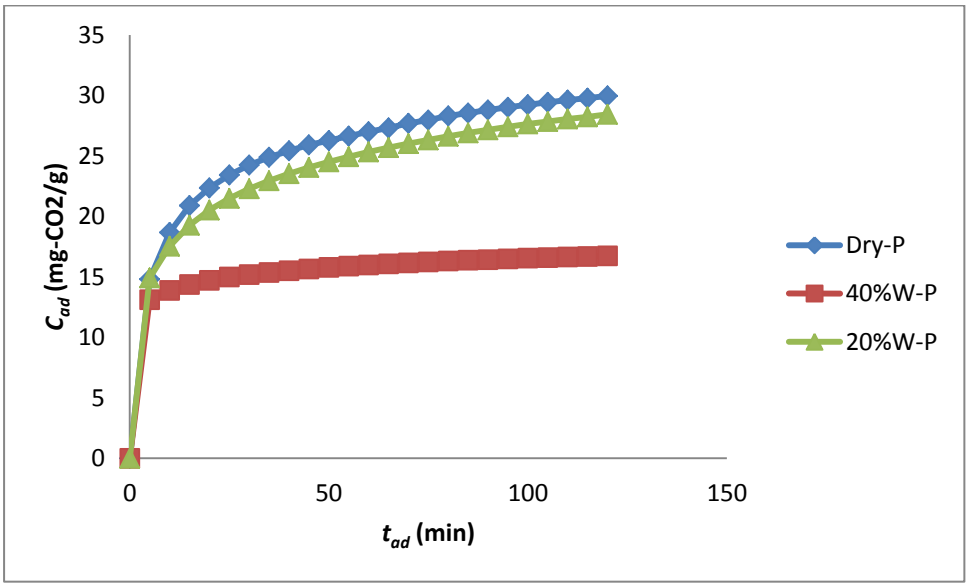


Figure 4.64: CO_2 adsorption from 14% CO_2 onto moist PAA at 35 °C

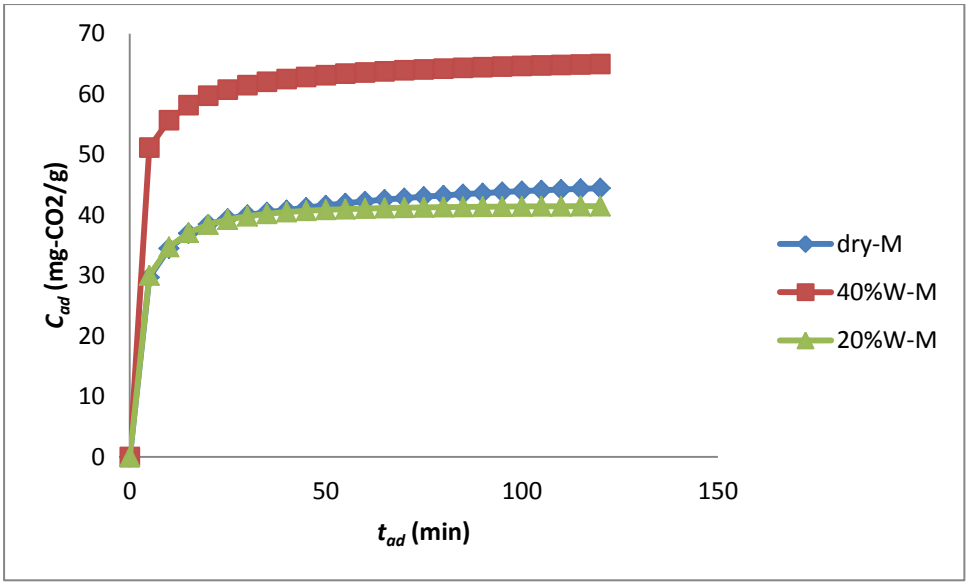


Figure 4.65: CO_2 adsorption from 14% CO_2 onto moist MWNT-PAA at 35 °C

C. CO_2 adsorption at 45 °C

At the temperature of 45 °C the presence of moist in PAA shows the increase of CO_2 adsorption capacity which was higher with 40% moist PAA sample; but slightly lower selectivity (Fig. 4.66 + Table 4.21). This shows that carbonate occurrence was more favorable at 45 °C, despite the poor geometry/structure in PAA which could disadvantage the potential interaction.

Table 4.21: Moisture effect on CO_2 adsorption using a flue gas of 14% CO_2 at 45 °C

Adsorbents	C_{ad} **mg/g**	X_{CO2} **%**
Dry PAA	25.5	92
20% Wet-PAA	28.2	90.4
40% Wet-PAA	29.4	89.1
Dry MWNT-PAA	40.0	90
20% Wet-MWNT-PAA	45.4	85
40% Wet-MWNT-PAA	48.1	86.6

With regard to the adsorbent MWNT-PAA, Figure 4.67 shows that the presence of moisture increased the CO_2 adsorption capacity at 45 °C. However, as previously discussed, the selectivity for CO_2 was reduced by significant amounts of O_2 that could be adsorbed under moist conditions of MWNT-PAA at 45 °C. Nevertheless, a high moisture levels flue gas is predicted to enhance the selectivity for CO_2. The carbonate formation through water and CO_2 was dominant at 45 °C. Thus, the humidification of flue gas may be a promising option for the enhancement of CO_2 adsorption capacity when the adsorption is intended to operate at 45 °C using the adsorbent MWNT-PAA.

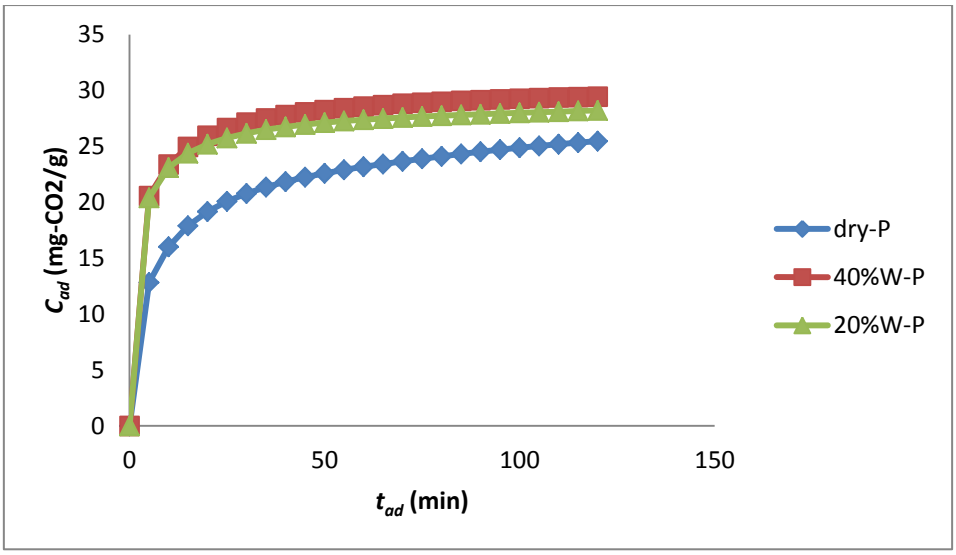


Figure 4.66: CO_2 adsorption from 14% CO_2 onto moist PAA at 45 °C

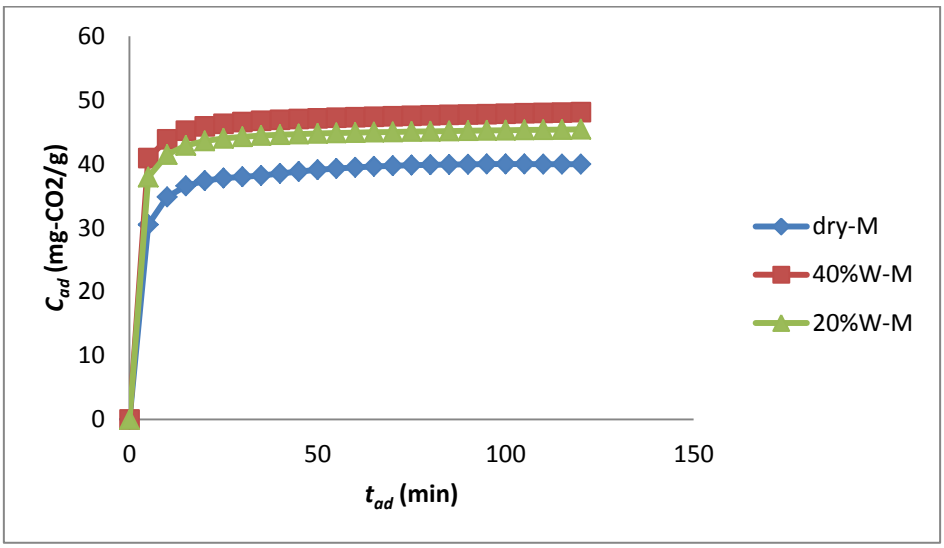


Figure 4.67: CO_2 adsorption from 14% CO_2 onto moist MWNT-PAA at 45 °C

D. CO_2 adsorption at 55 °C

The adsorption conducted at 55 °C with the use of PAA as adsorbent with 14% CO_2 flue gas (Figure 4.68) shows a slight increase of CO_2 adsorption capacity with 40% moist PAA, and a decrease with 20% moist PAA. The values of CO_2 adsorbed are reported in Table 4.22. The big concern to elucidate is the fluctuation in the increase and decrease of CO_2 adsorption capacity with large and small amounts of water in PAA, respectively. It is known that the increase of temperature increases the desiccation of the adsorbent. Thus, a wet adsorbent will progress to dry adsorbent when a part of water is lost as a result of temperature effects. Yet, the water is intended to increase the CO_2 uptake in the presence of the amine adsorbent. The 40% moist PAA presents enough water to increase CO_2 uptake through carbonate formation. In addition, the formation of bubbles with the increase of temperature is possible; especially with small quantity of water in the 20% moist PAA. The resistance to the breakdown of these bubbles increases with the presence of air in gas stream. Unless the potential interaction of CO_2-water-amine to form HCO_3^- and NH_3^+ is strong enough to break these bubbles, the decrease of CO_2 adsorption is inevitable. Furthermore, the selectivity for CO_2 was favorable even though it decreased with the increase of water in the PAA adsorbent. This is advantageous for CO_2 capture adsorption technology using PAA at 55 °C with a significant amount of water content in the gas stream.

Table 4.22: Moisture effect on CO_2 adsorption using a flue gas of 14%CO_2 at 55 °C

Adsorbents	C_{ad} **mg/g**	X_{CO2} **%**
Dry PAA	24.4	100
20% Wet-PAA	20.6	96.8
40% Wet-PAA	25.7	93.7
Dry MWNT-PAA	34.2	99
20% Wet-MWNT-PAA	31.2	74.3
40% Wet-MWNT-PAA	34.9	64.2

A similar trend was observed for the MWNT-PAA where a decrease in CO_2 adsorption capacity was noted for the 20% moist sample; while a slight increase was noted for the 40% moist sample (Fig. 4.69 and Table 4.22).

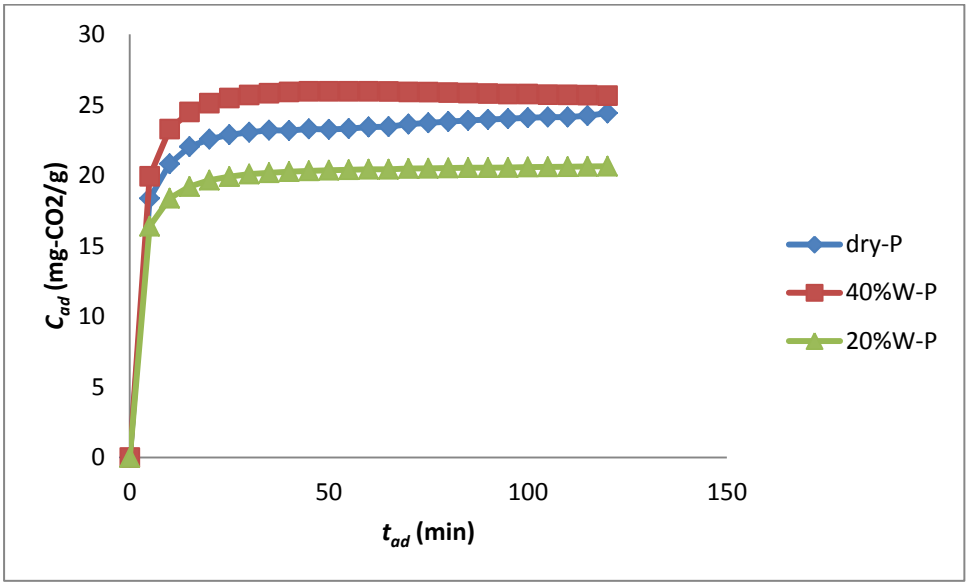


Figure 4.68: CO_2 adsorption from 14% CO_2 onto moist PAA at 55 °C

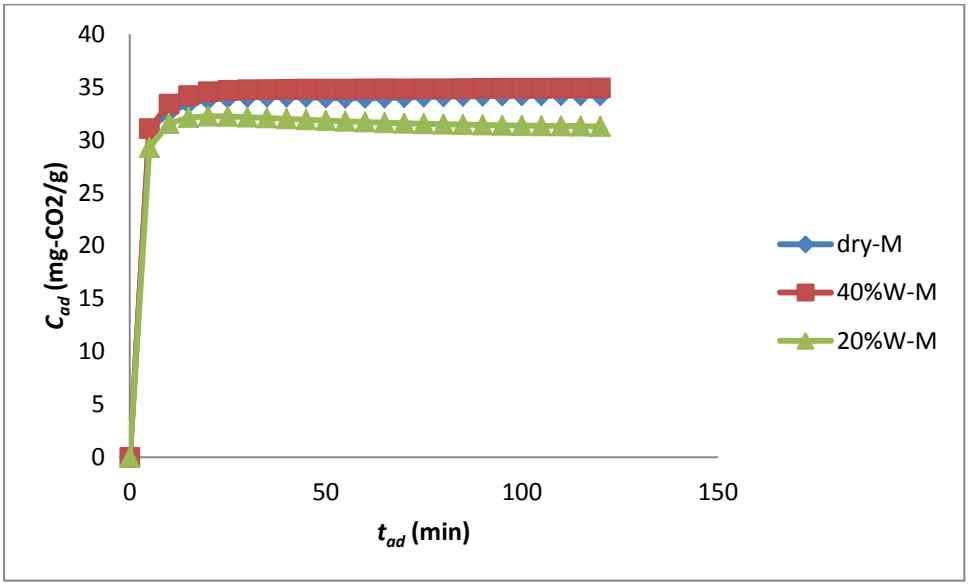


Figure 4.69: CO_2 adsorption from 14% CO_2 onto moist MWNT-PAA at 55 °C

4.6.2.3. Discussion of CO_2 adsorption using moist adsorbents at varying CO_2 concentration

For a gas streams with both 100 and 14% CO_2 contents, the presence of moisture in the adsorbent PAA reduced CO_2 adsorption capacity at the temperatures tested (25 and 35 ◦C). This shows that the formation of carbonate was not favorable at these temperatures. Moisture could be incorporated in the lattice of pores, blocking CO_2 from migrating to the available adsorption sites. Likewise, the adsorbent MWNT-PAA showed a decrease of CO_2 adsorption capacity with the increase of moisture at 25 °C, but only for the 100% CO_2 gas stream (Table 4.23). The CO_2 adsorption capacity was almost independent of water concentration for the gas stream of 14% CO_2. The presence of air with N_2 in the flue gas could sweep the water from the lattice pores in order to allow the migration of CO_2 into available adsorption sites. Note that the homogeneity, smoothness, and purity of the surface interacting particles influence the interparticle forces. Moreover, the presence of very small bubbles of gas on the surface of particles can significantly impact on the interparticle interaction [295]. Thus, the microbubbles occurring decrease CO_2 adsorption capacity. The phenomenon of microbubbles was important with the PAA at temperatures of 25 and 35 °C due to the poor geometry/structure of the adsorbent, i.e. its large pore size, small surface area and pore volume. Conversely, the microbubbles did not develop on the MWNT-PAA surface, due to the high hydrophobicity of the adsorbent and also the ability to form carbonate. Therefore, the adsorbent MWNT-PAA did not experience a significant decrease of CO_2 adsorption capacity with the presence of water in the adsorbent. Instead, the CO_2 adsorption capacity was either almost equal or higher with the increase of moisture in MWNT-PAA.

The adsorbent PAA was more efficient for the adsorption performed at 45 °C where the increase of moisture concentration in an adsorbent resulted in an increase of CO_2 adsorption. The adsorbent MWNT-PAA operated efficiently at all temperatures, with minimal reduced CO_2 adsorption recorded. A high CO_2 adsorption capacity for both gas streams with 100% CO_2 and 14% CO_2 contents were encountered at 35 °C when using the adsorbent MWNT-PAA. In addition, the adsorbent MWNT-PAA showed that a significant quantity of moisture in the flue gas resulted in high CO_2 adsorption capacity. This explains a continuous formation of carbonate through the interaction between H_2O, CO_2 and $–NH_2$ which resulted in HCO_3^-

and $-NH_3^+$ formation. When the quantity of water is small, the rise of temperature can limit the carbonate formation resulting in a decrease of the CO_2 adsorption capacity. The highest CO_2 adsorption capacity at 35 °C with the use of MWNT-PAA was 71 and 65 mg-CO_2/g for both flue gas with 100 and 14% CO_2 contents, respectively. This proved that the impact of O_2 is less when the CO_2 and O_2 are competing in the adsorption process. The increase of water enhanced the selectivity for CO_2 during the adsorption at 35 °C with the adsorbent MWNT-PAA, and for the adsorption in the temperature range 45 - 55 °C with the adsorbent PAA (Table 4.24). The O_2 adsorption drops significantly in the competition with CO_2 due to the latter's higher affinity for the amine adsorbent compared to O_2.

Note that the CO_2 adsorption capacity is expected to increase when the reactor with MWNT-PAA adsorbent is permanently fed with flue gas containing moisture, because the carbonate formation will be limited not by the saturation of water but by the saturation of the adsorbent. In this work the adsorbent was wetted before the adsorption process, which shows that the quantity of water could limit the carbonate formation while the adsorbent is still providing available sites for adsorption. The saturation of water before adsorbent saturation will obviously lead to carbamate formation instead of carbonate formation. This, according to stoichiometry of the reactions, ensures double the amount of CO_2 adsorption capacity compared to carbamate formation. In addition, the permanent flowing of flue gas with water content will never be subjected to the desiccation, therefore the CO_2 adsorption capacity and the selectivity for CO_2 can be higher.

Table 4:23: Moisture effects on CO_2 adsorption capacity from 100% CO_2 in gas stream

Adsorbents	C_{ad} (mg-CO_2/g)											
	25 °C			35 °C			45 °C			55 °C		
	%Mosture			%Moisture			%Moisture			%Moisture		
	dry	20%	40%	dry	20%	40%	dry	20%	40%	dry	20%	40%
PAA	52	24.3	13.5	52	46.4	26.5	39	43.4	47	43.7	22	35.7
MWNT-PAA	70	57	43.7	60	57	71	56	49.3	70.2	46.6	46.7	71

Table 4.24: Moisture effects on CO_2 adsorption capacity from gas stream of 14% CO_2

Adsorbents	25 °C		35 °C		45 °C		55 °C	
	C_{ad} mg/g	X_{CO2} %	C_{ad} mg/g	X_{CO2} %	C_{ad} mg/g	X_{CO2} %	C_{ad} mg/g	X_{CO2} %
Dry PAA	31	86	30	88	25.5	92	24.4	100
20% Wet PAA	27.6	88.3	28.5	83.2	28.2	90.4	20.6	96.8
40% Wet PAA	10.3	58.7	16.7	66	29.4	89.1	25.7	93.7
Dry MWNT-PAA	45.9	90	41.5	70	40.0	90	34.2	99
20% Wet MWNT-PAA	44.5	84.2	44.4	81.4	45.4	85	31.2	74.3
40% Wet MWNT-PAA	46.8	81.5	65	91.6	48.1	86.6	34.9	64.2

4.7. ADSORPTION-DESORPTION CYCLES

The regeneration efficiency of adsorbents is an important factor that needs to be investigated to determine the competiveness of the adsorbent. Regarding the economic feasibility and environment concerns, an adsorbent must not be discarded after being used only once. For the regeneration efficiency, the adsorbent must release the maximum gas adsorbed again in the desorption process. A high frequency of reuse with consistent gas recovery at acceptable temperature and pressure is required for the adsorbent to be competitive. Testing of the regeneration of the adsorbents was rendered possible through the adsorption-desorption process using a temperature swing adsorption (TSA) systems. The gas recovery evaluation was achieved by considering the difference between the maximum and minimum adsorption isotherm curve as the maximum amount of gas adsorbed; the difference was considered to be

the amount of gas recovered. Thus, the ratio of the amount of gas recovery and the maximum amount of gas adsorbed results in percentage gas recovery.

As discussed in Section 3.3.3, the assessment of adsorbents' regeneration was undertaken with 10 cycles of CO_2 adsorption-desorption runs at 25 °C for the adsorption process and 90-100 °C for desorption process at constant pressure in 100% CO_2 for the adsorption using MWNT, PSI, PAA and MWNT-PAA using the TGA. This is important to be lightened for the regeneration temperature for adsorbents when the physisorption is predominant (PSI, MWNT) and when the chemisorption is predominant (PAA, MWNT-PAA).

4.7.1. Adsorption at 25 °C with desorption at 90 °C for 10 Cycles

The adsorbent PSI showed a high regeneration efficiency (Fig. 4.70), where some cycles of adsorbed gas recovery were a little bit beyond 100% (104% as the highest, as shown) in Table 4.25. Since the temperature stability was up to 400 °C (Section 4.2.1.1), non-deformation of adsorbent was expected when running the adsorption below 400 °C, unless a breakable bond occurs in the adsorbent structure besides the reversible adsorption bond expected between adsorbate and adsorbent. When the recovery goes beyond 100%, two explanations can be mooted to justify the cause. The first explanation is a possible destruction of the adsorbent and that the desorption phase includes the total desorbed gas corresponding to 100% and the extra beyond 100% corresponding to the adsorbent decomposition by temperature effects. The second explanation is that the desorbed temperature was able to remove all the adsorbed gas corresponding to 100% plus other gases previously inserted in the lattice of adsorbent. Since the recovery for all cycles was almost 100%, the adsorbent PSI showed stable regeneration at temperature of 90 °C.

With regard to the adsorbent MWNT, the regeneration after 10 cycles of adsorption-desorption displayed the behavior shown in Figure 4.71 and it was very efficient. The recovery (Table 4.25) shows an average recovery of 96%. Thus, the regeneration of the

adsorbent MWNT was successful at 90 °C; however, it has demonstrated a low adsorption capacity.

Table 4.25: Capacity of CO_2 desorption at 90 °C after adsorption at 25 °C

	% CO_2 recovery in desorption process after 10 cycles of ads-desorption										
Adsorbents	1	2	3	4	5	6	7	8	9	10	Average
MWNT	97	99	93	97	93	99	95	93	95	98	96
PSI	104	101	102	100	99	101	100	98	100	97	100
PAA	86	92	89	87	83	86	83	84	84	80	85
MWNT-PAA	92	85	83	82	80	78	78	78	78	77	81

The evaluation of CO_2 desorption using the adsorbent PAA (Table 4.25) shows an average recovery of 85%. The outcome from the integration of 10 cycles of adsorption-desorption peaks (Figure 4.72) shows highest and lowest recovery of 92 and 80% respectively. The regeneration for PAA at 90 °C was not adequate and could be improved by changing other factors including pressure, temperature and purging gas.

Considering the adsorbent MWNT-PAA, the average of recovery was 81%, with 92 and 77% as the highest and the lowest recoveries after 10 cycles of adsorption and desorption. The regeneration for MWNT-PAA was unsatisfactory, therefore improvement is necessary.

The higher CO_2 desorption (Table 4.25) observed for PSI and MWNT shows the prevalence of physisorption during the adsorption process. Whilst PSI and MWNT have low CO_2 adsorption capacity, their regeneration at 90 °C was effective. Conversely, PAA and MWNT-PAA presented low CO_2 desorption at 90 °C. This shows that the use of an amine to modify the chemical surface has chemisorption through the formation of carbamate. Generally, in

TSA systems, chemisorption requires higher temperatures to complete adequate desorption, compared to physisorption where the van der Waals bonds break at low temperature. For instance, increasing the temperature was necessary for the evaluation of regeneration performance of PAA and MWNT-PAA as adsorbents where chemisorption was predominant during CO_2 adsorption process.

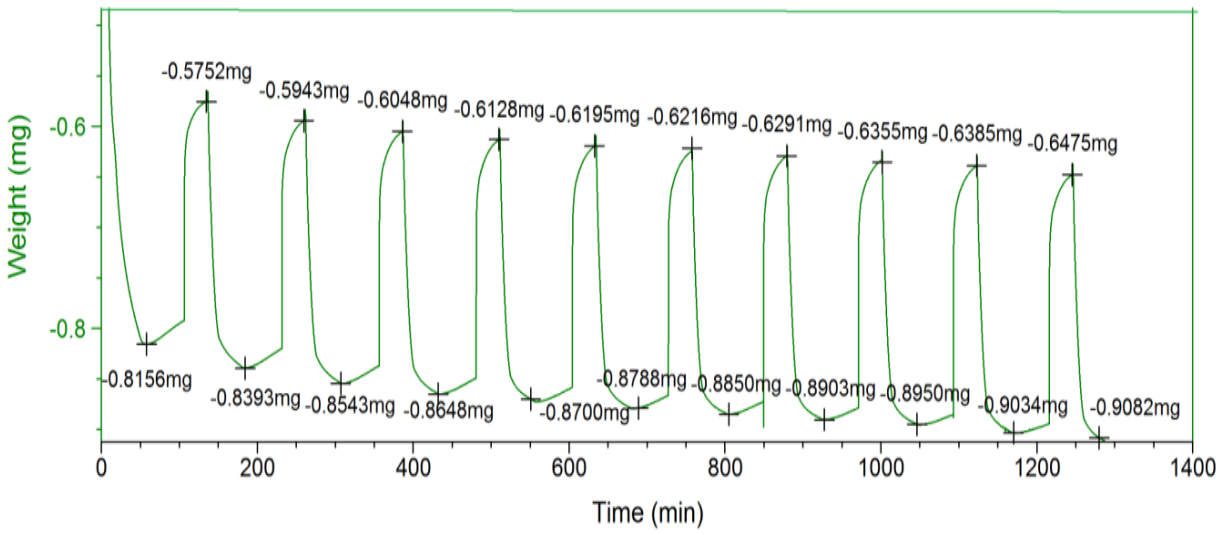


Figure 4.70: Adsorption (25 °C)-desorption (90 °C) Cycle for PSI

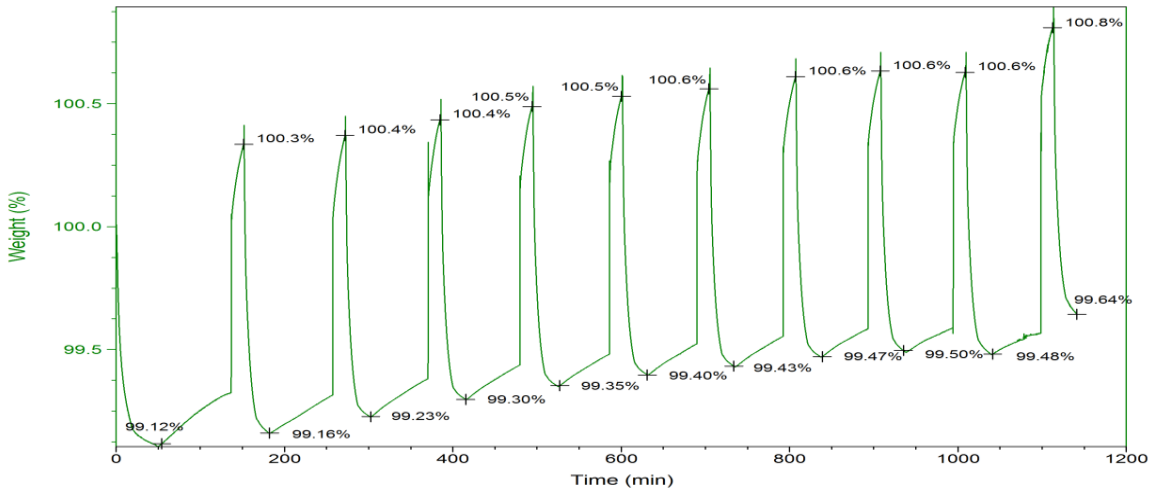


Figure 4.71: Adsorption (25 °C)-desorption (90 °C) Cycle for MWNT

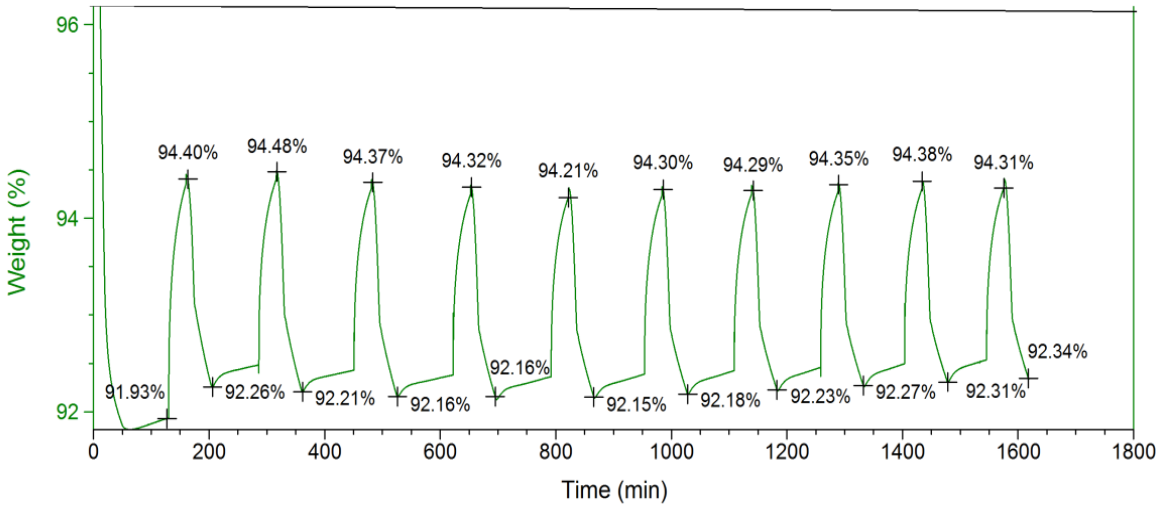


Figure 4.72: Adsorption (25 °C)-desorption (90 °C) Cycle for PAA

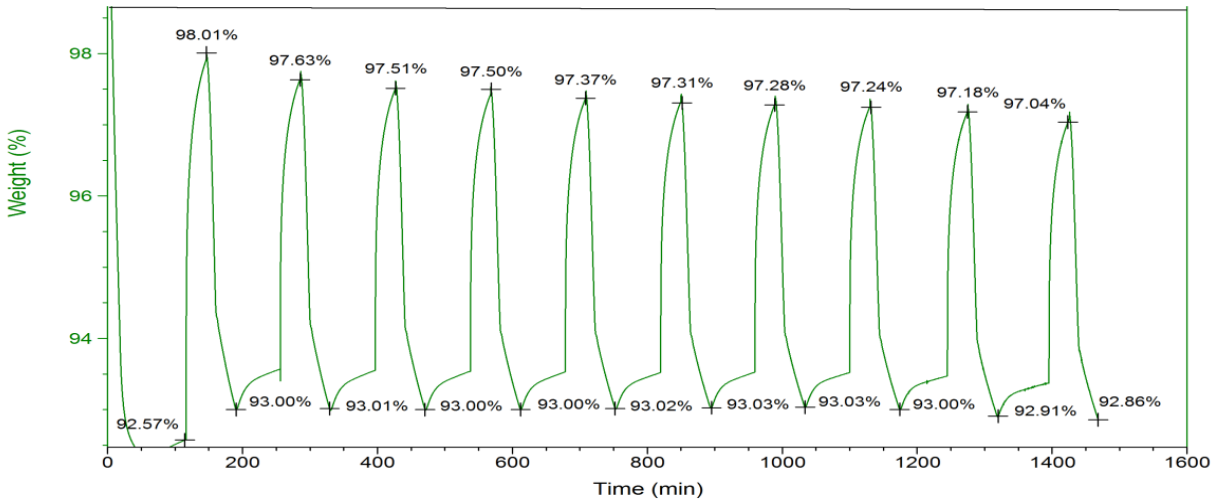


Figure 4.73: Adsorption (25 °C)-desorption (90 °C) Cycle for MWNT-PAA

4.7.2. Adsorption at 25 ℃ with Desorption at 100 ℃ for 10 Cycles

Overall, the increase of desorption temperature to 100 ℃ shows an increase of percentage CO_2 desorption. After integration of peaks in Figures 4.76 - 4.77, the percentage of CO_2 recovery was calculated as shown in Table 4.26. It is shown that the increase of desorption temperature to 100 ℃ has increased the average recovery from PSI to 123%. Thus, the

recovery using PSI as adsorbent has increased by 23% compared to the desorption performed at 90 °C. This increase of recovery above 100% must be avoided in order to prevent the adsorbent from gradual destruction. It is noticeable that the lifetime of the adsorbent relevant to the frequency of their replacement, is a factor of equal importance to CO_2 adsorption capacity, selectivity, and kinetics, with a direct impact on the economics of any commercial scale operation [296]. Nevertheless, the adsorbent can get more available adsorption sites, if, instead of adsorbent destruction, the desorption temperature is beneficial to remove the undesirable gas deeply located in the lattice of the adsorbent PSI. This can result in high adsorption capacity with efficient regeneration after a large number of adsorption cycles where the gas impurity will negatively affect the CO_2 concentration during the first adsorption-desorption cycles. Since desorption of PSI was more efficient at 90 °C, the increase of temperature to 100 °C will result in additional costs without associated increased efficiency or benefits.

Table 4.26: Capacity of CO_2 desorption at 100 °C after adsorption at 25 °C

	% CO_2 recovery in desorption process after 10 cycles of ads-desorption										
Adsorbents	1	2	3	4	5	6	7	8	9	10	Average
MWNT	104	109	107	105	103	101	108	108	109	102	106
PSI	123	121	124	123	123	123	123	121	123	125	123
PAA	100	102	100	99	97	97	97	96	96	95	98
MWNT-PAA	105	103	102	97	99	96	93	98	97	97	99

The same discussion applied to MWNT, where the adsorbent showed an average recovery of 106% at 100 °C (Table 4.26). This is above 100% whilst the average recovery was 96% at 90 °C. It is known that MWNT has high thermal stability up to 600 °C. This implies that no material destruction is expected, but that deep removal of unwanted gas previously located in the lattice of adsorbent is possible. Since the regeneration energy increased with the increase

of temperature, a temperature of 90 °C, resulting in average recovery of 96%, was an efficient temperature for desorption.

The average recovery over 10 cycles was 98 and 99% for PAA and MWNT-PAA, respectively. However, in the first three cycles the recovery for the adsorbent MWNT-PAA was just slightly above 100% (Table 4.26) and could be approximated to 100%. Thus, a suitable desorption temperature for PAA and MWNT-PAA is 100 °C. The carbamate formation through chemisorption by the amine of the CO_2 has been confirmed as reversible at a temperature of 100 °C.

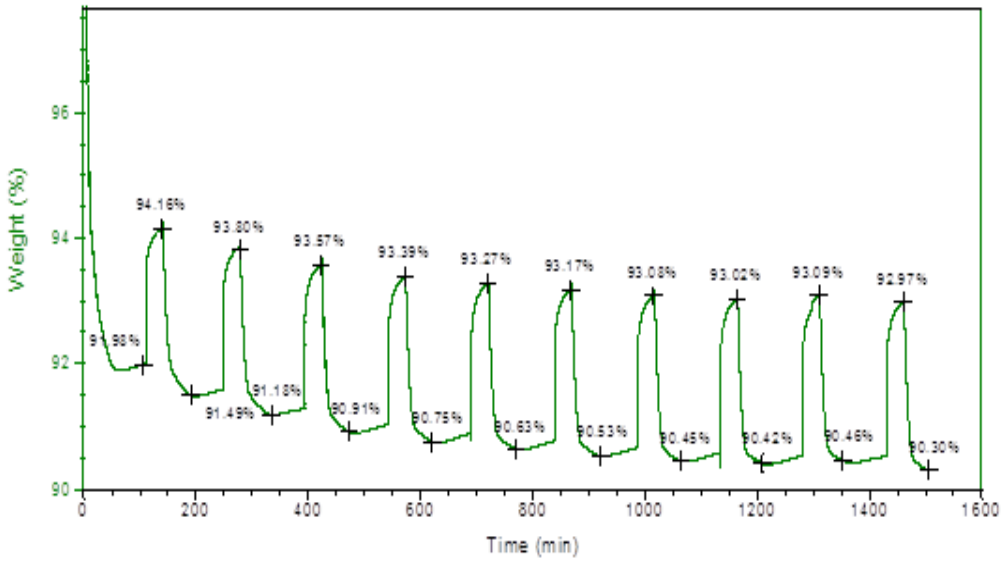


Figure 4.74: Adsorption (25 °C)-desorption (100 °C) Cycle for PSI

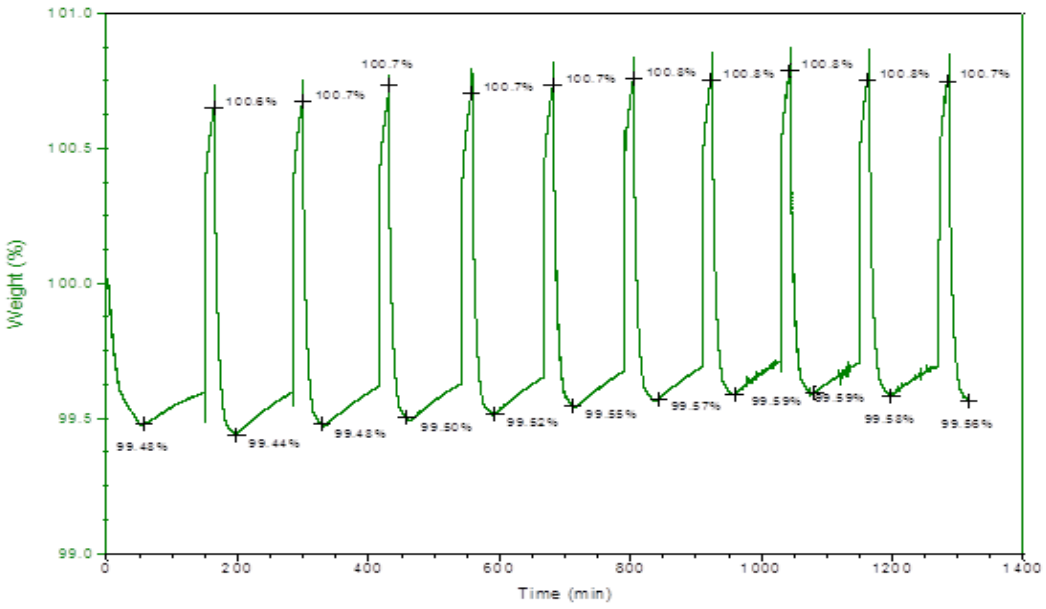


Figure 4.75: Adsorption (25 °C)-desorption (100 °C) Cycle for MWNT

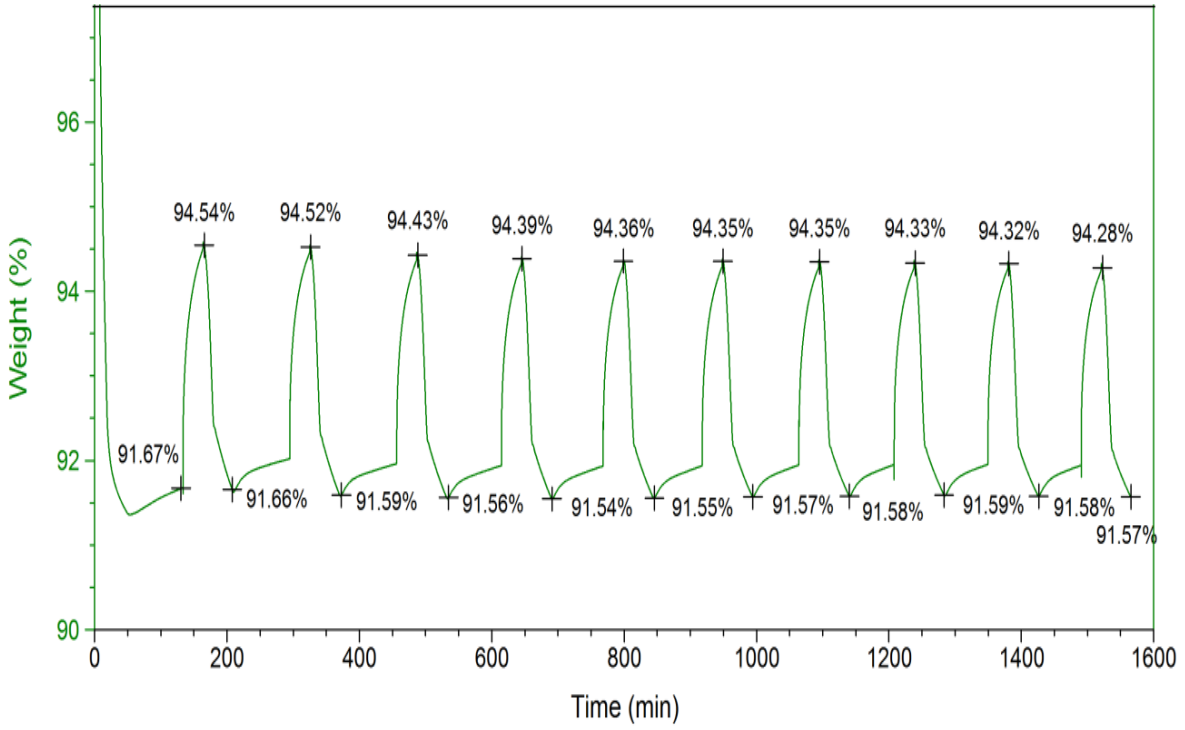


Figure 4.76: Adsorption (25 °C)-desorption (100 °C) Cycle for PAA

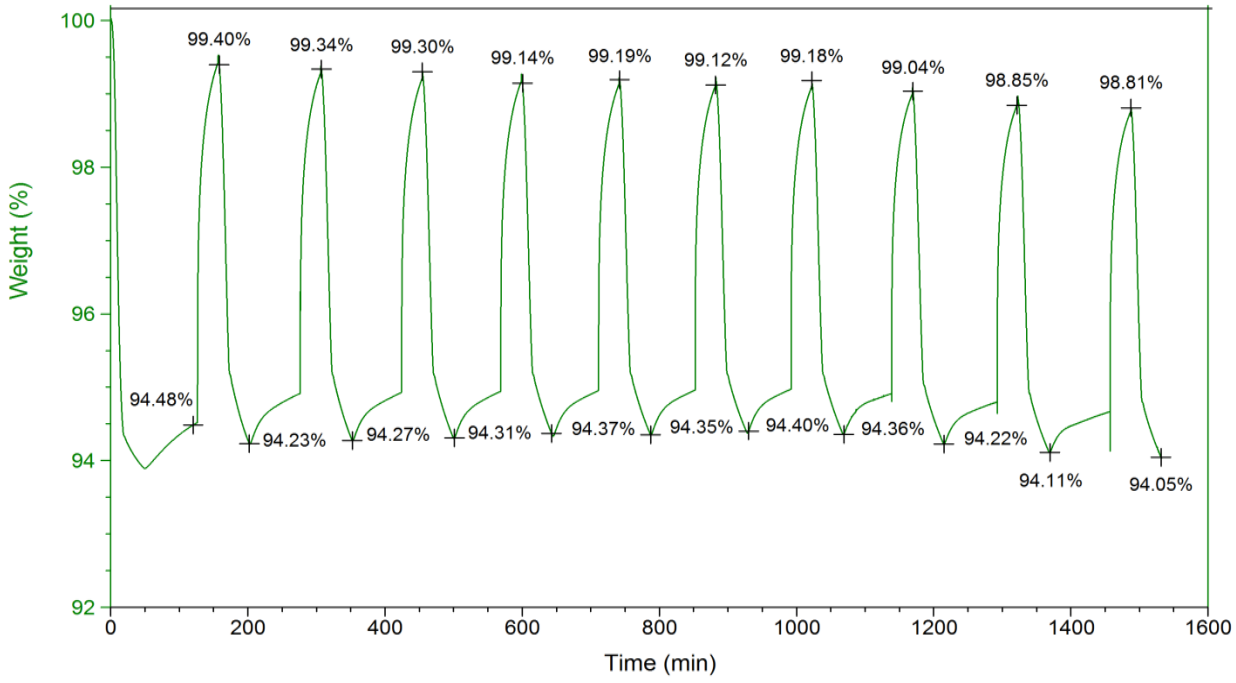


Figure 4.77: Adsorption (25 °C)-desorption (100 °C) Cycle for MWNT-PAA

4.8. THERMODYNAMIC EVALUATION OF THERMAL SWING ADSORPTION

Adsorption involves mechanical work, because adsorption is accompanied by the evolution of heat, and temperature changes affect the adsorption equilibrium and, in some cases, adsorption rate. If E is the energy of adsorption, then E = Q + H. The factor Q as the heat flux depends on bed geometry, flow rate, thermal diffusivity, temperature, fluid density, adsorbent surface area and heat capacity. H is the enthalpy of the reaction and heat is release for exothermic reactions and absorbed for endothermic reactions. When the system adsorbate-adsorbent releases the heat, the corresponding heat flow is negative. An exothermic reaction increases the temperature; therefore a temperature controller is needed in order to stabilize the temperature by switching off the energy from the source [297]. Consequently, there is gain in energy when the heat is released. In the case of an endothermic reaction, the temperature decreases [298] and the energy is needed from some source to maintain the temperature of work. This results in energy consumption. The important definitions of heat of adsorption are differential heat of adsorption and isosteric heat of adsorption. However, the enthalpy and internal energy depend on the initial and the final states. Different thermodynamics paths are necessary for the evaluation of heat flow in the adsorption process. A cycle of adsorption heat flow implies: (a) heat flow in the sweeping process; (b) heat flow in the adsorption process; and (c) heat flow in the desorption process.

4.8.1. Evaluation of heat flow in the sweeping process

The sweeping process was operated in three stages as follow: (a) the heating process from 21 °C (as ambient temperature) in the case of first cycle, or from adsorption temperature for all following cycles to 110 °C as the sweeping temperature; (b) 30 minutes of sweeping at 110 °C to complete the sweeping operation; and (c) the cooling process where the temperature changes from 110 °C to the adsorption temperature.

The values in Table 4.27 indicate that the heating of the reactor from the adsorption temperature to the sweeping temperature (110 °C) was marked by an increase of heat flow when the adsorption temperature increased. This observation is opposite to the formula $\Delta H = mC_p\Delta T$ where the heat flow (ΔH) is intended to increase with the increase of temperature change (ΔT). ΔT can increase only when the gap between the adsorption temperature and the sweeping temperature (110 °C) increases; resulting in decrease of adsorption temperature.

The explanation of this controversy is possible when considering Figures 4.78 and 4.79 for adsorbents PAA and MWNT-PAA, respectively. These figures depict three stages of the path as follows: (a) the heat flow relevant to the path ABCDEF as the sweeping stage; (b) the heat flow relevant to the path FGH as the adsorption stage; and (c) the heat flow relevant to the path HIJKLMN as the desorption stage. As both Figures 4.78 (b) and 4.79 (b) describe closed loops corresponding to hysteresis curves for a complete cycle where the point N as the end of a previous cycle coincide with the point A as the beginning of the next cycle.

Table 4.27: Heat relevant to the sweeping process

Temp ◦C	Heating Heat to 110 °C (kJ/kg)		Isothermal Heat at 110 °C (kJ/kg)		Cooling Heat from 110 °C to T^5_{ad}. (kJ/kg)		Total Heat in sweeping process (kJ/kg)	
	PAA	MWNT-PAA	PAA	MWNT-PAA	PAA	MWNT-PAA	PAA	MWNT-PAA
25	26.324	-173.361	8.767836	41.64702	-239.227	-157.802	-204.13	-289.5160
35	98.501	0.90349	8.767836	41.64702	-134.355	-71.5573	-27.086	-29.00679
45	144.908	51.31895	8.767836	41.64702	-74.443	-24.0513	79.2328	68.91467
55	174.375	81.69762	8.767836	41.64702	-24.3230	-0.37691	158.820	122.9677

In the sweeping process described by the path ABCDEF the section ABC shows the heat flow relevant to the heating step to reach 110 °C. The long the section ABC shows a release of heat from the system adsorbate-adsorbent in segment AB and an absorbance of heat in segment BC. Using the adsorbents PAA and MWNT-PAA, it is shown in the sweeping process from starting point A that the release of heat goes up to 61 and 72 °C at point B whatever the adsorption temperature, and afterwards the heat is absorbed to reach 110 °C at point C. This shows that the heat flow for absorbance stayed steady as long as the variable adsorption temperature is below 61 °C for PAA (Fig. 4.78(b)) and 72 °C for MWNT-PAA (Fig. 4.79(b)). Consequently, the heat flow relevant to the heating step to reach the sweeping temperature at point C will drop with the lowest adsorption temperature, because it is the resultant balance between the heat released and the absorbed heat. This means that a higher adsorption temperature will have a shorter heat release, because the temperature change from

[5] T_{ad}: adsorption temperature

adsorption temperature to 61 or 72 °C for PAA or MWNT-PAA will be reduced. As the heat absorbance is steady from 61 or 72 to 110 °C for PAA or MWNT-PAA, the heat flow as a result of the balance of heat released and heat absorbed is intended to be higher. Moreover, under the same temperature conditions, MWNT-PAA shows low heat flow in the heating phase represented by path ABC compared to PAA (Table 4.27). This is because the heat released goes from the adsorption temperature up to 72 °C for the adsorbent MWNT-PAA (Fig. 4.79 (b)); whilst it goes up to 61 °C for the adsorbent PAA (Fig. 4.78 (b)). Consequently the section ABC has generally resulted in absorbance of heat while the segment AB is marked by the release of heat. The release of heat in the segment AB is larger in MWNT-PAA than in PAA due to large specific surface area and small pore size in MWNT-PAA. Since the segment BC is steady, the resultant heat flow in the section ABC depends on the behavior in the AB section. The higher the heat release is in AB, the lower the heat absorbance is in ABC, with possibility to be converted to released heat if the heat flow in the segment AB surpasses it, as is the case for MWNT-PAA at 25 °C (Table 4.27). Also, a small change of temperature has a large effect on the change of heat flow relevant to the heating for both adsorbents PAA and MWNT-PAA, as showed in Table 4.27. Thus, the increase of temperature results in an increase of heat flow in the absorbance direction.

With regards to the isothermal heat for the sweeping process at 110 °C, the heat flow as shown in segment CD (Fig. 4.62 - 4.63) was steady and marked by heat absorbance with values of 8.77 kJ/kg and 41.65 kJ/kg for PAA and MWNT-PAA, respectively.

The cooling phase in path DEF, as showed in Figures 4.78 and 4.79, was marked by the release of heat as tabulated in Table 4.27. Under the same conditions, the release of heat was higher for PAA compared to MWNT-PAA. As it is the cooling phase, the larger pore size favored the heat flow for rapid cooling, in contrast to the heating phase, where the smaller pore size favors the heat flow. In addition, the lower the adsorption temperature is, the higher the heat flow is relevant to the release of heat for the reactor to cool from 110 °C to the adsorption temperature.

Finally, the resulting heat flow for the sweeping process along the path ABCDEF (Fig. 4.78 and 4.79) was marked by large heat release at 25 °C, which has decreased at 35 ◦C and shifted to absorbance heat at 45 °C and had become even more significant at 55 °C, as shown

by the values in Table 4.27. Moreover, under the same temperature conditions the adsorbent MWNT-PAA has the advantage of higher heat release and lower absorbance heat compared to PAA, as shown in Table 4.27. Note that the higher heat release and the lower heat absorbance lower the energy consumption in the sweeping process. Thus, the use MWNT-PAA is more energy efficiency in the sweeping process than PAA.

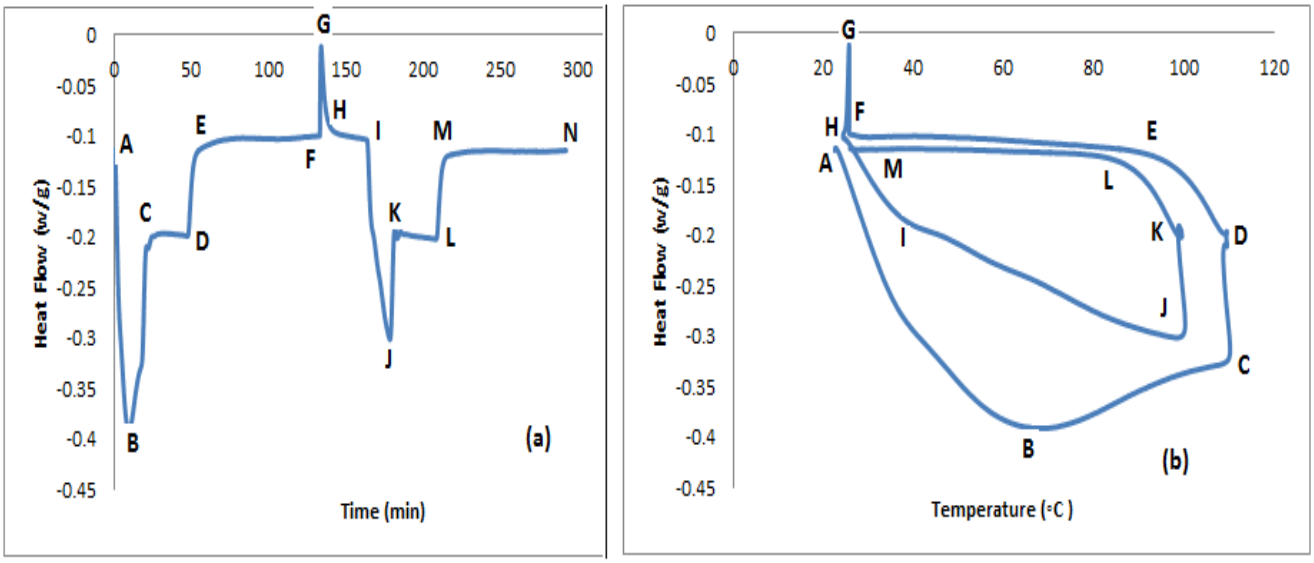


Figure 4.78: Heat Flow from DSC-TGA for a cycle of adsorption-desorption using PAA

a) Heat Flow versus time; b) Heat Flow versus temperature

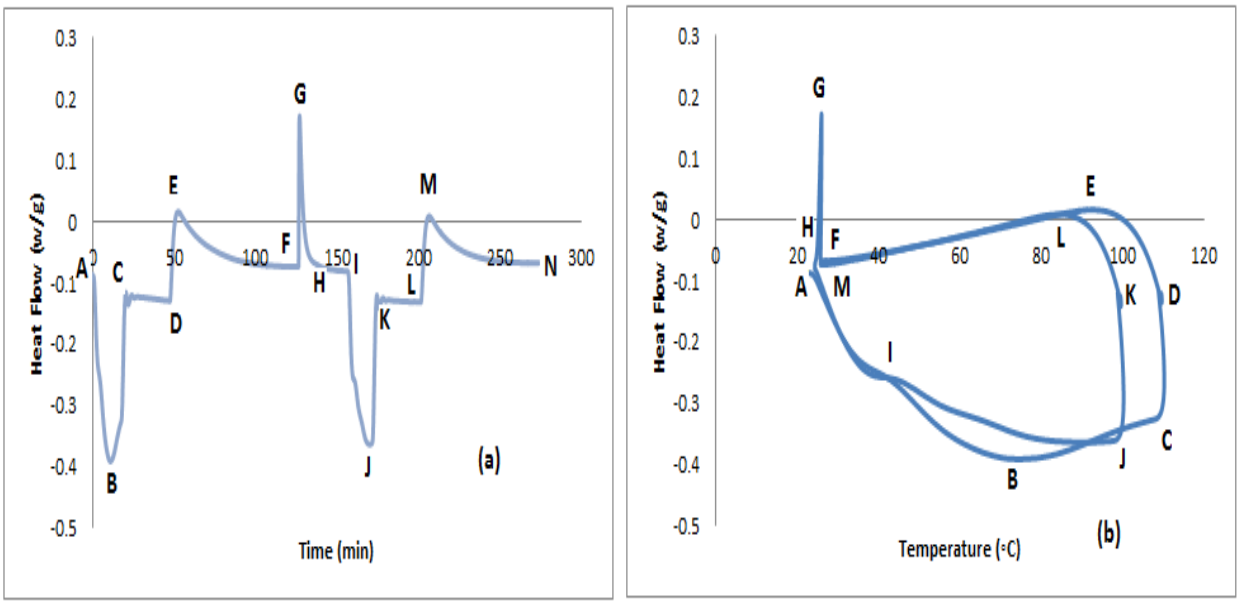


Figure 4.79: Heat Flow from DSC-TGA for a cycle adsorption-desorption using MWNT-PAA

a) Heat Flow versus time; b) Heat Flow versus temperature

4.8.2. Evaluation of heat flow in the adsorption process

The adsorption process relevant to the path FGH shown in Figures 4.78 and 4.79 was operated with variable adsorption temperatures, where the heat flow was marked by the release of heat. It is shown by the values in Table 4.28 that there is a large change of heat flow for a small change of adsorption time, and that the heat flow increases when the adsorption time increases. A long adsorption run will result in gain of energy due to higher heat release, regardless of other factors such as adsorption rate, adsorption kinetics which can be a disadvantage. Under the same condition of temperature, the heat flow for the adsorbent MWNT-PAA was always very higher than for the adsorbent PAA. This gives the adsorbent MWNT-PAA an advantage regarding the energy efficiency in an adsorption process. Thus, a good geometry/structure increases the exothermic heat in adsorption process compared to a poor geometry/ structure.

Table 4.28: Heat relevant to the adsorption process

Isotherm Time (min)	Adsorption Heat at 25 °C (kJ/kg)		Adsorption Heat at 35 °C (kJ/kg)		Adsorption Heat at 45 °C (kJ/kg)		Adsorption Heat at 55 °C (kJ/kg)	
	PAA	MWNT-PAA	PAA	MWNT-PAA	PAA	MWNT-PAA	PAA	MWNT-PAA
10	-61.0000	-151.698	-138.041	-202.210	-199.648	-291.359	-294.014	-340.564
20	-131.891	-341.501	-323.262	-459.178	-430.993	-683.154	-649.663	-723.650
30	-210.258	-717.096	-501.359	-694.97	-670.095	-1039.56	-1217.23	-1177.79
40	-286.756	-901.560	-666.300	-924.307	-968.375	-1410.60	-1431.16	-1686.12
50	-361.930	-1084.05	-821.474	-1140.05	-1186.09	-1784.68	-1680.58	-1898.16
60	-442.265	-1264.15	-957.220	-1344.76	-1331.90	-2000.02	-1952.45	-2205.68
70	-514.286	-1441.81	-1072.43	-1545.12	-1518.30	-2310.88	-2306.40	-2580.99
80	-585.229	-1619.91	-1207.47	-1776.75	-1699.02	-2605.57	-2621.04	-2958.69
90	-646.598	-1792.66	-1351.62	-2033.40	-1930.53	-2934.99	-2976.17	-3334.91
100	-714.613	-1965.47	-1490.33	-2257.87	-2138.31	-3272.15	-3265.83	-3708.03
110	-779.477	-2138.13	-1625.98	-2477.10	-2342.66	-3604.10	-3587.38	-4086.58
120	-842.125	-2316.20	-1751.39	-2693.90	-2550.51	-3991.50	-3911.57	-4466.59
130	-904.459	-2491.20	-1895.01	-2908.49	-2758.15	-4272.78	-4228.85	-4843.81
140	-965.265	-2660.20	-2032.81	-3122.34	-2964.12	-4615.49	-4558.88	-5219.18
150	-1026.00	-2826.74	-2171.27	-3336.27	-3176.03	-4961.11	-4894.70	-5599.76

4.8.3. Evaluation of heat flow in the desorption process

The heat flow in desorption process is indicated in Figures 4.78 and 4.79 by the path HIJKLMN, which can be divided into three parts as follows: (a) heat flow relevant to the heating phase from adsorption temperature to desorption temperature (100 °C), shown by section HIJ; (b) heat flow relevant to the isothermal heating at 100 °C as shown in the segment JK; and (c) heat flow relevant to the cooling phase from 100 °C back to the adsorption temperature represented by the path KLMN. The point N back to the adsorption temperature coincides with the point F.

The heat flow relevant to the heating process as shown in the section HIJ was marked by the release of heat, which decreases with an increase of temperature. Except at 25 °C, the heat flow in the section HIJ was a little bit higher for the adsorbent PAA than for the adsorbent MWNT-PAA (shown by the values in Table 4.29). This can be explained only by the investigation of the link PAA-CO_2 and (MWNT-PAA)-CO_2, which can sometime cause a fluctuation when the physisorption occurs over the monolayer formed through chemisorption.

The isothermal heat to complete the desorption process at 100 °C in the segment JK was marked by the absorbance of heat, which was steady with heat flow of 176.99 kJ/kg and 401.68 kJ/kg for the adsorbents PAA and MWNT-PAA, respectively.

The cooling was performed in section KLMN, where the point N coincides with F as starting point for the next cycle. Thus, the heat flow as shown by the values in Table 4.29 was marked by heat absorbance which decreases with the increase of temperature. Except at 55 °C, the absorbent PAA showed a higher heat flow for the cooling process than MWNT-PAA.

Table 4.29: Heat relevant to desorption process

Temp ◦C	Heating Heat to 100 °C (kJ/kg)		Isothermal Heat at 100 °C (kJ/kg)		Cooling Heat from 100 °C to T_{ad} (kJ/kg)		Total Heat in desorption process (kJ/kg)	
	PAA	MWNT-PAA	PAA	MWNT-PAA	PAA	MWNT-PAA	PAA	MWNT-PAA
25	-173.857	-239.936	176.9879	401.675	506.1669	417.9046	509.2978	579.6436
35	-100.065	-94.2775	176.9879	401.675	211.1939	168.4397	288.1168	475.8372
45	-66.8148	-60.5192	176.9879	401.675	134.5117	129.9369	244.6848	471.0927
55	-42.4447	-27.8276	176.9879	401.675	89.80651	105.4464	224.3497	479.2938

Finally, the resultant heat flow in desorption process was characterized by an endothermic process for both adsorbents PAA and MWNT-PAA where a higher heat flow was absorbed for the adsorption temperature set a 25 °C. However, afterward with the increase of temperature the heat flow decreased slightly for PAA and stayed almost constant for MWNT-PAA (see tabulated values in Table 4.29).

4.8.4. Heat flow depending on adsorption time

The heat flow for the complete cycle shows at all temperature high heat absorbance when the cycle is tailored to run at an adsorption time of 10 minutes (Table 4.30). However, the shorter adsorption time results in a larger CO_2 adsorption per day. A large amount of energy is required for a complete cycle, because the heat release increases with the increase of the adsorption time, which indicates a gain of energy as showed in Table 4.30. The heat flow for the complete cycle tailored to operate at adsorption times in the range of 10 to 70 minutes showed changes, especially for the adsorbent MWNT-PAA where the heat release decreased from 25 to 35 °C and increased afterwards, as shown by the values in Table 4.30. Regardless of some fluctuations, the use of the adsorbent MWNT-PAA for a complete cycle of adsorption-desorption results in higher heat release than in the case of the adsorbent PAA. Therefore, MWNT-PAA is predicted to be more beneficial regarding energy consumption compared to PAA for a complete cycle of adsorption-desorption.

Regarding the heat flow of the three phases (the sweeping process, the adsorption process and the desorption process) a higher heat absorbance was recorded in the desorption process

which confirms the endothermic nature of desorption process (Table 4.29). Therefore, more attention has to be given to the desorption process when the thermal swing adsorption (TSA) systems has to be optimized for efficient energy usage. The heat absorbance in the desorption process was significantly more with the adsorbent MWNT-PAA than for PAA. However, this was balanced by its higher heat release in the adsorption process, which resulted in a significant heat release for the whole cycle. A higher heat release was recorded in adsorption process which confirms the exothermic nature of the adsorption process (Table 4.28). As the heat flow relevant to a complete cycle was generally marked by heat release (Table 4.30), the adsorption process showed the largest effect on the overall energy efficiency.

With regard to the energy efficiency, a cycle of adsorption-desorption is effective when the TSA system is designed to operate continuously with a long adsorption time (Table 4.30). The disadvantage is that the adsorption rate decreases significantly during a long adsorption time, causing a very low CO_2 uptake in the last 70% of adsorption time, thus lowering the quantity of CO_2 adsorption per day. Therefore the optimization of a TSA system also requires attention to some other important factors such as sweeping, adsorption and desorption temperatures, time required for the sweeping, adsorption and desorption processes, CO_2 adsorption per day, numbers of beds for a continuous TSA system and energy consumption.

Table 4.30: Heat flow for a cycle with variable adsorption times

Time (min)	25 ℃ Heat flow kJ/kg		35 ℃ Heat flow kJ/kg		45 ℃ Heat flow kJ/kg		55 ℃ Heat flow kJ/kg	
	PAA	MWNT-PAA	PAA	MWNT-PAA	PAA	MWNT-PAA	PAA	MWNT-PAA
10	244.1678	138.4296	122.9898	244.6204	124.2696	248.6484	89.15570	260.65870
20	173.2768	-51.3734	-62.2312	-12.3476	-107.075	-143.147	-266.496	-122.4273
30	94.90980	-426.908	-240.328	-248.140	-346.177	-499.553	-834.060	-576.5673
40	18.41180	-611.432	-405.269	-477.477	-644.457	-870.593	-1047.29	-1084.897
50	-56.7622	-790.922	-560.443	-693.220	-862.172	-1244.67	-1297.41	-1296.937
60	-137.097	-974.022	-693.189	-897.930	-1007.98	-1460.01	-1569.28	-1604.457
70	-209.118	-1151.68	-811.399	-1098.29	-1194.38	-1770.87	-1923.23	-1979.467
80	-280.061	-1329.78	-946.439	-1329.92	-1375.10	-2065.56	-2237.87	-2357.467
90	-341.430	-1502.53	-1090.59	-1586.57	-1606.61	-2394.98	-2593.00	-2733.687
100	-409.445	-1675.34	-1229.30	-1811.04	-1814.39	-2732.14	-2882.66	-3106.807
110	-474.309	-1848.00	-1364.94	-2030.27	-2018.74	-3064.09	-3204.21	-3485.357
120	-536.957	-2026.07	-1490.35	-2247.07	-2226.59	-3451.49	-3528.40	-3865.367
130	-599.291	-2201.07	-1633.98	-2461.66	-2434.23	-3732.77	-3845.68	-4242.587
140	-660.097	-2370.07	-1771.88	-2675.51	-2640.20	-4075.48	-4175.71	-4617.957
150	-720.932	-2536.61	-1910.24	-2889.44	-2852.11	-4421.10	-4511.53	-4998.537

4.9. EVALUATION OF THE NUMBER OF BEDS FOR TSA SYSTEMS

The thermal swing adsorption (TSA) system includes three main stages: (a) sweeping of the adsorbent; (b) the adsorption process; and (c) the desorption process. Thus, knowledge of heating, isothermal and cooling times is required in order to evaluate the number of beds suitable for efficient continuous TSA systems. The investigation done for the TSA system evaluation was based on the dry flue gas without considering the moisture effect, which was beneficial for the adsorbent MWNT-PAA for CO_2 adsorption as shown previously.

The sweeping process was beneficial for the cleaning of the adsorbent in order to provide more available adsorption sites by stripping out the gas and water previously incorporated in the pores of adsorbent. Using N_2 as purge gas, the sweeping process was done at 110 ℃ from

ambient or adsorption temperature with an isothermal time of 30 minutes. Likewise, the process of desorption was done at 100 °C at different times, before the reactor was cooled down to the same adsorption temperatures (25, 35, 45 to 55 °C). An extensive length of cooling time was reported in Table 4.31 from the sweeping process at 110 °C or the desorption process at 100 °C to the adsorption process at 25 °C. This is a drawback for a continuous TSA system which is expected to complete a number of cycles at a fixed time. However, the heating time was not as challenging, as shown by the data in Tables 4.31 and 4.32. The higher the adsorption temperature, the shorter the length of cooling time is, as indicated by the data in Tables 4.31 and 4.32. Thus, it is an advantage for a TSA system to operate with an adsorption temperature close to the sweeping and desorption temperatures, unless a specific heat exchanger is used to enhance the cooling phase. However, this will increase the cost relevant to the implementation and the energy consumption. The change of heat flow was not so significant in the desorption process when the adsorption temperature increased (Table 4.29).

Table 4.31: The length of heating and cooling times in a sweeping process[6]

T_0 (°C)	T_s (°C)	T_{ad} (°C)	Heating time (min)	Sweeping time (min)	Cooling time (min)	Total time (min)
21	110	25	20	30	110	160
21	110	35	20	30	46	96
21	110	45	20	30	31	81
21	110	55	10	30	23	63

Table 4.32: The length of heating and cooling times with 30 minutes of desorption[7]

T_{ad} (°C)	T_{des} (°C)	Heating time (min)	Cooling time (min)
25	100	16	117
35	100	14	44
45	100	12	28
55	100	10	19

[6] T_0: ambient temperature; T_s: sweeping temperature; T_{ad}: adsorption temperature
[7] T_{des}: desorption temperature

It is obvious that the beginning of adsorption was always marked by a higher adsorption rate due to rapid adsorption kinetics, resulting in higher CO_2 adsorption per day for TSA systems. The implementation of TSA systems with the shortest adsorption time were beneficial regarding the daily CO_2 adsorption, as depicted by the data in Tables 4.30 - 4.33. The challenge is that the length of cooling time does not correlate with the short adsorption time for the TSA systems. Consequently, a large number of beds relevant to the temperature time cycle are required for the temperature time cycle to synchronize TSA systems in continuous operation mode. The shorter the adsorption time, the larger is the numbers of beds required for the synchronization of the TSA systems. This can produce a higher CO_2 adsorption per day. A large number of beds for the TSA systems become complex when taking into account additional factors such as space, bed equipment, adsorbent costs and energy cost. Large numbers of beds require a big space, together with expensive bed equipment, adsorbent costs and high energy costs. Furthermore, the heat flow for a cycle decreased with a shorter adsorption isothermal time. Is it because of disadvantage lies in the short adsorption time for the TSA systems that the approach of long adsorption time becomes beneficial? The TSA systems with longer adsorption times require fewer reactor beds, but the CO_2 adsorption per day is then significantly lower. In addition, almost 70% of the adsorption process with a long adsorption time had a very low adsorption rate with slow adsorption kinetics. Despite this, the heat release from such a process can be very high, as shown by the results in Table 4.30. Therefore, the optimization of all the relevant process parameters is necessary for the implementation of efficient TSA systems.

The results presented in Tables 4.31 and 4.32, show that the length of cooling time from 110 and 100 °C as sweeping and desorption temperatures respectively, to 25 °C as adsorption temperature, is quite extensive. Consequently, this will require a large numbers of beds, as is confirmed by the data in Table 4.33, especially compared to other adsorption temperatures shown in Tables 4.34, 4.35 and 4.36. A high adsorption temperature close to the sweeping and desorption temperatures will yield a small number of beds for the TSA systems in continuous operation mode. However, the adsorption capacity can be a weakness that needs to be kept in mind.

If the number of beds for a given TSA system is N at an adsorption time t, with a daily CO_2 adsorption of q, a multiple number of beds nxN result in a daily CO_2 adsorption of nxq. If an adsorption time of t' results in a number of beds N' = nN, the daily CO_2 adsorption will be q'

> nq if the length of bed temperature cycle for an adsorption time t'< t. As an example, consider the values in Table 4.33 with the adsorbent MWNT-PAA, where the gas stream is 100% CO_2, an adsorption time for the relevant temperature time cycle is 393 minutes. This will require 4 beds for the TSA system, and yield a daily CO_2 adsorption of 966 g-CO_2/kg. If 4 identical TSA system units with 4 beds each operate in parallel, the number of beds will be 4x4 = 16 and the daily CO_2 adsorption will be 4x966 = 3864 g-CO_2/kg, while the adsorption time will stay 100 minutes. However, by using only one TSA system with 16 beds the adsorption isothermal time will drop to 20 minutes, as shown in Table 4.33, while the CO_2 adsorption per day will increase to 4014 g-CO_2/kg. Thus, for a fixed temperature it is advantageous for the same numbers of beds to be set in series rather than to be split in multiple series of numbers of beds operating in parallel.

When the same numbers of beds are suitable for different adsorption times in TSA systems at a fixed temperature, the shortest adsorption time should be the most important consideration. This is due to the short length for temperature time cycle, high adsorption rate, rapid adsorption kinetics and large daily CO_2 adsorption that can then be achieved. Since the TSA systems have three stages, i.e. sweeping, adsorption and desorption, the use of four beds proved to be sufficient when space limitations exist. The first bed will cover the sweeping process, while the second bed will accommodate adsorption and the third bed will be the desorbing stage. The fourth bed will operate as guardian bed facilitating the synchronization of the TSA system in order to avoid probable delays which could interrupt the continuity. Considering 4 beds as a suitable number of beds for the TSA systems for the same adsorption temperature, and the shortest adsorption time will certainly result in high CO_2 adsorption per day. Regardless of the energy evaluation, when the choice of adsorption temperature has to be made for a TSA systems with 4 beds, the highest adsorption temperature close to the desorption temperature is beneficial due to a higher adsorption rate, rapid adsorption kinetics, short length for temperature time cycle and high CO_2 adsorption per day. However, increasing the temperature will increase the energy consumption. Energy consumption must be balanced with the short length of adsorption time, heating and cooling times. Typically a complete adsorption-desorption cycle shows a large heat release with the increase of temperature, as is depicted in Table 4.30. A large heat release is beneficial for energy consumption. Thus, the adsorption temperature of 55 °C gives a high adsorption per day whatever the CO_2 concentration in the gas stream, with short adsorption time and a short temperature time cycle, when using 4 beds to maintain the TSA system.

Table 4.33: Integration of number of beds for a TSA system at 25 °C

Adsorption Time (min)	Cycle Time (min)	Beds No for cont. operation	CO_2 adsorption (g-CO_2/kg) per day					
			14% CO_2		40% CO_2		100% CO_2	
			PAA	MWNT-PAA	PAA	MWNT-PAA	PAA	MWNT-PAA
10	303	31	2294	4176	2470	5184	3420	6984
20	313	16	1391	2407	1528	2968	2144	4014
30	323	11	1020	1710	1130	2102	1618	2860
40	333	9	810	1335	902	1626	1317	2230
50	343	7	673	1098	752	1324	1118	1831
60	353	6	577	934	645	1115	976	1553
70	363	6	500	812	558	962	869	1348
80	373	5	452	788	502	846	784	1191
90	383	5	409	650	452	754	715	1067
100	393	4	380	646	411	680	658	966
110	403	4	346	545	373	618	609	882
120	413	4	316	504	345	567	568	812
130	423	4	293	469	320	523	532	752
140	423	3	276	438	299	485	500	700
150	443	3	259	447	280	451	472	655

Table 4.34: Integration of number of beds for a TSA system at 35 °C

Adsorption Time (min)	Cycle Time (min)	Beds No for cont. operation	CO_2 adsorption (g-CO_2/kg) per day					
			14% CO_2		40% CO_2		100% CO_2	
			PAA	MWNT-PAA	PAA	MWNT-PAA	PAA	MWNT-PAA
10	164	17	2623	4769	2989	4952	4998	6863
20	174	9	1565	2588	1796	2859	2428	3792
30	184	7	1129	1737	1302	2010	2091	2641
40	194	5	883	1283	1025	1536	1640	2030
50	204	5	726	1012	846	1232	1353	1650
60	214	4	618	832	720	1023	1151	1389
70	224	4	541	702	627	869	1001	1198
80	234	3	481	607	553	754	882	1050
90	244	3	431	533	494	657	792	936
100	254	3	394	474	448	581	719	845
110	264	3	361	426	408	599	658	771
120	274	3	334	387	375	471	606	709
130	284	3	311	354	347	429	563	657
140	294	3	290	326	323	393	525	612
150	304	3	272	301	302	363	492	572

Table 4.35: Integration of number of beds for a TSA system at 45 °C

Adsorption Time (min)	Cycle Time (min)	Beds No for cont. operation	CO_2 adsorption (g-CO_2/kg) per day					
			14% CO_2		40% CO_2		100% CO_2	
			PAA	MWNT-PAA	PAA	MWNT-PAA	PAA	MWNT-PAA
10	131	14	2253	4033	2404	3992	4256	6920
20	141	8	1347	2301	1514	2506	2397	3712
30	151	6	973	1597	1132	1813	1689	2551
40	161	5	759	1230	906	1418	1315	1950
50	171	4	622	1007	758	1174	1070	1584
60	181	4	529	851	652	1001	900	1321
70	191	3	461	736	574	874	777	1137
80	201	3	408	647	511	775	684	997
90	211	3	367	576	460	697	613	889
100	221	3	335	519	421	633	555	803
110	231	3	308	471	386	580	508	732
120	241	3	285	431	358	535	467	671
130	251	2	265	397	331	497	431	620
140	261	2	248	368	307	463	401	576
150	271	2	233	341	286	434	374	537

Table 4.36: Integration of number of beds for a TSA system at 55 °C

Adsorption Time (min)	Cycle Time (min)	Beds No for cont. operation	CO_2 adsorption (g-CO_2/kg) per day					
			14% CO_2		40% CO_2		100% CO_2	
			PAA	MWNT-PAA	PAA	MWNT-PAA	PAA	MWNT-PAA
10	102	11	2997	4549	2997	4375	5549	5980
20	112	6	1625	2380	1625	2515	1978	3163
30	122	5	1107	1607	1107	1790	2077	2182
40	132	4	834	1210	834	1394	1562	1664
50	142	3	670	967	670	1156	1255	1332
60	152	3	562	807	562	983	1049	1113
70	162	3	486	693	486	850	899	954
80	172	3	429	609	429	750	787	835
90	182	3	383	542	383	670	699	742
100	192	2	347	489	347	605	629	668
110	202	2	316	445	316	554	572	607
120	212	2	293	408	293	508	524	556
130	222	2	270	376	270	469	484	514
140	232	2	252	349	252	436	450	477
150	242	2	235	325	235	407	420	445

4.10. COMPARISON OF DESIGNED ADSORBENTS TO THE EXISTING ADSORBENTS FOR CO_2 CAPTURE

The CO_2 adsorption performance of the adsorbents PAA and MWNT-PAA were compared to the existing adsorbents which include activated carbon, zeolite, silica gel and MOFs under the condition of pressure at 1.1 bar for CO_2 capture.

Zhang *et al.* (2013), investigating the CO_2 adsorption capacity for activated carbon at the temperature of 25 ^{o}C, found 37 mg-CO_2/g with a pressure of 1.1 bar. This CO_2 adsorption capacity increased to704 mg-CO_2/g with the increase of pressure at 36 bars. When grafting the activated carbon with amine, at the same temperature as previously, the CO_2 adsorption capacity was 55 mg-CO_2/g for 1.1 bar and 836mg-CO_2/g for 36 bars [299]. However, all the adsorption capacity was lost when testing with the moisture.

Stuckert *et al.* (2011) [300], found that the zeolite of types Li-LSX, K-LSX and NaX exhibited the CO_2 adsorption capacity of 75, 48 and 40 mg-CO_2/g respectively at 25 °C and 1.1 bar. However, the grafting with amine was a drawback to the CO_2 adsorption capacity. Furthermore, the moisture effect with relative humidity (RH) of 80% resulted in 96% loss of CO_2 adsorption capacity [242, 300]. Also, the adsorbent regeneration required high temperature in the range 180 – 240 °C for the efficiency [300].

Zhang *et al.* (2012) [301], using TGA at 1.1 bar, found the CO_2 adsorption capacity of silica gel (SG) was 5.1 mg-CO_2/g at 75 °C; when loading with PEI to compose SG-PEI, in dry conditions the CO_2 adsorption capacity increased significantly to 131.1 mg-CO_2/g. This CO_2 adsorption capacity kept increasing until 185 mg-CO_2/g when the SG-PEI was tested with moisture. However, the PEI was found non-biodegradable and toxic [219].

Sumida *et al.* (2011) [302], investigating the CO_2 adsorption capacity of different types of MOFs which include Cu-BTTri, Mg_2(dobdc), Be-BTB, Co(BDP), MOF-177, Caron JX101 and Zeolite 13X, found that Mg_2(dobdc) exhibited a higher CO_2 adsorption of 88 mg-CO_2/g at 35 °C and 5 bars. In addition, all types of MOFs showed a CO_2 adsorption capacity lower than 25 mg-CO_2/g at 35 °C and 1.1 bar.

The adsorbent PAA made with EDA exhibited a CO_2 adsorption capacity of 52mg-CO_2/g at 25 and 35 °C and 1.1 bar. In the presence of moisture, the highest CO_2 adsorption capacity was 47mg-CO_2/g, obtained at 45 °C. The adsorbent MWNT-PAA made with the purpose of enhancing the CO_2 adsorption capacity through the improvement of geometry/structure showed the CO_2 adsorption capacity of 70 mg-CO_2/g at 25 °C and 1.1 bar. This CO_2 adsorption capacity increased a bit to 71 mg-CO_2/g in the presence of moisture at 35, 45 and 55 °C and 1.1 bar. Thus, the adsorbents PAA and MWNT-PAA have demonstrated to be competitive in CO_2 capture when looking at the advantage relevant to the biodegradability, CO_2 adsorption capacity, CO_2 adsorption kinetics, water tolerance, and regeneration temperature and heat flow for TSA systems.

CHAPTER FIVE

SUMMARY, CONCLUSIONS AND RECOMMENDATIONS

5.1. SUMMARY

In order to reduce CO_2 emissions, much work has been done in the area of CCS to mitigate potential global climate change for the sustainability of the application of fossil fuels, which generate 85% of world electricity.

The current research was undertaken to investigate a new adsorbent synthesized from carbon nanotubes with polyaspartamide surfactant in order to provide a new material for application in adsorption technology for CO_2 capture. The polyaspartamide (PAA) was produced by grafting an amine to a synthesized long chain polymer, polysuccinimide (PSI), which operates as the hydrophobic and nontoxic backbone. The FTIR analysis confirmed the biodegradability of materials through the identification of the imide bond, a biofissionable bond. The PSI was grafted with three types of amines, namely 1,3 propanediamine (PDA), ethylenediamine (EDA), and monoethanoalamine (MEA), in order to produce three types of PAA, named PSI-PDA, PSI-EDA and PSI-MEA. All three PAAs have been successful regarding amine incorporation which was 92, 100 and 98.6% in the polymer for PDA, EDA and MEA respectively, as determined by ^1H NMR analysis. Their biodegradability was proven by the presence of an amide group as a biofissionable bond, evaluated through FTIR analysis. In addition, using FTIR, the PSI-PDA and PSI-EDA adsorbents showed the presence of amine group (NH_2) to provide the potential CO_2 anchoring sites during CO_2 adsorption. However, the geometry/structure and thermal stability of the three PAAs evaluated through BET and TGA have shown drawbacks compared to the crude PSI tested alone. The thermal stability decreased from 400 °C for the crude PSI to 200 °C for the three PAAs.

The design of adsorbent through the grafting of amine to PSI using PDA, MEA and EDA for PAA synthesis significantly decreased the CO_2 adsorption capacity for PAA equivalent to PSI-PDA and PSI-MEA. The CO_2 adsorption capacity was 13.5 mgCO_2/g and 9 mgCO_2/g for PSI-PDA and PSI-MEA exposed to 100% CO_2 at 25 °C and 1.1 bars, compared to 25 mg-

CO_2/g for crude PSI respectively. This demonstrated a drawback regarding the process of surface chemical improvement from PSI to PAA for CO_2 adsorption enhancement. Under the same conditions the CO_2 adsorption capacity was 52 mg-CO_2/g for PSI-EDA. This significant increase of CO_2 adsorption capacity from PSI to PSI-EDA (PAA) has confirmed the design of the adsorbent for chemical surface improvement using EDA grafted on PSI for PAA synthesis.

The investigation of the influence of temperature on CO_2 adsorption capacity for PSI-EDA, henceforth named PAA, at temperature ranging 25 – 55 °C showed a high CO_2 adsorption capacity of 52 mg-CO_2/g at 25 and 35 °C for CO_2 adsorption tests with a gas composition of 100% CO_2. The CO_2 adsorption capacity remained the same at 25 + 35 °C, and increased from 45 to 55 °C to confirm the chemisorption predominance occurrence (Table 5.1). This is contrary to physisorption, where the CO_2 adsorption capacity is intended to decrease with the increase of temperature. In addition, the CO_2 adsorption rate increased with the increase of temperature to confirm the Arrhenius principle. Considering the change of CO_2 concentration at 100, 40 and 14% CO_2 in air, the CO_2 adsorption performed at temperatures ranging 25 – 55 °C was consistently marked by higher CO_2 adsorption capacity at 25 and 35 °C, as shown in Table 5.1. Since the adsorbent PAA showed a decrease of N_2 and O_2 adsorption capacities with the increase of temperature, the selectivity for CO_2 increased with the increase of temperature. The adsorbent PAA showed the ability to increase CO_2 concentrate to 100% after the adsorption process at 55 °C from the flue gas with very low concentration of CO_2 (Table 5.1).

Table 5.1: CO_2 adsorption capacity and CO_2 purity (%) in adsorbed gas for PAA

Gas Stream	25 °C		35 °C		45 °C		55 °C	
	C_{ad} mgCO_2/g	X_{CO2} %	C_{ad} mgCO_2/g	X_{CO2} %	C_{ad} mgCO_2/g	X_{CO2} %	C_{ad} mgCO_2/g	X_{CO2} %
14%CO_2	26.8	86	27	88	24	92	24.5	100
40%CO_2	30.2	87	31	92	29.8	94	29.4	100
100%CO_2	52	100	51.7	100	39	100	43.7	100

It is obvious that the CO_2 adsorption capacity of PAA was improved from PSI through the grafting of EDA, however the geometry/structure was poor. Therefore, the necessity of improving the geometry/structure was an attempt to enhance the CO_2 adsorption capacity. The process of geometry/structure enrichment was rendered possible through the use of non-covalent functionalization of MWNT by the polymer. Using the polymers PSI and PAA for the non-covalent functionalization of MWNT, the adsorbents MWNT-PSI and MWNT-PAA were produced. The analysis done through BET confirmed the improvement of geometry/structure for both MWNT-PSI and MWNT-PAA compared to PSI and PAA, as depicted in Table 4.1.

FTIR analysis showed that all functionalities, including biodegradable bonds and amine bonds (NH_2) were reproduced. TEM analysis confirmed the nanotube structure for both absorbents MWNT-PSI and MWNT-PAA. The thermal stability investigated using the TGA showed a drawback for both MWNT-PSI and MWNT-PAA, with thermal stability only up to 200 °C, in comparison to the pristine MWNT, where the thermal stability was 600 °C.

The MWNT-PSI as the synthesized adsorbent produced with the objective to improve the adsorptivity properties, showed a disadvantage for CO_2 adsorption. The CO_2 adsorption capacity at 25 and 35 °C was 22 and 19.5 mg-CO_2/g for the MWNT-PSI; while for the crude PSI the CO_2 adsorption capacity was 25 and 20 mgCO_2/g respectively. The inconvenience of low CO_2 adsorption capacity on MWNT-PSI was due to the inadequate position of PSI on MWNT, where the PSI as long chain with structure of closed ring in each monomer could tightly twist around the MWNT, blocking the available adsorption sites. Thus, the absorbent MWNT-PSI was not found beneficial for CO_2 capture.

The highest CO_2 adsorption capacity using the MWNT-PAA with 100% CO_2 was 70 mg-CO_2/g. However, the CO_2 adsorption capacity decreased with the increase of temperature, as showed in Table 6.2. In a gas of 14 and 40% CO_2, the performance of MWNT-PAA decreased with the decrease of CO_2 concentration (Table 5.2). The highest CO_2 adsorption capacity for MWNT-PAA exposed to flowing gas of 14 and 40% CO_2 was 47 and 62.4 mg-CO_2/g obtained at 25 °C.

N_2 and O_2 adsorption tests performed over the temperature range on the MWNT-PAA showed the ability to adsorb significant amounts of O_2 at 35 and 45 °C where the O_2

adsorption capacity was 12.5 mg-O_2/g and 8.33 mg-O_2/g respectively. Therefore, the selectivity for CO_2 was reduced for the adsorption using a gas of 14 and 40% CO_2 in air. Thus, the concentration of CO_2 in the adsorbed gas was inadequated at 35 and 45 ℃ at 14 and 40% CO_2 (Table 5.2). Conversely, the potential of improving the selectivity for CO_2 to more than 90% CO_2 concentration in the adsorbed gas was possible at 35 ℃ by shortening the adsorption time to a maximum time of 30 minutes when exposing MWNT-PAA to flowing gas of 14 and 40% CO_2. This was because the kinetics of N_2 and O_2 adsorption at 35 ℃ was found to be very slow the first 30 minutes. However, at 25 ℃ the adsorbent MWNT-PAA showed high selectivity for CO_2 with 92 and 94% CO_2 concentration in adsorbed gas for the gas of 14 and 40% CO_2. This selectivity for CO_2 was much better at 55 ℃ with 99% CO_2 concentration in adsorbed gas for the adsorbent MWNT-PAA exposed to flowing of gas of 14 and 40% CO_2. Consequently, the adsorbent MWNT-PAA is declared to be efficient for dry flue gas from power plants when the adsorption is set to operate at 25 and 55 ℃. At the temperature of 35 ℃ the adsorbent MWNT-PAA can enhance the selectivity for CO_2 if the adsorption process is reduced to a maximum time of 30 minutes for the dry flue gas from power plants.

Table 5.2: CO_2 adsorption capacity and CO_2 purity in adsorbed gas for MWNT-PAA

Gas Stream	25 ℃		35 ℃		45 ℃		55 ℃	
	C_{ad} mgCO_2/g	X_{CO2} %	C_{ad} mgCO_2/g	X_{CO2} %	C_{ad} mgCO_2/g	X_{CO2} %	C_{ad} mgCO_2/g	X_{CO2} %
14%CO_2	43.2	92	31.5	70	28	77	39.3	99
40%CO_2	58.7	94	37.8	73.5	40.7	81.4	49.1	99
100%CO_2	70	100	60	100	56	100	44.6	100

The selectivity for CO_2 is predicted to be far higher for both PAA and MWNT-PAA. This is because the amount of O_2 is very low in the flue gas from post-combustion plants compared to the amount of O_2 in this work as the flue gas was composed of air and CO_2. In addition, CO_2 controls the adsorption due to its high affinity with amine. However, the CO_2 adsorption capacity decreased with the decrease of CO_2 concentration in the flue gas under the same conditions of temperature and pressure. Furthermore, the adsorbents PAA and MWNT-PAA showed high adsorption rate with the potential to cover almost 70% of their adsorption

capacity in the first 30 minutes; while to complete the total adsorption capacity required significantly longer time period.

The adsorbent water tolerance test showed an increase of CO_2 adsorption capacity with the increase of moisture for the adsorbent PAA exposed to gas where the CO_2 concentration was 100 and 14% at 45 °C. Thus, the adsorption performed at 45 °C for 20 and 40% moist PAA exposed to 100% CO_2 resulted in CO_2 adsorption capacity of 43.4 and 47 mgCO_2/g respectively (Table 4.18, Fig. 4.58). The use of flue gas of 14% CO_2 to flow through 20 and 40% moist PAA resulted in CO_2 adsorption capacity of 28.2 and 29.4 mg-CO_2/g at 45 °C (Table 4.21, Fig. 4.66), with minimum CO_2 concentration of 90.4 and 89.1% (Table 4.24). This is because the O_2 adsorption was not as significant at 45 °C when 20 and 40% moist PAA were exposed to 100% O_2 (Table 4.17).

The CO_2 adsorption capacity increased generally with the increase of moisture in the adsorbent MWNT-PAA. When using a gas stream with 100% CO_2 content, the higher CO_2 adsorption capacity of 71 mg-CO_2/g was obtained at temperatures range of 35 to 55 °C, with MWNT-PAA incorporated in 40% moisture. While using a gas of 14% CO_2, the higher adsorption capacity was 65 mg-CO_2/g with 92% CO_2 concentration at 35 °C where significant amount of O_2 was demonstrated to be adsorbed in 40% moist MWNT-PAA exposed to 100% O_2.

Regarding the regeneration, the adsorbents PAA and MWNT-PAA were demonstrated to be regenerable at 100 °C with the potential recovery of 98% and 99% of adsorbed gas respectively.

The thermodynamic studies showed very high heat release for the MWNT-PAA as resultant heat flow which includes sweeping, adsorption and desorption processes, compared to PAA, except at 55 °C where the heat release for both PAA and MWNT-PAA was almost similar. The heat release increased with the adsorption time and temperature for both PAA and MWNT-PAA. Although a high heat release has advantages for energy efficiency, a short adsorption time was demonstrated to be beneficial to operate with a higher adsorption rate in order to multiply the adsorption cycle resulting in a large CO_2 uptake per day.

The correlation of time for the synchronization of sweeping, adsorption and desorption processes has shown a big challenge to implement continuous TSA systems. The problem is due to the gap between the adsorption time and the cooling time where the temperature has to be taken from sweeping or desorption temperature to the adsorption temperature in order to complete a cycle and start a new cycle. It was found that the CO_2 adsorption rate of adsorbents PAA and MWNT-PAA decreased with the increase of adsorption time. Consequently, the shorter the adsorption time the higher is the adsorption rate resulting in larger total CO_2 adsorption per day. Thus, the integration of numbers of beds is recommended in order to synchronize the sweeping, adsorption and desorption processes for continuous TSA systems. However, the short adsorption time required large numbers of beds to correlate with the cooling time for the implementation of continuous TSA systems. When the adsorption temperature increases, the gap with the sweeping or desorption temperature is reduced, resulting in short cooling time and the numbers of beds are reduced as well. It was found that both PAA and MWNT-PAA operating in TSA systems release significant amount of heat, which becomes more emphasized with the increase of temperature. Therefore, the integration of 4 beds operating with 40 minutes of adsorption time at 55 °C was found beneficial for continuous TSA systems when using both PAA and MWNT-PAA with dry gas. Regarding the moist flue gas, the temperature of 55 °C is not beneficial because the moist MWNT-PAA showed large O_2 adsorption with reduced selectivity for CO_2, resulting in 64% CO_2 concentration. Since the maximum of 4 beds was favorable to circumvent the challenge relevant to the space cluttering and equipment cost, the implementation of TSA systems for MWNT-PAA designed to operate at 35 °C was demonstrated to be efficient with the flue gas of water content from post-combustion.

5.2. CONCLUSIONS

Fossil fuel utilization has increased due to the growth of world population which resulted in high energy demand; causing high CO_2 emissions into the atmosphere. CCS is the sole alternative of reducing CO_2 emissions with the sustainability of fossil fuel utilization, which otherwise must be suppressed for the environment safety. However, CO_2 diluted in flue gas must be separated from other gases to achieve plus 95% purity for the transport and storage efficiencies. Such requirement needs an advanced capture technology which justifies the reason of this work. The objective of this work is to improve the CO_2 capture technology through the design of adequate hydrophobic and biodegradable adsorbent. Thus, the key

question relevant to the development of efficient and cost-effective means for CO_2 capture was answered through the performance of adsorbents as stated below:

- Both adsorbents PAA and MWNT-PAA exhibit a biodegradable bond through FTIR. The grafting of EDA on PSI to produce PAA with NH_2 as available CO_2 anchoring site was beneficial to increase significantly the CO_2 adsorption capacity at all temperatures. However, the geometry/structure of PAA was poor. The use of MWNT to produce MWNT-PAA resulted in enhancement of geometry/structure with higher CO_2 adsorption capacity compared to PAA.
- Both adsorbents PAA and MWNT-PAA showed the possibility of increasing the CO_2 adsorption capacity in the presence of moisture.
- Both adsorbents PAA and MWNT-PAA showed a very higher affinity to CO_2 compared to O_2 and N_2. Therefore, the potential to capture CO_2 exhibited a higher selectivity for CO_2 with the purity in range 92 - 100% CO_2 concentration.
- The adsorption process was marked by higher CO_2 adsorption rate for both adsorbents PAA and MWNT-PAA in the way that almost 85% of the whole CO_2 adsorption capacity was achieved the first 30 minutes.
- An efficient regeneration for both PAA and MWNT-PAA was found at 100 °C with 98 and 99% CO_2 recovery respectively.
- The investigation of heat flow showed for both adsorbents a very higher heat release in adsorption process recognized exothermic. While a very low heat was absorbed in desorption and sweeping processes recognized endothermic. This is beneficial for energy efficiency gains, because the system can operate with the heat release minimizing the external source of energy.
- Thus, both PAA and MWNT-PAA showed to be competitive for advanced CO_2 capture plant using adsorption technology compared to other adsorbents including the existing adsorbents such as activated carbon, silica gel, zeolites and MOFs.

Regarding the performance of the adsorbent MWNT-PAA, a higher CO_2 adsorption capacity of 70 mg-CO_2/g was recorded under dry conditions at 25 °C when using 100% CO_2 at 1.1 bar. This CO_2 adsorption capacity was enhanced to 71 mg-CO_2/g at 35, 45 and 55 °C when using the moist MWNT-PAA. Using 14% CO_2 with air ($79N_2/21O_2$), the higher CO_2 adsorption

capacity was 46 mgCO_2/g under dry conditions obtained at 25 °C, which increased to 65 mg-CO_2/g at 35 °C when using moist MWNT-PAA. Concerning the energy efficiency, MWNT-PAA reached its maximum heat release of 5600 kJ/kg at adsorption temperature of 55 °C; while in sweeping and desorption processes operated at 110 and 100 °C the maximum heat absorbance was 123 and 500 kJ/kg respectively. Thus, the TSA systems resulted in high heat release of 5000 kJ/kg.

Thus, the implementation of efficient MWNT-PAA for CO_2 capture requires:

- The polymer used as backbone must be water insoluble, nontoxic and biodegradable.
- The incorporation of amine in polymer backbone on one hand must provide available CO_2 anchoring sites, but on the other hand must avoid being in excess.
- During the synthesis of polysuccinimide (PSI) the condition of operation must be respected and the expansion must be observed.
- In case of diamine incorporation on PSI to make PAA, the condition of operation as described in Section 3.3 must be carefully respected in order to avoid crosslinking.
- The carbon nanotubes used to make MWNT-PAA must have high purity and high quality in geometry/structure including surface area, pore volume and pore size.
- Before the mixing of carbon nanotubes with the polymer, the sonication of carbon nanotubes in the solvent is required for adequate dispersion. The sonication time beyond 20 minutes must be avoided in order to prevent the carbon nanotubes from being brittle.
- The ratio carbon nanotube with polymer must be respected as 1:30.
- Non-covalent functionalization at room temperature is favorable for the mixing of carbon nanotubes with polymer in order preserve the functionality of polymer.
- The adsorbents PAA and MWNT-PAA must be conserved in a cool place.
- The adsorbents PAA and MWNT-PAA must not be used beyond 180 °C for adsorption or desorption process.

5.3. RECOMMENDATIONS

The adsorption process was rendered possible through the use of TGA. However, the mass transfer is not efficient, because of the horizontal position of the gas pipeline which is separated from the crucible from right to left at the distance of 8 cm and from top to bottom a

the distance of 1 cm. Therefore, the contact between the adsorbent and the gas coming from the pipeline is poor. Consequently, the adsorption time was extended in order to complete the total adsorption capacity. The design of efficient equipment with specific size geometry of the bed operating at adequate conditions of temperature and pressure with the ability to provide moisture at different humidity rate in gas stream will obviously show a higher efficiency of both adsorbents PAA and MWNT-PAA. Moreover, the designed equipment must be able to assure adsorption-desorption cycles in order to predict the frequency of adsorbent replacement. A system has been designed and the adsorbents will be tested shortly.

Furthermore, the investigation of these adsorbents in pressure swing adsorption (PSA) and vacuum swing adsorption (VSA) systems is recommended for large application of the adsorbents.

With regard to capture plants, the adsorbents PAA and MWNT-PAA were predicted to perform better than have been with the use of TGA. As the efficiency of PAA in the presence of water was found at 45 °C, it is recommendable to prepare the flue gas with moisture content accordingly in order to provide high CO_2 uptake. Otherwise the removal of water is required for CO_2 uptake enhancement when the adsorbent PAA is intended to be used at other temperatures beside 45 °C.

The adsorbent MWNT-PAA offers a large domain of application concerning the temperature in the range 25 - 55 °C. Nevertheless, large adsorption capacity was obtained at 35 °C when using the flue gas with 14% CO_2 content under moist conditions. A flue gas with large quantity of moisture content is not concerning since the increase of water in MWNT-PAA showed the increase of CO_2 uptake. However, since the presence of O_2 could be a drawback, it is recommended to use the adsorbent MWNT-PAA at any temperature in the range 25 - 55 °C for post-combustion capture.

Finally, to complete a high daily CO_2 uptake when using PAA or MWNT-PAA, it advisable to shorten the adsorption isothermal time and improve the cooling system with efficient heat exchanger in order to correlate the time for adsorption-desorption cycle in TSA systems with minimum numbers of beds possible.

CHAPTER SIX

CONTRIBUTION OF THE WORK TO SCIENTIFIC ADVANCEMENT AND ACHIEVEMENTS

Within the framework of CCS research in the School of Chemical Engineering, at Wits, in collaboration with the Norwegian University of Science and Technology (NTNU), the present research presents a contribution to the scientific community with regards to novel CO_2 adsorbent development. It is noticeable that much work has been done in this area, but until now, very few if any have been successful in meeting the requirements for being the environmentally friendly, and meeting appropriate conditions of implementation and operation. Absorption technology, especially with the use of alkanolamines (Monoethanolamine, Diethanolamine and Triethanolamine) has gained the attention of many researchers in capture technology; however, its implementation is still at pilot scale stage due to certain inconveniences which include absorbent degradation, material corrosion and high energy requirement for regeneration, all requiring improvement. Adsorption technology is more attractive in its ability to procure high purity CO_2 and to separate diluted compounds in the flue gas mixtures. However, refinements in the field of CO_2 capture due to the large scale of the plants that it has to face. In addition, flue gas especially from fossil fuel plants, include moisture, variable temperatures and pressures, which affect efficient performance of adsorption technology.

Existing adsorbents, such as activated carbon, silica gel, zeolite, MOFs and others, have been ineffective where the flue gas contains moisture. Also they require difficult conditions of operation which include high temperature and pressure in order to adsorb and desorb CO_2 efficiently. These challenges restrict utilization, and have pushed researchers to develop approaches through the design of specific adsorbents for a large application of adsorption technology. Thus, through this research ("A CO_2 capture technology using carbon nanotubes with polyaspartamide surfactant.") a hydrophobic and biodegradable adsorbent with water tolerance characteristics, and the ability to operate efficiently for CO_2 adsorption and desorption under moderate conditions, which include low temperature and pressure, has been developed. Further work is required to test these adsorbents on a pilot scale.

6.1. ACHIEVEMENT OF ADSORBENTS DESIGN

The design of new adsorbent, termed MWNT-PAA, was rendered possible through the non-covalent functionalization of multi-walled carbon nanotubes (MWNT) by polyaspartamide (PAA) obtained from the polysuccinimide (PSI) grafted with ethylenediamine (EDA). The use of PSI made from the polycondensation of aspartic acid was intended to provide a polymer with biofissionable bonds for the biodegradability (the environmentally friendly aspect). The imide (CON) bond in PSI and amide (CONH) bond in PAA are biofissionable bonds able to be broken under enzymatic activity. The EDA was used to provide PAA with an NH_2 group as CO_2 anchoring site. The PAA was then intended to present two necessary bonds (NH_2 and CONH), which should operate as CO_2 anchoring and biofissionable bonds respectively. Thus, the design of PAA was successfully achieved as revealed by the characterization analysis done with the use of FTIR, which confirmed the presence of NH_2 and CONH. This shows that the adsorbent PAA has the potential of capturing CO_2 through NH_2. However, the regeneration behavior of the adsorbents has been demonstrated, the biodegradability aspect is much more important for the environment safety, because the adsorbent has always to be discarded after a frequency of being used. Furthermore, characterization of using ^1H NMR of the PAA shows the absence of free amine which could cause the corrosion of materials. Regarding the environment challenge where the polymer polyethylenimine (PEI), the polymer most extensively used in CO_2 capture, is non-biodegradable, the polymer PAA showed the potential of being biodegradable. Thus, the achievement of the design of PAA, a hydrophobic and biodegradable polymer amine adsorbent, revealed to be a contribution to the CCS research. The factors which include biodegradability, water tolerance and moderate conditions of operation for adsorption and desorption processes provide to PAA a large application in CO_2 capture technology.

The CO_2 adsorption capacity of PAA almost doubled compared to PSI; however the geometry/structure of PAA was a drawback. The design of MWNT-PAA was aimed at the improvement of the geometry/structure of the adsorbent with the goal of increasing CO_2 adsorption capacity. The non-covalent functionalization of MWNTs, a highly hydrophobic material with very good geometry/structure, was deliberately applied by PAA in order to preserve the previous functionality obtained on PAA and to enhance the hydrophobicity of the adsorbent as a factor recognized beneficial for the water tolerance property. The achievement of the designed MWNT-PAA was successful after showing the expected

information obtained through different characterizations. Since the MWNT-PAA showed the presence of NH_2 and CONH through FTIR characterization, the CO_2 anchoring site and the biodegradability were consistently kept after using a non-covalent functionalization process. Moreover, the geometry/structure of MWNT-PAA was highly enriched from PAA, resulting in approximately triple CO_2 adsorption capacity from the crude polymer PSI. In addition, the adsorbent MWNT-PAA appears to have a high water tolerance, with a significant increase of CO_2 adsorption capacity under moist adsorbent conditions. The adsorption and desorption processes was efficient at moderate conditions of operation including low temperature and pressure. One more important thing was achieved and must be highlighted is that the non-covalent functionalization of MWNT-PSI was a drawback for CO_2 adsorption capacity compared to PSI; however, the geometry/structure of MWNT-PSI was significantly improved. This is due to the presence of closed rings in the chemical structure of PSI compared to PAA, where the rings were open through the use of EDA. The closed rings have the ability to twist tightly the MWNT, resulting in the blockage of CO_2 from passing to the available adsorption sites. Thus, the technology of designing the adsorbent through the non-covalent functionalization of MWNT by polymer requires a specific chemical structure of polymer with open rings in order to enhance the CO_2 adsorption capacity. This approach is very important to the scientific community regarding the choice of polymer when the geometry/structure is intended to be improved for CO_2 adsorption capacity enhancement by the use of MWNT through non-covalent functionalization process.

The art of designing an adsorbent from PSI to MWNT-PAA via PAA resulted in improvements of the chemical surface on one hand, and enrichment of geometry/structure on the other hand, after preserving all necessary functionalities. This is a subtle creativity for an advanced technology which is beneficial for the scientific community to be enriched with novelty. However, as MWNTs are commercially expensive, the discoveries of simplified methods must present the perspective of lowering the price in future. There is research demonstrating the possibility of synthesizing MWNTs from coal using catalytic chemical vapor deposition (CCVD) process. Moreover, a very small quantity of MWNT (1:30 as ratio MWNT and PAA) was enough to design the adsorbent MWNT-PAA and to bring improvement from PAA.

6.2. ACHIEVEMENT OF ADSORPTION AND DESORPTION PROCESS

Operating in TSA systems, many factors were investigated in order to come out with consistent approaches which are necessary for a capture plant to operate in the TSA systems with efficient conditions.

Different isothermal adsorptions with variable temperatures were achieved in order to evaluate the CO_2 adsorption capacity and the adsorption kinetics of the adsorbent with changes of temperature. The investigations conducted show that the adsorption has corresponded to Langmuir model, where the adsorption rate was very high at the beginning of the adsorption process and decreased while the adsorption process was in progress. Therefore, it was discussed that the completion of the total adsorption capacity in TSA systems presented a drawback regarding the time and the quantity of CO_2 that supposed to be captured. The TSA systems where the adsorption time was reduced for high adsorption rate resulted in multiple adsorption cycle with increase of global quantity of CO_2 adsorbed. However, the reduced of adsorption time resulted in significant daily amount of CO_2 adsorption, the challenge of cooling time from the sweeping or desorption temperatures to the fixed adsorption temperature revealed to be an obstacle for the TSA systems. Thus, more beds are required for the reduced adsorption isothermal time to correlate with the cooling time from sweeping and/or desorption temperatures in order to implement the TSA systems. The more the adsorption isothermal time was reduced, the larger was the number of beds required for the synchronization of TSA systems. The large number of beds disadvantages the TSA systems due to the requirements of large space and cost of materials. Instead, the implementation of specific heat exchanger equipment could accelerate the cooling time resulting in mitigation of number of beds. Furthermore, it was demonstrated for the TSA systems connected to one source of flue gas, that the use of the beds placed in series is beneficial than the beds placed in parallel. Thus, the achievement of the discussion on TSA systems has provided the optimum conditions of implementation of adsorption technology for CO_2 capture. This is a contribution to the scientific community regarding the progress of CCS research in adsorption technology.

6.3. ACHIEMENT OF THERMODYNAMICS STUDIES

The investigation has shown that the exothermicity and endothermicity of the adsorption and desorption processes relevant to the heat release and heat absorbance increased from PAA to MWNT-PAA respectively. Thus, a high potential interaction provided by enhanced geometry/structure emphasized the heat flow either in release or in absorbance. Also, the heat release was significant and increased with the increase of temperature in such a way that the TSA systems could opt for the change of isothermal temperature using the heat release without external energy. Furthermore, the resultant heat flow for the TSA systems including sweeping, adsorption and desorption resulted in more heat release than heat absorbance. This is beneficial for the TSA systems to operate with less energy which in most cases is a determining factor for the viability of a technology.

6.4. PAPERS AND CONFERENCES PRESENTATIONS PRODUCED TO DATE

6.4.1. Papers

Paper 1: Ngoy, J.M.; Wagner, N.; Riboldi, L.; Bolland, O. (2014). "A CO2 capture technology using multi-walled carbon nanotubes with polyaspartamide surfactant." *Energy Procedia*, Volume 63, 2014, Pages 2230–2248. doi:10.1016/j.egypro.2014.11.242.

Paper 2: Ngoy, J.M.; Wagner, N..; Bolland, O.: Potgieter, H. "Influence of Moisture on CO_2 adsorption using Multi-walled Carbon Nanotube with Polyaspartamide." Paper submitted to the Journal of Adsorption.

Paper 3: Ngoy, J.M.; Wagner, N..; Bolland, O.: Potgieter, H. "Temperature effect on the selectivity for CO_2 using MWNT-PAA exposed to 14% CO_2 in gas mixture." Paper in process.

Paper 4: Ngoy, J.M.; Wagner, N..; Bolland, O.: Potgieter, H. "The Thermodynamics Study of MWNT-PAA for CO_2 capture." Paper in process

Paper 5: Ngoy, J.M.; Wagner, N..; Bolland, O.: Potgieter, H. "The impact of CO_2 adsorption kinetics on continuous TSA systems using MWNT-PAA for CO_2 capture." Paper in process

6.4.2. Conference presentations

1) **4th Carbon Capture and Storage Conference** "Capacitating South Africa for CCS" 20-21 October 2015, The Capital 20 West Hotel, Morningside, Johannesburg.
2) **8th Trondheim Conference on CO2 Capture, Transport and Storage (TCCS-8),** Trondheim, Norway June 16-18, 2015.
3) Fossil Fuel Conference held at the University of Cape Town from 27 to 28 November 2014.
4) **GHGT-12** (Greenhouse gas Technology) held at Austin (USA) from 05 to 09 October 2014.
5) **Carbon Capture Workshop**: Carbon Capture & Clean Environment. University of the Western Cape, Cape Town 24-26 March 2014 (South Africa).
6) **Third CCS Conference** of South African Centre for Carbon Capture and Storage (SACCCS). The 3rd and 4th of October 2013 in Cedar Park Hotel/ Woodmead/ Johannesburg (South Africa).
7) **7th Trondheim Conference on CO2 Capture, Transport and Storage (TCCS-7),** Trondheim, Norway June 4-6, 2013.
8) **7th Framework Programme Conference Agenda CCS-EU/RSA Partnership.** A focus on Carbon Capture by OCTAVIUS. The 13th and 14th of February 2013 at ESKOM academy of learning/ Dale Road/ Johannesburg (South Africa)
9) **Indaba 2012, 13 & 14 November** in the 17th Southern African Conference (Fossil Fuel Foundation) Bytes Conference Center, Midrand/ Johannesburg (South Africa).
10) **The 11th of July 2012 SACCCS** (South African Centre for Carbon Capture and Storage meeting participation on discussion of the recently launched European Commission FP7 Project – OCTAVIUS (South Africa).
11) **Northwest University (NWU)** Research proposal Students Colloquium at June 2012, North-West University in South Africa.

REFERENCES

[1] Weart, S.R. (2008). "The Discovery Of Global Warming". *Havard University Press, Revised And Expanded Edition,* 31 Oct 2008, Nature – 230 pages. ISBN-13: 9780674031890.

[2] Maslin, M. (2008). "Global warming: a very short introduction". *Oxford University Press,* 27 Nov 2008, Nature - 216 pages.

[3] Callendar, G. S. (1938). "The artificial production of carbon dioxide and its influence on temperature." *Quarterly Journal of the Royal Methodological Society*, ***64***: 223-240.

[4] Seeing the light "Callendar, G.S. and Carbon dioxide theory of Climate change." *Archive hub at the centre of great research*. Archiveshub.ac.uk. American Meteorological Society, November 2007.

[5] Keeling C.D. (1960). "The Concentration and Isotopic Abundances of Carbon Dioxide in the Atmosphere". *Tellus*, ***12***: 200-203.

[6] Keeling, C. D. (1998). "Rewards and Penalties of Monitoring the earth." *Annual Review of Energy and Environment* ***23***: 25-82. Doi: 10.1146/annurev.energy.23.1.25.

[7] Fung, I. Y.; Doney, S. C.; Lindsay, K.; and John, J. (2005). "Evolution of Carbon Sinks in a Changing Climate." *PNAS*. ***102***(32): 11201-11206.

[8] Le Quéré, C.; Rödenbeck, C.; Buitenhuis, E. T.; Conway, T. J.; Langenfelds, R.; Gomez, A.; Labuschagne, C.; Ramonet, M.; Nakazawa, T.; Metzi, N.; Gillett, N. and Heimann, M. (2007). "Saturation of the Southern Ocean Sink Due to Recent Climate Change." *Science Journals*. ***316***(58832): 1735-1738. Doi: 10.1126/science.1136188

[9] IPCC "Fourth Assessment Report: Climate Change". An Assessment of the Intergovernmental Panel on Climate Change. IPCC Plenary XXVII (Valencia, Spain, 12-17 November 2007).

[10] Cline, W.R. (1991). "Scientific Basic for the Greenhouse effect." *The Economic Journal*, ***101***: 904-919.

[11] ECOWORLD 03 May 2008. "The reality of fossil fuel as it account for 80% of our Global Energy Supply". *Nature & Technology in Harmony*.

[12] Pacala S. and Sokolow R. (2004). “Stabilization Wedges: Solving the Climate problem for the Next 50 Years with Current Technologies”. *Science*, Vol 305. Toward a Hydrogen Economy Review. www.sciencemag.org

[13] Rojey A. (2008). “Energie et climat, Réussir la transition énergetique (English title: Energy and Climate: How to achieve a Successful Energy Transition)”, *Editions Technip*, Paris, 59-61.

[14] https://careers.slb.com/whoweare/news/climatechange.aspx

[15] Eberhard A. (2011). “The future of South African Coal; Market, Investment and Policy Challenges”. Program on Energy and Sustainable Development (PESD) Stanford. Working paper # 100.

[16] Boden, T.A., G. Marland, and R.J. Andres. (2011). Global, Regional, and National Fossil-Fuel CO_2 Emissions. Carbon Dioxide Information Analysis Center, Oak Ridge National Laboratory, U.S. Department of Energy, Oak Ridge, Tenn., U.S.A. doi 10.3334/CDIAC/00001_V2011

[17] COP17/CMP7 (2011). Durban: A climate for change, Transforming Africa’s Future. Durban South Africa

[18] Darde, A., Prabhakar, R., Tranier, J.P., and Perrin, N. (2009). “Air Separation and flue gas compression and purification units for oxy-coal combustion systems.” *Energy Procedia*. ***1***: 527-534

[19] Keeling, C.D., and Whorf, T.P. (2005). “Atmospheric CO_2 Records From Sites in the SIO Air Sampling Network.” In Trends: A Compendium of Data on Global Change. Carbon Dioxide Information Analysis Center, Oak Ridge National Laboratory, U.S. Department of Energy, Oak Ridge, Tenn., U.S.A. http://cdiac.esd.ornl.ornl.gov/trends/co2/sio-mlo.htm

[20] Orr, F.M., Jr. (2004). “Storage of Carbon Dioxide in Geologic Formation,” *J. Pet. Tech.*, ***56***(9), 90-97.

[21] Finkenrath M. (2011). “Cost and Performance of Carbon Dioxide Capture from Power Generation”. *OECD/IEA.* http://www.iea.org/papers/2011/costperf_ccs_powergen.pdf

[22] OECD/IEA (2010). “Power Generation from Coal: Measuring and Reporting, Efficiency Performance and CO_2 Emissions.” *Coal Industry Advisory Board (CIAB)*

[23] Resnik, K.P.; Yeh, J.T.; and Pennline, H.W. (2004). "Aqua Ammonia Process for Simultaneous Removal of CO_2, SO_2, and NO_x." *Int. J. Envr. Tech. Mgmt,* ***4***(1/2): 89-104.

[24] Darde, V.; Thomsen, K.; van Well, W.J.M.; Stemby, E.H. (2010). "Chilled ammonia process for CO_2 capture." *Int. J. of Greenhouse Gas Control,* ***4***(2): 131-136

[25] Rao, A.B.; and Rubin, E.S. (2002). "A Technical, Economic, and Environmental Assessment of Amine-Based CO_2 Capture Technology for Power Plant Greenhouse Gas Control." *Environ. Sci. Technol.,* ***36***: 4467-4475.

[26] Practical guide for Emission and Process Measurements (2004). "Flue gas Analysis in Industry." *Testo 0981.2773/hd/R*/08.2004.

[27] Finkenrath, M.; Smith J.; and Volk, D. (2012). "CCS RETROFIT Analysis of the Globally Installed Coal-Fired Power Plant Fleet." *International Energy Agency: OECD/IEA,* 2012.

[28] Spath, P. L.; Mann, M. K.; Kerr, D. R. (1999). "Life Cycle Assessment of Coal-fired Power Production." *National Renewable Energy Laboratory; NREL/TP-570-25119*

[29] Hodges A. W., and Rahmani M. (2012). "Fuel Sources and Carbon Dioxide Emissions by Electric Power Plants in the United States." *University of Florida IFAS Extension.* Publication #FE796.

[30] Bridwater, A.V., D. Meier, and D. Radlein, "An overview of fast pyrolysis of biomass." *Organic Geochemistry* ***199***(30): 1479-1493.

[31] Demirbas, A. (2008). "Biofuels sources, biofuel policy, biofuel economy and global biofuel projections." *Energy Conversion and Management,* ***49***: 2106-2116.

[32] Demirbas, M.F. and Balat, M. (2006). "Recent advances on the production and utilization trends of bio-fuels: A global perspective". *Energy Conversion and Management*. ***47***: 2371-2381.

[33] Bhattacharya, A.V., Meier, D., and Radlein, D. (1999), "An overview of fast pyrolysis of biomass". *Organic Geochemistry*. ***30***: 1479-1493.

[34] McKendry, P. (2002), "Energy production from biomass (part 2): conversion technologies". *Bioresource Technology* ***83***: 47-54

[35] Perlack, R.D. (2005). “Biomass and a feedstock for a bioenergy and bioproducts industry: The technical feasibility of a billion-ton annual supply., O.R.N. Laboratory, U.S. Department of Energy U.S. Department of Agriculture.

[36] Duminda A., Gunawardena and Sandun D., Fernando. (2013). “Methods and Apllication of Deoxygenation for the Conversion of Biomass to Petrochemical Products.” *Ed. Miodrag Dorko Matovic 552* P., April, 2013. DOI: 10.5772/ 53983.

[37] Clarke, M.C. (2013). “Low Rank Coal/ Lignite Upgrading Technologies” *Energy Generation, Coal Technologies*, 50-53.

[38] Alper, B.; Lemos De Sousa, M.J.; Flores, D. (1989). “A progress report on the Alpen Coal Classification” *International Journal of Coal Geology*, ***13***(1-4): 1-19.

[39] Alfred, D; Chandler, Jr. (1972). “Anthracite coal and the Beginnings of the Industrial Revolution in the United States.” *Business History Review*. **46**(02).

[40] “MIN 454: Underground Mining Methods handout; from course at the University of Alaska Fairbanks” Archived from the original on 26 March 2009. Retrieved 2009-05-05.

[41] International Energy Annual 2006. Energy Information Administration. 2008. Archived from the original on 23 May 2011.

[42] "International energy statistics". U.S. Energy Information Administration. Retrieved 10 March 2014.

[43] Jaramillo, P; Giffin, W.M.; Matthews, H.S. (2007). “Comparative Life-Cycle Air Emissions of Coal, Domestic Natural Gas, LNG, and SNG for Electricity Generation.” *Environ. Sci. Techol.*, ***41***, 6290-6296.

[44] Nuwer, Rachel (2012-08-17). A 20-Year Low in U.S. Carbon Emissions. Blogs.nytimes.com

[45] Moore H., (1935). “Liquid fuels”. *The Technical Press LTD*, London 263 pages.

[46] Snyder, L. R.; Buell, B. E.; and Howard, H. E. (1968). “Nitrogen and Oxygen Compound Types in Petroleum. Total Analysis of a 700-850 ◦F Distillate form a California Crude Oil” *Union Oil Co. of California, Union Research Center, Brea, Calif.* ***40*** (8): 1303.

[47] Phillips, F. C. (2012). "The Composition oand Fuel Value of Natural Gas". *HardPress*, 52 pages. ISBN: 1407665340, 9781407665344

[48] Speight, J. G. (2013). "Shale Gas Production Processes." *Gulf Professional Publishing*, Science -170 pages

[49] Kelkar, M. (2008). " Natural Gas Production Engineering." *PennWell*, pages 15-21.

[50] Tek, M.R. (2012). "Underground Storage of Natural Gas: Theory and Practice." *Springer Science & Business Media. Science* - 472 pages

[51] Nijaguna, B. T. (2006). "Biogas Technology." *New Age International*, Biogas - 298 pages

[52] Deublein, D.; Steinhauser, A. (2011). "Biogas from Waste and Renewable Resources: An Introduction." *John Wiley & Sons*, Technology & Engineering -578 pages

[53] FÜssel Hans-Martin (2009). "An updated assessment of the risks from climate change based on research published since the IPCC Fourth Assessment Report". *Climate Change* ***97***, 469-482.

[54] Rostrup-Nielsen, J.; Christiansen, L. J. (2011). "Concepts in Syngas Manufacture." *World Scientific, Technology & Engineering* – 379 Pages.

[55] Moulijn, J. A.; Figueiredo, J. L. (2012). "Carbon and Coal Gasification : Science and Technology." *Springer Science & Business Media*, Science – ***655***: 16-21.

[56] Breault R. W. (2010). "Gasification Processes Old and New: A Basic Review of the Major Technologies." *Energies, **3***: 216-240; doi:10.3390/en3020216. ISSN 1996-1073. www.mdpi.com/journal/energies

[57] Zeng, Z.; Pei, P. (2012). "Study on Underground Coal Gasification Combined Cycle Coupled with On-site Carbon Capture and Storage." *Carbon Sequestration*, 360 pages.

[58] Osborne, D. (2013). "The Coal Handbook: Towards Cleaner Production: Coal Production." *Elsevier, Business & Economics* – ***776***: 9-15.

[59] Marland G., Boden R. C., Griffin S. F., Huang P., Kanciruk, and Nelson T. R. (1989). "Estimate of CO_2 Emissions from Fossil Fuel Burning and Cement Manufacturing*". Based on the United Nationals Energy Statistics and the U.S. Bureau of Mines Cement*

Manufacturing Data. Report No. #ORNL/CDIAC-25, Carbon Dioaxide Information Analysis Centre, Oak Ridge National Laboratory, Oak Ridge, Tennessee, USA.

[60] Fahim, M. A.; Al-Sahhaf, T. A.; Elkilani, A. (2009). "Fundamentals of Petroleum Refining." *Elsevier, Technology & Engineering* – ***516***: 35-36.

[61] IPCC. (2006): 2006 IPCC Guidelines for National Greenhouse Gas Emissions. *Energy **2***. http://www.ipcc-nggip.iges.or.

[62] Draft iron and Steel production-Guidance (2003). "Direct Emissions from iron & Steel Production". Climate Leaders Greenhouse Gas inventory Protocol core module Guidance. U.S. Environmental Protection Agency.

[63] Benchaita T. (2013). "Greenhouse Gas Emissions from New Petrochemical Plants." *Inter-American Development Bank IDB.* Background Information Paper for the Elaboration of Technical Notes and Guidelines for IDB projects.

[64] International Energy Agency (IEA). 2006a. *Energy Technology Perspectives, Scenarios and Strategies to 2050*. Paris: OECD/IEA.

[65] STANFORD UNIVERSITY (2005). An Assessment on Carbon Capture Technology and Research Opportunities. GCEP Energy Assessment Analysis Spring. http://gcep.stanford.edu

[66] Xu, X ; Song, C. ; Wincek, R ; Andresen, J.M.; Miller, B.G. and Scaroni, A.W. (2003). "Separation of CO_2 from Power Plant Flue Gas Using a Novel CO_2 'Molecular Basket' Adsorbent." *Fuel Chemistry Division Preprints, **48***(1): *162.*

[67] Commission Energie – Centre d'Analyse Strategique (Avril 2007) – Rapport d'orientation "Evolutions technologiques" – *Perspectives energetiques de la France à l'horizon* 2020-2050.

[68] De Visser, E.; Hendriks, C.; Barrio, M. ; Molnvik, M. J. ; de Koeijer, G. ; Liljemark, S. ; Le Gallo, Y. (2008). "Dynamis CO_2 quality recommendations." *International Journal of Greenhouse Gas Control*, ***2***: 478-484.

[69] IEA GHG R&D Programme. (2004). "Impact of impurities on CO_2 Capture, Transport and storage". *IEAGreenhouse gas, R & D Programme*. http://www.worldcat.org

[70] Santos, S. (2012). "CO_2 Transport via Pipeline and Ship." *Ieaghg, September 2012,* CCS Opportunities in CCOP Region, CCOP-EPPM. Workshop (Indonesia).

[71] Botero, C.; Finkenrath, M.; Belloni, C; Bertolo, S; D'Ercole, M.; Gori, E.; and Tacconelli, R. (2009). "Thermoeconomic Evaluation of CO_2 Compression Strategies for Post-Combustion CO_2 Capture Applications." *ASME,* ***4*** : 517-526.

[72] Lecomte F., Broutin P., and Lebas E. (2009). "CO_2 Capture Technologies to Reduce Greenhouse Gas Emissions." *Editions TECHNIP*. 176 pages.

[73] http://www.kbr.com/Technologies/Process-Technologies/CO_2-Compression-and-Sequestration/

[74] IEA Greenhouse Gas R&D Programme (2008). "Geologic Storage of Carbon Dioxide: Staying Safely Underground." *Ieaghg, January 2008*, 28 pages.

[75] Cooper, C. D. (2014). "Introduction to Environment Engineering." *Waveland Press, Technology & Engineering,* pp 14, 121, 122, 164. 405 pages.

[76] Maroto-Valer, M. M. (2010). "Developments and Innovation in Carbon Dioxide (CO_2) Capture and Storage Technology: Carbon Dioxide (CO_2) Capture, Transport and Industrial Applications." *Elsevier,* - Technology & Engineering pp158, 560 pages.

[77] White, C.M., Straziser, B. R., Granite, E. J., Hoffman, J. S., and Pennline, H. W. (2003). "Separation and capture of CO_2 from large stationary sources and sequestration in geological formations—coalbeds and deep saline aquifers". *Journal of the Air & Waste Management Association,* ***53***: 645-715.

[78] Guide technique, méthodologique (2007). CO_2 Capture and Storage in the Subsurface. Media Library, Entreprises et fédérations professionnelles, Secteur public, October 2007 - 64 p. - Réf. 6175.

[79] Engelbrecht, A., Golding, A, Hietkamp, S., Scholes, B. (2004). "The potential for sequestration of carbon dioxide in South Africa. [Online] Pretoria (Issuing organization: Manufacturing and Materials Technology, CSIR) Available at: http://www.dme.gov.za/pdfs/energy/coal/carbon_dioxide.pdf. [Accessed on 27 April 2010]

[80] Abdullah, K.; Al-Fattah, S. M.; Barghouty, M. F.; Dabbousi, O. B. (2011). "Carbon Capture and Storage: Technologies, Policies, Economics, and Implementation Strategies." *CRC Press*, Technology & Engineering pp 176-195, 404 pages.

[81] Sheng, J. (2013). "Enhanced Oil Recovery Field Case Studies." *Gulf Professional Publishing*, - Science pp 389-391, - 712 pages.

[82] Wilson, M. (2007). Capturing CO_2- the opportunities, Commercial Viability and Challenges. CO2 Capture and Storage Conference. *Calgary, Canadian Institute*.

[83] IPCC "Special Report on Carbon Capture and Storage, pp. 181 and 203 (Chapter 5, "underground Geological Storage")" Retrieved 2010-04-14

[84] IPCC-CCS (2005). IPCC Special Report on Carbon Dioxide Capture and Storage. Cambridge, United Kingdom and New York, NY, USA, Cambridge University Press.

[85] Ceglarska-Stefanska, G. and Zarebsks, K. (2002). "The Competitive Sorption of CO_2 and CH4 with regard to the release of Methane from Coal". *Fuel Processing Technology, **77***(78): 423-429.

[86] Bustin, R.M., Clarkson, C.R, (199). "Binary gas adsorption/ desorption isotherms: effect of moisture and coal composition upon carbon dioxide selectivity over methane. *International Journal of Coal Geology. **42***(200): 241-271.

[87] Shi, J. Q., Durucan, S. (2005). Oil & Gas Science and Technology. [e-book] London: Institut francais du petrole. Available at: Innovation Energy Environment/ http://ogst.ifp.fr/index.php?option =article&access=standard&Itemid=129&url=/articles/ogst/pdf/2005/03/shi1_vol60n3.pdf. [Accessed on 3 May 2010].

[88] CO_2 Capture project (2008). "Rock formations suitable for CCS". www.co2captureproject.com.; http://www.hostgeni.net/host-info/co2captureproject.org

[89] CMr Energy. "Large-Scale Storage of CO_2 on the Norwegian Shelf Report." Ref. no: CMR-13-F75003-RA-1, Rev: 02 Date: 09.06.2013. Page 12 of 47.

[90] Sinayuç,C. (2012). "Deep Saline Formations: The Largest Potential Volumes for Geological Storage of CO_2". Middle East Technical University Petroleum Research Center. CO_2 Capture and Storage – Regional Awareness Raising Workshop – 13-14 June 2012 – METE Ankana - TURKEY

[91] Caldeira, K., Wickett, M.E. (2003). "Antropogenic carbon and ocean pH". *Nature* ***425***(6956), 365-365. Bibcode: 2001 AGUFMOS11C0385C. doi:10.1038/425365a. PMID 14508477.

[92] Millero, Frank, J. (1995). "Thermodynamics of the carbon dioxide system in the oceans". *Geochimica et Coamochimica Acta* ***59***(4): 661-677. Bidcode: 1995GeCoA.. 59..661M. doi:10.1016/0016-7037(94)00354-O.

[93] Feely, R. A.; et al. (July 2014). "Impact of Anthropogenic CO_2 on the $CaCO_3$ System in the Oceans" *Science* ***305***(5682): 362-366. Bibcode: 2004 Sci…305..362F. doi: 10.1126/science.1097329. PMID 15256664.

[94] Edenhofer, O.; Flachsland, C.; Jakob, M.; Lessmann, K. (2013). "The Atmosphere as a Global Commons – Challenges for International Cooperation and Governance." *Harvard Kennedy School. The Harvard Project on Climate Agreements,* August 2013, Discussion Paper 13-58.

[95] Heinrich J. (2012). "Legal implications of CO_2 Ocean Storage" Laboratory for Energy and the Environment, Massachusetts Institute of Technology, 77 Massachusetts Avenue. Cambridge, MA 02139-4307, Working Paper July 2002.

[96] Newall, P.S., Clarke, S.J., Haywood, H.M., Scholes, H., Clarke, N.R., King, P.A., Barley, R. W., (2000). "CO_2 storage as carbamate minerals, report PH3/17 for IIEA Greenhouse Gas R&D Programme, CSMA Consultants Ltd, Cornwall, UK

[97] Butt, D. P., Lackner, K. S., (1997). "A Method for Permanent Disposal of CO_2 in Solid Form. *World Resource Review* ***9***(3): 324-336.

[98] Bearat, H., McKelvy, M. J., Chizmeshya, A. V. G., Sharma, R., Carpenter, R. W. (2002). "Magnesium Hydroxide Dehydroxylation/ Carbonation Reaction Processes: Implications for Carbon Dioxide Mineral Sequestration. *Journal of the American Ceramic Society*: ***85***(4): 742-48.

[99] Zevenhoven, R., Kavaliauskaite, I. (2004). "Mineral carbonation for long-term CO_2 storage: an exergy analysis. *Int. J. Thermodynamics,* ***7***(1): 23-31.

[100] Figueroa, J.D., Fout, T. (2008). "Advances in CO_2 Capture technology — The U.S. Department of Energy's Carbon Sequestration Program." *International Journal of Greenhouse Gas Control*. ***2***(1): 9-20.

[101] Aresta, M. and Dibenedetto A. (2007). "Utilisation of CO₂ as a chemical feedstock: Opportunities and challenges." *Dalton Transactions* **28**: 2975-2992.

[102] Department of National Treasury, Republic of South Africa (2013). "Reducing greenhouse gas emissions and facilitating the transition to a green economy." Carbon Tax Policy Paper (May 2013).

[103] Tokyo Metropolitan Government (2013). "The Tokyo Cap-and-Trade Program achieved 23% reduction in the 2nd year." Bureau of Environment Urban and Global Environmental Division, 21 January 2013.

[104] National Treasury Department, Republic of South Africa (2013). "CARBON TAX POLICY PAPER Reducing greenhouse gas emissions and facilitating the transition to a green economy." *POLICY PAPER FOR PUBLIC COMMENT*, May 2013 – 91 pages.

[105] Al-Juaied, M.; Whitmore, A. (2009). "Realistic Costs of Carbon Capture." Energy Technology Innovation Policy." *Energy Technology Innovation Policy, Harvard Kennedy*, Discussion paper 2009-08. energytechnologypolicy.org

[106] OECD/IEA 2006. "CO_2 Capture & Storage." *IEA Energy Technology Essentials*. December 2006.

[107] Finkenrath M. (2011). "Cost and Performance of Carbon Dioxide Capture from Power Generation". IEA Greenhouse Gas R & Programme. (Energy) http://www.iea.org/papers/2011/costperf_ccs_powergen.pdf

[108] WorleyParsons, Schlumberger (2011). "Economic Assessment of Carbon Capture and Storage Technologies." Global CCS Institute

[109] Christensen J., Tosen G. "Cost and economic potential." IPCC special Report on carbon dioxide and storage.

[110] Davison J. (2006). "Performance and costs of power plants with capture and storage of CO2". IEA Greenhouse Gas R & D Programme. *Energy*. **32**(2007): 1163-1176 http://info.ornl.gov/sites/carboncapture/

[111] Yu, C. H.; Huang, C. H.; Tan, C. S. (2012). "A Review of CO_2 Capture by Absorption and Adsorption." *Aerosol and Air Quality Research, **12***: 745–769.

[112] da Silva E.F. (2005) "Computational Chemistry Study of Solvent for Carbon Dioxide Absorption". Doctoral thesis; *Norwegian University of Science and Technology*.

[113] Ma'mun, S., Svendsen, H., Hoff, K.A., and Juliussen, O. (2004). "Selection of New Absorbents for Carbon Dioxide Capture," GHGT-7 Conference, Vancouver B.C., Canada, September 5-9.

[114] Petrakopoulou, F., Tsatsaronis, G., Boyano, A. and Morosuk, T. (2011) "Post-Combustion CO_2 Capture with Monoethanolamine in a Combined-Cycle Power Plant: Exergetic, Economic and Environmental Assessment". *GHG-Emission, Measurement and Management.*

[115] "Glossary." The Brownfields and Land Revitalization Technology Support Center. Retrieved 2009, 12-21.

[116] Davidson, R.M. (2007). "Post-combustion Carbon Capture from coal fired plants-solvent scrubbing." *IEA Clean Coal Centre, CCC*/125.

[117] Wang M., Lawal A., Stephenson P., Sidders J., Ramshaw C., and Yeung H. (2011). "Post-combustion CO_2 capture with chemical absorption: A state-of-the-art Review". *Chemical Engineering Research and Design. **89***(9): 1609-1624.

[118] Baker, R. W. (2012). "Membrane Technology and Applications." *John Wiley & Sons*, - *Technology & Engineering* - 592 pages

[119] CO_2 CRC: "CO_2 capture/separation technologies**:** Membranes." "http://www.co2crc.com.au/aboutccs/cap_membranes.html"

[120] Carapellucci, R., and Milazzo, A. (2004). "Carbon Dioxide Removal via a Membrane System in a Natural Gas Combined-Cycle Plant," *J. Power and Energy, **218***(Part A): 219-229.

[121] Wark, K, Jr. (1995). "Advanced Thermodynamics for Engineers", New York, N.Y.: *Mcgraw-Hill*. 564 pages.

[122] Suzuki, M. (1990). "Adsorption Engineering". *Kodanha LTD., Tokyo and Elsevier Science Publishers B.V., Amsterdam-Oxford-New York-Tokyo* 295 pages.

[123] Foo, K.Y.; Hameed, B.H. (2010). "Insights into the modeling of adsorption isotherm systems". *Chemical Engineering Journal* ***156*** (1): 2–10. doi:10.1016/j.cej.2009.013. ISSN 1385-8947.

[124] Mantell, C.L., Ph.D. (1951). " Chemical Engineering: Adsorption" *MCGRAW-HILL BOOK COMPANY Second Edition* ***634***: 7

[125] Boden N., Cullis C. F., and Fish A. (2007) "Spontaneous ignition in carbon adsorption beds" *Journal of Applied Chemistry*. ***12***(4).

[126] Frankenburg, W. G. (1952). "Advances in Catalysis and Related Subjects: Physical Adsorption." Academic Press Inc., ***4***: 212-258, 456 pages.

[127] Klaus Unger (1972) "Structure of Porous Adsorbents" *Angew. Chem. Internat.* ***Edit. /Vol. I1*** 1 No. 4

[128] Ralph T. Yang (2003). "Adsorbents, Fundamentals and Applications." Wiley-Interscience. Page 8.

[129] Harrison, L.D.; Brunner, K.M., and Hecker, W.C. (2013). "A combined packed-bed friction factor equation: extension to higher Reynolds number with wall effects". *AIChE J*., ***59***.(3): 703-706.

[130] McCabe, W.E.; Smith, J.C., and Harriott, P. (2001). "Unit Operations of Chemical Engineering". *McGraw Hill, New York.*

[131] Patel, C.; Belady, C. (1997). "Modeling and Metrology in High Performance Heat Sink Design". Proceedings of the 47th Electronic Components and Technology Conference, IEEE, P. 296, San Jose, California. www.electronics. Cooling.com/197/09/standardizing-heat-sink-characterization-for-forced-convection/

[132] Shalliker, R. A.; Broyles, B. S.; Guiochon, G. (2003). "Axial and radial diffusion coefficients in a liquid chromatography column and bed heterogeneity" *Journal of Chromatography A,* ***994***: 1-12

[133] Shaverdi, G. (2012). "Developing a Model for Mass Transfer in Adsorption Packed-bed Filters." A Thesis in the Department of Mechanical and Industrial Engineering, University of Concordia, Montreal, Quebec, Canada, August 2012.

[134] Ranz, W.E.; Marshall, W.R. (1952). "Evaporation from drops part I." *Chemical Engineering Progress, **48**(3)*: 141-146.

[135] Thoenes, D.; Kramers, H. (1958). "Mass transfer from spheres in various regular packing to a flowing fluid." *Chemical Engineering Science*, ***8***: 271-283.

[136] Walkao, N.; Funazkri, T. (1978)." Effect of fluid dispersion coefficients on particle to fluid mass transfer coefficient in packet beds." *Chemical Engineering Science*, ***33***: 1375-1384.

[137] Yang, X.; Otto, S.R.; Al-Duri, B. (2003). "Concentration-dependent surface diffusivity model (CDSDM) numerical development and application." *Chemical Engineering Journal, **94***, 199-209.

[138] Young, D.M.; Crowell, A.D (1962). "Physical Adsorption of Gases." *Butterworth*, London

[139] Ruthven, D. M. (1984). "Principles of Adsorption and Adsorption Processes." Wiley, New York

[140] Wakao N., and Kaguei S. (1930). "Heat and Mass Transfer in Packed Beds". *Gordon and Breach Science Publishers* pp 31-71

[141] Ertl, G.; Rhodin, T.N. (1979). "*The Nature of the Surface Chemical Bond"*. *North Holland Publishing*, Ch. V, pp. 315 - 380.

[142] Chungsying Lu, Hsunling Bai, Bilen Wu, Fengsheng Su, and Jyh Feng Hwang (2008). "Comparative Study of CO2 Capture by Carbon Nanotubes, Activated Carbons, and Zeolites". *Energy & Fuels* **22**: 3050-3056.

[143] Myers, A. L. (2002). "Thermodynamics of adsorption in porous materials". *A.I.Ch.E. J.*, **48**: 145–160.

[144] Bonjour, J.; Chalfen, J.B., & Meunier, F. (2002). "Temperature swing adsorption process with indirect cooling and heating." *Industrial Engineering and Chemistry Research, **41***: 5802-5811.

[145] Clause, M., Bonjour, J., & Meunier, F. (2003). "Influence of the presence of CO_2 in the feed of an indirect heating TSA process for VOC removal." *Adsorption, **9***: 77-85.

[146] Chi, C. W. and Cummings, W. P. (1978). " Adsorptive separation processes: gases. *In Kirk Othner Encyclopedia of Chemical Technology*, 3rd Ed., Vol. I. Wiley Interscience, New York.

[147] Pajonk, G.M.; Teichner, S.J.; and Germain, J. E. (1983). "Spillover of Adsorbed Species." *Studies in surface science and catalysis,**17***, ISBN 0-444-42224-2

[148] Ruthven, D.M. (1984). "Principles of adsorption and adsorption processes," *New York: Wiley*, p. 433.

[149] Yang, R.T. (1997). "Gas separation by adsorption processes." *Series on Chemical Engineering, **1***: 352 London: Imperial College Press.

[150] Knaebel, K.S. (1991) "High purity oxygen and nitrogen." The Ohio State University. Patents. Publication number: US5032150A

[151] Zhang, J.; Webley, P. A. and Xiao, P. (2008). " Effect of process parameters on power requirements of vacuum swing adsorption technology for CO_2 capture from flue gas." *Energy Conversion and Management, **49***(2): 346-356.

[152] Finamore, N. K.; Liu, C.; Mohanty, P.; Moore, D. T.; and Landskron, K. "Electric Field Swing Adsorption for Carbon Capture Applications". *Department of Chemistry, Lehigh University, Bethlehem,* PA 18015. Co-principal investigators

[153] Petrovska, M. ; Tondeur, D. ; Grevillot, G. ; Granger, J. ; Mitrovic, M. (1991). "Temperature swing gas separation with electrothermal deposition step*." Sep. Sci. Technol., **26***: 425-44

[154] Burchell, T.D. ; Judkins, R.R. ; Rogers, M.R. ; Williams, A.M. (1997). "A novel process and material for the separation of carbon dioxide and hydrogen sulphide gas mixtures" *Carbon, **35***: 1279-1294

[155] Saysset, S. ; Grevillot, G. ; Lamine, A.S. (1999). "Adsorption of Volatile Organic Compounds on Carbonaceous Adsorbent and Desorption by direct Joule Effect." *Recent Progress in Genie des Procedes, No. 68.* Proceedings of the 2nd European Congress of Chemical Engineering, Montpelier, France, pp. 389-396.

[156] Sullivan, P.D. (2003). Organic vapor recovery using activated carbon fiber cloth and electrothermal deposition, Ph.D. Thesis. University of Illinois at Urbana.

[157] Grande, C. A., Rodrigues, A. E. (2008). "Electric Swing Adsorption for CO_2 removal from flue gases". *International Journal of Greenhouse Gas Control.* ***2***(2), 194-202.

[158] Jakobsen, H. A (2014). " Chemical Reactor Modeling: Multiphase Reactive Flow." *Springer Science & Business Media*, 2nd Ed. pp 1056-1085, 1604 pages.

[159] CO2CRC. "CO_2 capture/separation technologies: Adsorption." www.CO2crc.com.au/aboutccs/cap_adsorption.html

[160] CO2CRC – Leaders in research into Carbon Capture and Storage. http://www.CO2crc.com.au/publications/all_factsheets.

[161] Ruthven, D (2011). "CO_2 Capture by Adsorption General Principles." University of Maine, Orono, ME 04469. *Stanford University, May 26 – 27th 2011*.

[162] Trambouze, P. and Euzen, J.P. (2002). "Chemical Reactors From Design to Operation." Ed. Technip, Paris. pp 454-459.

[163] Kunii, D.; Levensipiel, O.; (1991). "Fluidization Engineering", *second ed. Butterworth-Heinemann, Boston.*

[164] Jakobsen, H. A (2014). "Chemical Reactor Modeling: Multiphase Reactive Flow." *Springer Science & Business Media*, 2nd Ed. pp 1020-1050, 1604 pages.

[165] https://upload.wikimedia.org/wikipedia/commons/3/37/Fluidized_Bed_Reactor_Graphic.JPG

[166] Liang, Y.; Harrisson, D.P.; Gupta, R.P. ; Green, D.A. ; McMichael, W.J. (2004). "Carbon dioxide capture using dry sodium-based sorbens." *Energy. Fuel.* ***18***: 569-575.

[167] Zhou, L.; Liu, X. W.; Li, J. W.; Wang, N.; Wang, Z.; Zhou, Y. P. (2005). "Synthesis of ordered mesoporous carbon molecular sieve and its adsorption capacity for H2, N_2, O_2, CH_4 and CO_2." *Chemical. Physics. Letters.* ***413***(1-3): 6–9.

[168] Ottiger, S.; Pini, R.; Storti, G.; Mazzotti, M. (2008) "Measuring and Modeling the Competitive Adsorption of CO_2, CH_4, and N_2 on a Dry Coal." *Langmuir*, ***24***: 9531–9540.

[169] Bonelli, B.; Onida, B.; Fubini, B.; Arean, C. O.; Garrone, E. (2000). "Vibration and thermodynamic study of the adsorption of carbon dioxide on the zeolite." *Langmuir, **16***: 4976–4983.

[170] Zhang, J.; Singh, R.; Webley, P. A. (2008). "Alkali and alkaline-earth cation exchanged chabazite zeolites for adsorption based CO_2 capture." *Microporous Mesoporous Material **111***(1-3): 478–487.

[171] Miller, S. R.; Pearce, G. M.; Wright, P. A.; Bonino, F.; Chavan, S.; Bordiga, S.; Margiolaki, I.; Guillou, N.; Fe´rey, G.; Bourrelly, S.; Llewellyn, P. L. (2008). "Structural Transformations and Adsorption of Fuel-Related Gases of a Structurally Responsive Nickel Phosphonate Metal−Organic Framework, Ni-STA-12." *J. Am. Chem. Soc.*, ***130***: 15967–15981.

[172] Nune, S.K.; Thallapally, P.K.; Dohnalkova, A.; Wang, C.; Liu, J. and Exarhos, G.J. (2010). "Synthesis and properties of nano zeolitic imidazolate frameworks." *Chem. Commun.*, ***46***: 4878-4880

[173] Li W., Zhang L. B., Peng J. H., Li, and Zhu X. Y. (2008). "Preparation of high surface area activated carbons from tobacco stems with K_2CO_3 activation using microwave radiation." *Science Direct. Industrial Crops and Products **27***: 341-347.

[174] Michael M. and Enggelhard, P.E. Corporation (2012) "Molecular gate adsorption system for the removal of carbon dioxide and/ or Nitrogen from coalbed and coal mine methane". *Moleculargate* 8 pages. http://www.moleculargate.com/nitrogen-rejection-N2-removal/2005%20SME%20Molecular%20Gate%20Paper%205.pdf

[175] Coulson J.M., Richardson J.F. (1996). "Chemical Engineering". *Butterworth-Heinner Pub. 4th Ed, **2***: 530-550.

[176] Hyun-Kon Son, Kil Won Cho, Kun-Hong Lee (1998). "Adsorption of Carbon dioxide on the chemically modified silica adsorbents". *Journal of Non-Crystalline Solids* **242**: 69-80

[177] Calsavara, V.; Machada N.R.C.F.; Bernardi Jr and Sousa-Anguiar E.F. (2000). "On the acidity and/or basicity of usy zeolites after basic and acid treatment." *Braz. J. Chem. Eng. **17***(1) Säo Paulo.

[178] Yang R.T. (1997). "Gas Separation by Adsorption Processes". *Series on Chemical Engineering. **1***: 364. London: Imperial College Press.

[179] Breck D.W. (1974). “Zeolite Molecular Sieves: Structure, Chemistry and Use”. *New York: John Wiley & Sons*, Inc. 771 p.

[180] Li, H.; Eddaoudi, M.; O'Keeffe, M. and Yaghi, M.O. (1999). ” Design and synthesis of an exceptionally stable and highly porous metal-organic framework.” *Nature* ***402***: 276-279. doi:10.1038/46248;

[181] Rowsell, J.L.C.; Yaghi, O.M. (2004). “Metal-organic frameworks: a new class of porous materials” *Microporous Mesoporous Mater*. ***73***(1-2): 3-14.

[182] Chae, H.K.; Siberio-Perez, D.Y.; Kim, J.; Go, Y.B.; Eddaoudi, M.; Matzger, A.J.; O’Keeffe, M.; Yaghi, O.M. (2004). “Synthesis, Characterization and Physical Adsorption Properties for Coordination Polymers Synthesized from Transition-metal Ions and Carboxylate-Containing Pyridine.” *Nature*, ***427***: 523-527.

[183] Li, H. ; Eddaoudi, M. ; O’Keeffe, M. ; Yaghi, O.M. (1999). “Design and synthesis of an exceptionally stable and highly porous metal-organic framework.” *Nature*, ***402***: 276-279.

[184] Eddaoudi, M. ; Kim, J. ; Rosi, N. ; Vodak, D. ; Wachter, J.; O’Keeffe, M.; Yaghi, O.M. (2002). “Systematic design of size and functionality in isoreticular MOFs and their application in methane storage. *Science*, *18*; **295** (5554): 469-72.

[185] Millward, A. R. ; Yaghi, O. M. (2005). “Metal-Organic Frameworks with Exceptionally High Capacity for Storage of Carbon Dioxide at Room Temperature” *J. AM. CHEM. SOC.* ***127***(51): 17999.

[186] Llewellyn, P.L.; Bourrelly, S.; Serre, C.; Vimont, A.; Daturi, M.; Hamon, L.; De Weireld, G.; Chang, J.S.; Hong, D.Y.; Hwang, Y.K.; Jhung, S.H.; and Férey, G. (2008). “High Uptakes of CO_2 and CH4 in Mesoporous Metal-Organic Frameworks MIL-100 and MIL-101.” *Langmuir*, ***24***: 7245-7250

[187] Yazaydin, A.O ; Benin, A.I ; Faheen, S.A. ; Jakubczak, P. ; Low, J.J. ; Willis, R.R. ; Snurr, R.Q. (2009). “Enhanced CO_2 adsorption in metal-organic frameworks,” *J. Phys. Chem*. *C* ***111***: 15350-15356.

[188] Xiao, P.; Zhang, J.; Webley, P.; Li, G.; Singh, R.; Todd, R. (2008). “Capture of CO2 from flue gas streams with zeolite 13X by vacuum-pressure swing adsorption.” *Adsorption*, ***14***(4-5): 574-582.

[189] Ho, M. T.; Allinson, G. W. and Wiley, D. E. (2008). "Reducing the Cost of CO_2 Capture from Flue Gases Using Pressure Swing Adsorption." *Ind. Eng. Chem. Res.* ***47***: 4883**.**

[190] Himeno, S.; Komatsu, T.; Fujita, S. (2005). "Development of a New Effective Biogas Adsorption Storage Technology." *Adsorption*, ***11***(1): 899-904.

[191] Zhou, L.; Wu, J.; Li, M.; Wu, Q.; Zhou, Y. (2005). "Prediction of multicomponent adsorption equilibrium of gas mixtures including supercritical components." *Chem. Eng. Sci.* ***60***(11): 2833-2844.

[192] Belmabkhout, Y.; Serna-Guerrero, R.; Sayari, A. (2009). "Adsorption of CO_2 from dry gases on MCM-41 silica at ambient temperature and high pressure. 1: Pure CO_2 adsorption *Chem. Eng. Sci.*, ***64***(14): 3721-3728.

[193] Caskey, S. R.; Wong-Foy, A. G.; Matzger, A. J. (2008). "Dramatic Tuning of Carbon Dioxide Uptake via Metal Substitution in a Coordination Polymer with Cylindrical Pores." *J. Am. Chem. Soc.* ***130***(33): 10870-10871**.**

[194] Figueroa, J. D., Fout, T., Plasynski, S., Mcllvried, H., Srivastava, R. D. (2008). "Advances in CO_2 capture technology—the US Department of Energy's Carbon Sequestration Program." *Int. J. Greenhouse Gas Control*. ***2***(1): 9-20..

[195] Aaron, D., Tsouris, C. (2005). "Nanotechnology for the Energy Challenge." *Sep. Sci. Technol*. ***40***: 321.

[196] Strazisar, B. R., Anderson, R. R. White, C. M. (2003). "Environmental and Energy Law ." *Energy Fuels*. ***17***: 1034.

[197] Caplow, M. (1968). "Kinetics of carbamate formation and breakdown." *J. Am. Chem. Soc.*, ***90***(24): 6795–6803. DOI: 10.1021/ja01026a041

[198] da Silva, E.F.; and Svendsen, H.F. (2004). "Ab Initio Study of the Reaction of Carbamate Formation from CO_2 and Alkanolamines." *Ind. Eng. Chem. Res.*, 2004, ***43***(13): 3413–3418. DOI: 10.1021/ie030619k

[199] McCann, N.; Phan, D.; Wang, X.; Conway, W.; Burns, R.; Attalla, M.; Puxty, G.; and Maeder, M. (2009). "Kinetics and Mechanism of Carbamate Formation from CO_2(aq), Carbonate Species, and Monoethanolamine in Aqueous Solution." *J. Phys. Chem. A*, ***113***(17): 5022–5029. DOI: 10.1021/jp810564z

[200] Caplow, M. (1968). "Kinetics of Carbamate Formation and Breakdown*." J. Am. Chem. Soc*. ***90***, 6795-9803. *Contribution from the Department of Biochemistry, Yale University, New Haven, Connecticut 06510. Recsived May 23, 1968*

[201] Arstad, B., Blom, R., Swang, O. (2007). "CO_2 absorption in aqueous solutions of alkanolamines: mechanistic insight from quantum chemical calculations". *J. Phys. Chem.* ***111***: 1222-1228.

[202] Tsuda, T.; Fujiwara, T. (1992). "Polyethyleneimine and Macrocyclic Polyamine Silica Gels Acting as Carbon Dioxide Absorbents" *J. Chem. Soc., Chem. Commun.* 1659.

[203] Leal, O.; Bolivar, C.; Ovalles, C.; Garcia, J. J.; Espidel, Y. (1995). "Reversible adsorption of carbon dioxide on amine surface-bonded silica gel." *Inorg. Chim. Acta,* ***240***: 183.

[204] Gray, M. L.; Soong, Y.; Champagne, K. J.; Pennline, H. W.; Baltrus, J.; Stevens, R. W., Jr.; Khatri, R.; Chuang, S. S. C. (2004). "Capture of carbon dioxide by solid amine sorbents" *Int. J. En*V*iron. Technol. Manage,* ***4***(1/2): 82-88.

[205] Knowles, G. P.; Graham, J. V.; Delaney, S. W.; Chaffee, A. L. (2005). "Organic/ Inorganic Hybrid Amine and Sulfonic Acid Tethered Silica Materials." *Fuel Proc. Technol.* ***86***: 1435.

[206] Eoghan P. Dillon, Christopher A. Crouse, and Andrew R. Barron Richard E. Smalley (2008). "Synthesis, Characterization, and Carbon Dioxide Adsorption of Covalently Attached Polyethyleneimine- Functionalized Single-Wall Carbon Nanotubes." *Institute for Nanoscale Science and Technology* ***2*****(**1): 156–164.

[207] Thitakamol, B.; Veawab, A.and Arroonwilas, A. (2006). "Environmental assessment of the integration of amine-based CO_2 capture unit to coal-fired power plants for greenhouse gas mitigation." *IEEE EIC Climate Change Conference*

[208] Allam, R. J.; Bredesen, R. and Drioli, E. (2003). "Carbon dioxide separation technologies." *M.Aresta (ed.), Carbon Dioxide Recovery and Utilization,* ***2***: 53-120.

[209] Sona, M. H.; Borgnes, D. and Torstensen, S. (2009), CO_2-Kårstø - KU - Fagrapport sikkerhet, akutte utslipp og beredskap, samt avfall, report from Norsk Energi, 2009,

[210] Shao, R. and Stangeland, A. (2009). "Amines Used in CO_2 Capture - Health and Environmental Impacts". *The Bellona Foundation*. Bellona Report Oslo, Norway, September.

[211] Technical Bulletin (May 1999) "Choosing an adsorption system for VOC: Carbon, Zeolite, or Polymers?" *CAT, EPA* **456**/F-99-004.

[212] Colina, C. M. (2010) "Carbon Dioxide Adsorption in Novel Amorphous Polymers: A Computational Study" *Pennsylvania State University*. Under Sponsorship of the ACS Petroleum Research Fund 55th Annual Report.

[213] Satyapal, S.; Filburn, T; Trela, J. and Strange, J. (2001). "Performance and properties of a solid amine sorbent for carbon dioxide removal in space life support applications" *Energy & Fuel* ***15***: 250-255.

[214] Xu, X.; Song, C; Andrésen, J.M.; Miller, B.G.; Scaroni, A. W. (2002). "Novel Polyethylenimine-modified mesoporous molecular sieve of MCM-41 type as high-adsorbent for CO_2 Capture." *Energy & Fuel* **16**: 1463-1469.

[215] Xu, X.; Song, C.; Andrésen, J.M.; Miller, B.G.; Scaroni, A. W. (2003). " Preparation and characterization of novel CO_2 'molecular basket' adsorbents based on polymer-modified mesoporous molecular sieve MCM-41" *Microporous and Mesoporous Materials*, ***62***(1-2): 29-45.

[216] Xu, X.; Song, C.; Miller, B. G.; Scaroni, A. W. (2005). "Influence of Moisture on CO_2 Separation from Gas Mixture by Nanoporous Adsorbent Based on Polyethylenimine – Modified Molecular Sieve MCM-41." *Ind. Eng. Chem. Res.* ***44***(21): 8113-8119.

[217] Hunter, A. C. (2008). "Molecular hurdles in polyfectin design and mechanistic background to polycation induced cytoxicity." *Advanced Drug Delivery Reviews* ***58***: 1523-1531.

[218] Moghimi, S.M. et al. (2005). "A two-stage poly(ethylenimine)-mediated cytoxicity: implications for transfer/therapy." *Molecular Therapy* ***11***: 990-995.

[219] Yuting, W.; Shirong, P.; Xin, L.; Xuan, Z.; Wei, Z. and Min, F.(2009). "A Biodegradable Low Molecular Weight Polyethylenimine Derivative as Low Toxicity and Efficient Gene Vector." *Bioconjugate Chem.* ***20:*** 322-332.

[220] https://en.wikipedia.org/wiki/Polyethylenimine#/media/File:G4_dendrimer_PEI.png

[221] Ji, S.; Liu, C.L.; Zhang, B.; Yang, F.; Xu, J.; Long, J.; Jin, C.; Fu, D.; Ni, Q.; Yu, X. (2010). "Carbon nanotubes in cancer diagnosis and therapy." *Biochimica et Biophysica Acta* ***1806***: 29–35

[222] Xia, W.; Wang, Y.; Bergstra, R.; Kundu, S.; and Muhler, M. (2007). "Surface characterization of oxygen-functionalized multi-walled carbon nonotubes by high-resolution X-ray photoelectron spectroscopy and temperature-programmed desorption". *Applied Surface Science*, **254**: 247-250.

[223] Bilalis, P.; Katsigiannopoulos, D.; Avgeropoulos, A. and Sakellariou, G. (2014). "Non-covalent functionalization of carbon nanotubes with polymers." *RSC Adv.*, ***4***: 2911

[224] pubs.rsc.org/en/content/articlehtml/2013/dt/c3dt52365a

[225] Patent US20020048632 – Polymer-wrapped single wall carbon nanotubes – Google Patents -

[226] Bovarnick, M.; Fieber, S.; Bovarnick, M. R.; and Kozlowski, J. (1953). "Rate of Excretion of Glutanyl Polypeptide and Its Polymers in Humans." *Exp. Biol. Med.* ***83*****(**2): 253-254.

[227] Kessler, B. J.; DiGrado, C. J.; Benante, C.; Bovarnick, M.; Silber, R. H.; and Zambito, A. J. (1955). "Comparison of Excretion Rates of Linear Glutamyl Peptides in Humans and Dogs." *Exp. Biol. Med.* ***88***(4): 651-653.

[228] Loebl, W. Y.; Ulimann, T. D.; Yaron, A.; Sela, M.; Berger, A.; and Katchalski, E. (19661). "Evaluation of Multichain Polyglutamic Acid as a Possible Plasma Expander." *Exp. Biol. Med.* ***108***(3): 661-663.

[229] Masayuk, T.; Takeshi, N.; Shigeyuki, M.; Toyoji, K. (1997). "Convenient Synthesis of high molecular weight poly(succinimide) by acid-catalysed polycondensation of L-aspartic acid." *Polymer* ***38***(18): 4733-4736.

[230] Haoron, C.; Wen, X.; Tongyu, C.; Wuli, Y.; Jianghua, H.; Changchun, W. (2005). "Aggregation of biodegradable amphiphilic poly(succinimide-co-N-propyl aspartamide) and poly(N-dodecyl aspartic-co-N-propyl aspartamide) in aqueous medium and its preliminary drug-released properties". *Polymer* ***46***: 1821-1827.

[231] Antoni, G.; Neri, P. (1974). "Hydrodynamic Properties of a New Plasma Expander: Polyhydroxyethylaspartamide" *Biopolymers.* ***13***: 1721-1729.

[232] N'Da, D. D (2004). "Synthesis of Methotrexate and Ferrocene Conjugate as Potential Anticancer Agents." (Thesis) *Faculty of Science, University of the Witwatersrand.*

[233] Ngoy, J. M.; Iyuke, S. E.; Yah, C. S., Neuse, E. W. (2011). "Kinetic Optimization of Folic Acid Polymer Conjugates for Drug Targeting". *American Journal of Applied Sciences* ***8***(6): 508-519.

[234] Caldwell, G.; Meirim, M. G.; N'Da, D. D.; Neuse, E. W. (2006). "Carrier-bound Methotrexate II. Water-soluble Polyaspartamide-Methotrexate Conjugates with amide Links in the Polymer Spacer. *J. Appl. Polym. Sci*. ***100***: 3415-3424.

[235] Haoron, C.; Wen, X.; Tongyu, C.; Wuli, Y.; Jianghua, H.; Changchun, W. (2005). "Aggregation of biodegradable amphiphilic poly(succinimide-co-N-propyl aspartamide) and poly(N-dodecyl aspartic-co-N-propyl aspartamide) in aqueous medium and its preliminary drug-released properties". *Polymer* ***46***: 1821-1827.

[236] Bartha, L.; Kis, G.; Hancsok, J.; Baladncz, J. (2004). "Engine oil compositions based on PIB-Succinimide combinatoires." *Lubrication Science* ***16***(4): 347-359.

[237] PERP Program – Maleic Anhydride – New Report Alert. Nexant's *Chem Systems. Maleic Anhydride (03/04-7).* April 2005.

[238] Nakato, T.; Kusuno, A.; Kakuchi, T. (2000). "Synthesis of poly(succinimide) by bulk polycondensation of L-aspartic acid with an acid catalyst." *Journal of Polymer Science. Part A: Polymer Chemistry,* ***38***(1): 117-122.

[239] Swarts, J. C.; Neuse, W. E.; Lamprecht, G. J. (1994). "Synthesis and Characterization of Water-Soluble Polyaspartamide-Ferrocene Conjugates for Biomedical Applications." *Journal of Inorganic and Organometallic Polymerrs.* ***4***(2).

[240] Eller, K., Henkes, E., Rossbacher, R., Höke, H. (2005). "Amines, Aliphatic" in Ullmann's Encyclopedia of Industrial Chemistry. Wley-VCH Verlag, Weinheim. Doi: 10.1002/14356007. A02_001.

[241] Trade mark of The Dow Chemical Company ("Dow"). (March 2009). "Ethylenediamine (EDA) CAS #0000107-15-3, 1,2-diaminoethane" Form No. 108-01351-0309 AMS. Printed in USA

[242] Jadhav, P. D.; Chatti, R. V.; Biniwale, R. B.; Labhsetwar, N. K.; Devotta, S.; Rayalu, S. S. (2007). "Monoethanol Amine Modified Zeolite 13X for CO_2 Adsorption at Different Temperatures" *Energy Fuels*, ***21***(6): 3555–3559.

[243] Su, F.; Lu, C.; Chen, W.; Bai, H.; Hwang, J. F. (2009). "Capture of CO_2 from flue gas via multiwalled carbon nanotubes" *Sci. Total Environ.*, ***407***(8) : 3017–3023.

[244] Wang, X.; Schwartz, V.; Clark, J. C.; Ma, X.; Overbury, S.; Xu, X.; Song, C. (2009). "Infrared Study of CO_2 Sorption over "Molecular Basket" Sorbent Consisting of Polyethylenimine-Modified Mesoporous Molecular Sieve." *J. Phys. Chem. C*, ***113***(17): 7260–7268.

[245] Harlick, P.J.E. and Abdelhamid Sayari, A. (2006). "Applications of Pore-Expanded Mesoporous Silicas. 3. Triamine Silane Grafting for Enhanced CO_2 Adsorption." *Ind. Eng. Chem. Res.* ***45****:* 3248-3255

[246] Huang, H. Y.; Yang, R. T. ; Chinn, D. ; Munson, C.L. (2003). "Amine Grafted MCM-48 and Silica Xerogel as Superior Sorbents for Acidics Gas Removal from Natural Gas." *Ind. Eng. Chem. Res.* ***42***: 2427.

[247] Hiyoshi, N.; Yogo, D.K.; Yashima, T. (2004). "Adsorption of Carbon Dioxide on Amine Modified SBA-15 in the Presence of Water Vapor." *Chem. Lett*. ***33***: 510.

[248] Su, F.; Lu, C.; Kuo, S.C and Zeng, W. (2009). "Adsorption of CO_2 on Amine-Functionalized Y-Type Zeolites." *Energy Fuels*, ***24***: 1441–1448 : DOI:10.1021/ef901077k

[249] Wurzbacher, J.A.; Gebald, C. and Steinfeld, A. (2011). "Separation of CO_2 from air by temperature-vacuum swing adsorption using diamine-functionalized silica gel." *Energy Environ. Sci.*, **4**: 3584-3592.

[250] Jacobsen, N. E. (2007). "NMR SPECTROSCOPY EXPLAINED: Simplified Theory, Applications and Examples for Organic Chemistry and Structural Biology." WILLEY Pages 1-2.

[251] Shah, N; Sattar, A; Benanti, M; Hollander, S; Cheuck, L (2006). "Magnetic resonance spectroscopy as an imaging tool for cancer: a review of literature." *The Journal of the American Osteopathic Association* ***106***(1): 23-27.

[252] Campion, A.; Kambhampati, P. (1998). "Surface-enhanced Raman scattering." *Chemical Society Reviews*, ***27***: 241-250.

[253] Griffiths, P. R; de Haseth, J.A. (2007). "Fourier Tranform Infrared Spectrometry" *Wiley 2nd Ed.* pp 1-43

[254] Smith, B.C. (2011). "Fundamentals of FOURIER TRANSFORM INFRARED SPECTROSCOPY" *CRC Press Taylor and Francis Group. 2nd Ed.* pp 8-9.

[255] Spence, J.C.H. (1980). "Experimental high-resolution electron microscopy". *New York: Oxford U. Press.* ISBN 0-19-505405-9.

[256] Pease, R.F.W.; Nixon, W.C. (1965). "High resolution scanning electron microscopy." *Jounal of Scientific Instruments.* ***42*** (81): 2. Doi: 10.10888/0950-7671/42/2/305

[257] Joy, D.C.; Pawley, J.B. (1992). "High-resolution scanning electron microscopy." *Ultramicroscopy.* ***47***(1-3): 80-100.

[258] Crewe, A.V.; Wall, J. and Welter, L.M. (1968). " A High-Resolution Scanning Transmission Electron Microscope." J. Appl. Phys. 39, 5861. http://dx.doi.org/10.1063/1.1656079

[259] Emmett, (1945). "Advances in Colloid Science". *Emmett, Ind. Eng. Chem.,* ***1*** (37), 1-36. 639 pages

[260] Hatakeyama, T.; Quinn, F.X. (1999). "Thermal Analysis, Fundamentals and Application to Polymer Science," *John Wiley & Sons Ltd.*

[261] Cheremisinoff, N.P. (1996). "Polymer Characterization, Laboratory Techniques and Analysis," *Noyes Publications*.

[262] Puccini, M.; Seggiani, M.; Vitolo, S. (2013). "Lithium Silicate Pellets for CO_2 Capture at High Temperature." *CHEMICAL ENGINEERING TRANSACTIONS,* ***35***: 373-378.

[263] Harlick, P.J.E. and Sayari, A. (2006). "Applications of Pore-Expanded Mesoporous Silicas. 3. Triamine Silane Grafting for Enhanced CO_2 Adsorption." *Ind. Eng. Chem. Res.,* ***45***: 3248-3255.

[264] Xu, X; Song, C; Andresen, J.M.; Miller, B.G. and Scaroni, A.W. (2002). "Novel Polyethylenimine-Modified Mesoporous Molecular Sieve of MCM-41 Type as High-Capacity Adsorbent for CO_2 Capture." *Energy & Fuels,* ***16***: 1463-1469

[265] Heydari-Gorji, A.; Belmabkhout, Y.; and Sayari, A. (2011). "Polyethylenimine-Impregnated Mesoporous Silica: Effect of Amine Loading and Surface Alkyl Chains on CO_2 Adsorption*" Langmuir, **27***: 12411–12416. dx.doi.org/10.1021/la202972t.

[266] Xu, X.; Graeffe, B.; and Song, C. (2004). "Effect of Type of Polymers Loaded in Mesoporous Carbon Dioxide "Molecular Basket" Adsorbent on Carbon Dioxide Separation from Gas Mixtures." *Prepr. Pap.-Am. Chem. Soc., Div. Fuel Chem., **49***(1): 259

[267] Zheng, F.; Tran, D.N.; Busche, B.; Fryxell, G.E.; Addleman, R.S.; Zemanian, T.S.; Aardahl, C.L. (2004). "ETHYLENEDIAMINE-MODIFIED SBA-15 AS REGENERABLE CO2 SORBENTS." *Prepr. Pap.-Am. Chem. Soc., Div. Fuel Chem., **49***(1): 261

[268] Clarke, S.; Petro, F. (2011). "Biomass Burn Characteristics." *Factsheet.* Order No 11-033, AGDEX 737/120, June 2011.

[269] SeriesTM Getting Started Guide (2010). "SDT Simultaneous DSC-TGA Q." *TA Instruments Revision H Issued March 2010*.

[270] TA Instrument SDT-Q600 Simultaneous TGA / DSC. Artisan, Technology Group. www.artisantg.com/Scientific/74393-1/TA_Instruments_SDT_Q600_Simultaneous_TGA_ DSC.

[271] GÜven, O. (1990). "Crosslinking and Scission in Polymers." Serie C Mathematical and Physical Science, ***202***.

[272] Kricheldorf, H.R. (1987). In: α-amino acid N-carboxyanhydride and related heterocycles. *Springer-verlag*, 3-58.

[273] Neri, P.; Antoni, G.; Benvenutti, F.; Cocola, F.; and Gazzei, G. (1973). Synthesis of α,β-poly[(2-hydroxyethyl)-DL-aspartamide], a new plasma expander. *J. Med. Chem.* ***16***, 893–897.

[274] Tomida, M.; Nakato, T. ; Matshunami, S.; Kakuchi, T. (1997). In Convenient synthesis of high molecular weight polymer. *Polymer*, **38**: 4733-4736.

[275] IUPAC (1972). "Manual of Symbols and Terminology", Appendix 2, Pt. 1. *Pure Appl. Chem.* ***31***, 578.

[276] Sasaki, K.; Tokura, Y.; Sogawa, T. (2013). "The Origin of Raman D Band: Bonding and Antibonding Orbitals in Graphene." *Crystals, **3***: 120-140; doi: 10.3390/cryst3010120.

[277] Hodkiewicz, J. (2010). "Characterization Carbon Materials with Raman Spectroscopy." *Thermo Fisher Scientific, Madison, WI, USA.* Application Note: 51946.

[278] Hodkiewicz, J. (2010). "Characterization Carbon Materials with Raman Spectroscopy." *Thermo Fisher Scientific, Madison, WI, USA.* Application Note: 51901.

[279] Kudin, K. N.; Ozbas, B.; Schniepp, H.C.; Pud'homme, R.K.; Aksay, I.A.; and Car, R. (2008). "Raman Spectra of Graphite Oxide and Functionalized Graphene Sheets." *Nano Letters* ***8***(1): 36-41.

[280] Liu, Z.; Davis, C.; Cai, W.; He, L. ; Chen, X. ; and Dai, H. (2008). "Circulation and long-term fate of functionalized, biocompatible single-walled carbon nanotubes in mice probed by Raman spectroscopy." *PNAS* ***105***(5): 1410-1415.

[281] US Department of energy National Carbon Capture Center (2008). "Post-Combustion Carbon Capture." *Cooperative Agreement DE-NT0000749* signed in September 2008.

[282] Duan L., Zhao C., Zhou W., Liang C., Chen X., 2009. "Sulfur evolution from coal combustion in O_2/CO_2 mixture". *Journal of Analytical and Applied Pyrolysis* ***86***: 269-73.

[283] Glasstone, S. (1946). "Physical Chemistry: Surface phenomena." *MacMillan and Co. 2nd Ed.* Page 1204.

[284] Thomas, W. J.; Crittenden, B. D. (1998). "Adsorption Technology and Design." *Butterworth-Heinemann* pages 67-76.

[285] Lide, D. R (2005). CRC Handbook of Chemistry and Physics (86th Ed). *Boca Raton (FL): CRC Press*. ISBN 0-8493-0486-5

[286] Glen, E. (2010). "The Physics Hypertexbook Viscosity". Physics.info. Retrieved 2010-09-14. http://physics.info/viscosity/

[287] Mori, K; Yamaguchi, K; Mizugaki, T; Ebitani, K; and Kaneda, K. (2001). "Catalysis of a hydroxyapatite-bound Ru complex: efficient heterogeneous oxidation of primary amines to nitriles in the presence of molecular oxygen." *Chem. Commun, 461-462. Doi: 10.1039/B009944I*

[288] Noguera, J. A. H.; Quintana, H. A. R and Gomez, W. D. F. (2014). "The influence of water on the oxidation of asphalt cements". *Construction and Building of Materials* ***71***: 451-455

[289] Rooney P. C.; Daniel, D. D. (1998). "Oxygen solubility in various alkanolamine/water mixtures." *Petroleum Technology Quarterly.* Spring, 97-101.

[290] Ogino, T.; Suzuki, T.; Sawada, K. (1987). "The formation and transformation mechanism of calcium carbonate in water." *Pergamon Journals.* ***51***: 2757 – 2767.

[291] Dell, R. M.; Weller, S. W. (1959). "The thermal decomposition of nesquehonite $MgCO_3$. $3H_2O$ and magnesium ammonium carbonate $MgCO_3$. $(NH_4)_2CO_3$. $4H_2O$. *Transactions of the Faraday Society* ***55***(12*)*: 2203-2220.

[292] Davies, P. J.; Bubela, B. (1970). "Transformation of nesquehonite into hydromagnesite." *Chemical Geology* ***12***(4): 289 – 300.

[293] Zhang, Z. P. ; Zhang, Y. J. ; Ni, Y. W. ; Liu, Z. M. ; Chem, J. P. ; Liang, X. M. (2006). "Temperature and pH-dependent morphology and FT-IR analysis of magnesium carbonate hydrates." *Journal of Physical Chemistry B* ***110***(26): 12969 – 12973.

[294] Fernandez, A. L.; Chimenos, J. M. ; Segarra, M. ; Fernandez, M. A. ; Espiell, F. (2000). "Procedure to obtain hydromagnesite from a MgO-containing residue. Kinetic study. *Industrial & Engineering Chemistry Research* ***39***(10): 3653 – 3658.

[295] Mishchuk, N.; Ralston, J.; and D. Fornasiero (2002). "Influence of Dissolved Gas on van der Waals Forces between Bubbles and Particles." *J. Phys. Chem. A,* ***106***: 689-696.

[296] Sayari, A.; and Belmabkhout, Y. (2010). "Stabilization of Amine-Containing CO_2 Adsorbents: Dramatic Effect of Water Vapor." *J. AM. CEM. SOC.* ***132***, 6312-6314.

[297] Tyldesley, J. R. (1977). "An Introduction to Applied Thermodynamics and Energy Conversion." Longman. Pages 155-173.

[298] Sundén, B.; Brebbia, C. A. (2008). "Advanced Computational Methods and Experiments in Heat Transfer X." WIT Press. Pages 100-125.

[299] Zhang, C; Son, W.; Sun, G.; Xie, L.; Wang, J. ; Li, K. ; Sun, C. ; Liu, H ; Snape, C.E. ; and Drage, T. (2013). "CO2 Capture with Activated Carbon Grafted by Nitrogenous functional groups." *Energy Fuels, **27***: 4818-4823.

[300] Stuckert, N.R.; and Yang, R.T. (2011). "CO_2 Capture from the Atmosphere and Simultaneous Concentration Using Zeolites and Amine-Grafted SBA – 15." *Environ. Sci. Technol. **45***: 10257-10264. dx.doi.org/10.1021/es202647a.

[301] Zhang, Z.; Ma, X.; Wang, D.; Song, C.; and Wang, Y. (2012). "Development of Silica-Gel-Supported Polyethylenimine Sorbents for CO_2 Capture from Flue Gas." AIChE Journal, ***58***(8): 2495-2502. DOI 10.1002/aic

[302] Sumida, K.; Rogow, D.L.; Mason, J.A.; McDonald, T.M.; Bloch, E.D.; Herm, Z.R.; Bae, T.; and Long, J.R. (2012). "Carbon Dioxide Capture in Metal-Organic Frameworks." Chem. Rev., ***112***: 724-781. dx.doi.org/1021/cr2003272.

APPENDICES

APPENDIX 1: TGA GRAPHS OF CO_2 ADSORPTION FOR DRY ADSORBENTS WITH 100% CO_2

APPENDIX 2: TGA GRAPHS OF N_2 ADSORPTION FOR DRY ADSORBENTS WITH 100% N_2

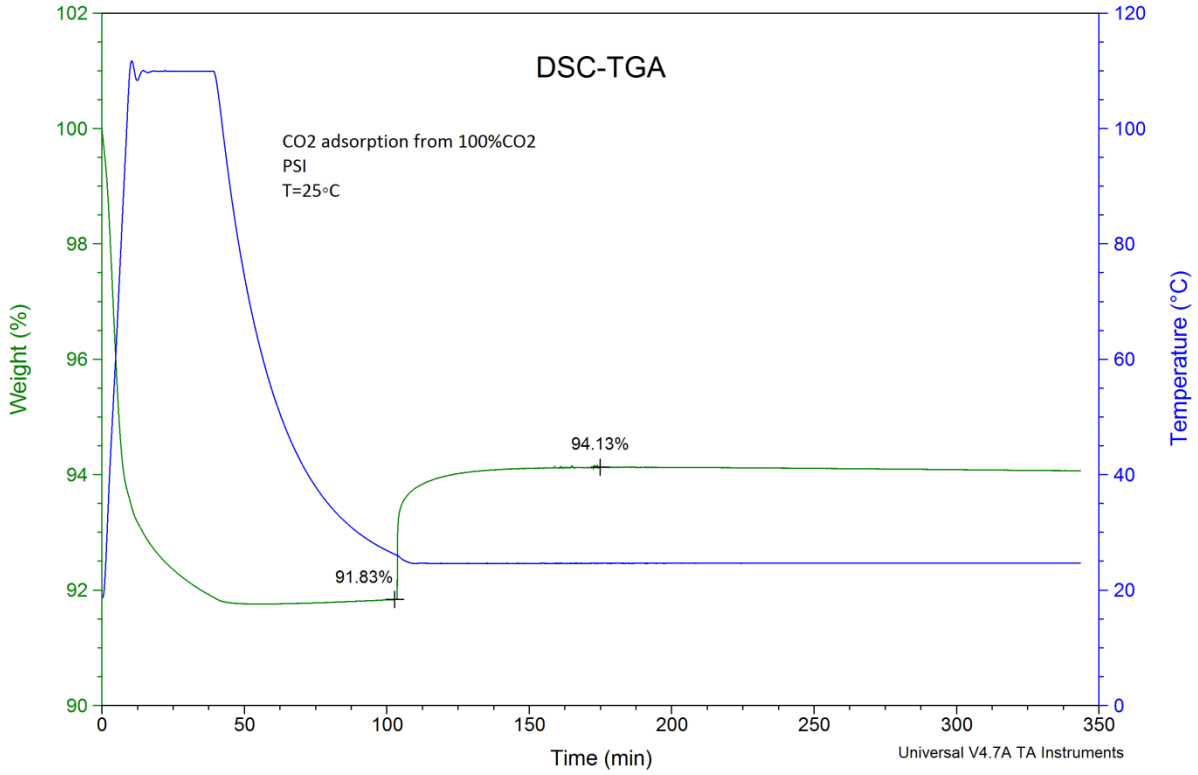
APPENDIX 3: TGA GRAPHS OF O_2 ADSORPTION FOR DRY ADSORBENTS WITH 100% O_2

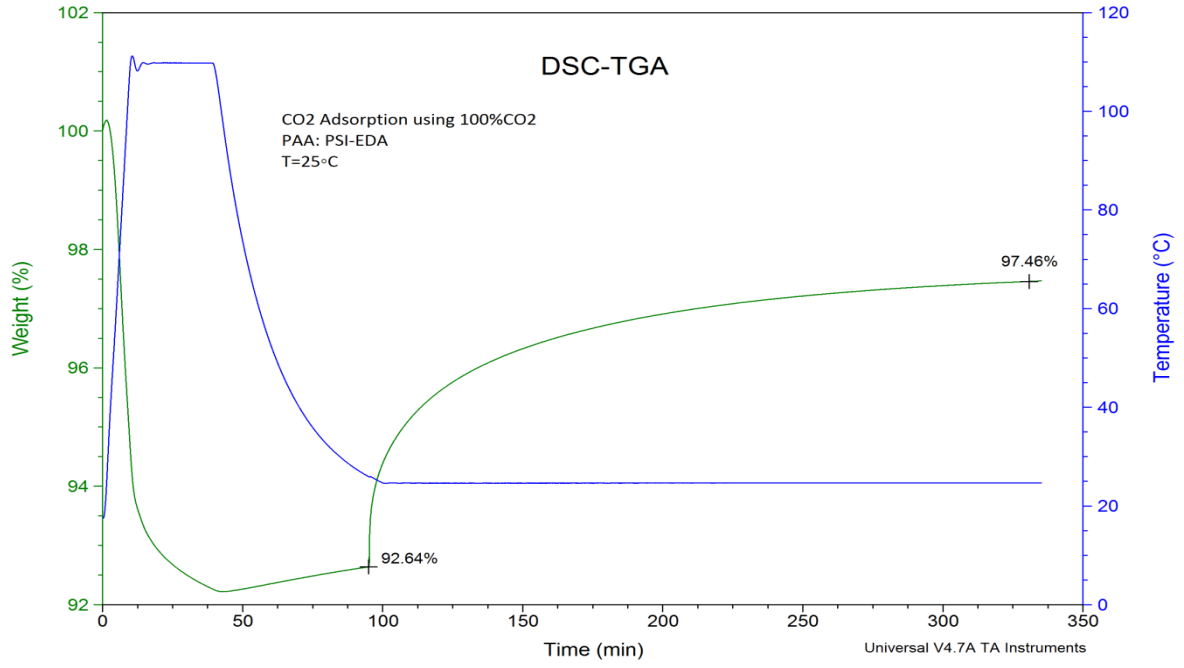
APPENDIX 4: TGA GRAPHS OF O_2 ADSORPTION FOR MOIST ADSORBENT WITH 100% O_2

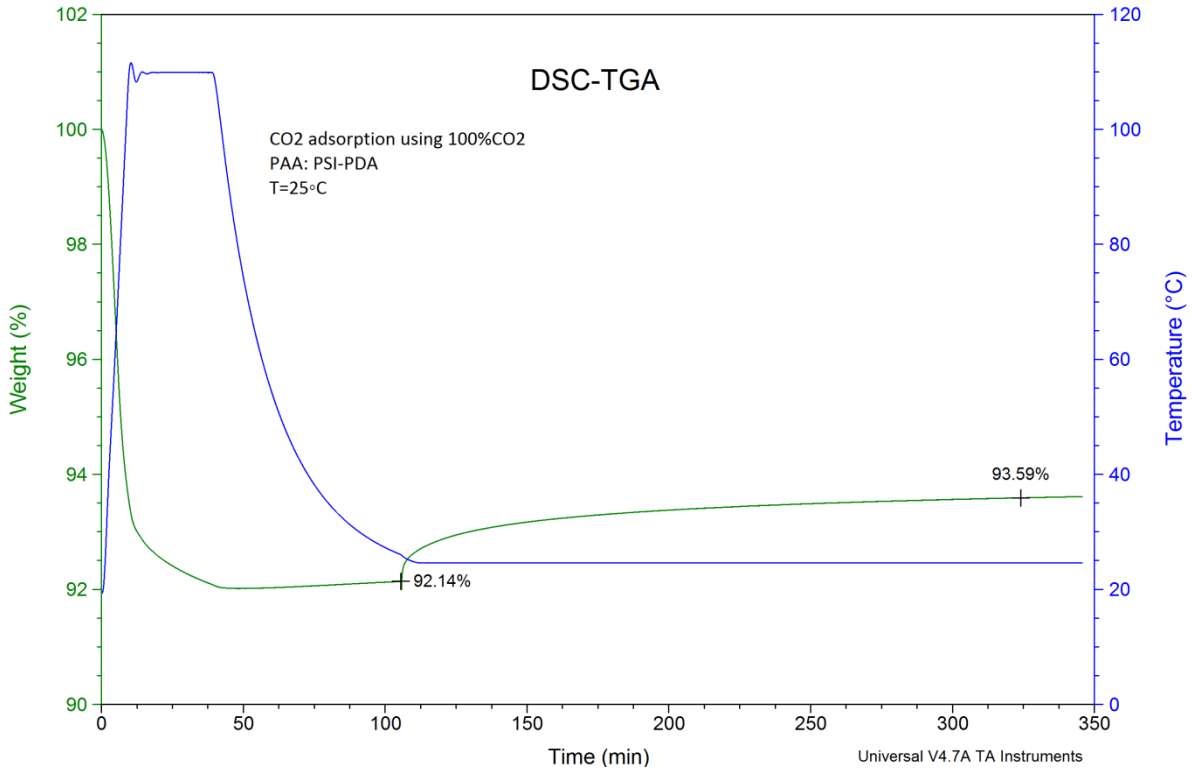
APPENDIX 1

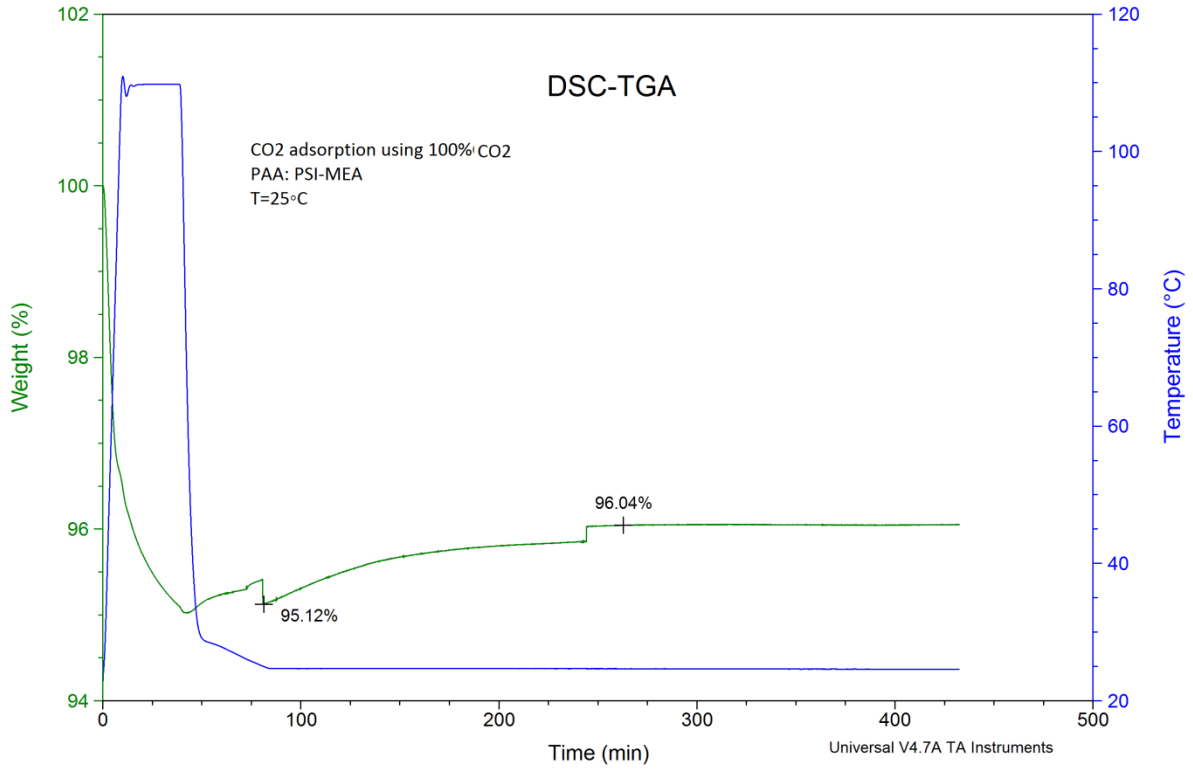
TGA GRAPHS OF CO_2 ADSORPTION FOR DRY ADSORBENTS

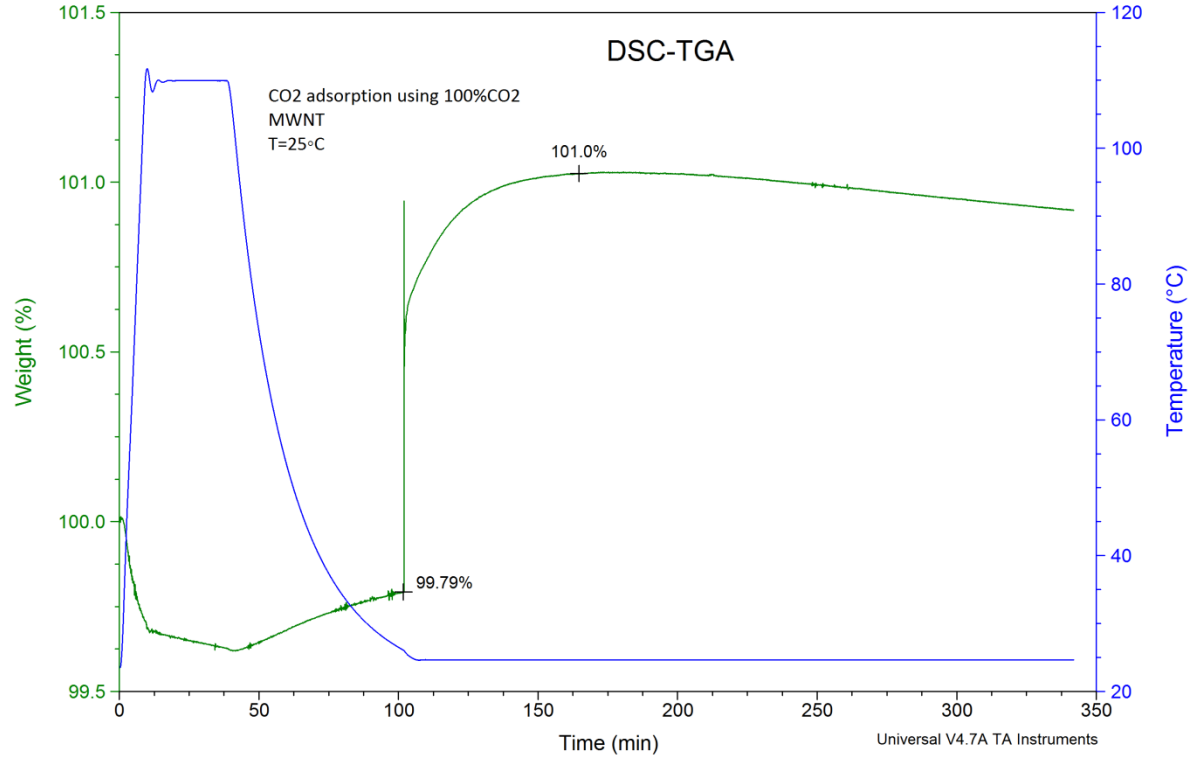
WITH 100% CO_2

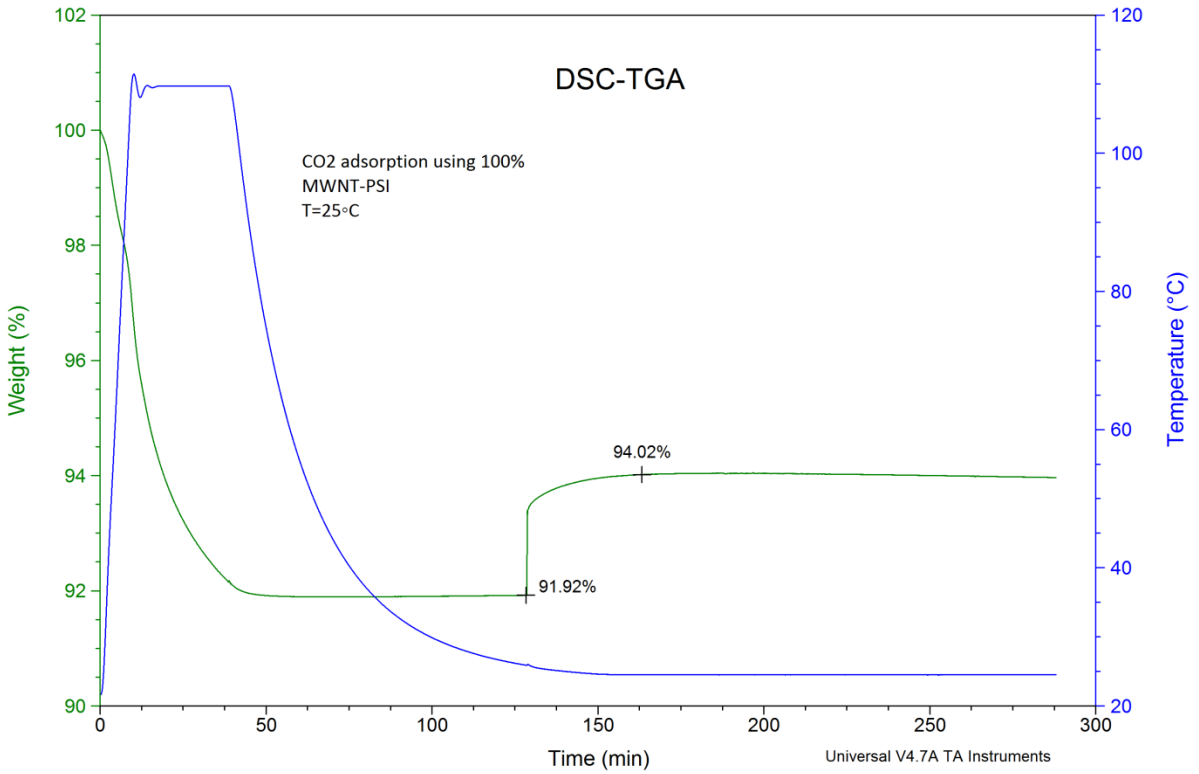


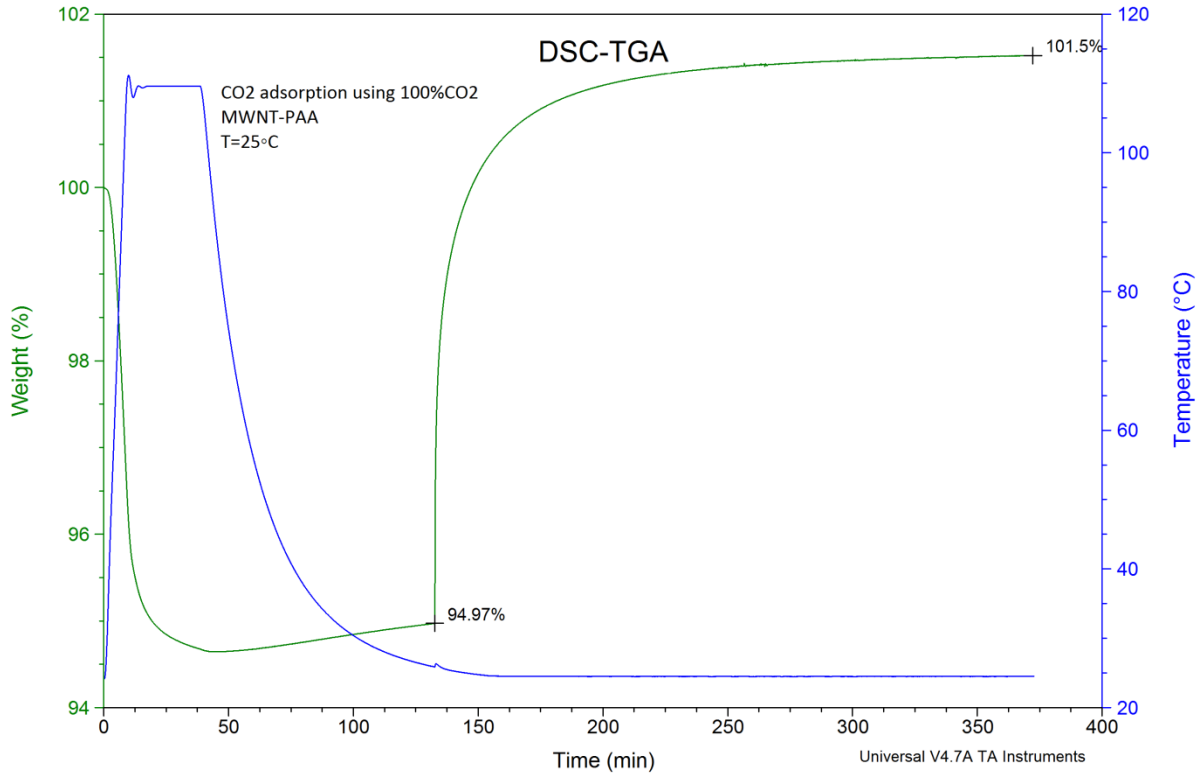


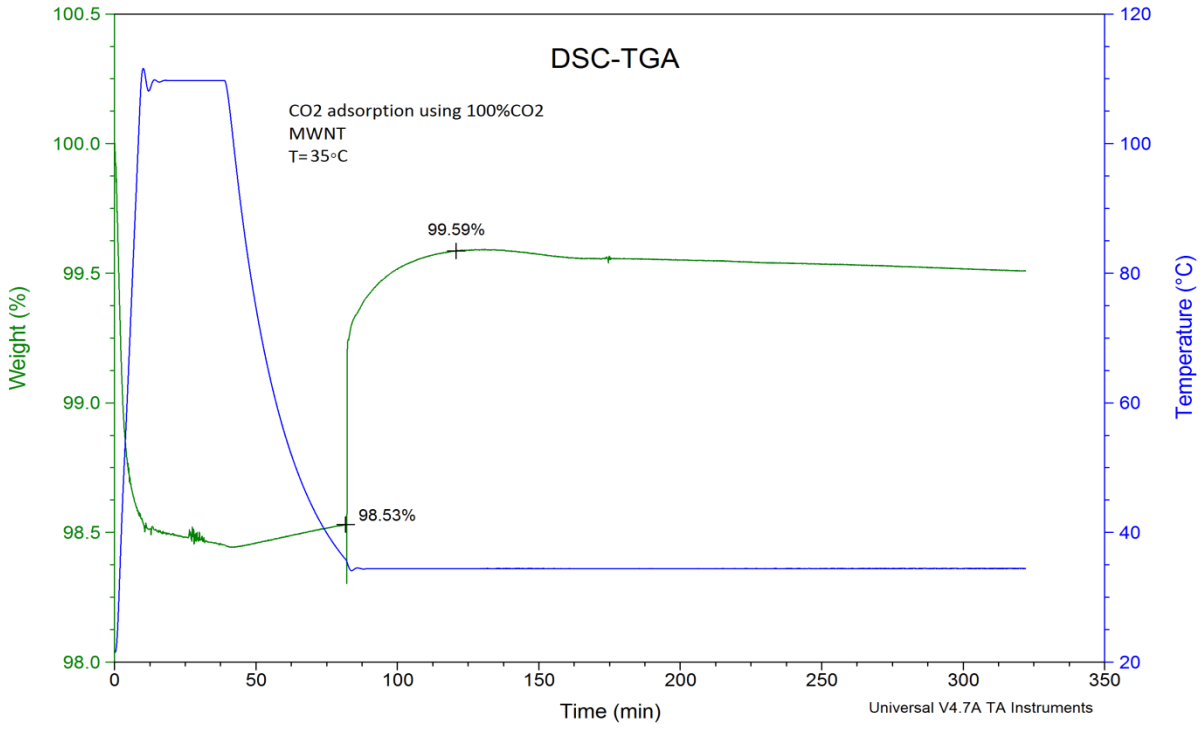

DSC-TGA
CO2 adsorption using 100%CO2
PAA: PSI-PDA
T=25◦C
93.59%
92.14%
Weight (%)
Temperature (°C)
Time (min)
Universal V4.7A TA Instruments

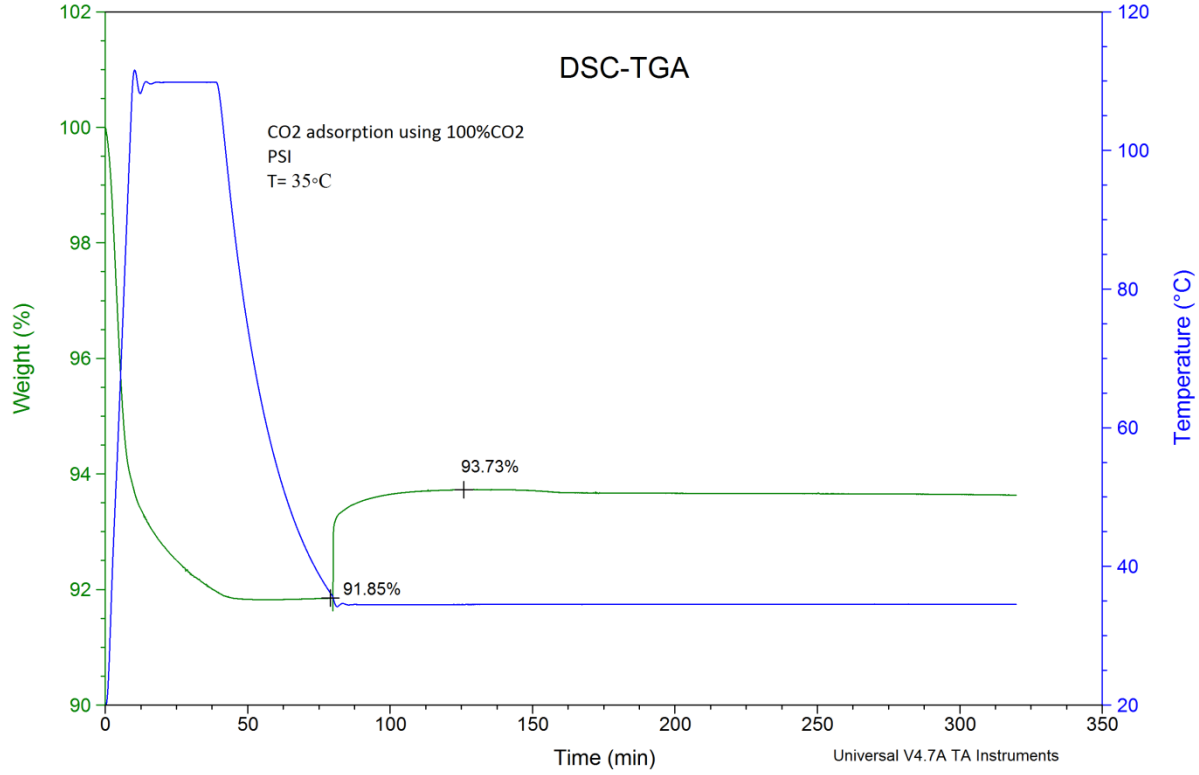

DSC-TGA
CO2 adsorption using 100% CO2
PAA: PSI-MEA
T=25◦C
96.04%
95.12%
Weight (%)
Temperature (°C)
Time (min)
Universal V4.7A TA Instruments

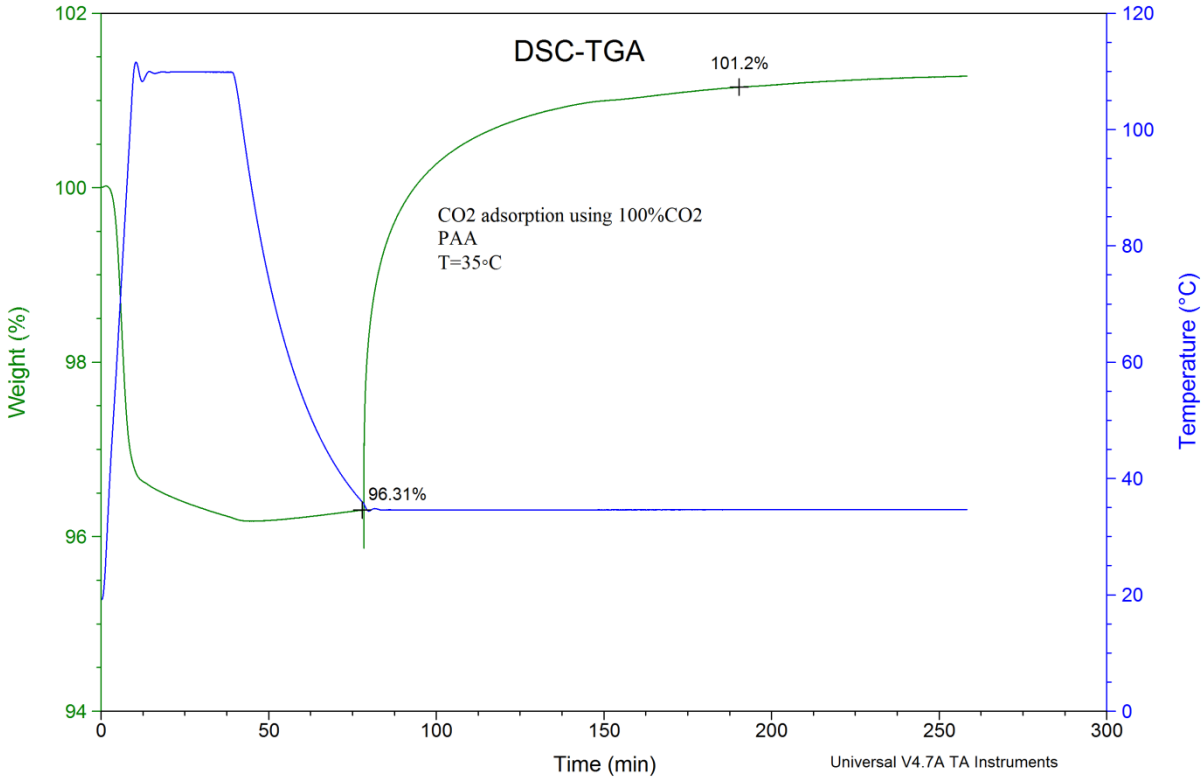

DSC-TGA
CO2 adsorption using 100%CO2
MWNT
T=25◦C
101.0%
99.79%
Weight (%)
Temperature (°C)
Time (min)
Universal V4.7A TA Instruments

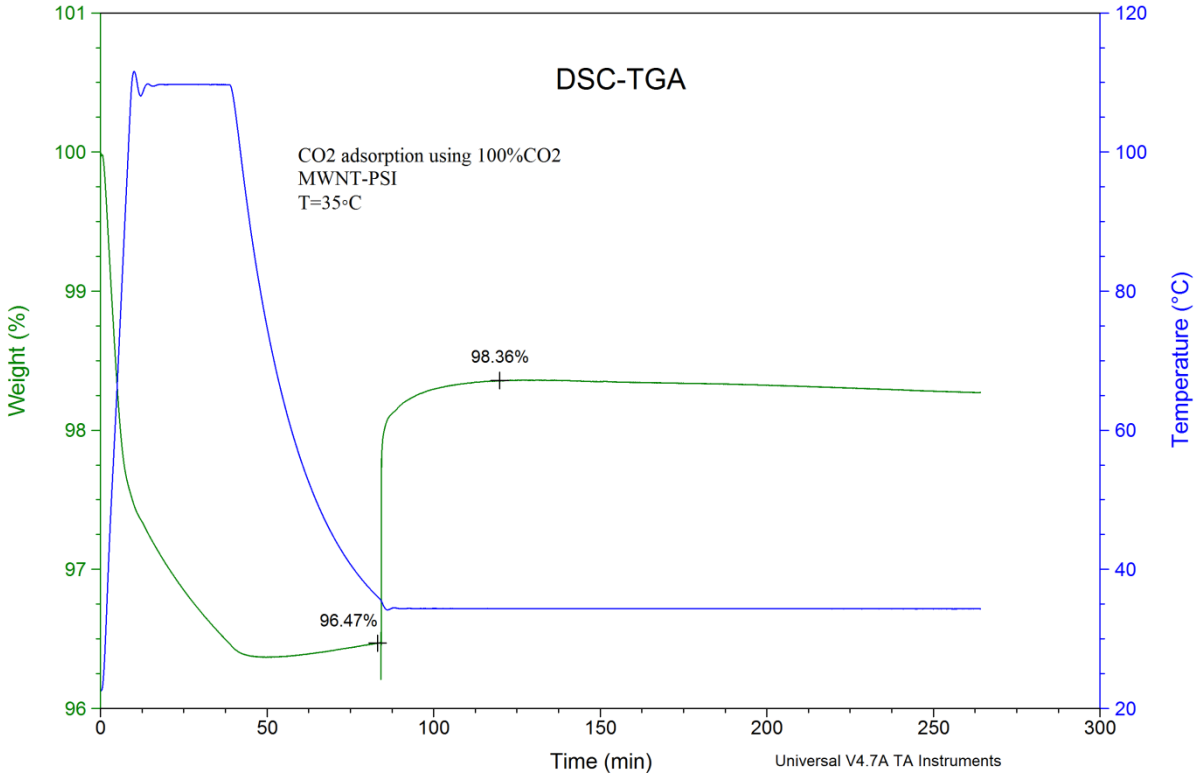

DSC-TGA
CO2 adsorption using 100%
MWNT-PSI
T=25◦C
94.02%
91.92%
Weight (%)
Temperature (°C)
Time (min)
Universal V4.7A TA Instruments

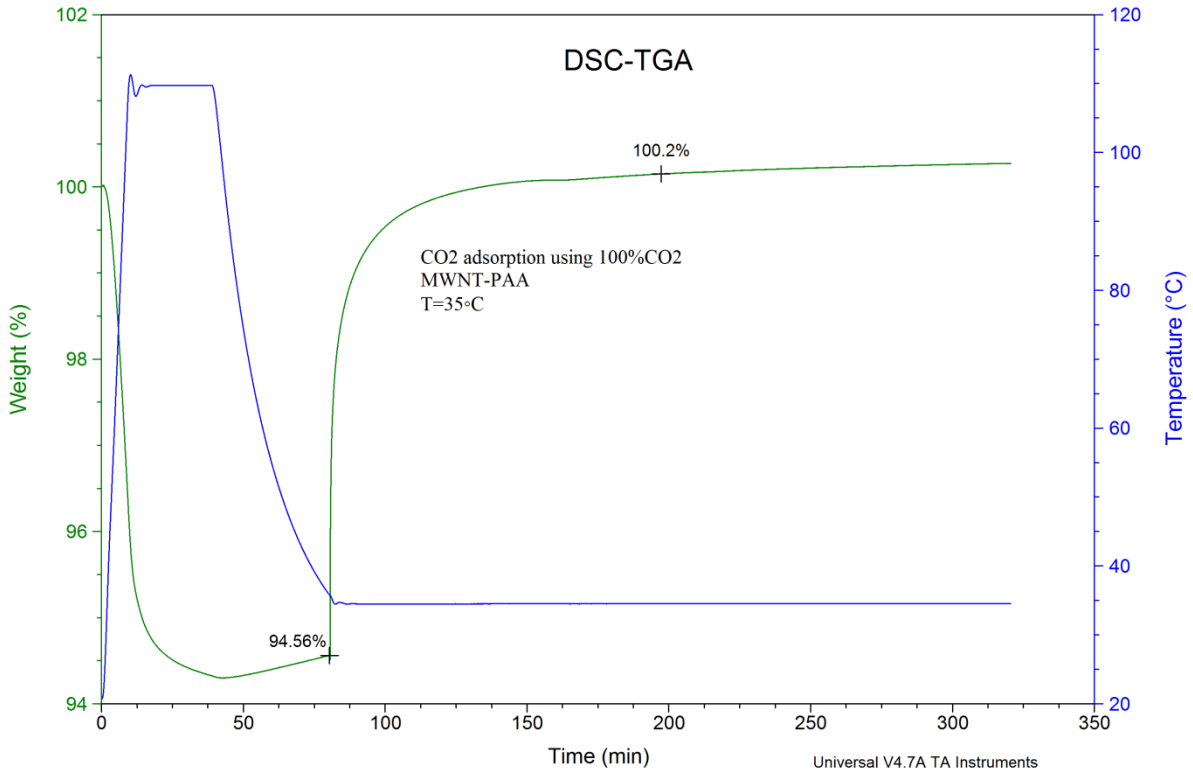

DSC-TGA
CO2 adsorption using 100%CO2
MWNT-PAA
T=25◦C
101.5%
94.97%
Weight (%)
Temperature (°C)
Time (min)
Universal V4.7A TA Instruments

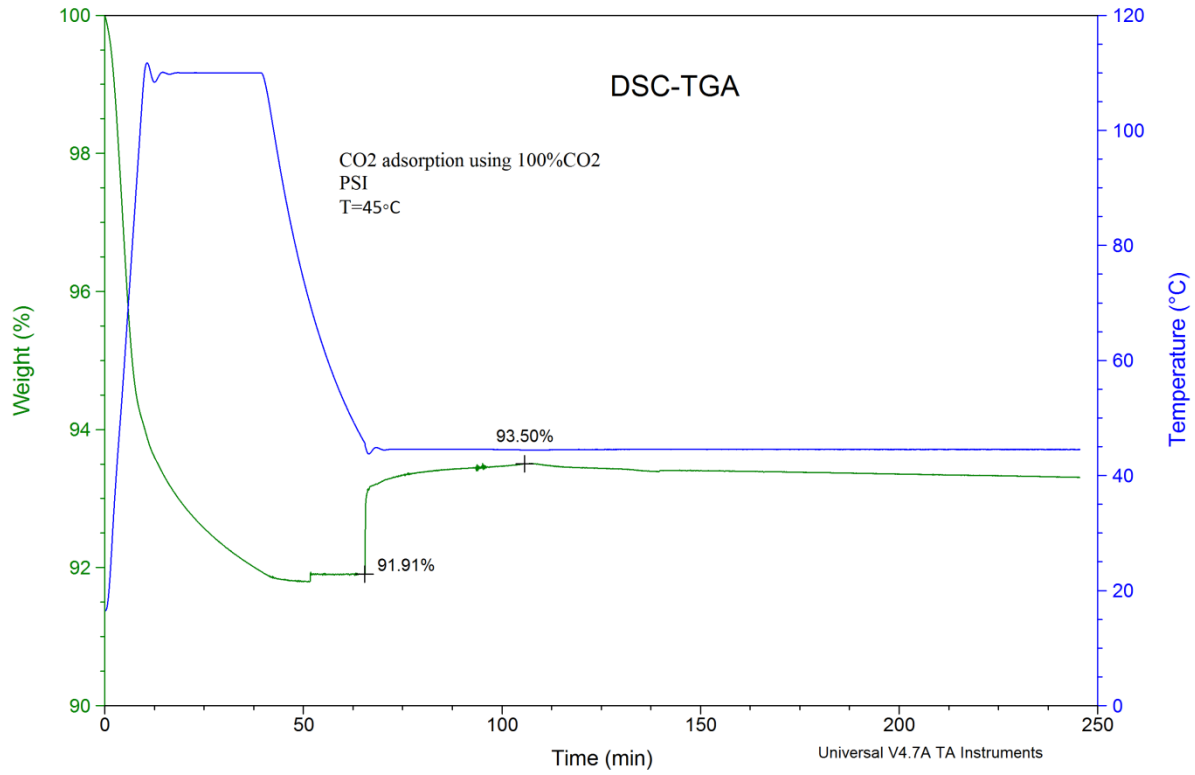

DSC-TGA
CO2 adsorption using 100%CO2
MWNT
T=35◦C
99.59%
98.53%
Weight (%)
Temperature (°C)
Time (min)
Universal V4.7A TA Instruments

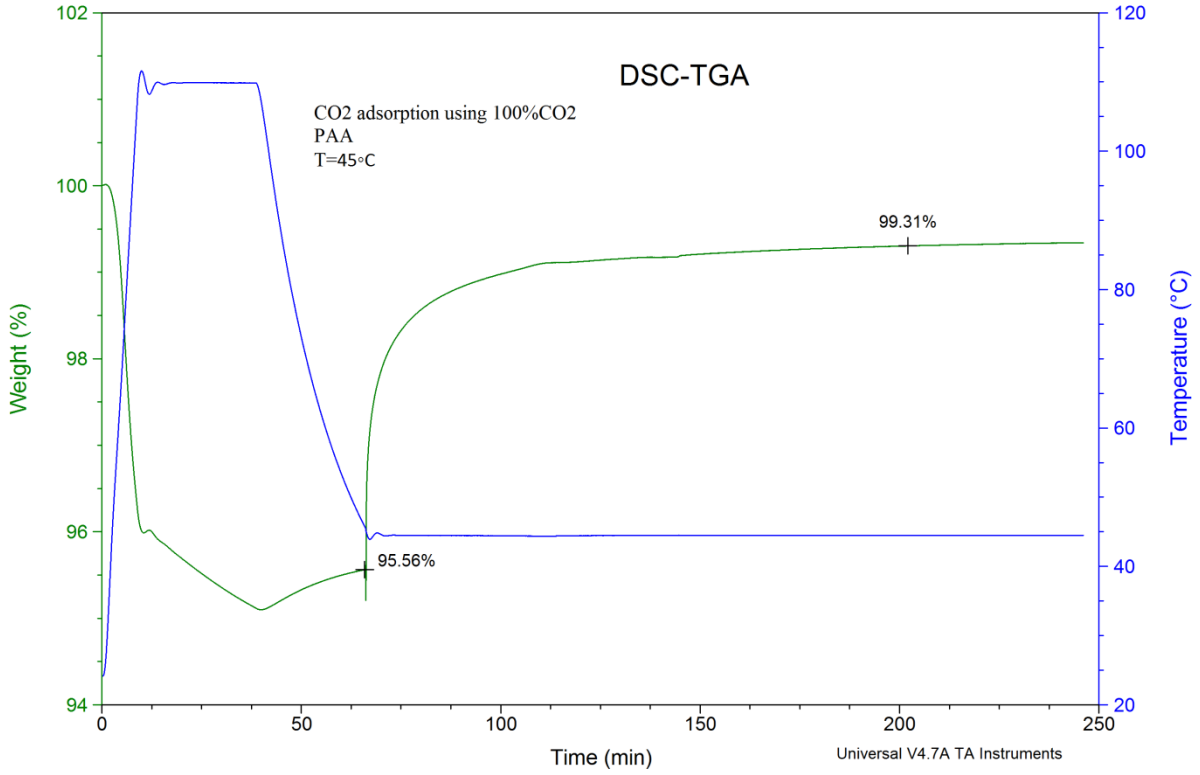

DSC-TGA
CO2 adsorption using 100%CO2
PSI
T= 35◦C
93.73%
91.85%
Weight (%)
Temperature (°C)
Time (min)
Universal V4.7A TA Instruments

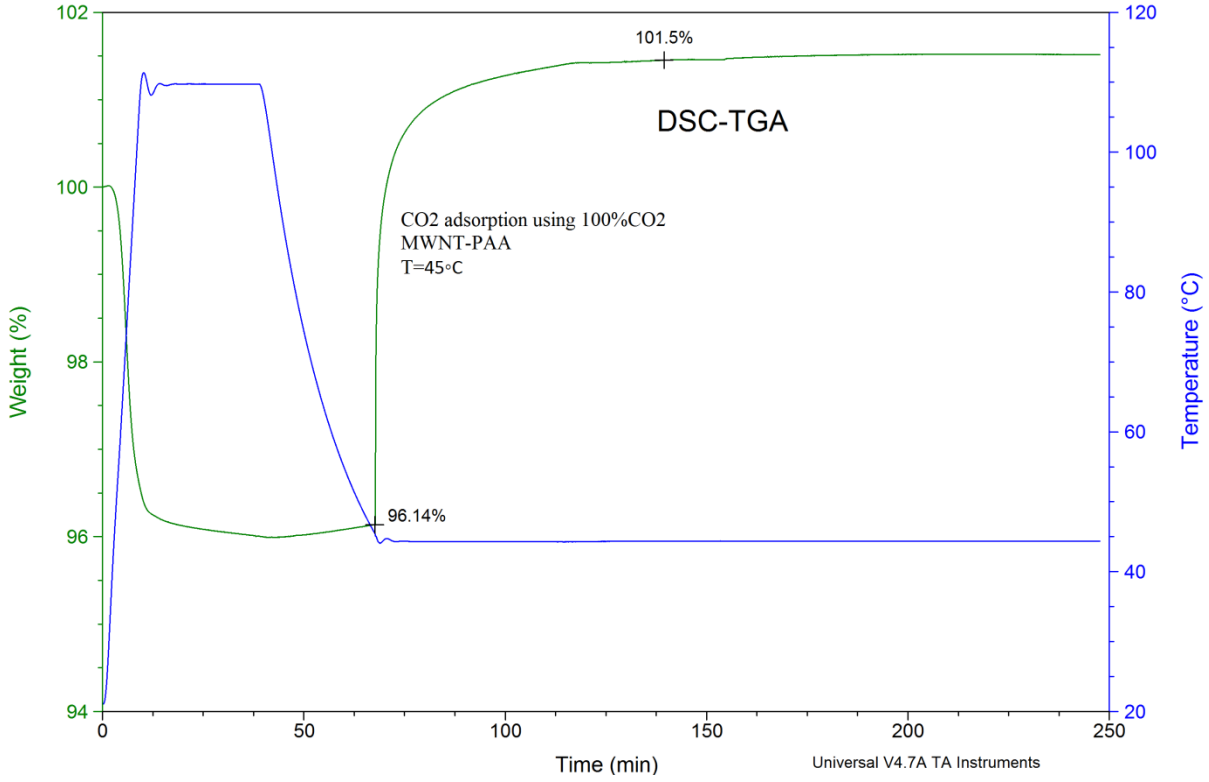

DSC-TGA
101.2%
CO2 adsorption using 100%CO2
PAA
T=35◦C
96.31%
Weight (%)
Temperature (°C)
Time (min)
Universal V4.7A TA Instruments

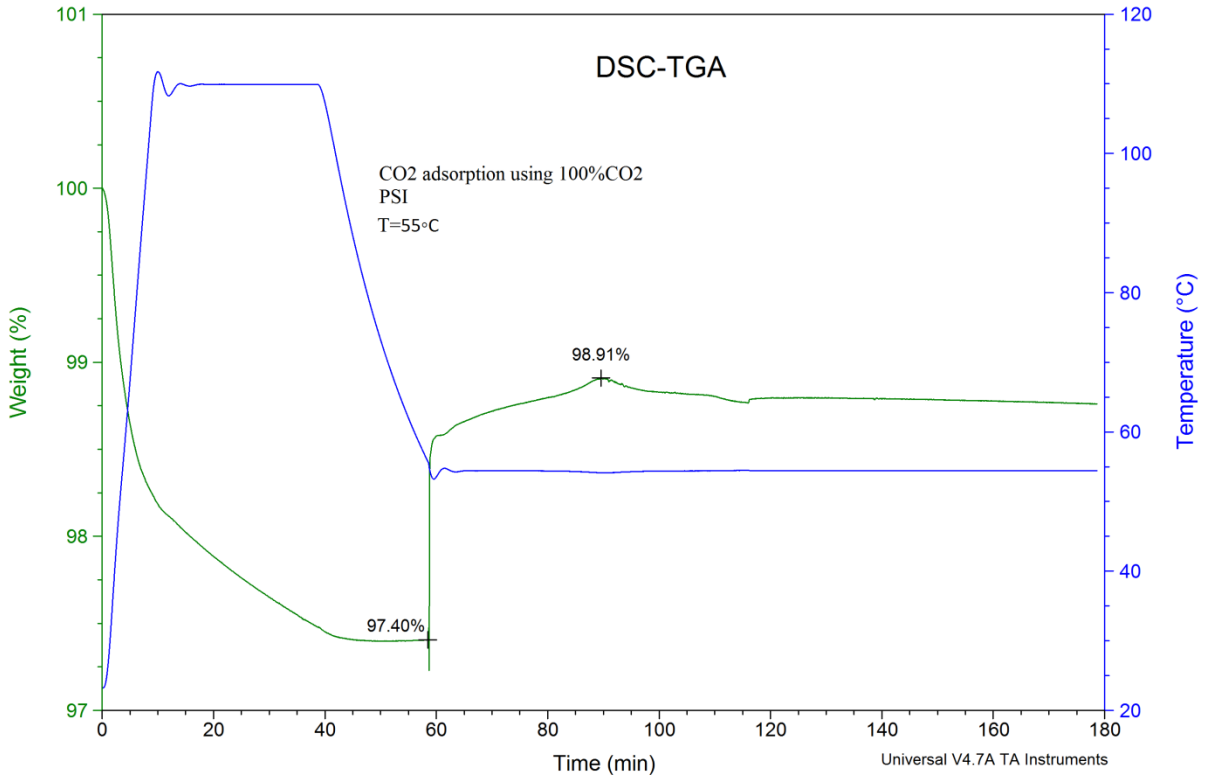

DSC-TGA
CO2 adsorption using 100%CO2
MWNT-PSI
T=35◦C
98.36%
96.47%
Weight (%)
Temperature (°C)
Time (min)
Universal V4.7A TA Instrumentsl

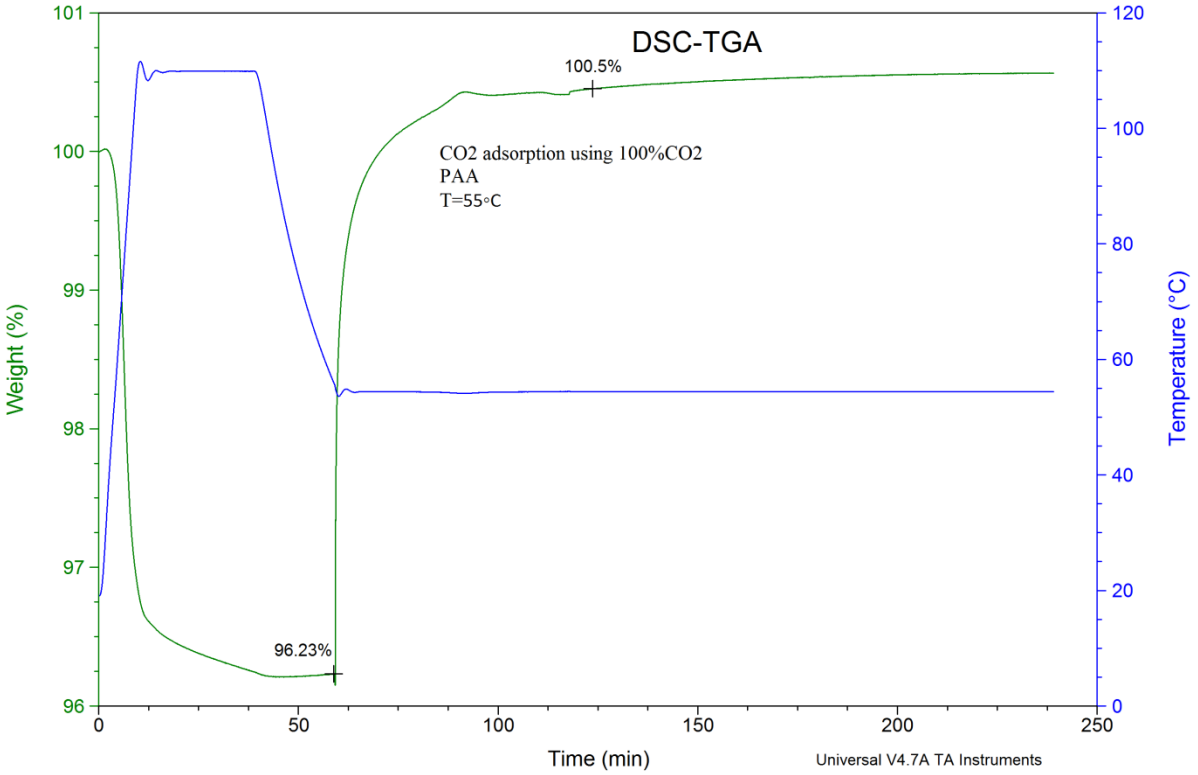

DSC-TGA
100.2%
CO2 adsorption using 100%CO2
MWNT-PAA
T=35◦C
94.56%
Weight (%)
Temperature (°C)
Time (min)
Universal V4.7A TA Instruments

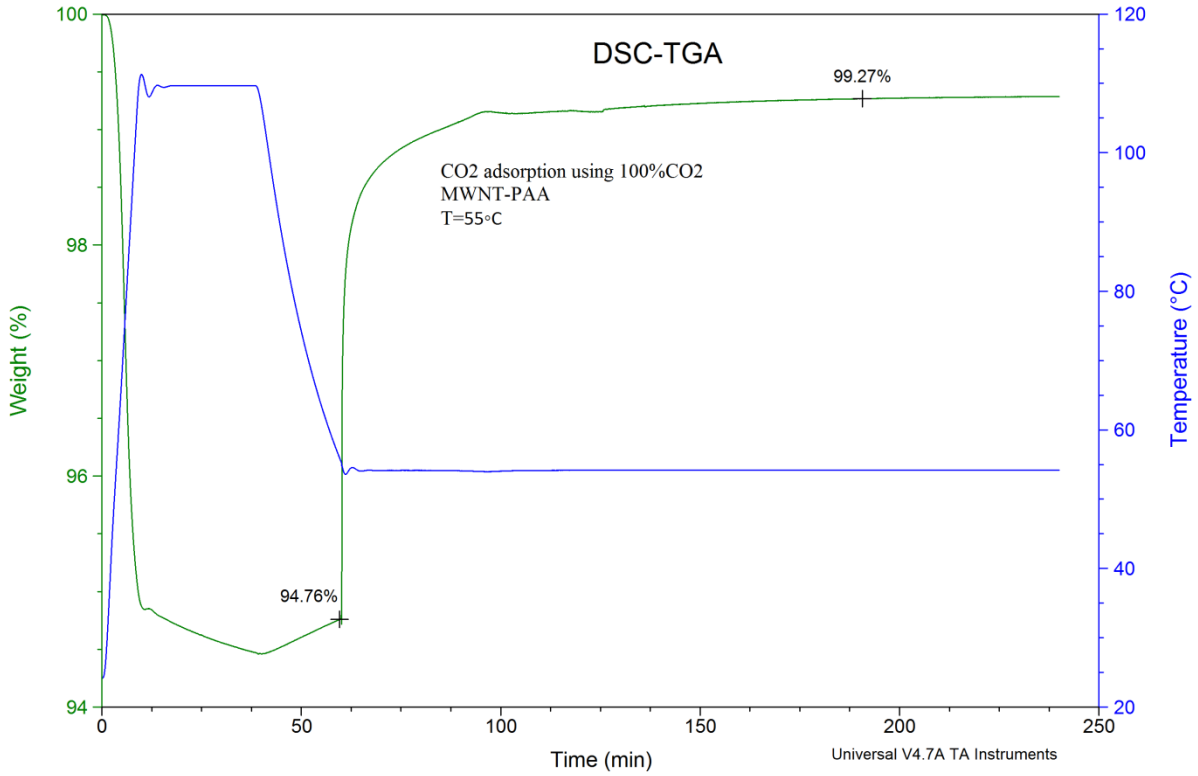

DSC-TGA
CO2 adsorption using 100%CO2
PSI
T=45◦C
93.50%
91.91%
Weight (%)
Temperature (°C)
Time (min)
Universal V4.7A TA Instruments

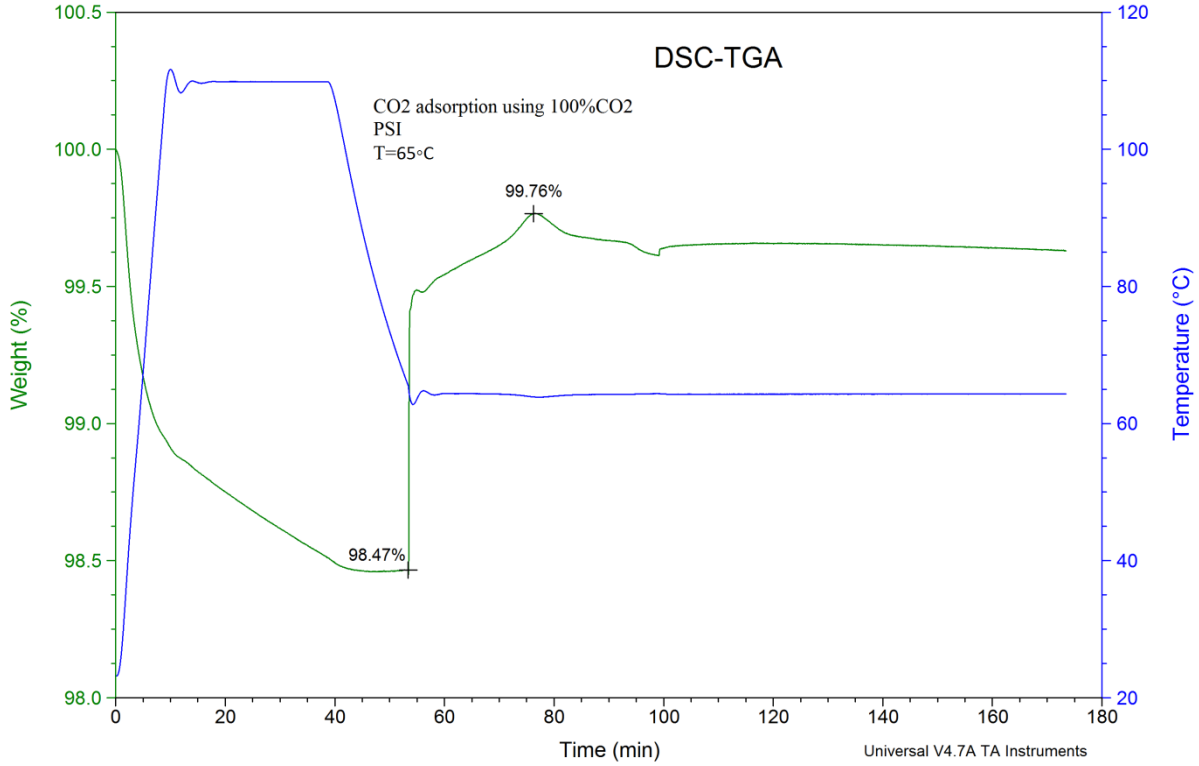

DSC-TGA
CO2 adsorption using 100%CO2
PAA
T=45◦C
99.31%
95.56%
Weight (%)
Temperature (°C)
Time (min)
Universal V4.7A TA Instruments

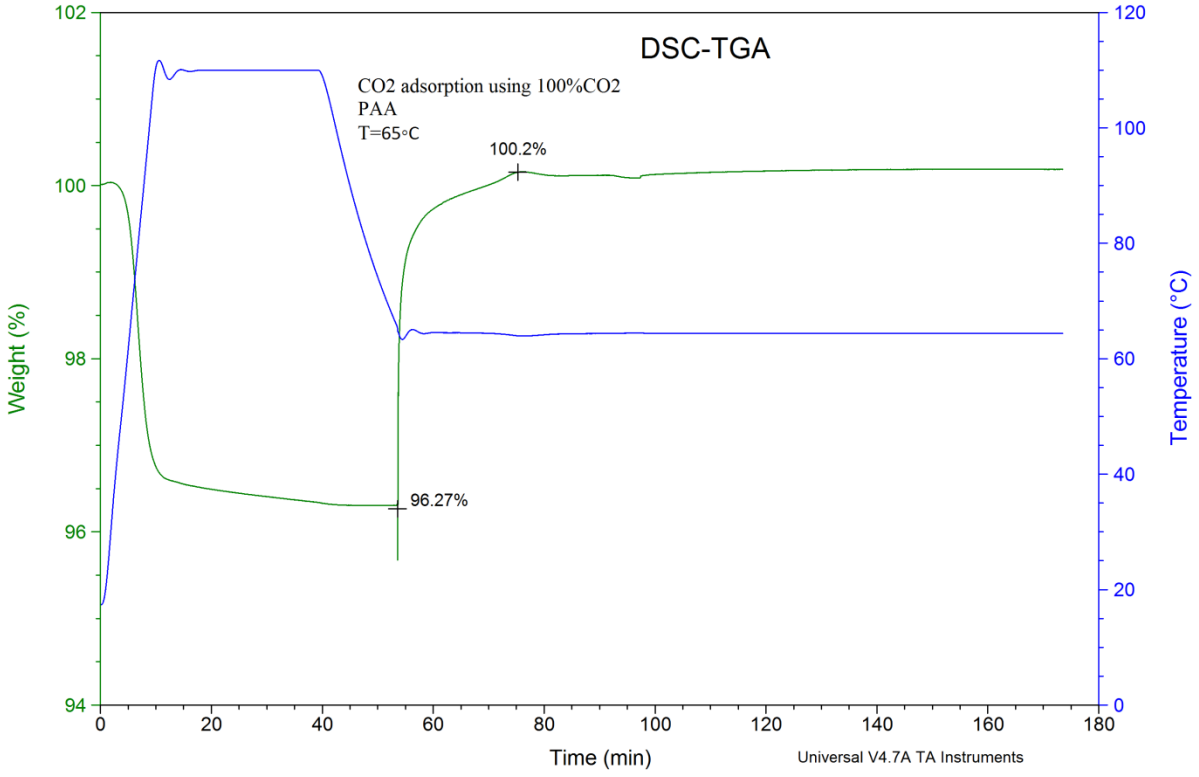

DSC-TGA
CO2 adsorption using 100%CO2
MWNT-PAA
T=45◦C
101.5%
96.14%
Weight (%)
Temperature (°C)
Time (min)
Universal V4.7A TA Instruments

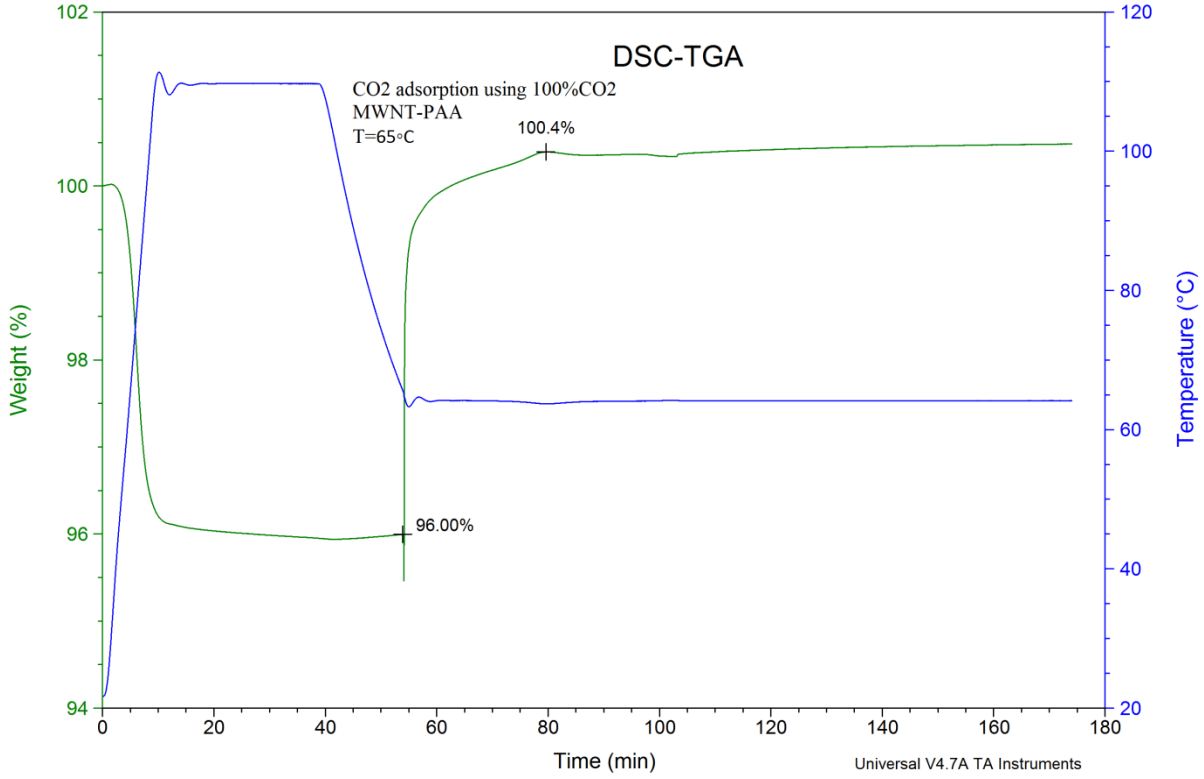

DSC-TGA
CO2 adsorption using 100%CO2
PSI
T=55◦C
98.91%
97.40%
Weight (%)
Temperature (°C)
Time (min)
Universal V4.7A TA Instruments

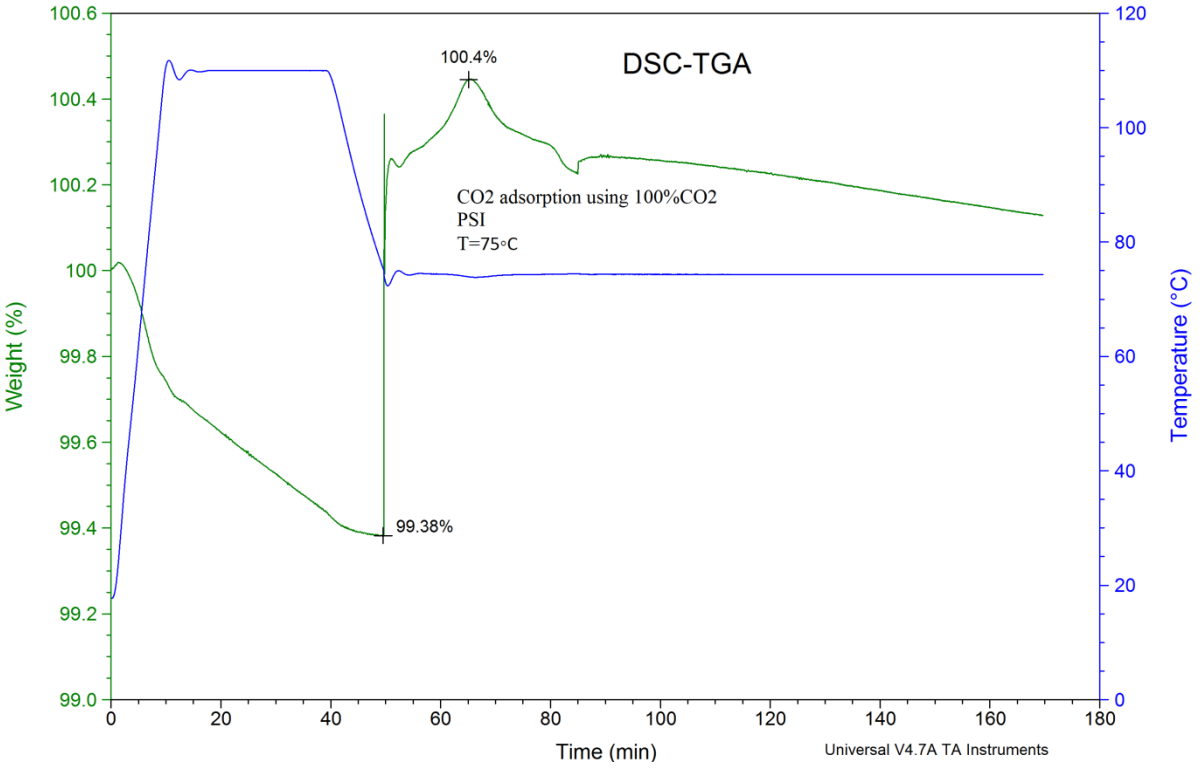

DSC-TGA
100.5%
CO2 adsorption using 100%CO2
PAA
T=55◦C
96.23%
Weight (%)
Temperature (°C)
Time (min)
Universal V4.7A TA Instruments

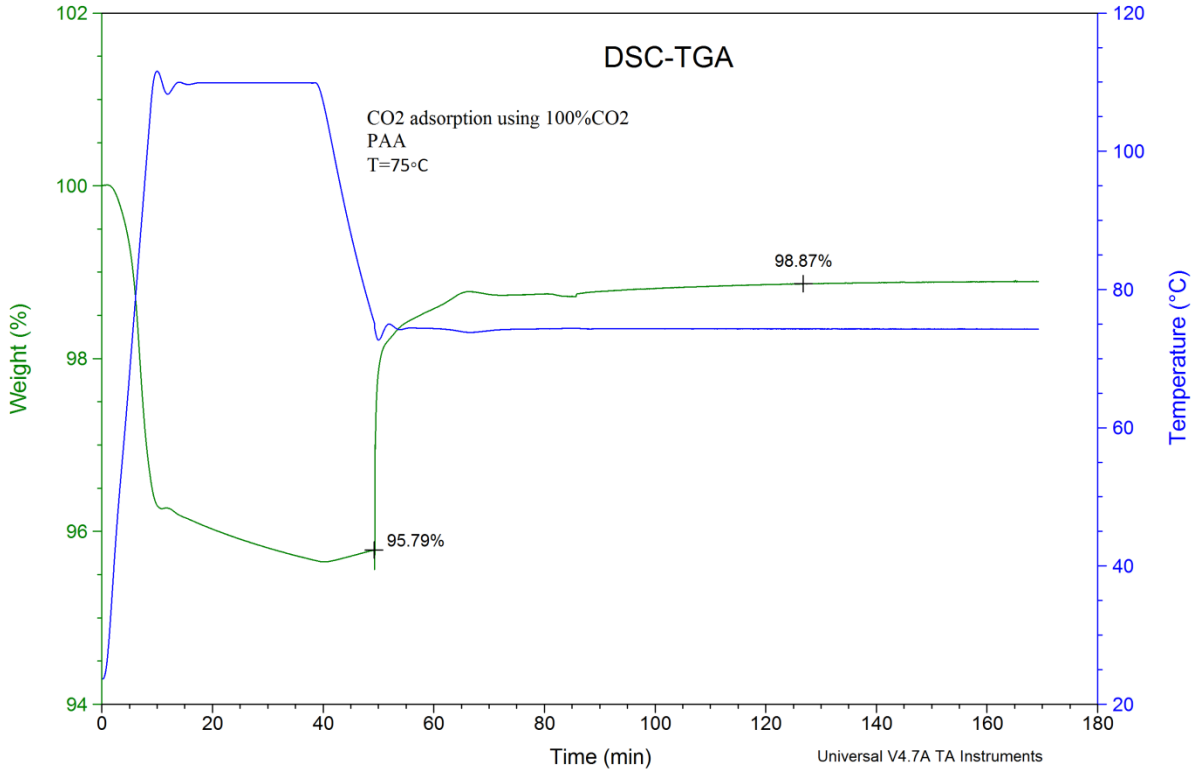

DSC-TGA
99.27%
CO2 adsorption using 100%CO2
MWNT-PAA
T=55◦C
94.76%
Weight (%)
Temperature (°C)
Time (min)
Universal V4.7A TA Instruments

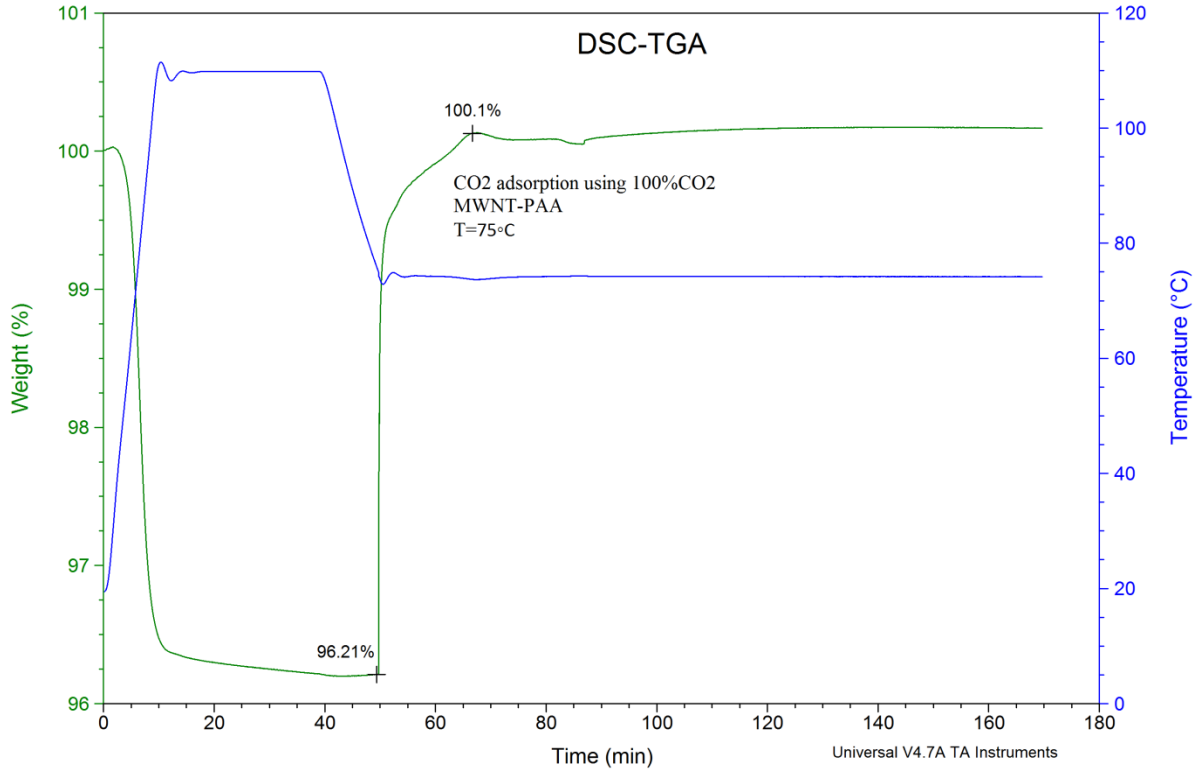

DSC-TGA
CO2 adsorption using 100%CO2
PSI
T=65◦C
99.76%
98.47%
Weight (%)
Temperature (°C)
Time (min)
Universal V4.7A TA Instrumentsn

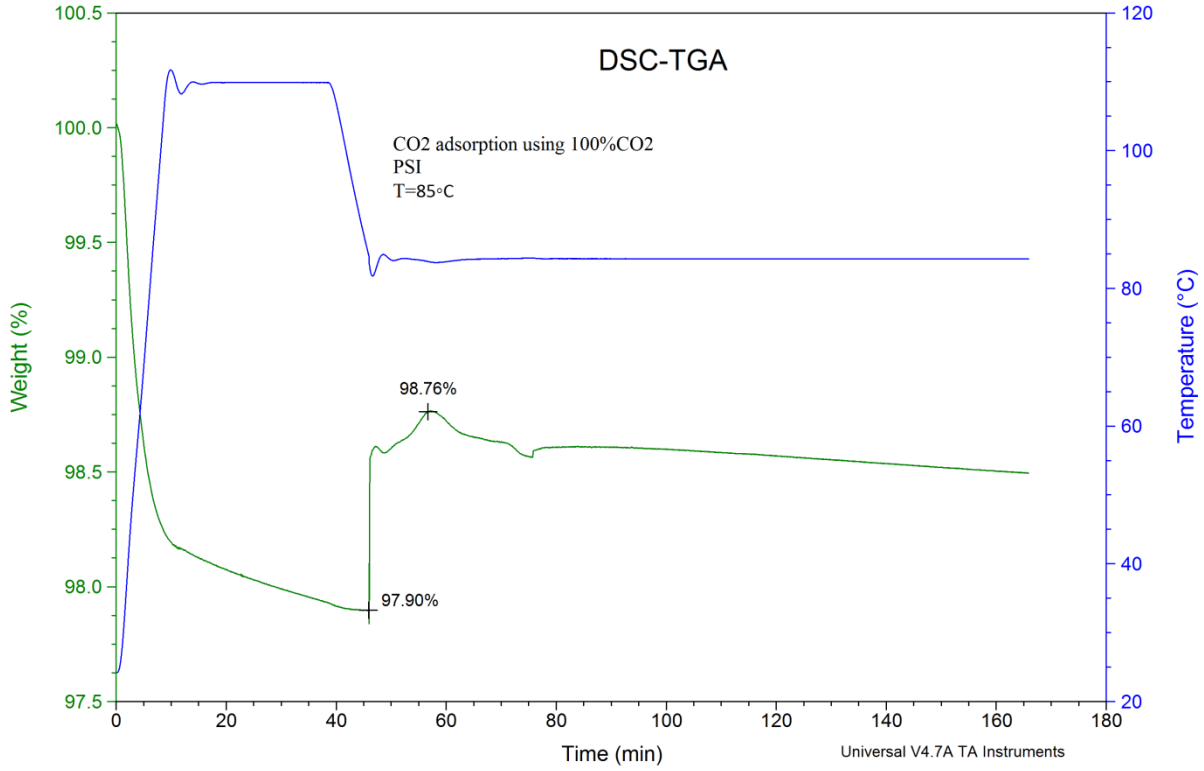

DSC-TGA
CO2 adsorption using 100%CO2
PAA
T=65◦C
100.2%
96.27%
Weight (%)
Temperature (°C)
Time (min)
Universal V4.7A TA Instruments

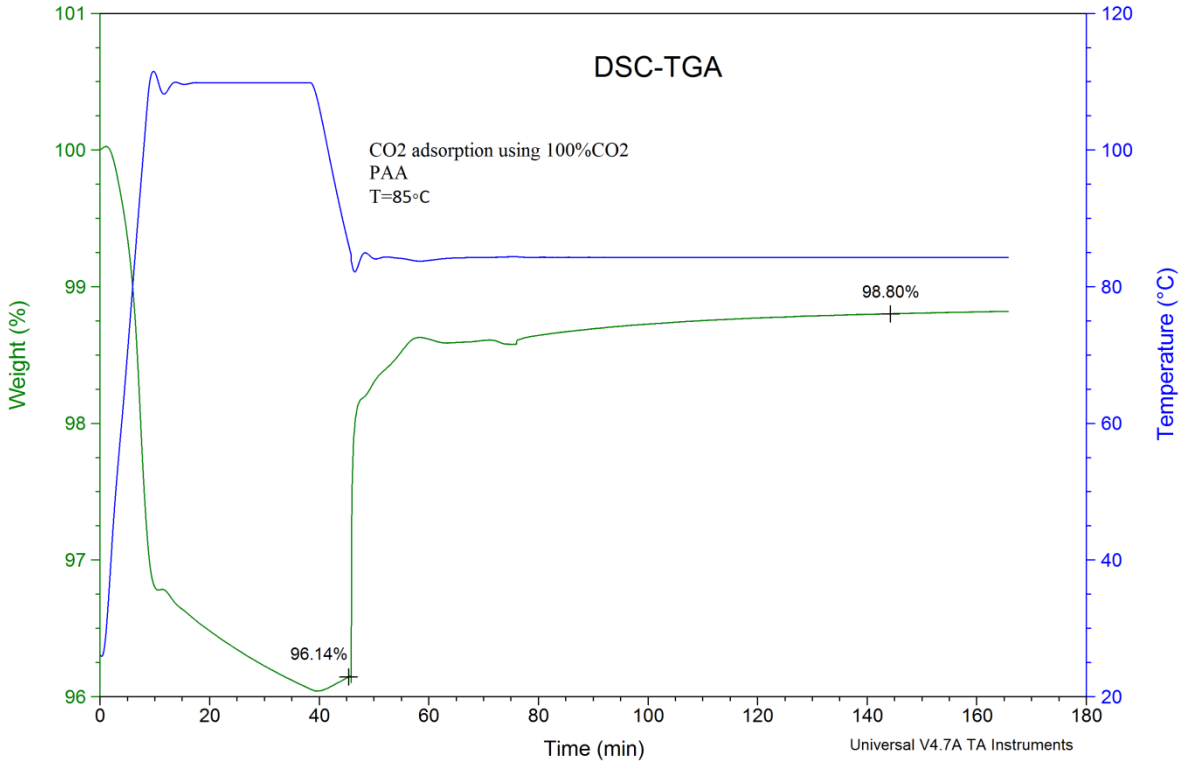

DSC-TGA
CO2 adsorption using 100%CO2
MWNT-PAA
T=65◦C
100.4%
96.00%
Weight (%)
Temperature (°C)
Time (min)
Universal V4.7A TA Instrumentsts

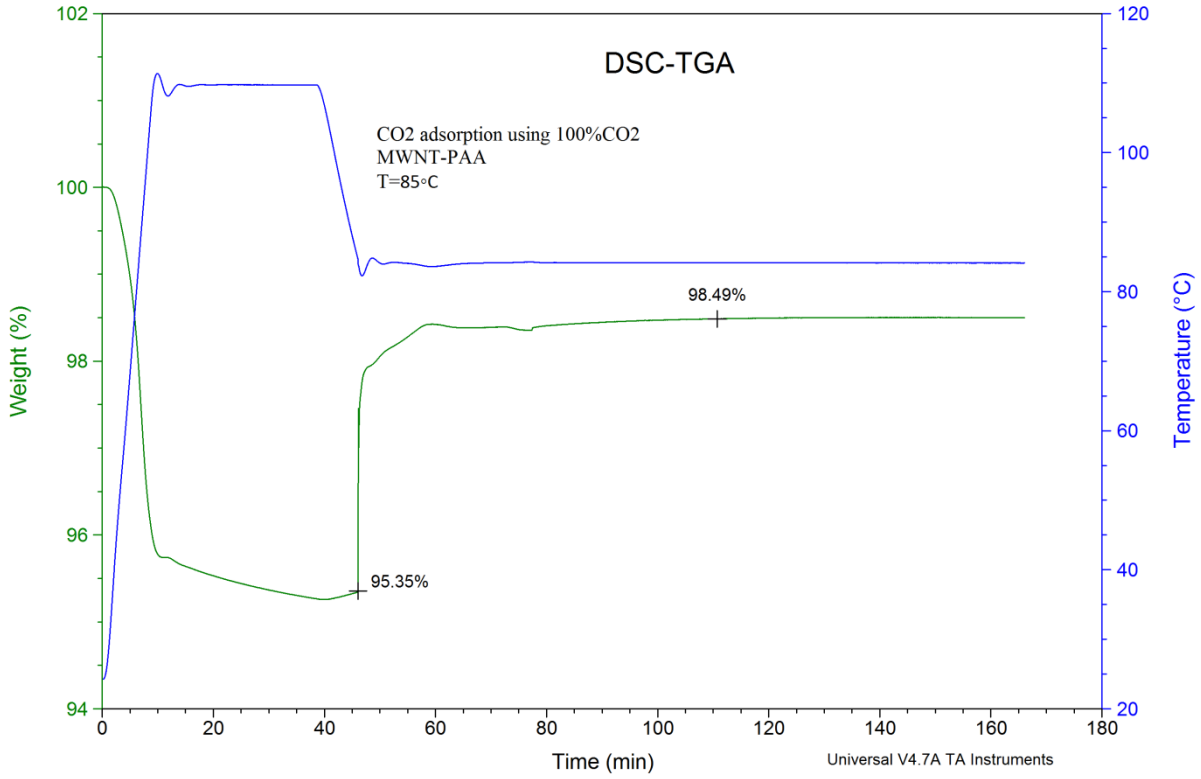

DSC-TGA
100.4%
CO2 adsorption using 100%CO2
PSI
T=75◦C
99.38%
Weight (%)
Temperature (°C)
Time (min)
Universal V4.7A TA Instrumentsts


DSC-TGA
CO2 adsorption using 100%CO2
PAA
T=75◦C
98.87%
95.79%
Weight (%)
Temperature (°C)
Time (min)
Universal V4.7A TA Instruments


DSC-TGA
100.1%
CO2 adsorption using 100%CO2
MWNT-PAA
T=75◦C
96.21%
Weight (%)
Temperature (°C)
Time (min)
Universal V4.7A TA Instruments

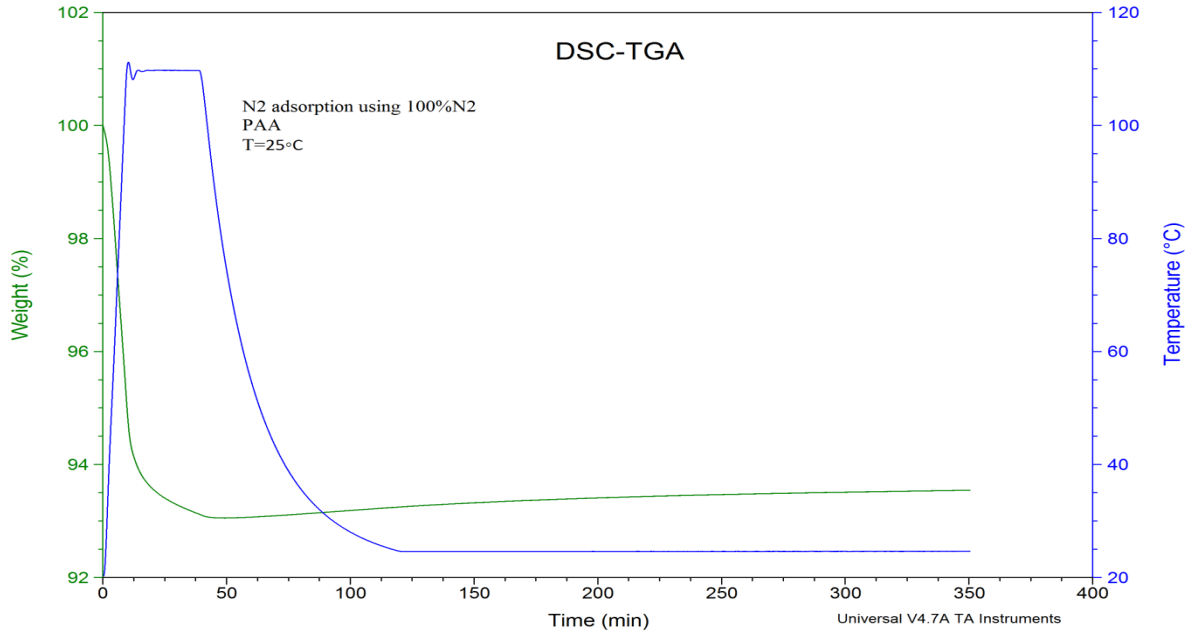

DSC-TGA
CO2 adsorption using 100%CO2
PSI
T=85◦C
98.76%
97.90%
Weight (%)
Temperature (°C)
Time (min)
Universal V4.7A TA Instruments

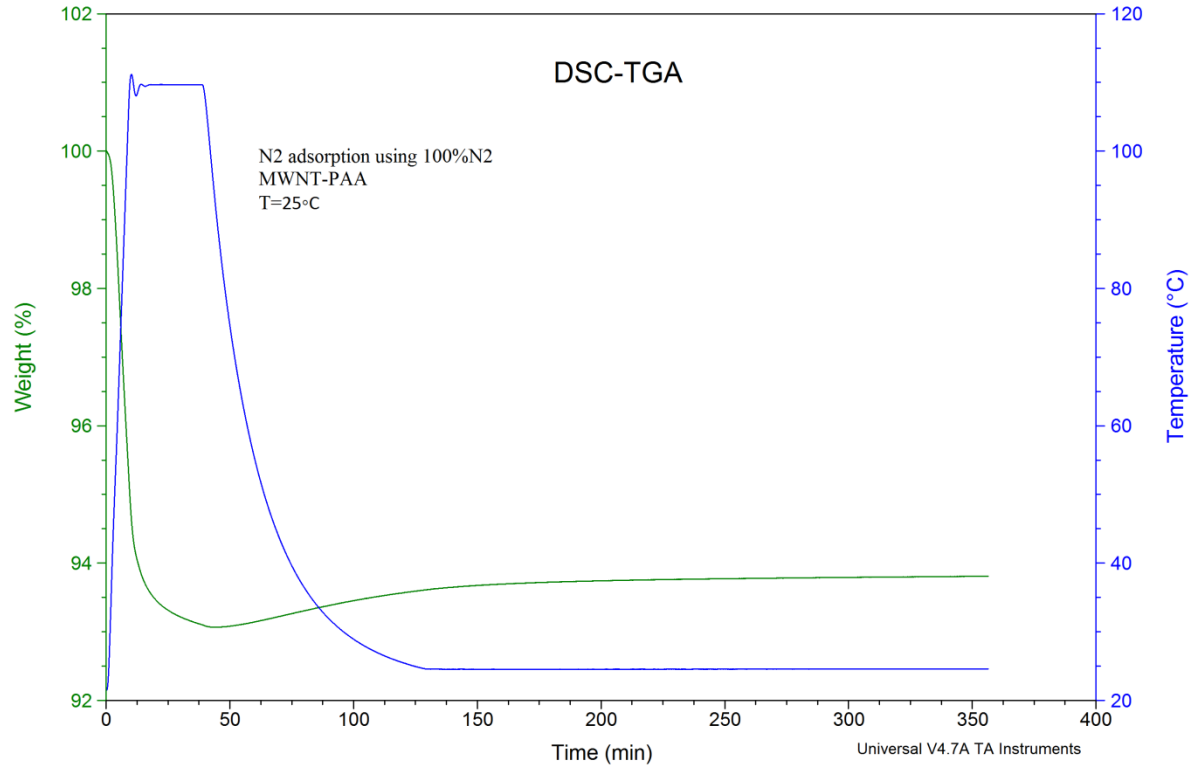

DSC-TGA
CO2 adsorption using 100%CO2
PAA
T=85◦C
98.80%
96.14%
Weight (%)
Temperature (°C)
Time (min)
Universal V4.7A TA Instruments

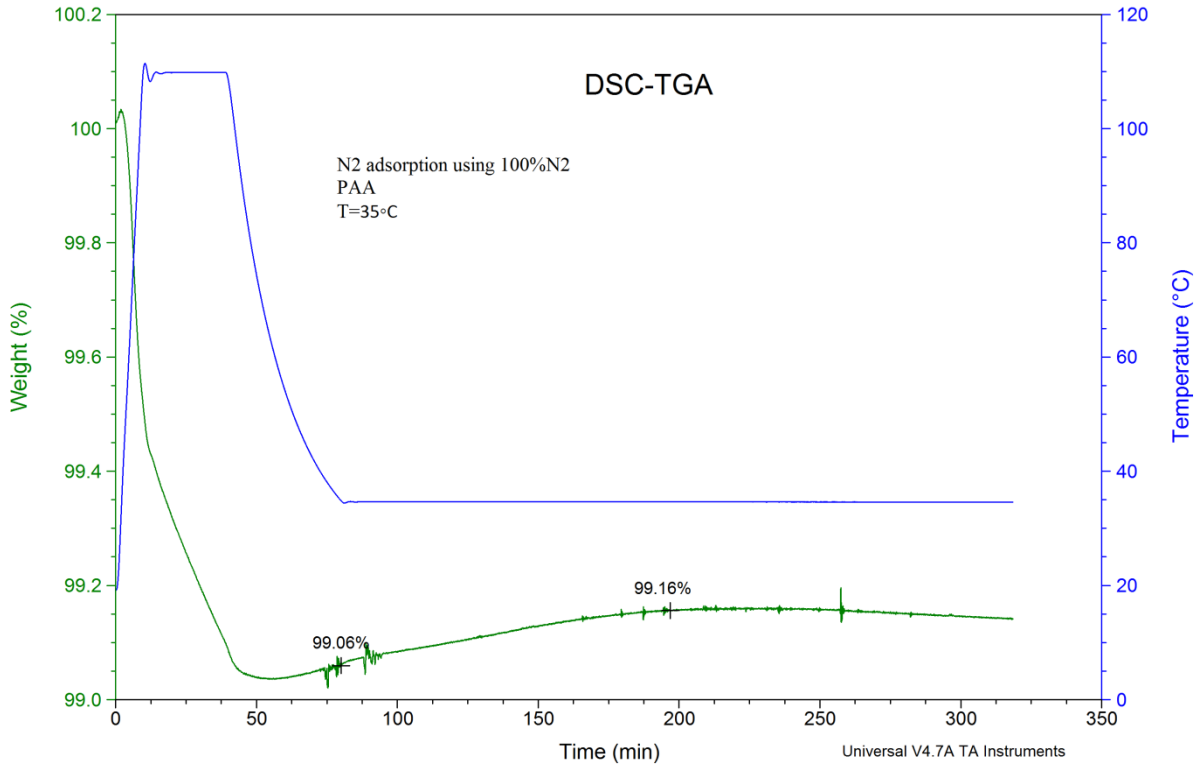

DSC-TGA
CO2 adsorption using 100%CO2
MWNT-PAA
T=85◦C
98.49%
95.35%
Weight (%)
Temperature (°C)
Time (min)
Universal V4.7A TA Instruments
102
100
98
96
94
120
100
80
60
40
20
0
20
40
60
80
100
120
140
160
180

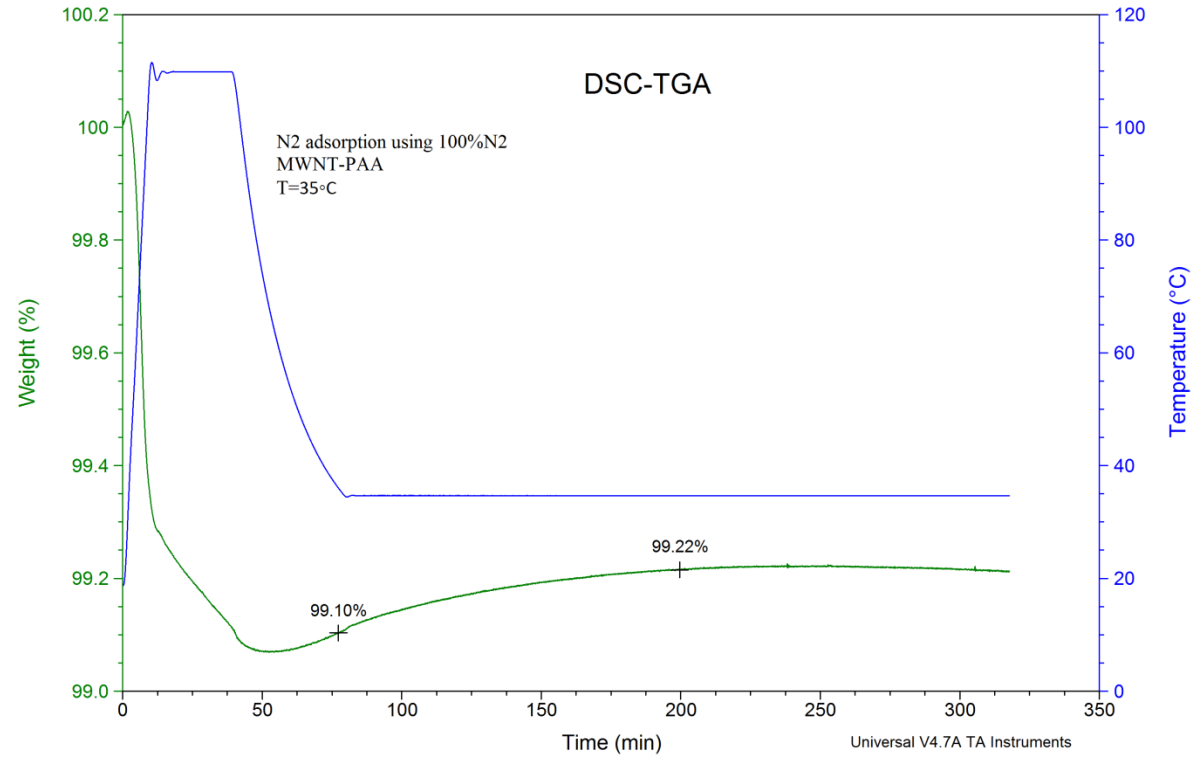
APPENDIX 2

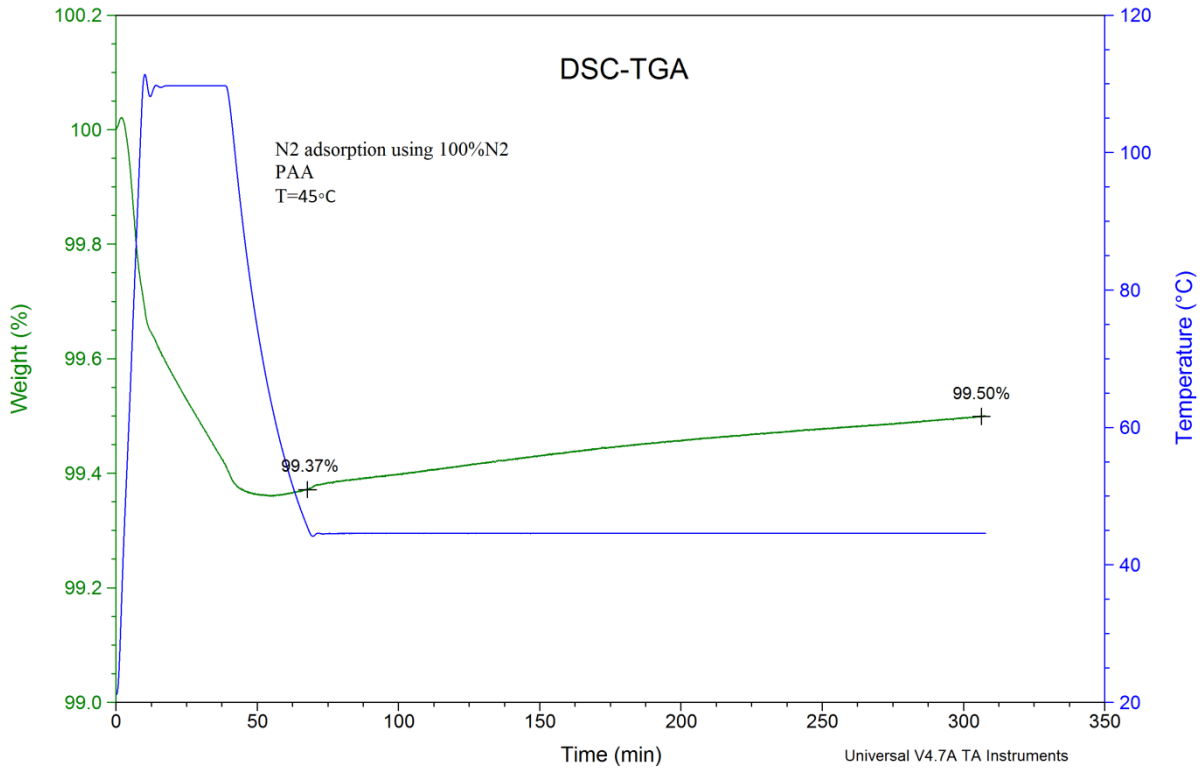
TGA GRAPHS OF N_2 ADSORPTION FOR DRY ADSORBENTS WITH 100% N_2

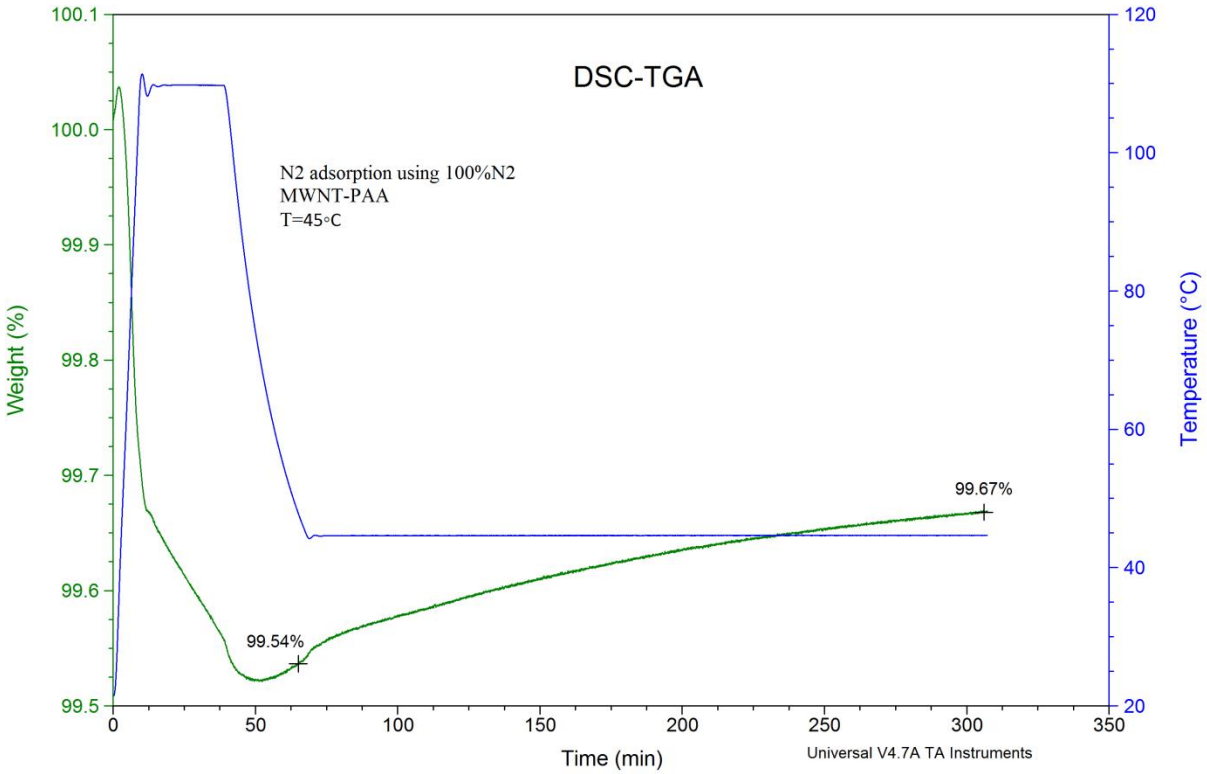


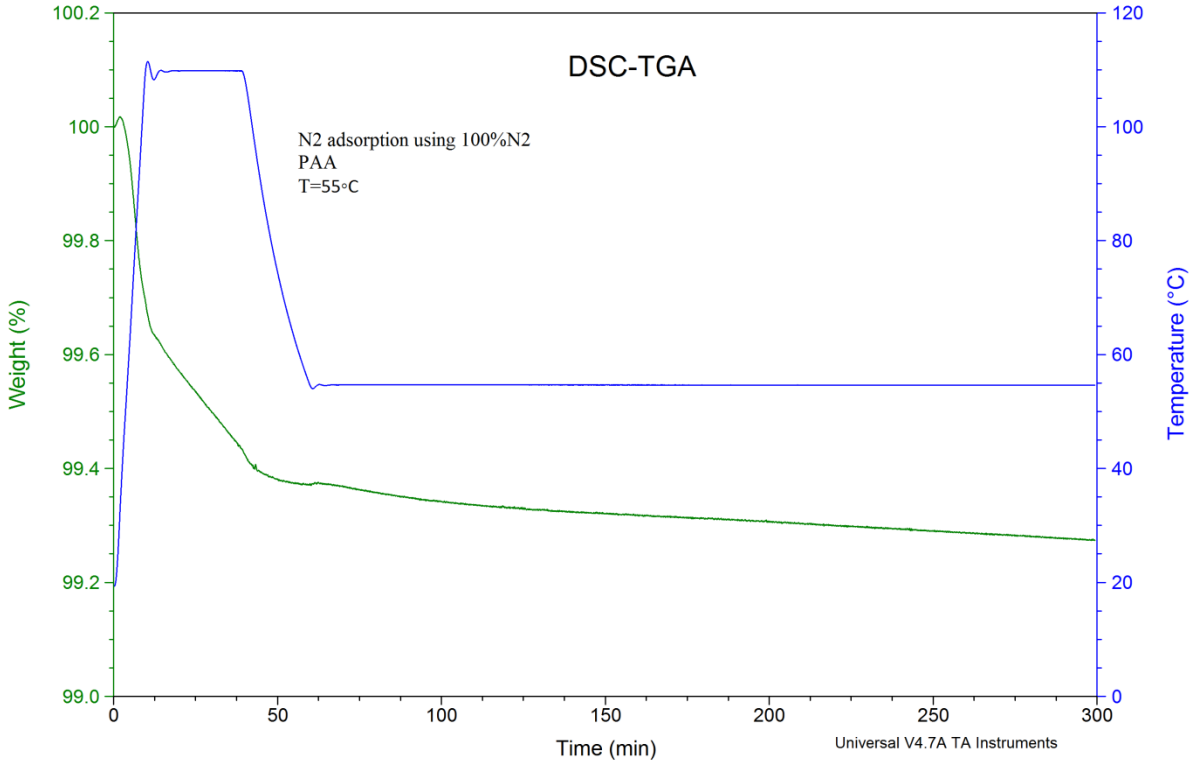


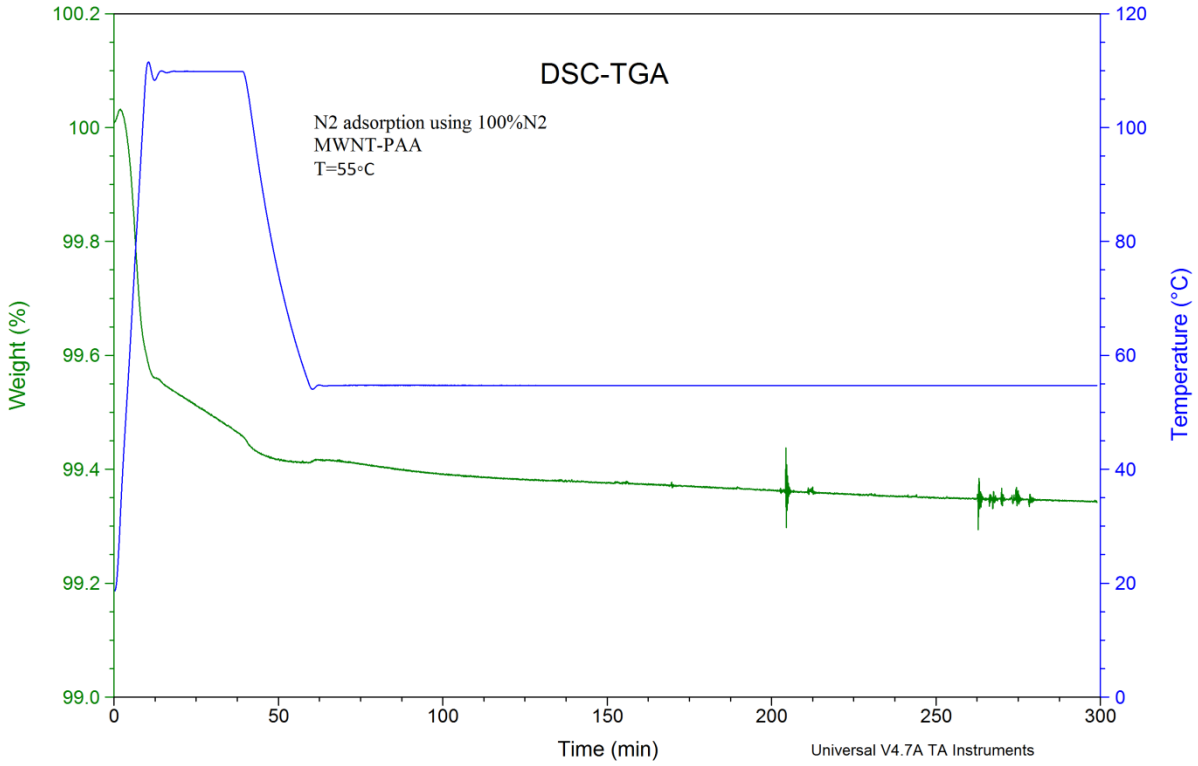

DSC-TGA
N2 adsorption using 100%N2
PAA
T=35◦C
99.16%
99.06%
Weight (%)
Temperature (°C)
Time (min)
Universal V4.7A TA Instruments


DSC-TGA
N2 adsorption using 100%N2
MWNT-PAA
T=35◦C
99.22%
99.10%
Weight (%)
Temperature (°C)
Time (min)
Universal V4.7A TA Instruments


DSC-TGA
N2 adsorption using 100%N2
PAA
T=45◦C
99.37%
99.50%
Weight (%)
Temperature (°C)
Time (min)
Universal V4.7A TA Instruments

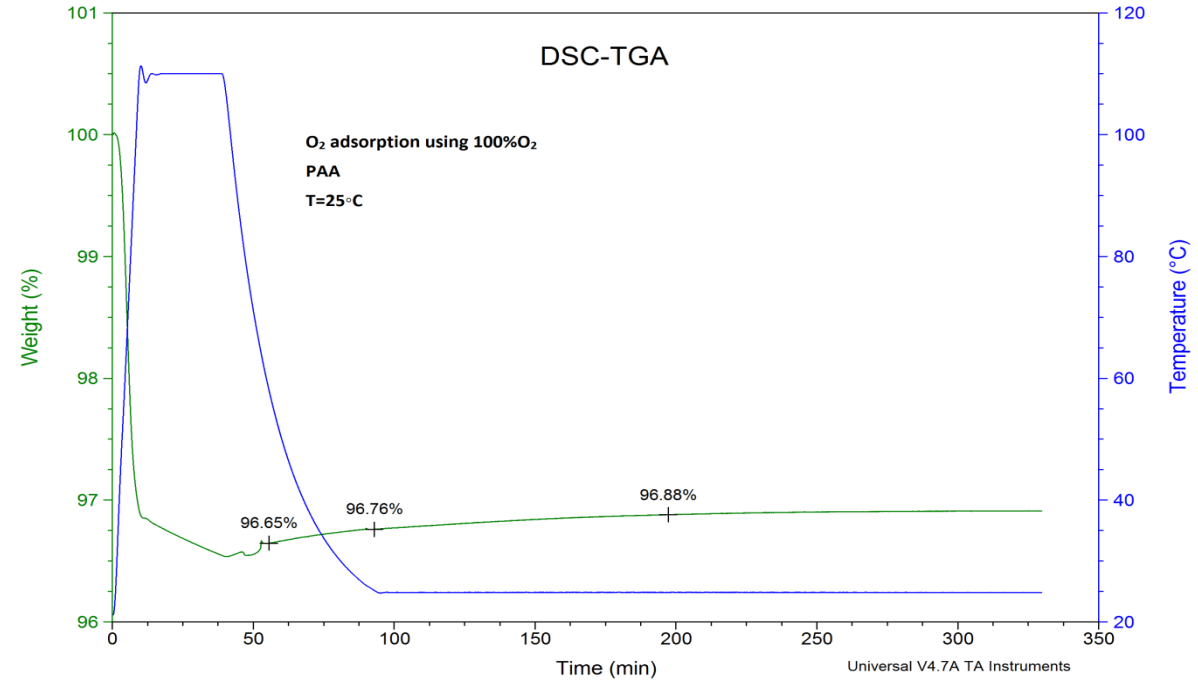

DSC-TGA
N2 adsorption using 100%N2
MWNT-PAA
T=45◦C
99.54%
99.67%
Weight (%)
Temperature (°C)
Time (min)
Universal V4.7A TA Instruments

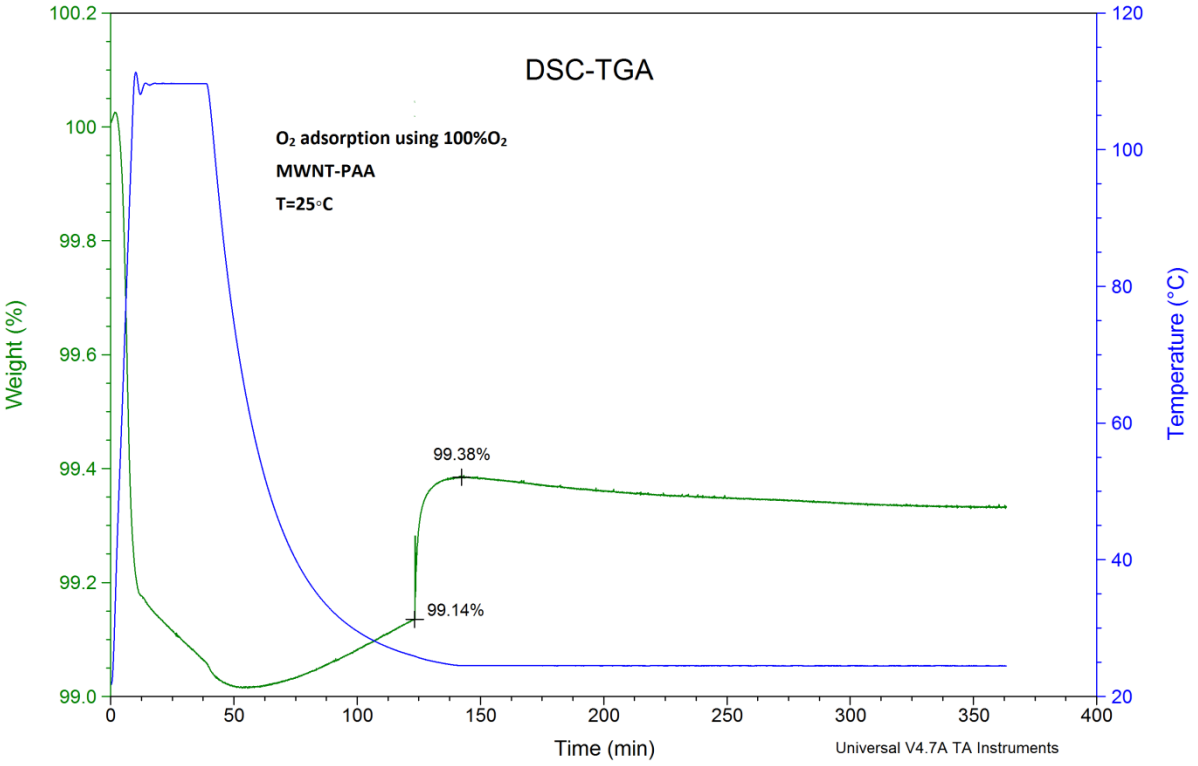

DSC-TGA
N2 adsorption using 100%N2
PAA
T=55◦C
Weight (%)
Temperature (°C)
Time (min)
Universal V4.7A TA Instruments

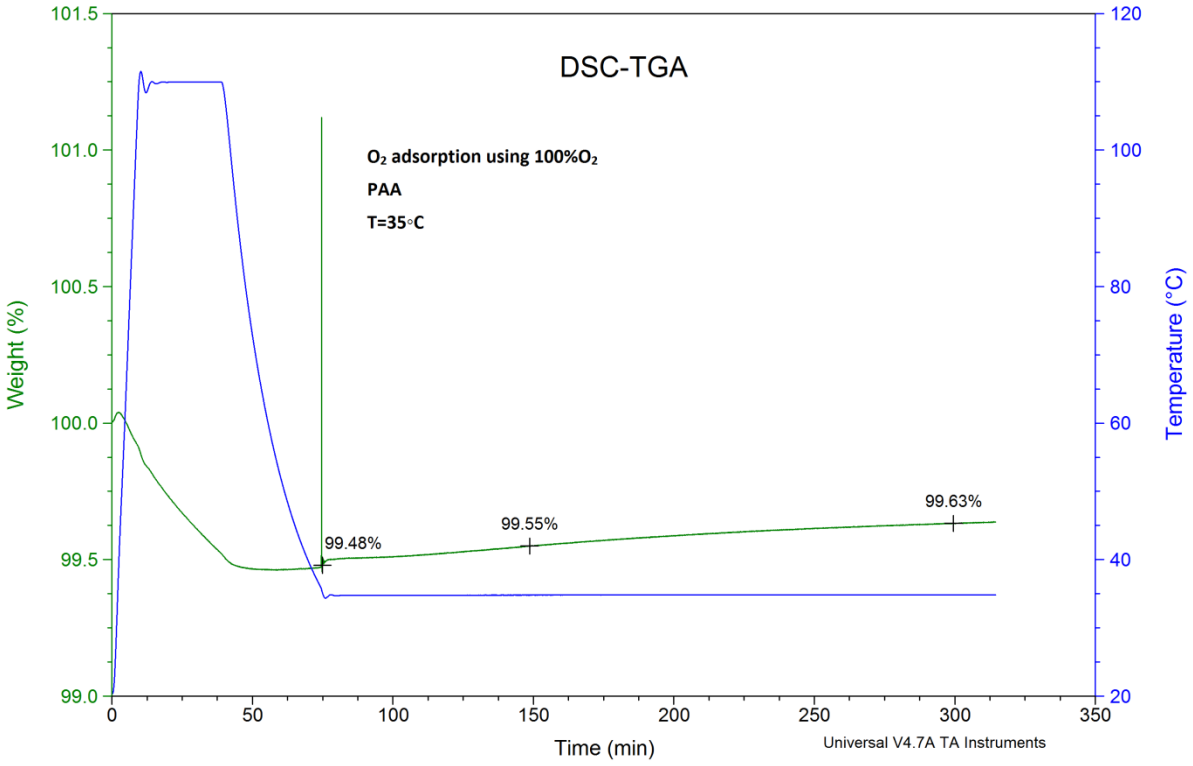

DSC-TGA
N2 adsorption using 100%N2
MWNT-PAA
T=55◦C
Weight (%)
Temperature (°C)
Time (min)
Universal V4.7A TA Instruments

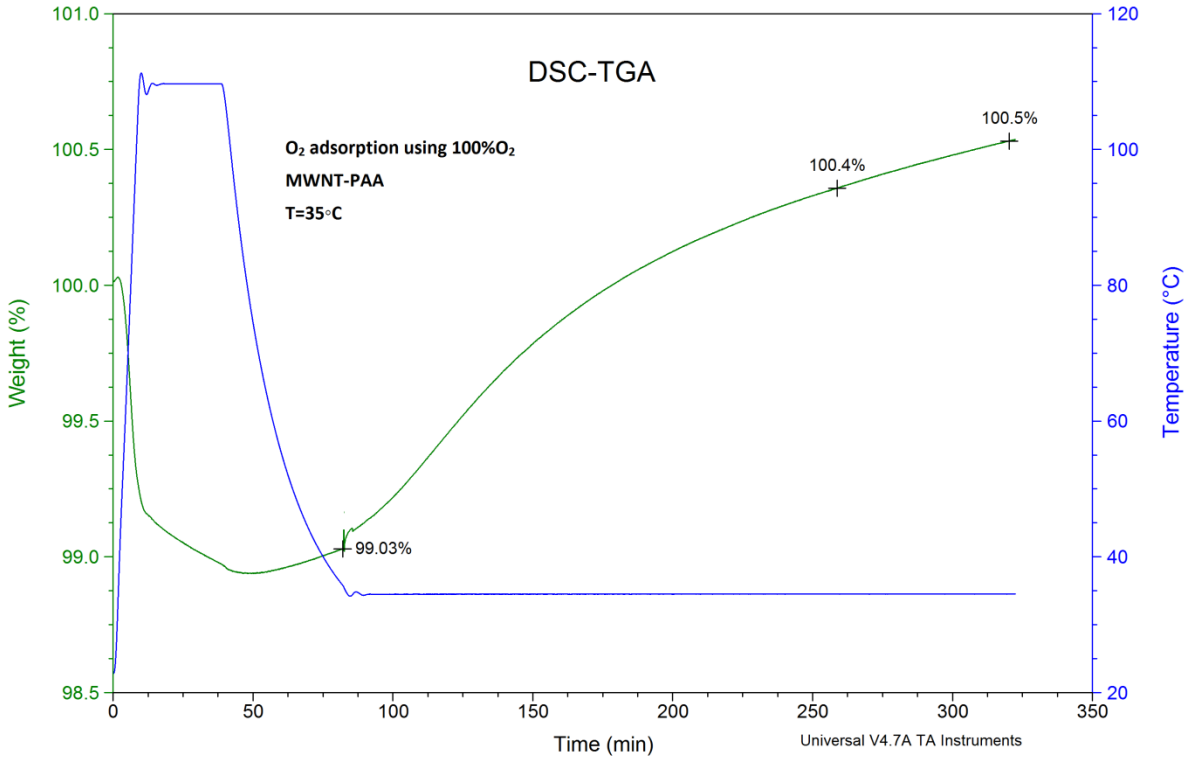
APPENDIX 3

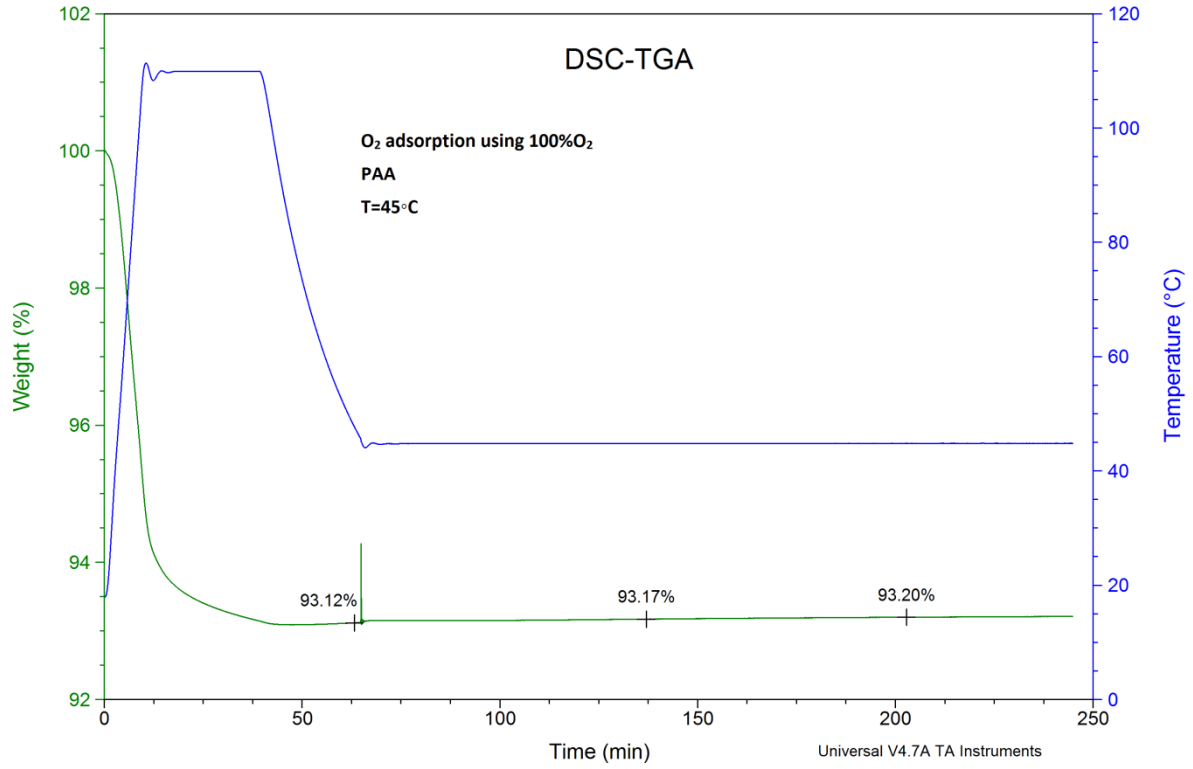
TGA GRAPHS OF O_2 ADSORPTION FOR DRY ADSORBENTS WITH 100% O_2

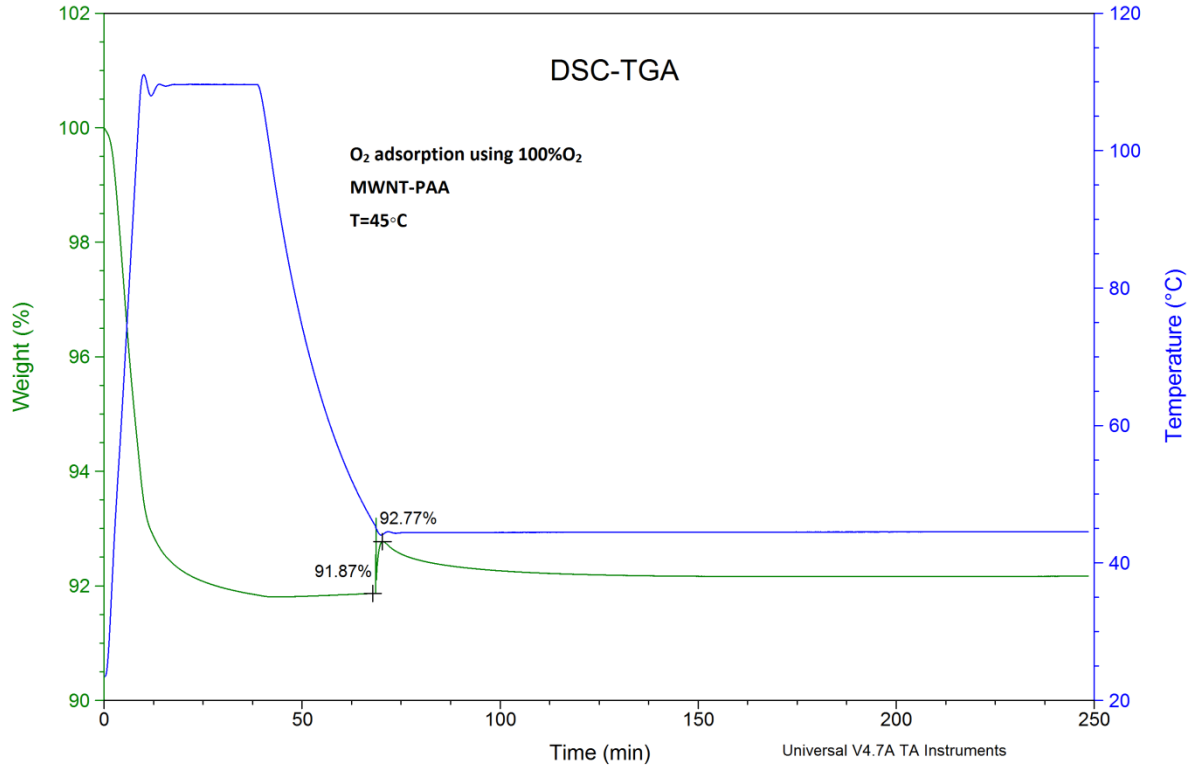


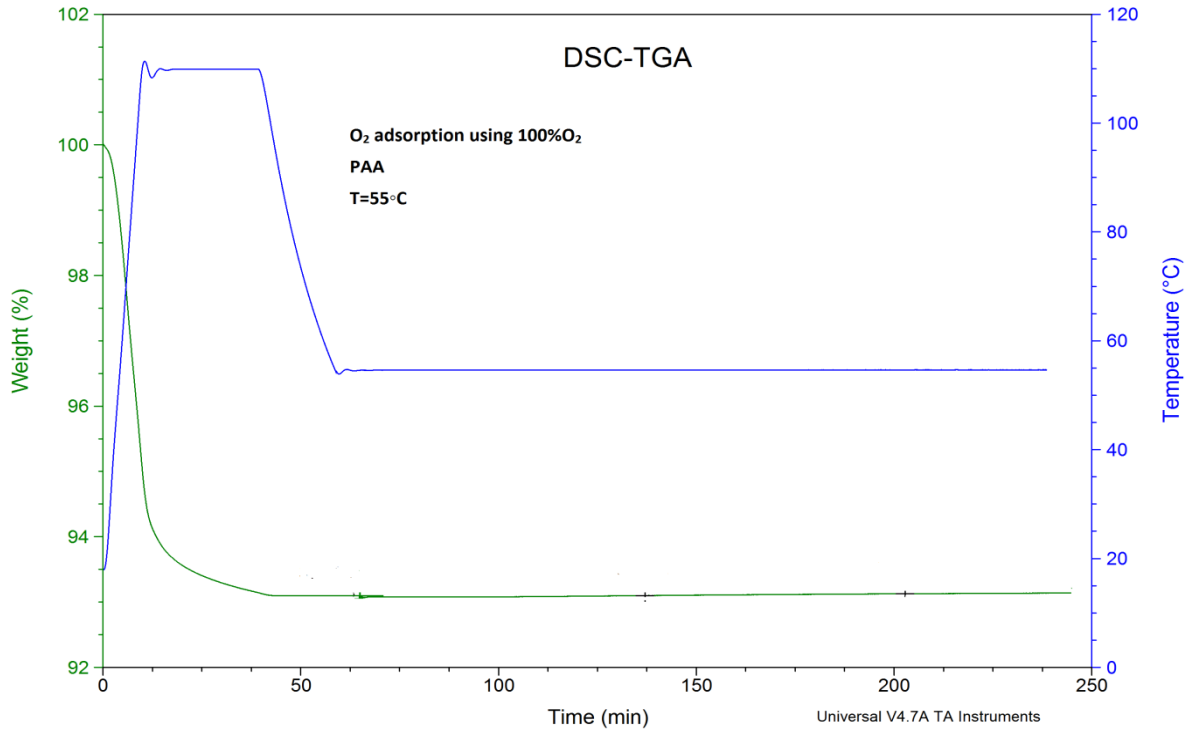


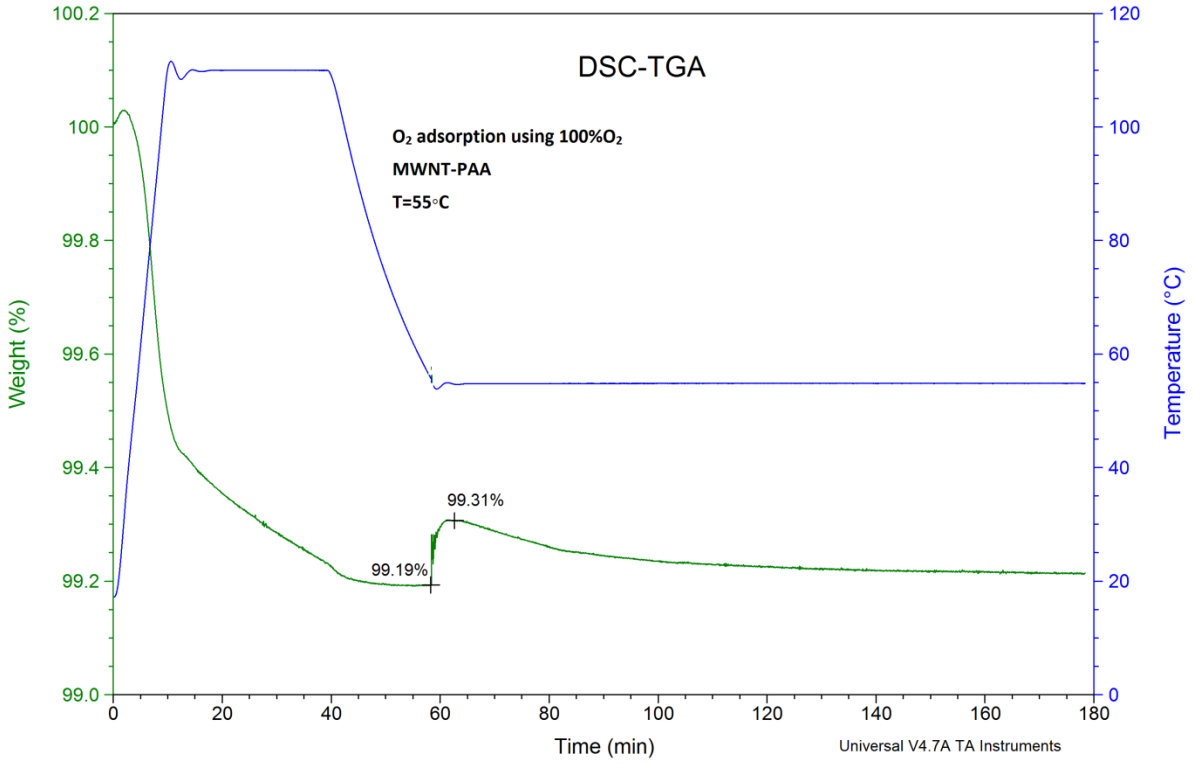

DSC-TGA
O2 adsorption using 100%O2
PAA
T=35◦C
99.48%
99.55%
99.63%
Weight (%)
Temperature (°C)
Time (min)
Universal V4.7A TA Instrumentsl


DSC-TGA
O2 adsorption using 100%O2
MWNT-PAA
T=35◦C
99.03%
100.4%
100.5%
Weight (%)
Temperature (°C)
Time (min)
Universal V4.7A TA Instruments


DSC-TGA
O2 adsorption using 100%O2
PAA
T=45◦C
93.12%
93.17%
93.20%
Weight (%)
Temperature (°C)
Time (min)
Universal V4.7A TA Instrumentsl

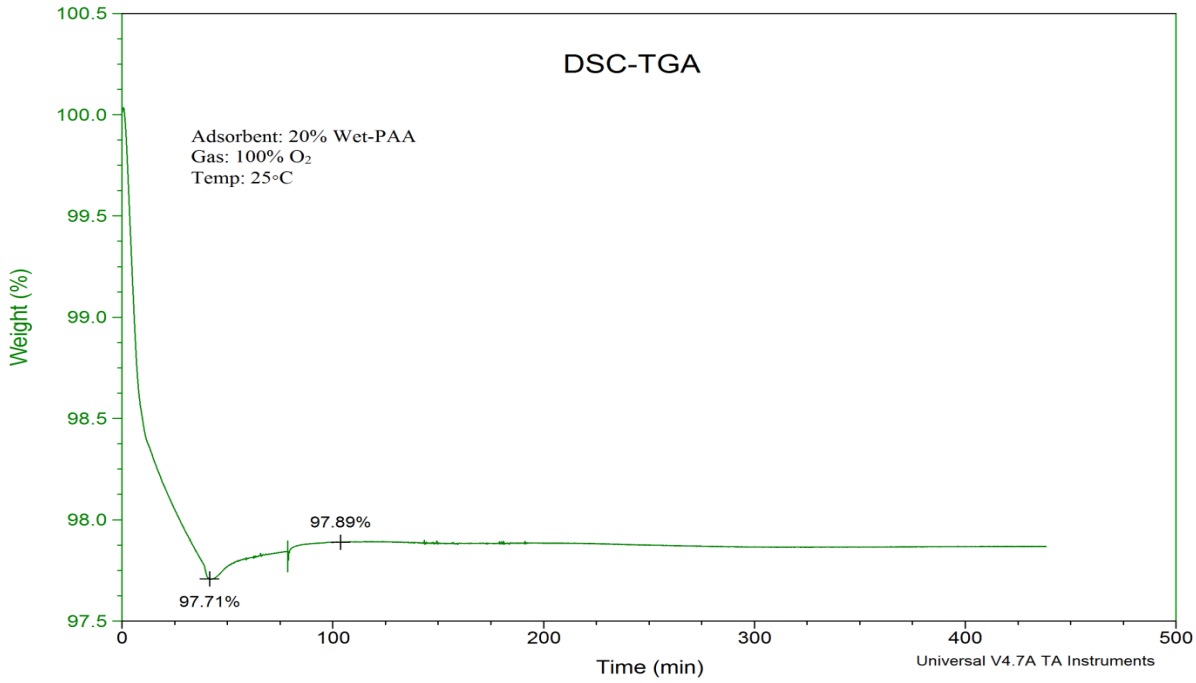

DSC-TGA
O2 adsorption using 100%O2
MWNT-PAA
T=45◦C
92.77%
91.87%
Weight (%)
Temperature (°C)
Time (min)
Universal V4.7A TA Instruments

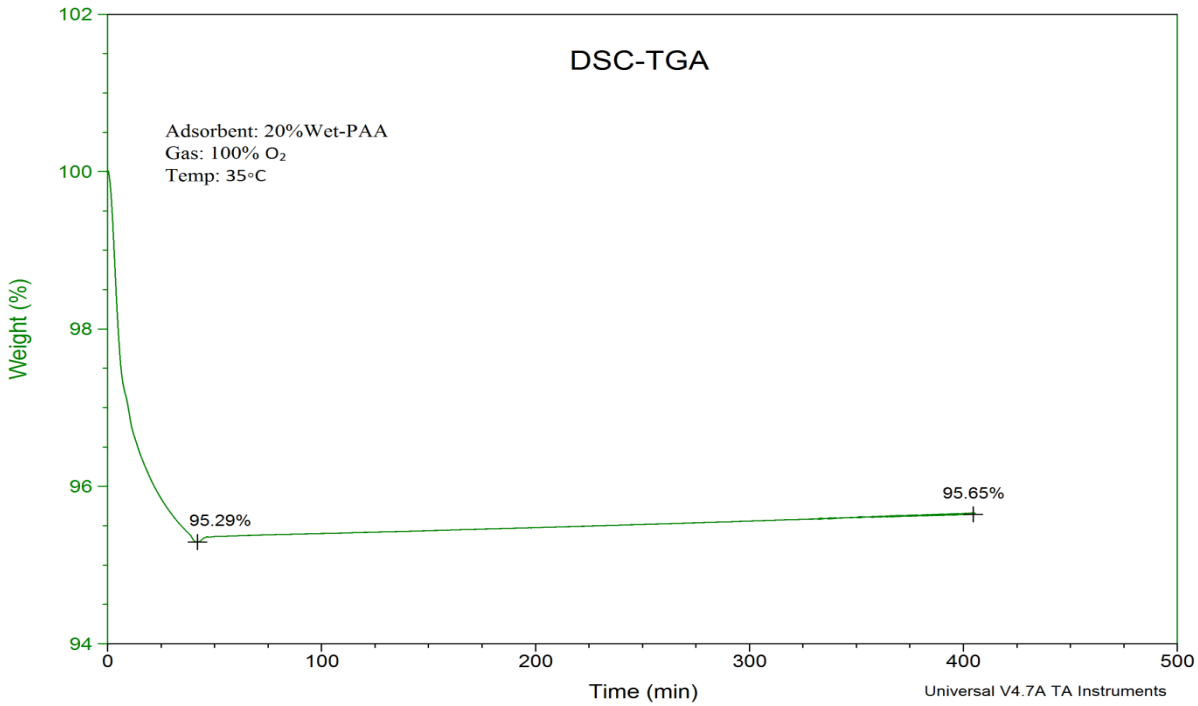

DSC-TGA
O_2 adsorption using 100%O_2
PAA
T=55°C
Weight (%)
Temperature (°C)
Time (min)
Universal V4.7A TA Instruments

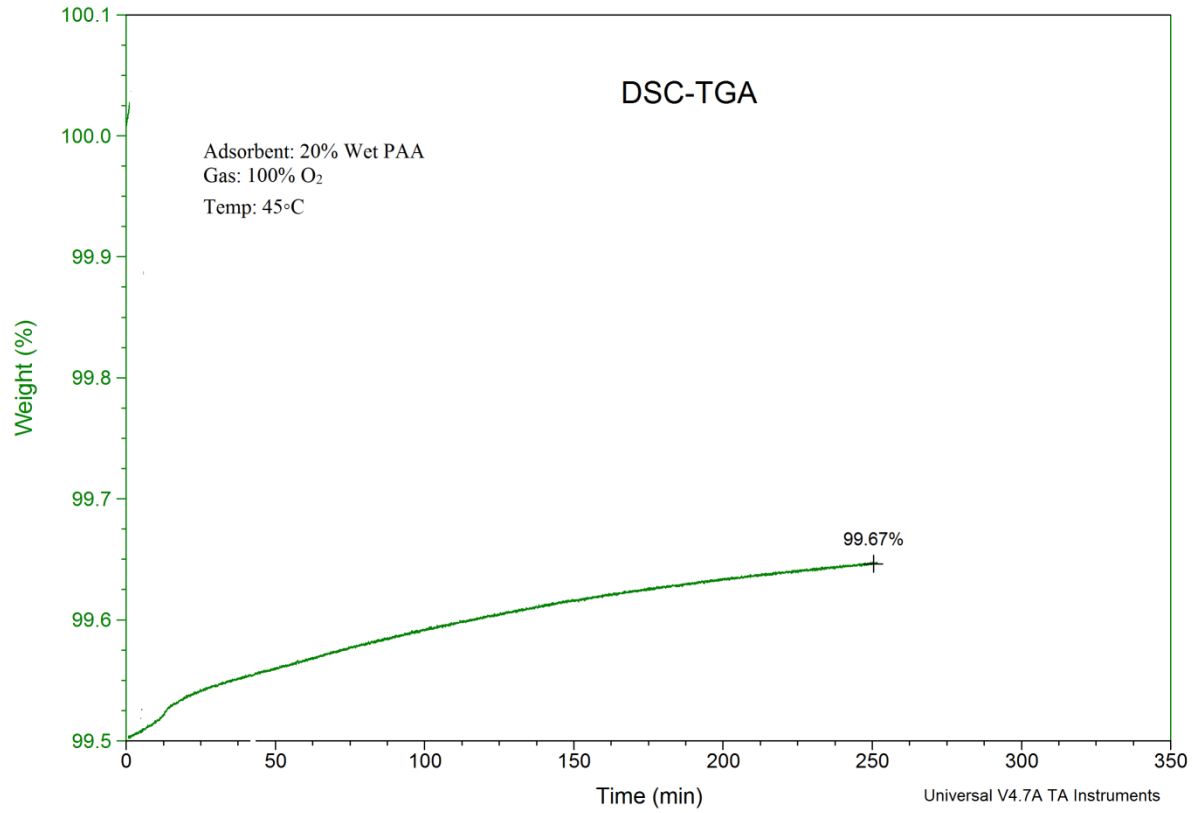

DSC-TGA
O_2 adsorption using 100%O_2
MWNT-PAA
T=55°C
99.31%
99.19%
Weight (%)
Temperature (°C)
Time (min)
Universal V4.7A TA Instruments

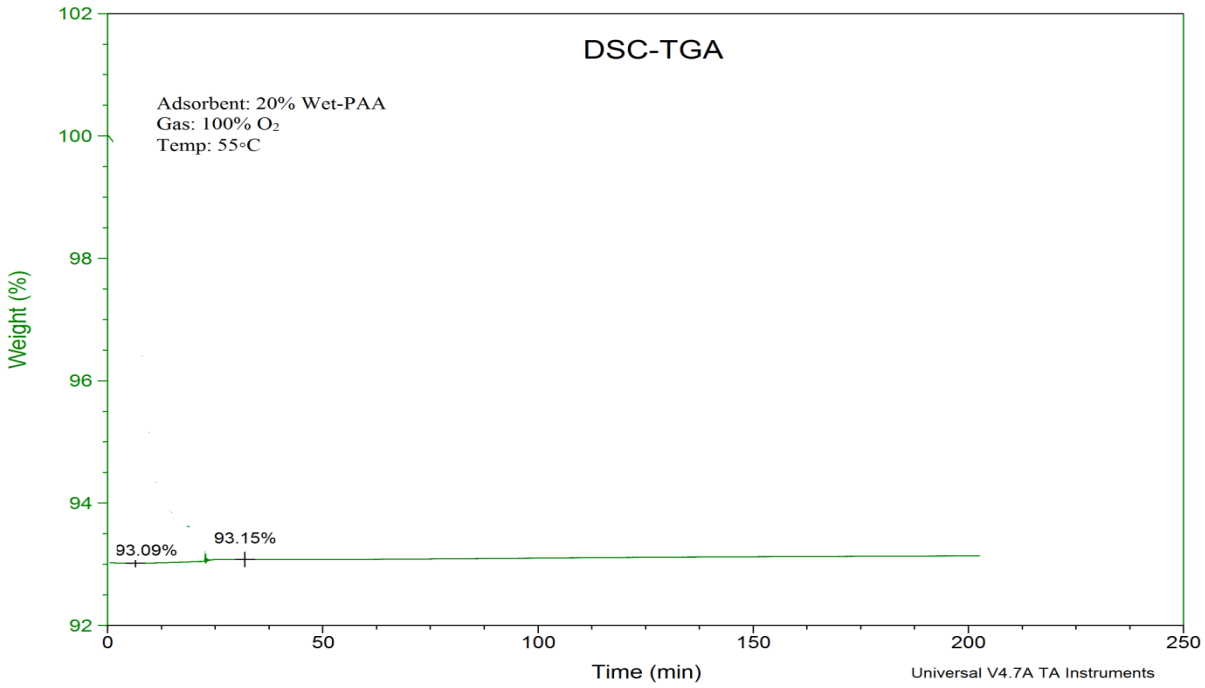
APPENDIX 4

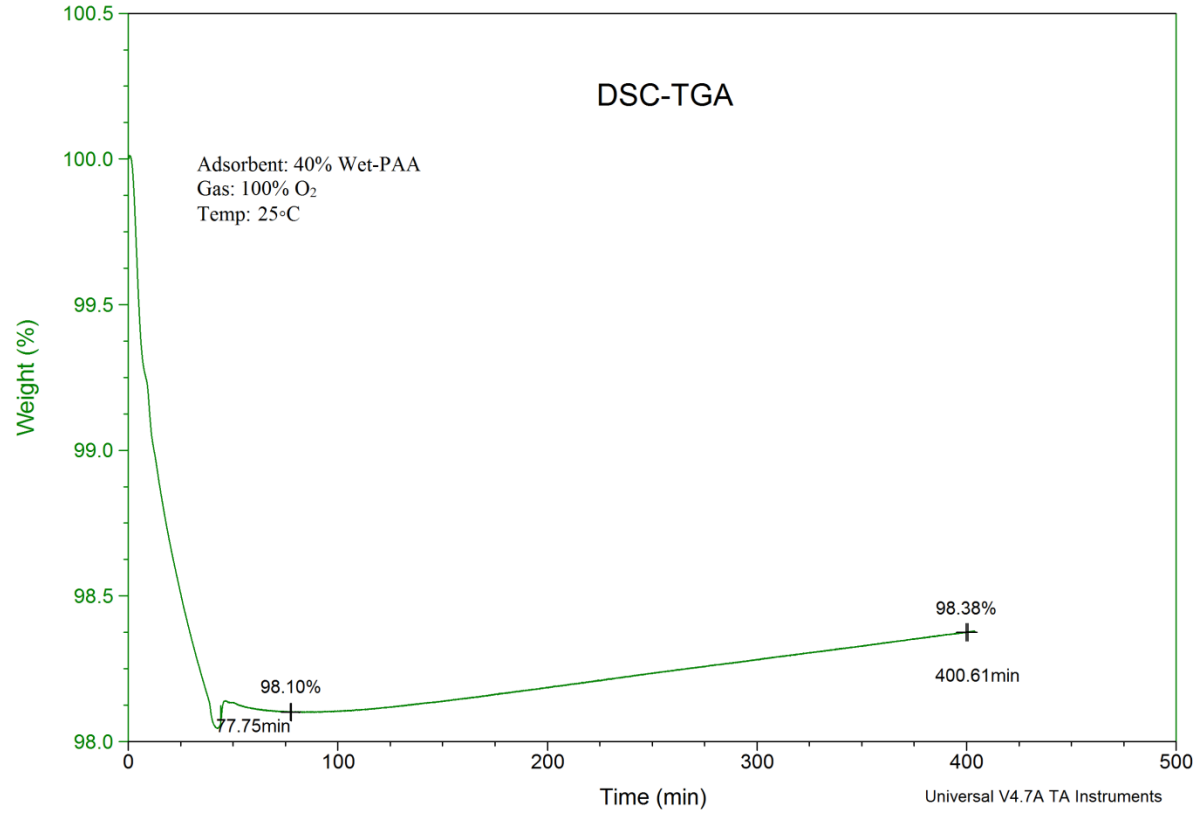
TGA GRAPHS OF O_2 ADSORPTION FOR MOIST ADSORBENT WITH 100% O_2

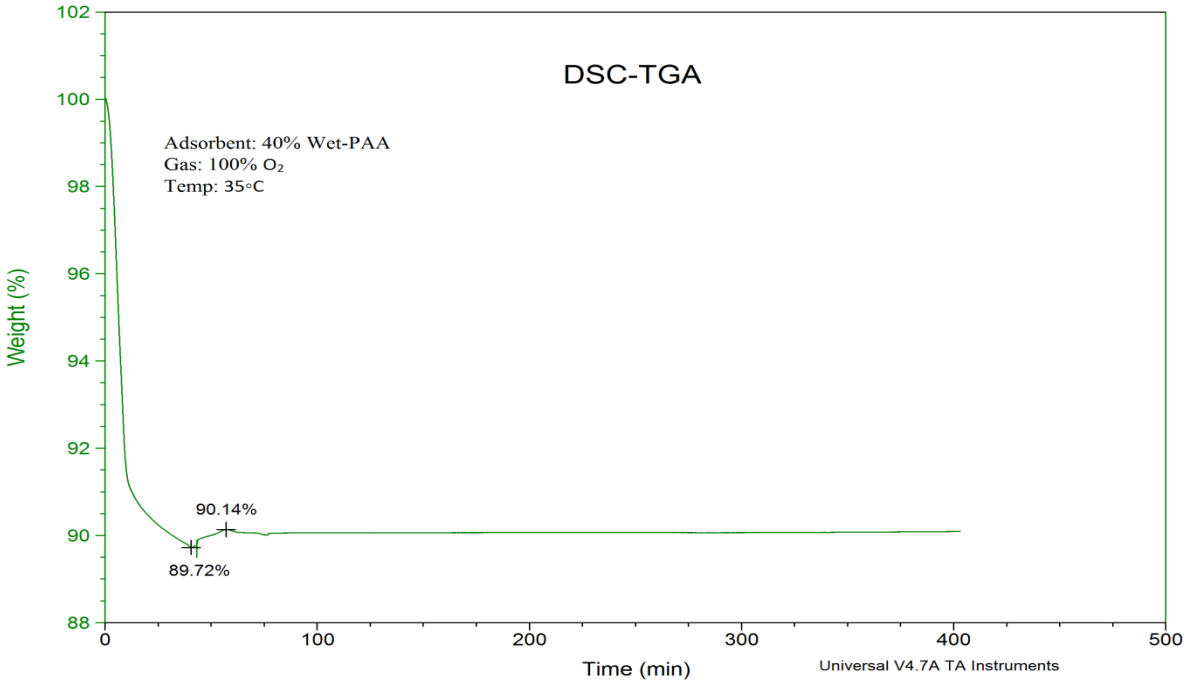


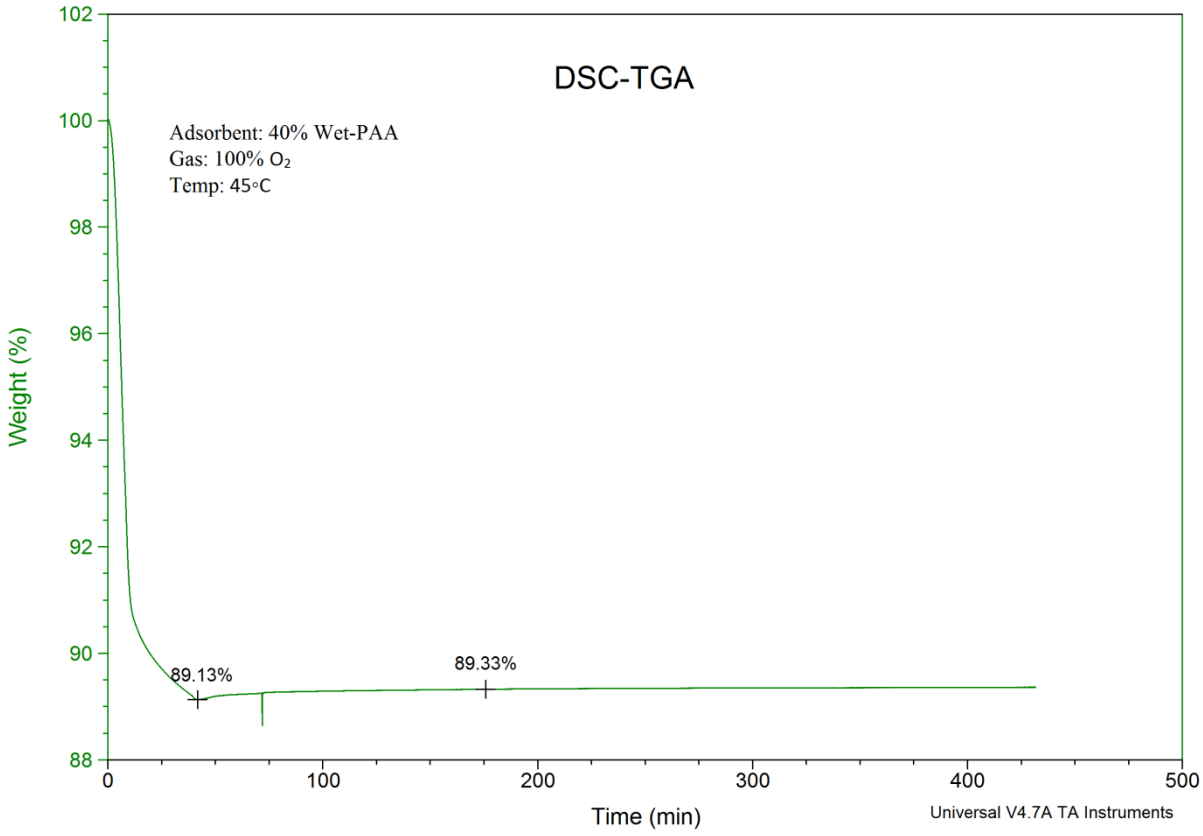


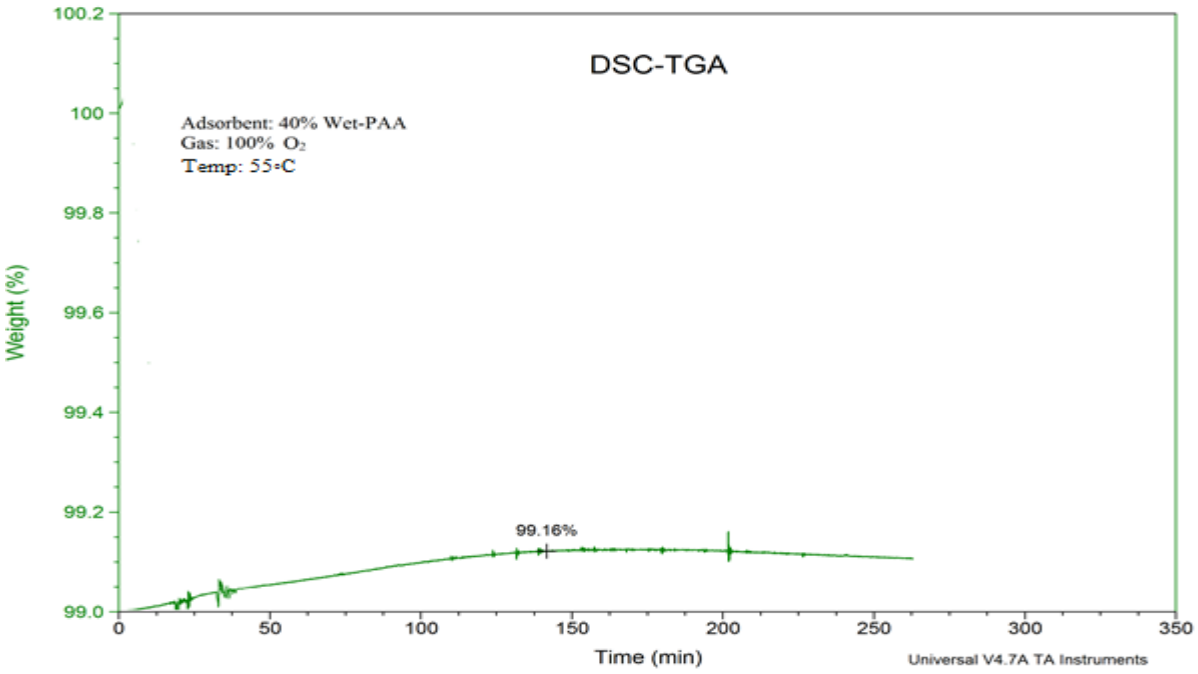

DSC-TGA
Adsorbent: 20% Wet PAA
Gas: 100% O2
Temp: 45◦C
Weight (%)
Time (min)
99.67%
Universal V4.7A TA Instrumentsn

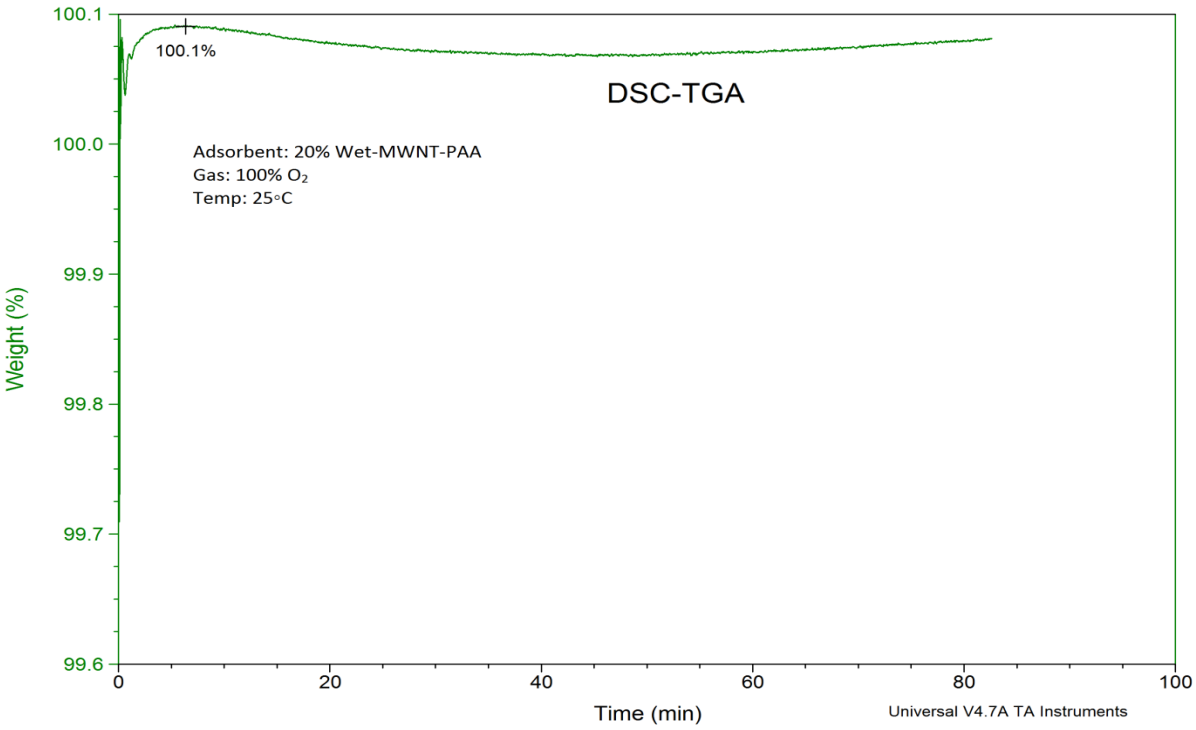

DSC-TGA
Adsorbent: 20% Wet-PAA
Gas: 100% O2
Temp: 55◦C
Weight (%)
Time (min)
93.09%
93.15%
Universal V4.7A TA Instruments

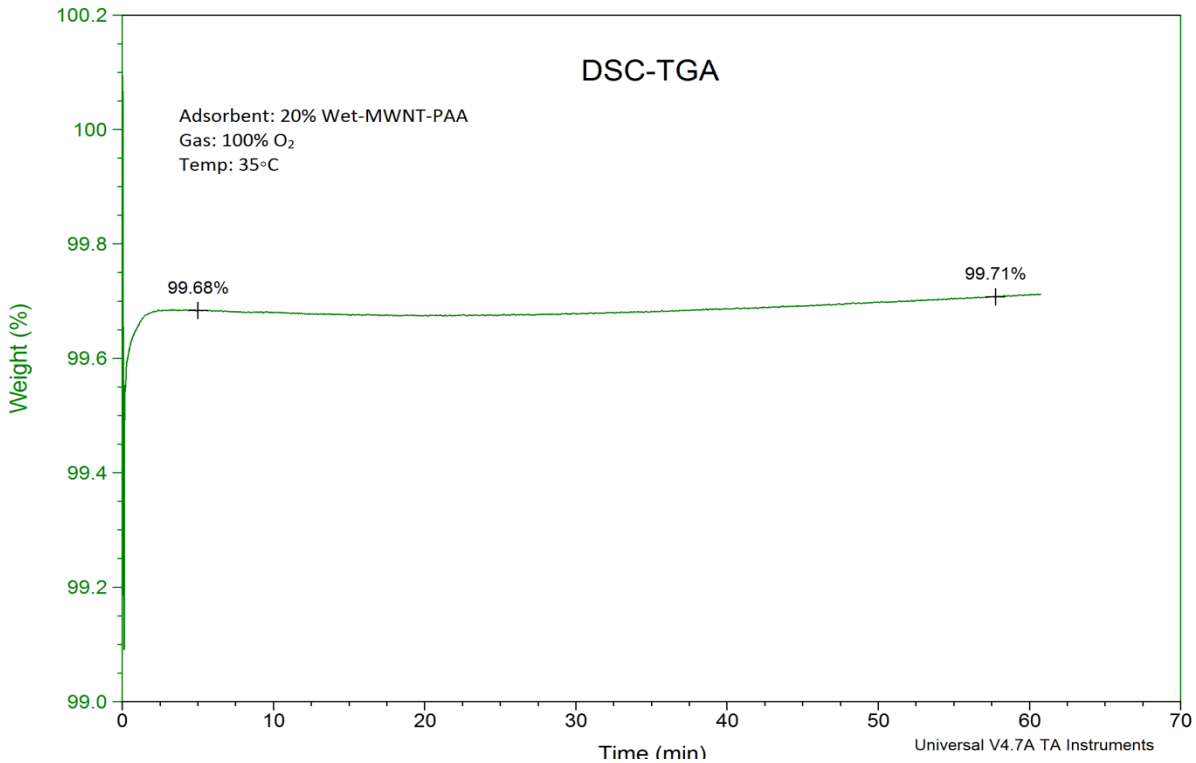

DSC-TGA
Adsorbent: 40% Wet-PAA
Gas: 100% O2
Temp: 25◦C
Weight (%)
Time (min)
98.38%
400.61min
98.10%
77.75min
Universal V4.7A TA Instruments

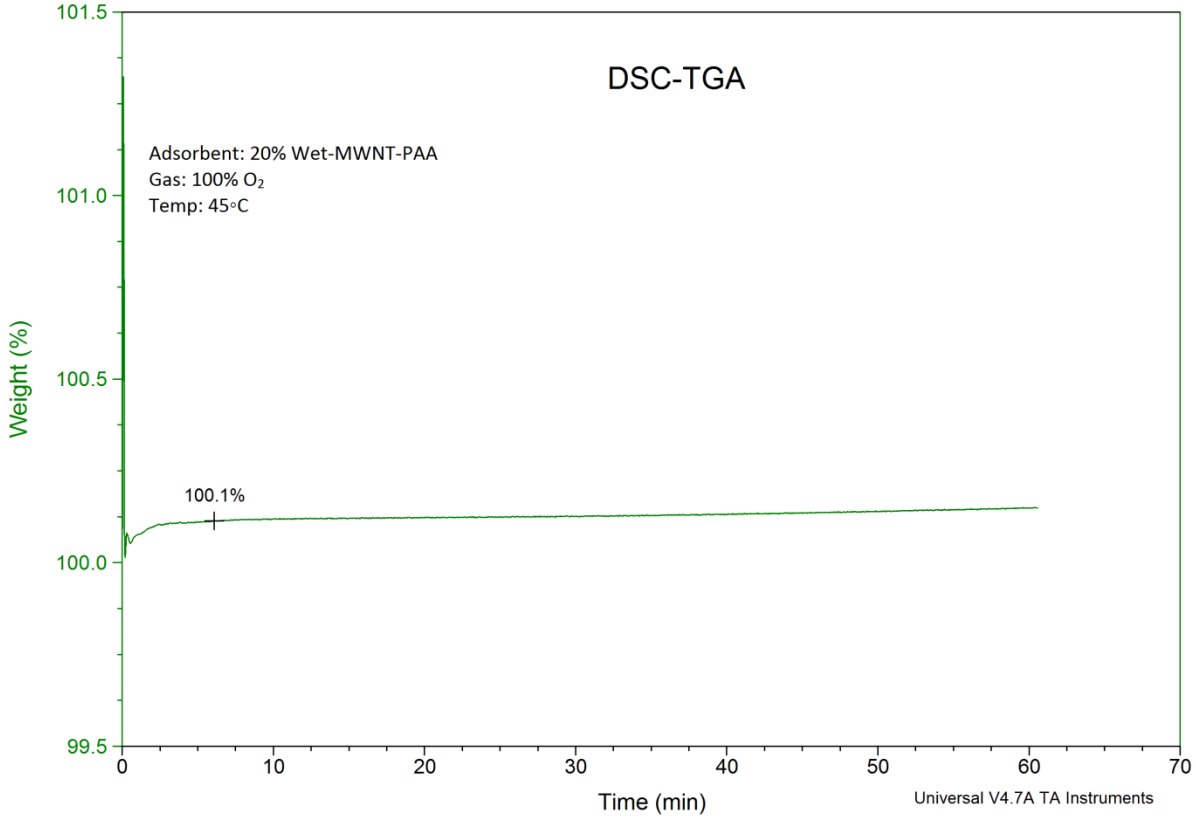

DSC-TGA
Adsorbent: 40% Wet-PAA
Gas: 100% O2
Temp: 35◦C
Weight (%)
Time (min)
90.14%
89.72%
Universal V4.7A TA Instruments

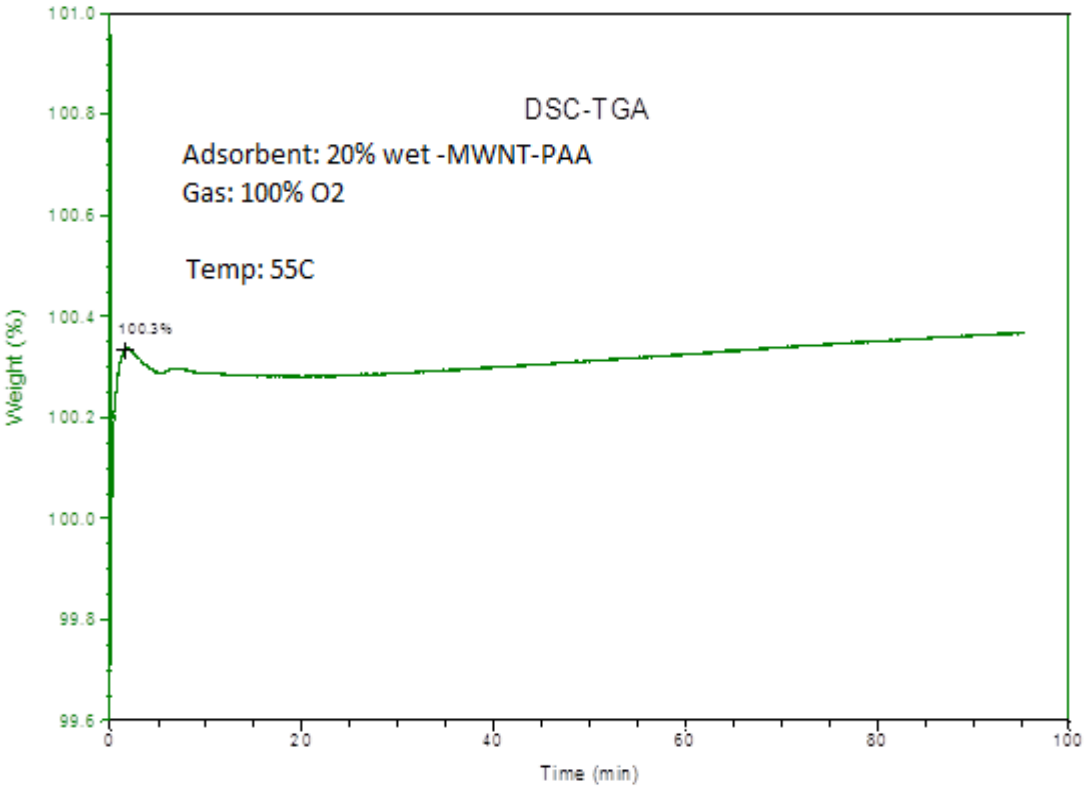

DSC-TGA
Adsorbent: 40% Wet-PAA
Gas: 100% O2
Temp: 45◦C
Weight (%)
102
100
98
96
94
92
90
88
89.13%
89.33%
0
100
200
300
400
500
Time (min)
Universal V4.7A TA Instruments

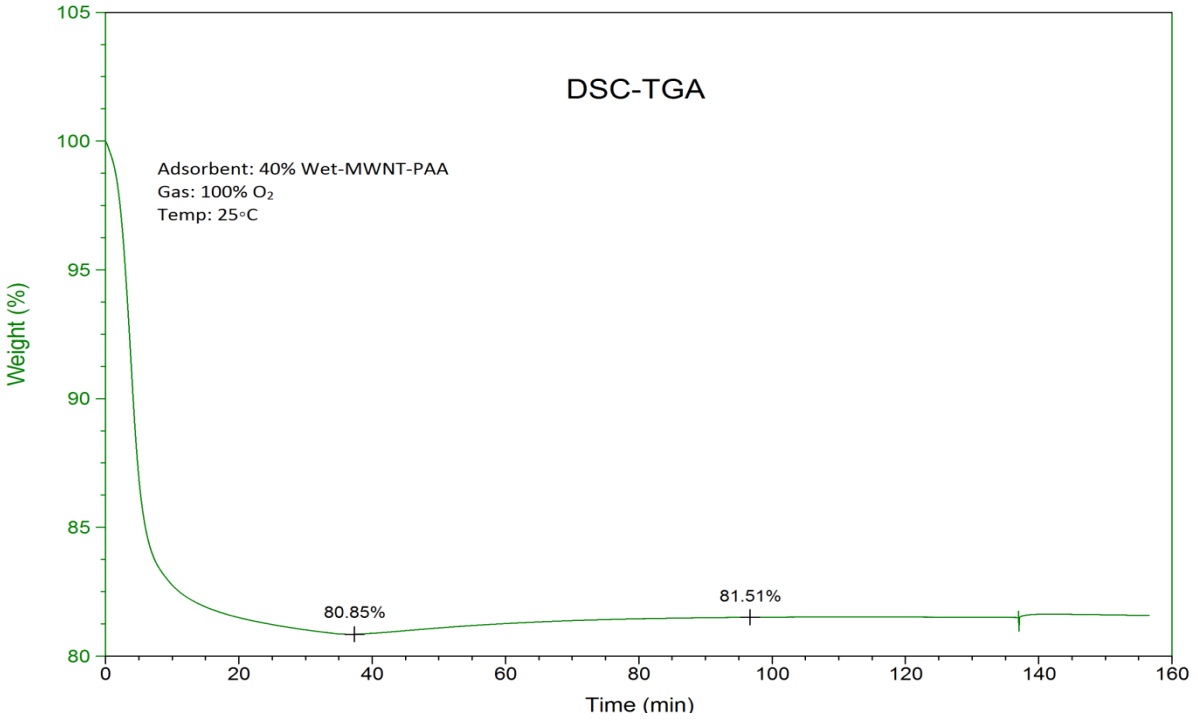

DSC-TGA
Adsorbent: 40% Wet-PAA
Gas: 100% O2
Temp: 55◦C
Weight (%)
100.2
100
99.8
99.6
99.4
99.2
99.0
99.16%
0
50
100
150
200
250
300
350
Time (min)
Universal V4.7A TA Instruments

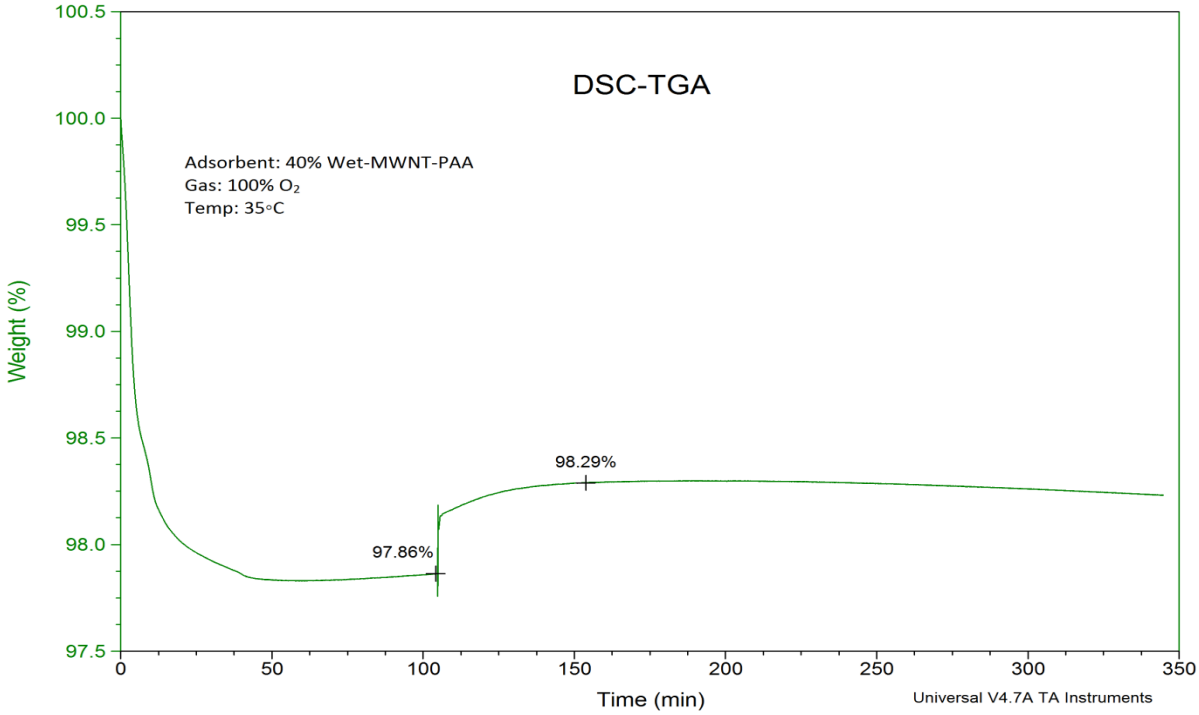

DSC-TGA
Adsorbent: 20% Wet-MWNT-PAA
Gas: 100% O2
Temp: 25◦C
100.1%
Weight (%)
Time (min)
Universal V4.7A TA Instruments

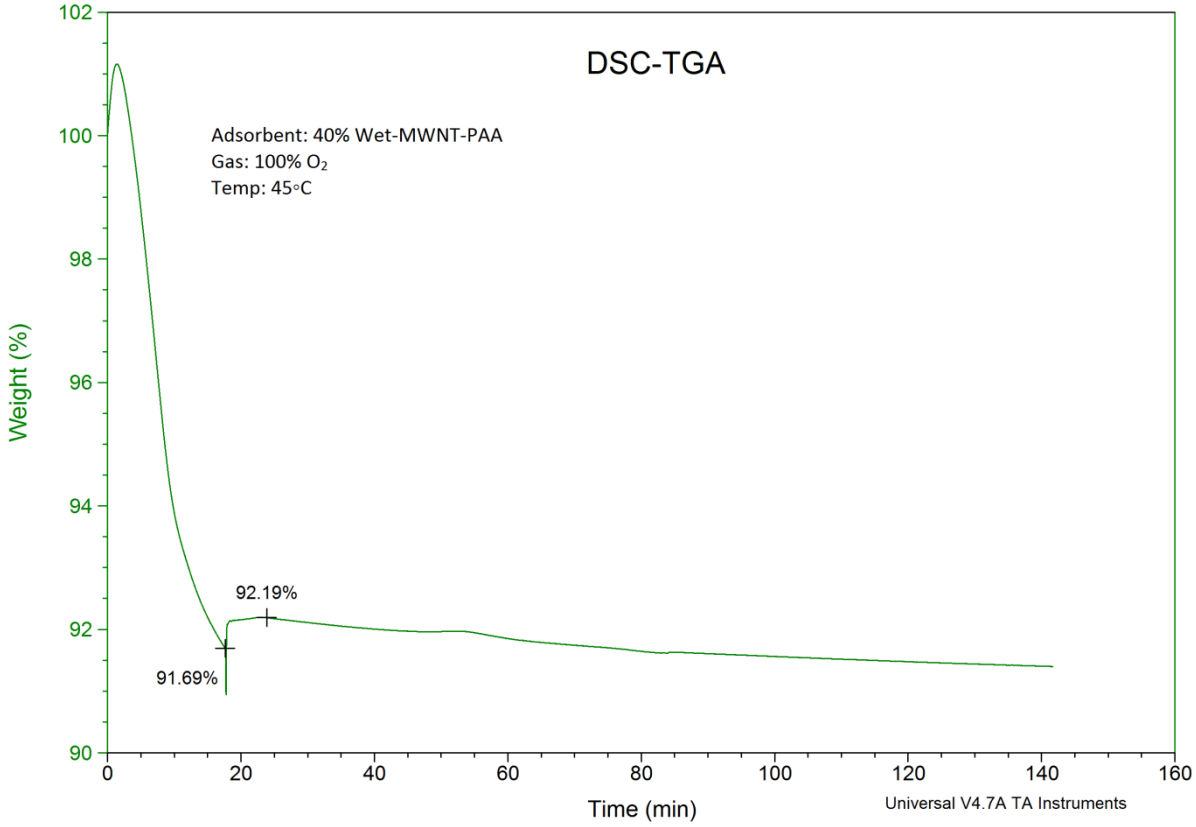

DSC-TGA
Adsorbent: 20% Wet-MWNT-PAA
Gas: 100% O2
Temp: 35◦C
99.68%
99.71%
Weight (%)
Time (min)
Universal V4.7A TA Instruments

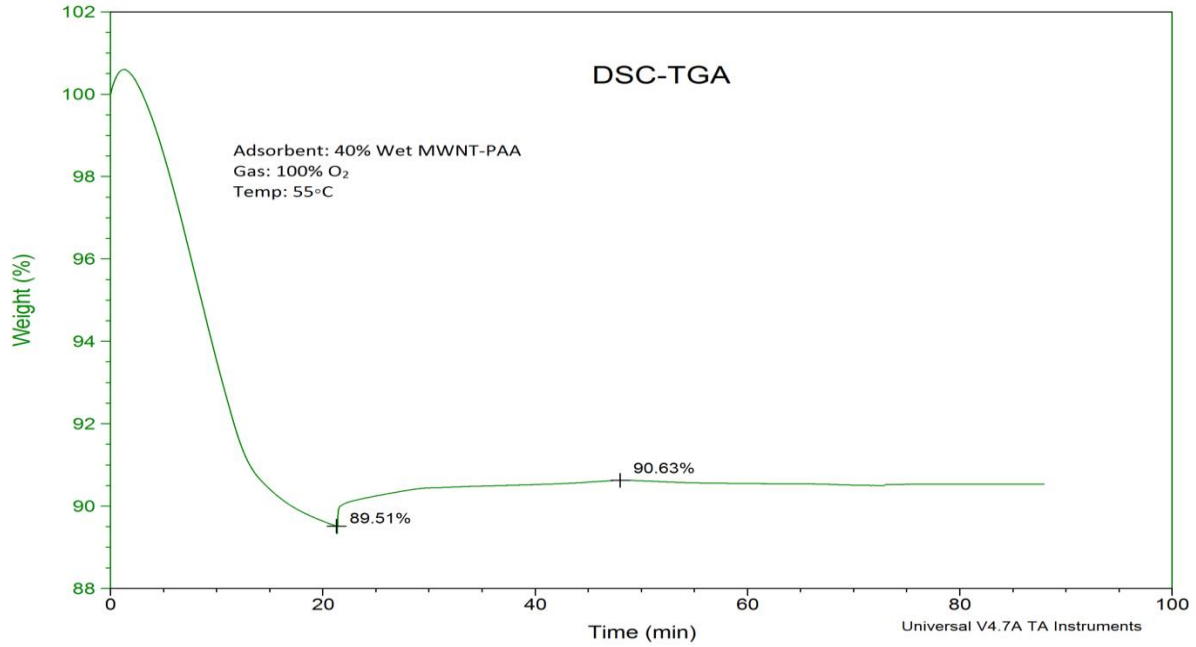

DSC-TGA
Adsorbent: 20% Wet-MWNT-PAA
Gas: 100% O_2
Temp: 45◦C
100.1%
Weight (%)
Time (min)
Universal V4.7A TA Instruments


DSC-TGA
Adsorbent: 20% wet -MWNT-PAA
Gas: 100% O2
Temp: 55C
100.3%
Weight (%)
Time (min)


DSC-TGA
Adsorbent: 40% Wet-MWNT-PAA
Gas: 100% O2
Temp: 25◦C
Weight (%)
Time (min)
80.85%
81.51%


DSC-TGA
Adsorbent: 40% Wet-MWNT-PAA
Gas: 100% O2
Temp: 35◦C
Weight (%)
Time (min)
97.86%
98.29%
Universal V4.7A TA Instruments


DSC-TGA
Adsorbent: 40% Wet-MWNT-PAA
Gas: 100% O2
Temp: 45◦C
92.19%
91.69%
Weight (%)
Time (min)
Universal V4.7A TA Instruments


DSC-TGA
Adsorbent: 40% Wet MWNT-PAA
Gas: 100% O2
Temp: 55◦C
90.63%
89.51%
Weight (%)
Time (min)
Universal V4.7A TA Instruments